# FLOW INTERFERENCE BETWEEN GROUPS OF THREE AND FOUR EQUISPACED CYLINDERS

A THESIS

by

A.T. SAYERS (BSc., MSc., Pr.Eng., M.I.Mech.E., C.Eng.)

Submitted to the Department of Mechanical Engineering of the University of Cape Town as a requirement for the degree of Doctor of Philosophy

1989

## ABSTRACT

This thesis is a study of the interference forces acting on one cylinder comprising a group of three and four cylinders when situated in a free stream flow. The spacing of the cylinders was such that the lines joining their axes formed an equilateral triangle, and a square respectively. The study is split into two parts,

(a) potential flow over the groups of cylinders

(b) real flow over the groups of cylinders

(a) The potential flow study developed equations for the complex potential of the flow over the groups of cylinders based on the method of images for doublets exterior to a cylinder in a potential flow field. From the complex potential equations thus formed, the absolute velocity on the surface of a cylinder was determined, and thence the pressure and force coefficients for that cylinder. The equations were solved numerically by computer programme and lift and drag data for one cylinder in the groups of three and four are presented and discussed.

(b) The real flow study was carried out in an open jet wind tunnel test section at a nominal sub critical Reynolds number of $3 \times 10^4$. Open jet wind tunnel blockage corrections were first investigated. Drag force data, relating to variable area ratio bluff bodies, and measured with a strain gauge balance, enabled blockage correction factors for the open jet wind tunnel to be determined. These were found to decrease as

the distance of the bodies from the mouth of the wind tunnel increased.

Base pressure measurements along the span of a single cylinder spanning the open jet test section confirmed the existence of three dimensional flow over the cylinder due to end flow effects at the interface of the wind tunnel jet and surrounding quiescent atmosphere. The fitting of end-plates to the cylinder within the jet boundaries was found to give a spanwise base pressure distribution and circumferential pressure distribution pertaining to those found in two dimensional flow over a single cylinder of infinite length. This experimental arrangement was used to study the flow interference between the groups of three and four cylinders since these regimes formed a standard experimental base on which to establish much needed design data.

The lift and drag coefficients on one cylinder of the group were determined from static pressure measurements around the cylinder at various angular orientations to the free stream flow direction, and for cylinder spacings in the range $1.1<S/D<5$. The total lift and drag coefficients for, and the direction of the resultant force acting on the structures as a whole were also determined for the various free stream directions.

Although the main thrust of the thesis is towards steady state time averaged flow interference, some dynamic effects in the form of flow visualisation, vortex shedding and cylinder frequency response are included as an addendum.

In presenting this thesis the author is claiming the following contributions to the field of flow interference over

groups of cylinders:

1. Lift and drag coefficients in potential flow over groups of three and four cylinders are calculated for varying inclination angles, and spacing ratios, of the groups to the free stream.
2. Blockage correction factors for bluff body flow in an open jet wind tunnel have been determined experimentally.
3. An experimental base has been established for the formulation of design codes based on zero wind tunnel blockage and zero end effects.
4. Force coefficients acting on groups of three and four equispaced cylinders have been determined experimentally for the ranges $1.1<S/D<5$ and $0<\alpha<180$ degrees, and show that sudden changes in magnitude and direction occur randomly as the incident free stream direction is changed.
5. The magnitude and direction of the force coefficients are highly dependent on the cylinder spacing, a fact supported by experiment.
6. Comparisons between the potential and real force coefficients acting on groups of three and four cylinders are made.
7. Pressure distributions around the cylinders comprising each group are presented as design code data for immediate use by designers.

In summary the lift, drag and pressure coefficient data presented in this thesis will prove valuable in the design of heat exchangers where force coefficients resulting from fluid flow through tube bundles are of importance: in the design of

chemical plant where flow around adjacent chimneys and stacks is of immediate concern; and in the design of semi-submersible oil rigs and production platforms, a topic of increasing importance to South Africa.

That the results of this thesis are of significant importance to the industrial aerodynamicist, is exemplified by the publication of three papers in the international literature. These papers are cited at the end of the thesis and copies may be found attached to the back cover.

## ACKNOWLEDGEMENTS

The author wishes to acknowledge his indebtedness to Messrs. L.R. Watkins, D.M. Finlayson and M.A.H. Batho of the Department of Mechanical Engineering workshops for construction of the experimental apparatus, and to T.V. Appleton who patiently prepared many of the graphs and figures.

Thanks are extended to Professor R.K. Penny for his encouragement and advice during the course of this study, whilst special thanks are due to Associate Professor J. Gryzagoridis for his advice and criticism, patience and understanding in his capacity as supervisor of this thesis.

Finally, the author wishes to express his deep appreciation to his wife, Susan, for her constant encouragement and understanding during the period of this project.

# PREFACE

The designer of cylindrical structures lying in close proximity to each other in a liquid or gas flow field, should be aware of the aerodynamic forces incident upon the respective cylinders comprising the structure. Data relating to the flow over a single cylinder in a uniform free stream is well represented in the literature but when cylinders are moved into close proximity to each other, the flow pattern about each cylinder can differ radically from the single cylinder pattern and this leads to changed force coefficients.

A literature survey reveals that many investigators have experimentally determined, in wind tunnels, the interference force coefficients acting on two cylinders in close proximity. In most cases, little or no account has been taken of wind tunnel blockage effects and cylinder end effects, the important criteria usually being to solve a particular problem as quickly as possible.

The author has therefore identified the requirement for a standard design data base to be established, this data being determined in terms of two dimensional flow over groups of three and four infinitely long cylinders, in a rational and precise way. This thesis deals with a number of aspects relating to the establishment of analytical and experimental techniques used in achieving the above mentioned flow criteria and hence the determination of the force coefficients acting on the cylinders comprising the group.

# NOMENCLATURE

| Symbol | | Units |
|---|---|---|
| A | cross sectional area of tunnel test section | $m^2$ |
| AR | aspect ratio (= s/D) | dimensionless |
| a | projected area of bluff body | $m^2$ |
| | radius of cylinder in potential flow | m |
| a/A | area ratio | dimensionless |
| $C_D$ | drag coefficient | dimensionless |
| $C_{Dc}$ | corrected drag coefficient | dimensionless |
| $C_{DT}$ | total drag coefficient for a group of cylinders | dimensionless |
| $C_L$ | lift coefficient | dimensionless |
| $C_{LT}$ | total lift coefficient | dimensionless |
| $C_p$ | pressure coefficient | dimensionless |
| $C_{pb}$ | base pressure coefficient | dimensionless |
| D | drag force | Newtons |
| | cylinder diameter | m |
| $D_0$ | drag on sting in wind tunnel | Newtons |
| $D_1$ | drag on plate in an infinite free stream | Newtons |
| $D_2$ | drag on plate in wind tunnel | Newtons |
| $D_3$ | drag on sting and plate in wind tunnel | Newtons |
| e | exponential (also exp) | dimensionless |
| F | resultant force per unit length | N/m |

| | | |
|---|---|---|
| f | distance of doublet from cylinder centre | m |
| | frequency | Hz |
| f' | distance from centre of cylinder to image doublet (the inverse point) | m |
| I | imaginary part of a number | dimensionless |
| i | imaginary number ($\sqrt{-1}$) | dimensionless |
| L | lift force | Newtons |
| m | total number of doublets | dimensionless |
| p | static pressure | Pa |
| $p_\infty$ | free stream static pressure | Pa |
| q | absolute velocity on surface of cylinder (= $\|V(z)\|$) | m/s |
| R | real part of a number | dimensionless |
| Re | Reynolds number (= $UD/\nu$) | dimensionless |
| r | radial co-ordinate | m |
| S | distance between cylinder centres | m |
| (S/D) | cylinder spacing ratio | dimensionless |
| St | Strouhal number (= fD/U) | dimensionless |
| s | effective span | m |
| U | free stream velocity | m/s |
| $U_c$ | corrected free stream velocity | m/s |
| u | velocity component in x direction | m/s |
| V | complex velocity | m/s |
| v | velocity component in y direction | m/s |
| w | complex potential (= $\phi + i\psi$) | $m^2/s$ |
| X | longitudinal distance between cylinder centres | m |

| | | |
|---|---|---|
| x | horizontal co-ordinate | m |
| Y | transverse distance between cylinder centres | m |
| y | vertical co-ordinate | m |
| z | complex variable (= x + iy) | m |

Greek

| | | |
|---|---|---|
| $\alpha$ | inclination of cylinder group to free stream | degrees |
| $\beta$ | angle subtended by cylinder 4 2 from cylinder 1 | degrees |
| $\gamma$ | angle of resultant force | degrees |
| $\delta$ | inclination of a doublet in potential flow | degrees |
| $\theta$ | angle around circumference of cylinder | degrees |
| $\mu$ | doublet strength (= $Ua^2$) | $m^3/s$ |
| $\mu'$ | strength of image doublet | $m^3/s$ |
| $\pi$ | operator (= 3.142) | dimensionless |
| $\rho$ | density of fluid | $kg/m^3$ |
| $\sigma$ | angle subtended by line joining causing doublet and its image | degrees |
| $\nu$ | kinematic viscosity of air (= $17 \times 10^{-6}$) | $m^2/s$ |
| $\phi$ | velocity potential | $m^2/s$ |
| $\psi$ | stream function | $m^2/s$ |

# TABLE OF CONTENTS

Page

Page

# LIST OF TABLES

# CHAPTER 1

# REVIEW OF PREVIOUS INVESTIGATIONS OF FLOW INTERFERENCE BETWEEN GROUPS OF CYLINDERS

## 1.1 INTRODUCTION

Although many engineering structures rely on cylindrical components or elements which, when assembled, form the whole, it is a fact that very little basic data relating to the forces acting on groups of more than two cylinders actually exists!. Of the data that does exist, this appears to have been obtained in response to a specific industrial requirement with the result that no standard code can be referred to by a designer as a starting point for a design. Zdravkovich (1977) [1] stressed this point in stating that investigations of the flow around groups of cylinders is an example of the unsystematic and fragmentary research carried out mainly to solve immediate practical problems.

Some of the variables used by other authors have been

1) Number of cylinders in the group
2) Cylinder spacing
3) Free stream Reynolds number
4) Cylinder aspect ratio
5) Wind tunnel blockage effects
6) Open or closed jet wind tunnel
7) Method of force measurement

In this chapter, details of previous work on interference

flow between groups of two or more cylinders will be discussed with reference to the aforementioned variables. It will be seen that whilst flow interference between two cylinders has been well documented, albeit in a haphazard way, it does never-the-less represent a body of data to which a designer could turn when carrying out initial design calculations. In contrast, for flow interference between groups of more than two cylinders, experimental data is very scarce and because of the lack of any standard experimental procedures, could not readily be included in a standard code.

To provide an understanding of the interference flow over groups of more than two cylinders, the author has obtained new data, collected under standard conditions, which, it is suggested forms the basis for a library of standard design codes to which design data that have been obtained under similar experimental conditions may be added.

## 1.2 HISTORICAL BACKGROUND

Applications of flow around cylinders started in the aeronautical field with the study of flows around twin struts and support wings and then moved to hydronautical engineering in examining the vibrations of periscopes, snorkels and radar masts. Civil engineering joined the field with studies of wind flows around chimney stacks and buildings and latterly of sea flows around jetties and other offshore structures. In electrical engineering, twin conductor transmission line vibration stimulated research whilst in mechanical and chemical engineering, heat exchanger tube vibration and pipe rack forces gave impetus to further studies.

The development of technology in historical terms has caused the study of flows over cylinders to move from one cylinder, to two cylinders, to three or more cylinder configurations. This natural progression makes it convenient to chronologically review the previous work carried out, first in terms of two cylinders and then for multi-cylinder configurations.

## 1.3 FLOW OVER TWO CYLINDERS

In the case of two cylinder flow, three configurations of the cylinders are possible. There is first the tandem arrangement where the cylinders are arranged one behind the other parallel to the direction of the free stream. Secondly, the cylinders can be set transversely, i.e. side by side, in a line perpendicular to the free stream. The third arrangement is staggered, and applies to any configuration other than the former two.



### Cylinders in tandem

Studies in flow around two circular cylinders arranged in tandem, began in aeronautical engineering in the early era of biplanes. This was because of the then common practice of employing cylindrical struts (later superceded by streamlined struts) to connect the two wings. Pannell, Griffiths and Coales (1915) [2] reported the results of force measurements on two parallel circular wires, the centre line distance between the wires (S/D) varying from 1 to 6. With both wires exposed to the wind, the combined drag force was measured at

inclination angles up to 20 degrees from the fully tandem (one behind the other) arrangement, the inclination angle being that between the line joining the centres of the cylinders and the wind direction. They noted that when the wires were in contact, (S/D=1), the total drag force amounted to only 40 percent of that on a single wire and that this was due to the streamlining of the overall flow pattern in the latter case. The wire diameter was 12.5 mm and the Reynolds number $9.72 \times 10^3$.

Biermann and Herrnstein (1933) [3] reported on drag force measurements for each cylinder in a group of two, the cylinder spacing being extended to nine diameters. They found that for a cylinder centre line spacing of four diameters or more, there was practically no interference. For spacings less than four diameters the interference drag, defined as, the difference between the drag of the cylinders in combination and the sum of the drags of the cylinders measured in isolation, could be either positive or negative depending on both the Reynolds number and the cylinder gap.

Spivak (1946) [4], using a hot-wire anemometer, carried out a detailed investigation of the predominant frequencies in the flow field behind a pair of tandem cylinders over a Reynolds number range from about $1.5 \times 10^4$ to $9.3 \times 10^4$ and spacing $1<S/D<7$. He discovered three fairly distinct regimes of flow. For cylinder spacings greater than 2 diameters the frequency of vortex shedding from the upstream or leading cylinder was the same as that for a single body, whereas for gaps of less than 1.5 diameters the shedding frequency appeared to be associated with a body of width equal to twice the cylinder diameter. At intermediate gap widths the flow was less well

behaved and frequencies associated with a single and double body could both be detected. These results of Spivak [4] and later those of Hori (1959) [5], confirmed Biermann and Herrnstein's [3] findings that the wakes behind the two cylinders were different for spacings of less than 2 diameters, even though the geometrical arrangement is symmetrical with respect to the free stream.

The cylinders used by Spivak [4] were of aspect ratio 12.3 and spanned a closed jet test section wind tunnel. The blockage, defined as the percentage of the test section cross-sectional area taken up by the total projected area of the cylinders (a/A), was 16%.

Pressure distributions around two cylinders in tandem arrangement were measured by Hori (1959) [5]. The pressure distributions are shown in polar coordinates in Fig. 1.1, for three cylinder spacings of 1.2, 2.0 and 3 diameters. It can be seen that only the rear part of the upstream cylinder was affected by the presence of the downstream cylinder and as the cylinder spacing increased, so the base pressure coefficient increased and consequently the drag on the upstream cylinder decreased. They concluded that the decrease of the interference drag coefficient was caused by the drop in the base pressure only.

On the part of the downstream cylinder facing the gap, low negative pressures of the same order of magnitude as the upstream cylinder base pressure are observed. This indicates that the flow in the gap is almost stagnant. Also, the negative gap pressure coefficient of the downstream cylinder exceeds that on the base side of the same cylinder resulting in a negative drag force or thrust in the upstream direction.

Two symmetrically positioned maximum pressures are to be observed at the points "x" in Fig. 1.1 and these correspond to the reattachment points on the downstream cylinder, of the flow which has separated from the upstream cylinder. The angular distance between the reattachment points decreased as the cylinder spacing increased from 2 to 3 diameters.

Time average pressure coefficient distributions around the downstream cylinder of two cylinders in tandem at a Reynolds number of $10^5$, were determined by Zdravkovich and Stanhope (1972) [6] and are shown in Fig. 1.2. They found that for small spacings up to 3.5 diameters the pressure distributions were similar, and displayed the same features as those found by Hori (1959) [5]. For cylinder spacings beyond 3.5 diameters, a second similar group of curves, including one for the pressure distribution around a single cylinder, are formed, all of them showing only one maximum pressure at the stagnation point and no sign of the reattachment peaks. They concluded that for small spacing, up to S/D=3.5, there are two symmetric peaks, presumably corresponding to the reattachment points, whilst for greater spacings, there is a single peak corresponding to the stagnation point.



Transverse cylinders

Biermann and Herrnstein (1933) [3] also measured the drag forces on two cylinders spaced transversely and found that the interference drag was zero for all spacing ratios greater than 5 but increased as the spacing was reduced to 2.25 diameters. For smaller spacings the flow pattern became bi-stable, changing randomly from one flow pattern to another. In these

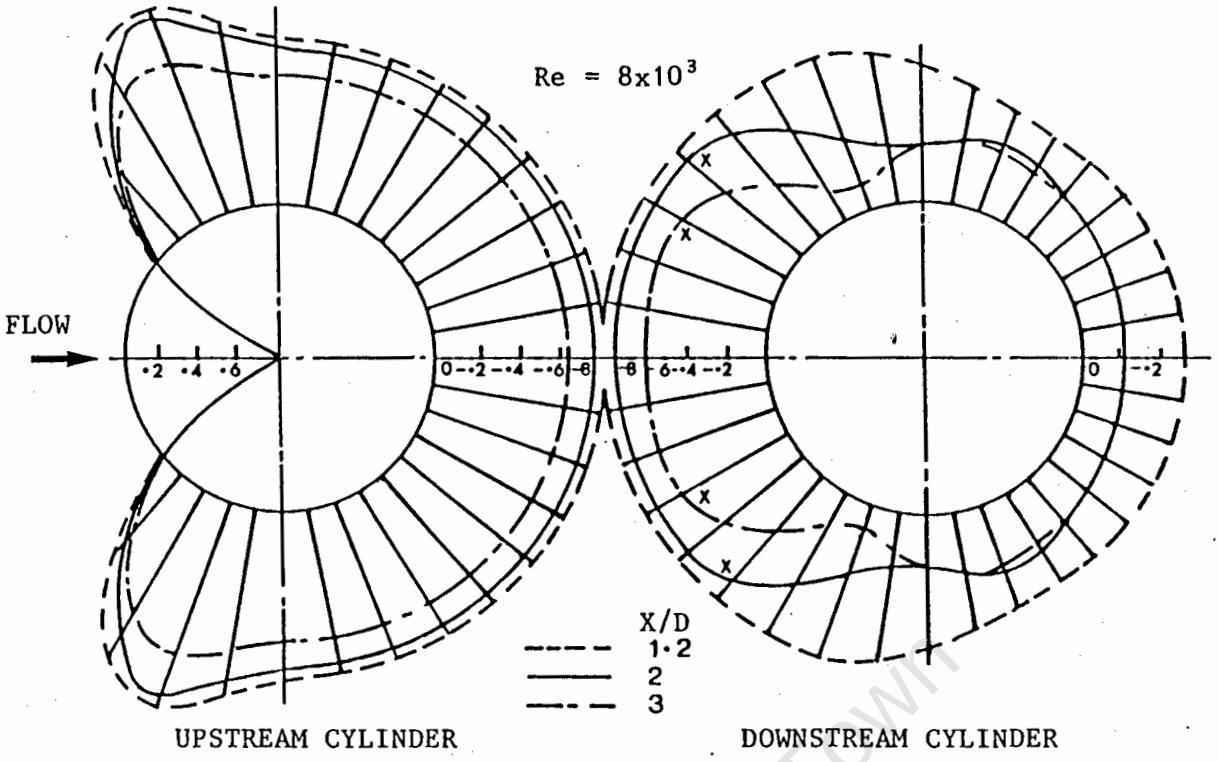


Fig. 1.1 Pressure distribution around two cylinders in tandem [5]

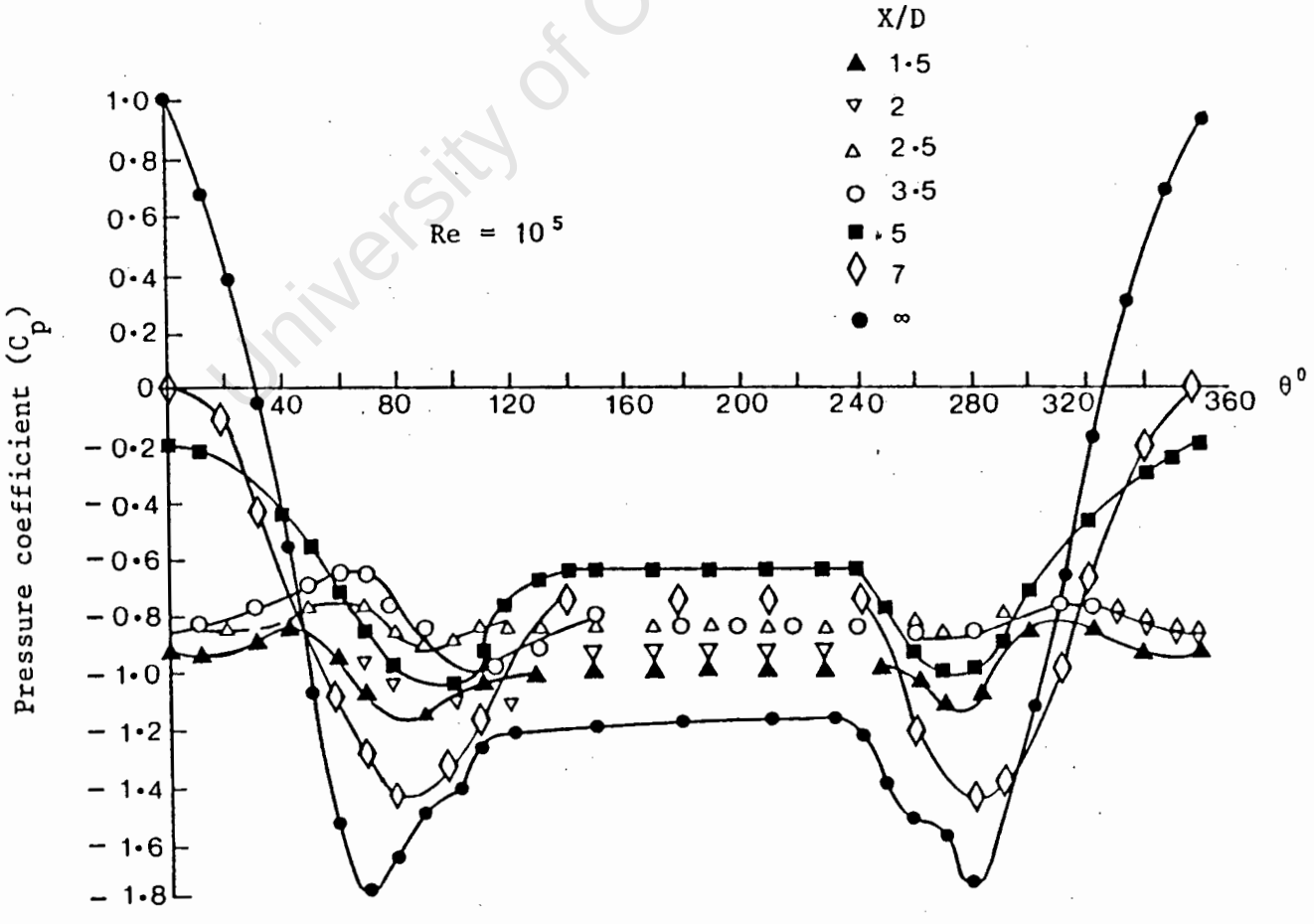


Fig. 1.2 Pressure distribution around downstream cylinder in various tandem arrangements [6]

tests, the cylinders spanned an open jet wind tunnel with their ends protruding through the air stream boundary, and even allowing for the relatively large aspect ratio of 48, end flow effects would cause errors in the pressure distribution around the cylinder and therefore in the drag force. The worst blockage, encountered in the transverse position when two cylinders are fully exposed to the air stream was 6% which is not likely to have had any effect on the results.

It is rather unfortunate that a Reynolds number of approximately $10^5$ was chosen, since this is in the transition region from a laminar to a turbulent boundary layer in flow over a single cylinder, and whilst the flow pattern might be quite stable at the higher cylinder spacings, instability could in part be responsible for the fluctuating interference drag at the smaller spacings.

Using the Schlieren optical method, Ishigai, et al. (1972) [7] photographed the flow patterns around two transverse cylinders and showed that for spacings greater than 2.5 diameters the vortex formation and shedding is coupled and symmetric about the axis of the gap, whilst at spacings less than 1.5, the vortex shedding is uncoupled and weak, and the gap flow biased to one side. This leads to wide and narrow wakes being formed behind the cylinders, the biased flow in the gap being bi-stable, and easily changed from one cylinder to another when a flow disturbance occurs.

Simultaneous measurements by Bearman and Wadcock (1973) [8] of the base pressures of both cylinders in the transverse arrangement revealed that for cylinder spacings between 1.1 and 2.3 diameters, the base pressure on each cylinder was different and that it changed from one steady state value to

another or simply fluctuated between the two extremes. They also found that stopping and starting the tunnel again could cause the pressure to change over. Their measurements were carried out in a closed jet tunnel, correction for blockage being in accordance with Maskell (1965) [9]. The Reynolds number of the flow was $2.5 \times 10^4$, the cylinder aspect ratio 30, whilst at worst before correction, the blockage amounted to only 3.8%.

Staggered arrangement

The staggered arrangements may be classified into five regions of interference force:

1) Negligible lift force and reduced drag force.
2) Small lift force (repulsive) and reduced drag force.
3) A lift force (repulsive) and increased drag force.
4) Negligible lift force and increased drag. A small region beyond which the cylinders behave singly.
5) Negative lift force and decreased drag force. A dominant region for the downstream cylinder.

Regions 1, 2 and 3 apply only to the upstream cylinder whilst the downstream cylinder can be in all regions.

Hori (1959) [5] carried out systematic measurements of the pressure distribution about each cylinder in staggered arrangement, and from them calculated the lift and drag coefficients. From these coefficients the resultant interference force coefficients were calculated and are plotted as arrows in Fig. 1.3, the interference effects being

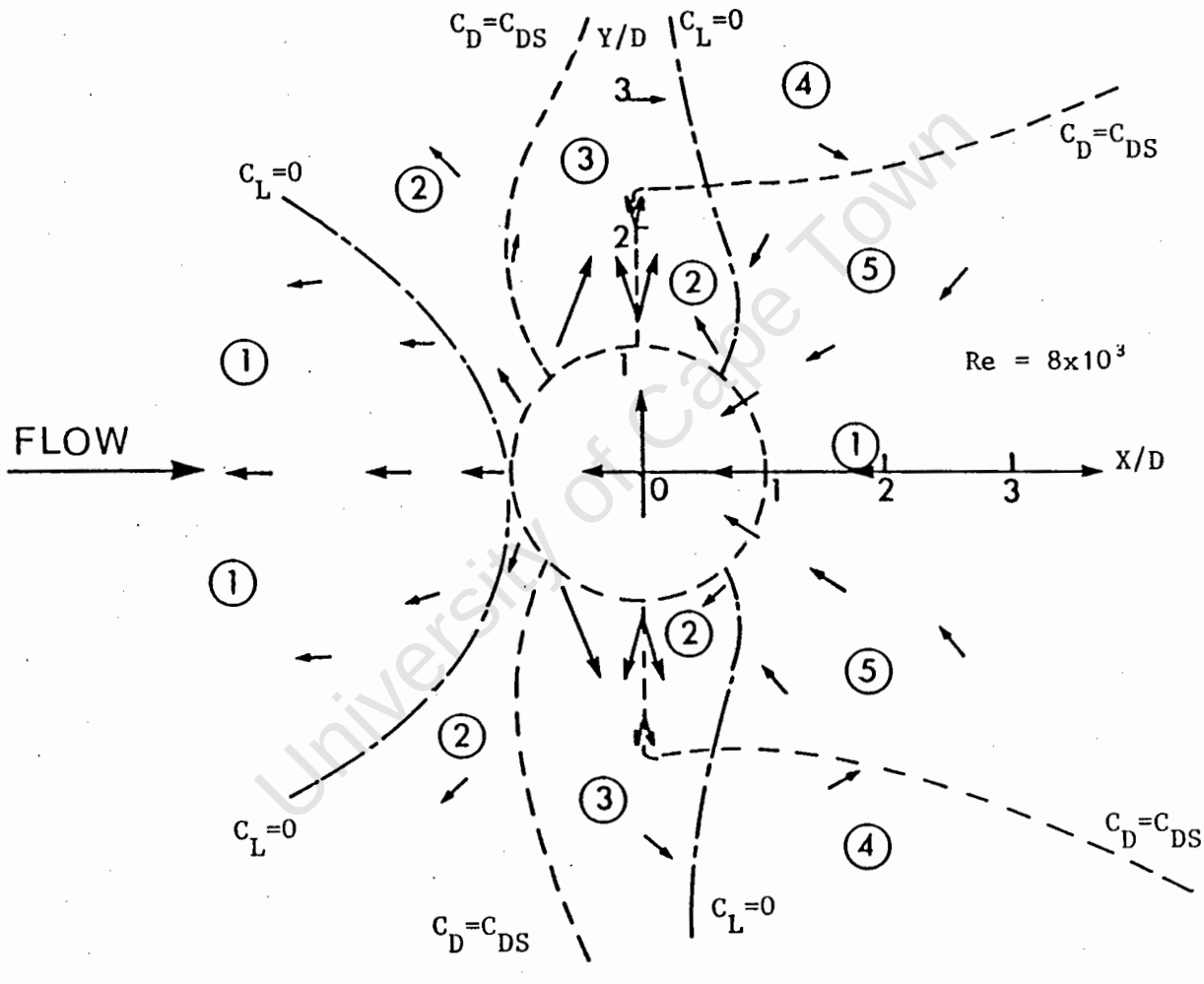


Fig. 1.3 Interference force coefficients for all cylinder positions [5]

proportional to the length of the arrows. The inclination of the arrows show the resultant interference effect direction whilst the position of the arrows relative to the origin indicates whether it applies to an upstream or downstream cylinder. An arrow to the left would indicate an interference force coefficient less than that for the single cylinder (that is negative) whilst an arrow to the right indicates a positive interference force coefficient. It is evident from Fig. 1.3 that small changes in relative position can give rise to large fluctuations of the force coefficients in both magnitude and direction.

Zdravkovich and Pridden (1977) [10] determined the lift and drag coefficients of the downstream cylinder in a group of two over a range of staggered arrangements from tandem to transverse. They showed that small changes in cylinder spacing can produce large changes in the flow pattern and resulting lift and drag forces. They also found that there are discontinuous changes in the flow pattern around the downstream cylinder, and in the forces acting on the downstream cylinder at some critical spacings. In this case, two types of flow pattern produce two values of forces, and both flows intermittently change over.

In the tandem arrangement, a discontinuity occurred at a cylinder spacing of about 3.5 diameters for $4.0\times10^4 < Re < 5.1\times10^4$, when two flow patterns interchanged. The first showed almost no flow in the gap, but reattachment of the separated flow from the surface of the upstream cylinder took place on the downstream cylinder. The second flow pattern showed an almost fully developed flow in the gap impinging on the downstream cylinder. Drag coefficients for the downstream

cylinder were negative for cylinder spacings from 1 to 2.1 diameters, and thereafter positive for all other spacings, the measurements being taken at a Reynolds number of $6x10^4$. The corresponding lift coefficients were zero except for the range $2.6<S/D<4$ where they were positive.

Zdravkovich and Pridden (1977) [10] plotted the loci of lift and drag coefficients for the downstream cylinder in terms of its transverse and longitudinal position in the flow field and at a Reynolds number of $6.1x10^4$. These are shown in Figs. 1.4 and 1.5, where in addition to the two instabilities found for the tandem and transverse arrangements, a third instability exists at approximately the position X/D=3 and Y/D=0.25. In this region, lift coefficients ranging from 0 to -0.8 are to be found and these change intermittently and at random. The forces acting on the downstream cylinder were measured using a three component mechanical balance in a closed jet test section. Cylinder end flow effects were minimised by leaving an 0.5 mm gap between the ends of the cylinder and two dummy cylinders attached to the walls of the test section. However, no pressure measurements along the length of the cylinder were reported to confirm two dimensional flow. Blockage amounted to 9% which the author considers to be high enough to have a profound effect on the measured forces.

Dalton and Szabo (1977) [11] also carried out a comprehensive study of flow interference around two cylinders. The cylinders were rotated about an axis placed mid-way along a line joining their centres such that the inclination of the cylinders, to the approaching free stream, could be varied. They measured lift and drag coefficients on one of the

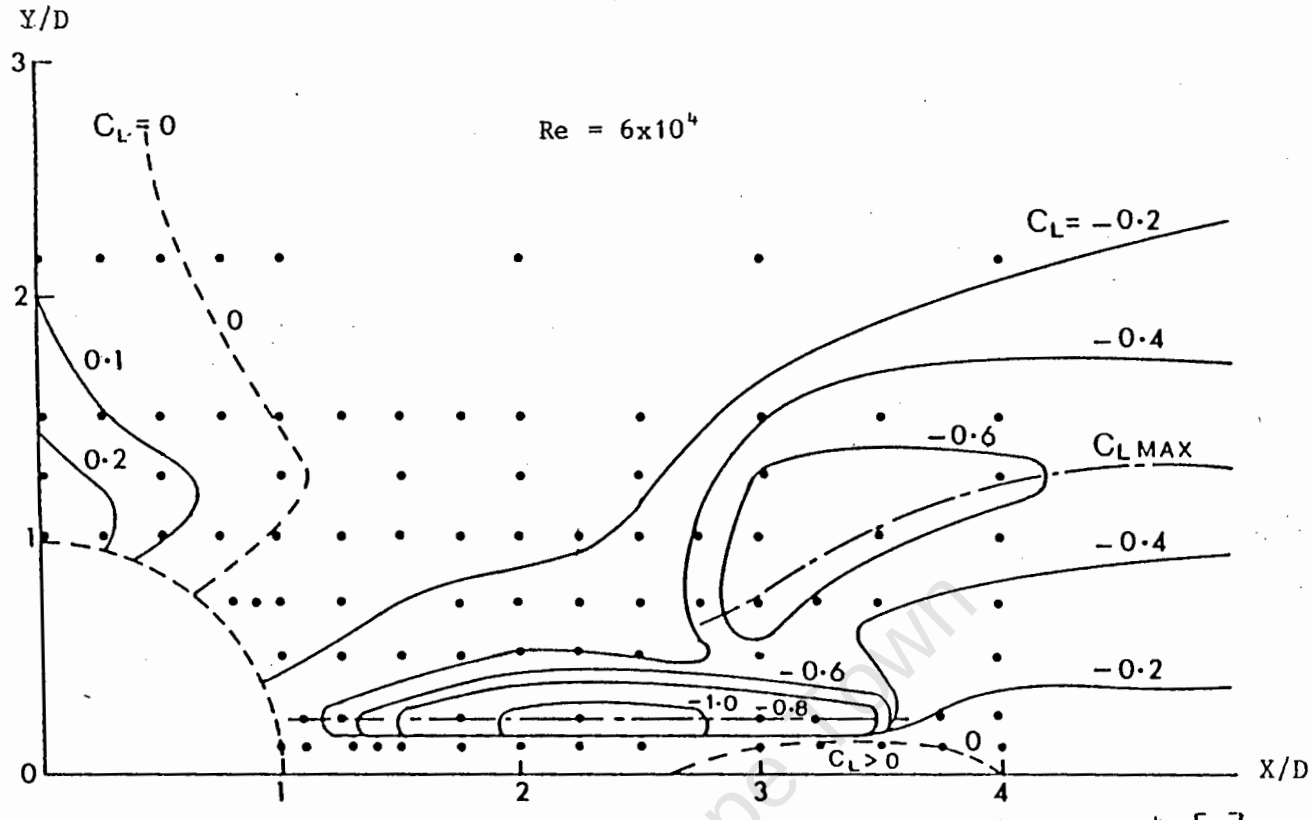


Fig. 1.4 Lift force coefficient for downstream cylinder at Re = $6x10^4$ [10]

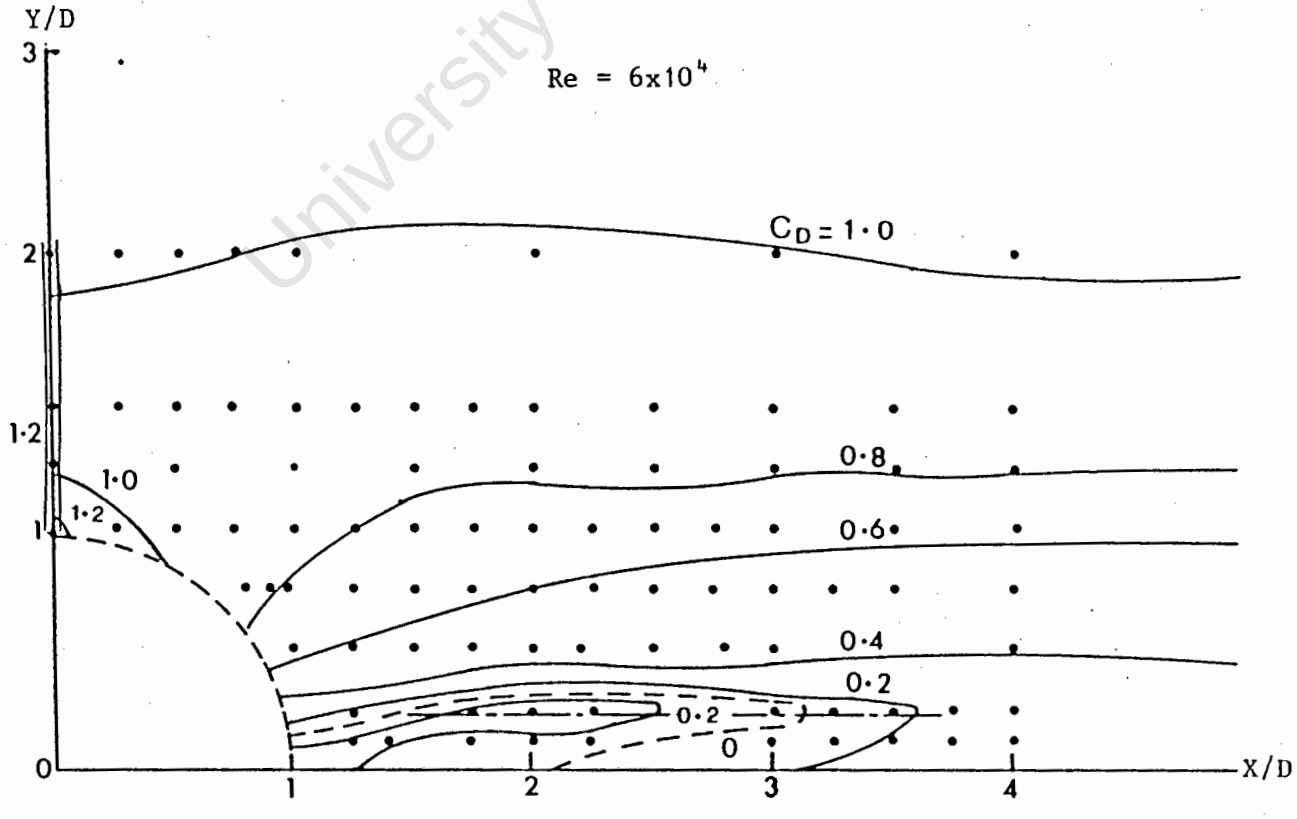


Fig. 1.5 Drag force coefficient for downstream cylinder at Re = $6x10^4$ [10]

cylinders for inclination angles between 0 degrees (tandem) and 90 degrees (transverse), at cylinder spacing of $1<S/D<5$, over a Reynolds number range of $2.78\times10^4<Re<7.82\times10^4$. They concluded that the drag coefficient on the trailing cylinder is strongly affected by spacing and orientation and weakly affected by Reynolds number; the drag coefficient becomes fairly constant at spacing ratios of 5 or more diameters; and that the drag coefficient on the upstream cylinder is more dependent on spacing and orientation than on Reynolds number.

All the measurements were carried out in a closed jet wind tunnel. The cylinders, which had an aspect ratio of 16, were mounted on a turntable in one wall of the tunnel and were free at the other end with the gap between it and the other tunnel wall being 6 mm. The drag or lift force on an individual cylinder was measured by calibrated deflection strain gauges attached to the surface. The worst blockage was 12.3% in the transverse arrangement and 6.2% in the tandem arrangement, but this blockage was corrected by the method of Allen and Vincenti (1944) [12] as amended by Dalton (1971) [13]. However, it is interesting to note that at an inclination angle of 0 degrees (tandem), the measured data correlated very well with that of Biermann and Herrnstein [3], but at an inclination angle of 90 degrees (transverse), the drag coefficients were about 10 percent lower than those of Biermann and Herrnstein [3]. It would seem therefore that the blockage correction technique employed by Dalton and Szabo is not very reliable at the higher blockage ratios whilst in the tandem arrangement, the low value of blockage did not have any measurable effect on the results. It is difficult to comment on the accuracy of the Reynolds number effect since this could

be masked by cylinder end flow effects caused by the 6 mm gap.

## 1.4 FLOW OVER MULTIPLE CYLINDERS

One of the first reports relating to measurements of the force acting on a cylinder in a group of more than two was by Roberts (1966) [14]. In studying the aeroelastic vibrations of an alternately staggered cascade of closely spaced cylinders, he determined the drag coefficients from pressure distribution measurements around the cylinder. The study did not involve wind direction variations, therefore shielding or buffeting of a trailing cylinder did not occur.

Mair and Maull (1971) [15] reported on the wake of two-dimensional bodies, emphasizing the properties of the wake which influence the drag on other bodies placed in it. They carried out experiments on a group of five cylinders arranged in two parallel rows of three and two, with their centres equispaced at 2 diameters. The Reynolds number based on the diameter was $1.5 \times 10^5$ and the cylinders were 18 diameters high. With the three cylinder row upstream, they determined the variation of the mean resultant force on one of the cylinders in the rear row as the orientation of the flow was varied, and showed that for a particular orientation, the force coefficient could vary from 0.67 to 1.17 for a change in wind direction of 2 degrees. One of their most pertinent conclusions was, "Theoretical work to predict the flow around groups of structures seems at the moment to present large difficulties. Theory, however, might give some guidance in planning and interpreting wind tunnel experiments. There is a danger of ad

hoc testing leading to a proliferation of undigested and uncorrelated data". No details of the size of wind tunnel used by them were given, and therefore no estimation of the blockage can be made.

Dalton and Szabo (1977) [11] extended their work to a study of the flow over three cylinders. The cylinders were equispaced along a line joining their centres, and were rotated about the axis of the centre cylinder. The lift and drag forces on a cylinder were measured, as before, over the same inclination, spacing and Reynolds number range. The worst blockage in the transverse position increased to 18% due to the addition of the third cylinder and it is therefore most likely that the results are subject to serious error especially at the higher inclination angles.

Gerhardt and Kramer (1981) [16] acknowledged the scarcity of code information concerning the static wind loads and wind-induced vibrations of groups of stacks. They chose to perform tests at a simulated high Reynolds number of the order $10^7$, based on diameter and velocity. The cylinders were arranged transversely in groups of three and four; as an equilateral triangle at various orientations to the wind; and as a group of five in the form of a square with a larger diameter cylinder in the centre, each group once again being set at various orientations to the wind. The cylinders stood with their free ends in the wind stream with aspect ratios of 28.6. No details of the cylinder diameter or size of tunnel test section were given and therefore no estimation of the blockage can be made. Drag coefficients at cylinder spacings up to 5 diameters were determined from pressure distributions but these are not readily comparable with the results of Dalton

and Szabo (1977) [11] because of the super-critical nature of the flow. They concluded that the largest static wind loads for groups of stacks occur for transverse arrangements and wind directions perpendicular to the plane of the centre line of the stacks, and that to avoid large static wind loads for groups of chimneys in transverse arrangements, spacings of $S/D<1.5$ and $2.5<S/D<3.5$ should be avoided.

The need for reliable force data for the fluid elastic stability of structures was noted by Price and Paidoussis (1984) [17]. They stated that for the range of Reynolds numbers in which they were interested, only one paper, by Eastop and Turner (1982) [18], existed. However, this paper confined itself to flows over three cylinders in tandem or transverse arrangement. Price and Paidoussis [17] arranged their cylinders such that two were positioned transversely at a fixed spacing whilst a third downstream cylinder could be moved parallel or perpendicular to the plane of the front row. Force measurements were made on the upstream and downstream cylinders for various positions of the downstream cylinder in a Reynolds number range $1.7\times10^4<Re<8.6\times10^4$. The three cylinders, with an aspect ratio of 24, were mounted as cantilevers across the height of the tunnel test section leaving a gap of 1 mm between their ends and the tunnel walls. One cylinder acted as the measuring cylinder and was clamped at its lower end to a force balance, which was in turn mounted in the wind tunnel floor. Maximum blockage was 8.3% and no correction was made for it.

They concluded that for the cylinder spacings investigated, the fluid forces on one cylinder in a group of three when subject to a cross flow have many similarities to the fluid

forces on one in a group of two cylinders and that for Reynolds numbers in the range $5.1x10^4 < Re < 5.8x10^4$, the force coefficients are not significantly affected by the value of Reynolds number. This statement lends support to Dalton and Szabo's [11] conclusions, especially so, since the blockage has been more than halved. Also for their data, Price et al showed that "to within a reasonable degree of accuracy, the force coefficients on one of three cylinders may be calculated, using a principle of superposition, from the force coefficients on one cylinder in a group of two". The inclusion of this last statement is for completeness, since the author doubts its validity, even with regard to the data from which it is derived.

In a private communication with Zdravkovich (1985) [19], Bardowicks (1980) [20], presented lift and drag coefficients acting on one cylinder in a group of three arranged as an equilateral triangle. The Reynolds number was $2x10^5$; cylinder spacing varied between 2 and 5 diameters; and the cylinders of aspect ratio 10, had free flow over one end, the other end being attached to a floor balance. No further information was given and hence blockage effects are unknown. The results would be useful were it not for the fact that the choice of Reynolds number is once again particularly unfortunate as it is in the transition region. A lack of detail of the cylinder end flow and blockage conditions also detract from the results.

Drag coefficients for cylinders in square clusters at S/D=5 in a simulated high Reynolds number flow were measured by Pearcey et al (1982) [21]. The clusters were in rows and

were found for the upstream and downstream cylinders in the 2x2 cluster. However, in the 3x3 cluster, a drag coefficient occurred in the third row which was less than in the second row and this was at variance with the drag coefficient measured on three (tandem) tubes in the sub critical state. The overall fluid force coefficients acting on the groups were found to be almost the same irrespective of the number of cylinders in the group, but the overall drag coefficient for the group is not representative of any cylinder in it.

## 1.5 SUMMARY OF PREVIOUS WORK

The papers reviewed show that the most complete physical picture of the flow around groups of cylinders has only been developed for two cylinders in various arrangements. Although in many of the papers cited, wind tunnel blockage was ignored, it was by default, small enough not to have a significant effect on the results. In more recent work [10],[11],[17] end flow conditions were recognised as being of importance and care was taken to minimise them. With some exceptions [14], most research has been carried out in the sub-critical flow regime in the Reynolds number range $10^4 < Re < 10^5$ where it has been shown [11],[17] that Reynolds number effects are negligible. Because of the range of values of the variables used by the different authors, it is impossible to correlate their results graphically but Table 1.1 summarises the important experimental conditions pertaining to the various authors.

There is then, for the two cylinder arrangement, a sound body of data in a stable flow regime to which the designer can turn for information relating to the interference forces act-

ing on the cylinders. When groups of more than two cylinders are considered, only a very limited and unclassified data base exists and this has been determined in an unsystematic manner. The basic two cylinder interference flow regime is not sufficient to describe the additional interaction of cylinders in groups of three or more and therefore definitive experimental data obtained under controlled wind tunnel blockage conditions and at a stable and representative sub critical Reynolds number is required for these flow regimes. This data will enable direct comparisons with the two cylinder flow regime to be made and will form the basis of an as yet non existant standard data code for designers.

The remainder of this thesis describes a potential flow solution for flow interference between three and four cylinders; the establishment of standard experimental flow conditions which minimises the error caused by blockage and cylinder end effects; the determination of the force coefficients acting on a single cylinder in a group of three and four, and the overall force coefficients for each group as a whole.

| Reference | Year | Tunnel | AR | a/A(%) | Rex$10^{-4}$ | Turb(%) |
|---|---|---|---|---|---|---|
| [3] Biermann, et al | 1933 | Open Jet | 48 | 1.23-1.6 | 6.5-16.3 | (?) |
| [4] Spivak | 1946 | Closed | 12.3 | 16.2 | 8 | 0.02 |
| [5] Hori | 1959 | Closed | 120 | 0.8-1.7 | 0.8 | (?) |
| [15] Mair, et al | 1971 | (?) | 18.2 | (?) | 15 | (?) |
| [6] Zdravkovich, et al | 1972 | Closed | 7 | 10 | 10-22 | 2 |
| [8] Bearman, et al | 1973 | Closed | 20 | 3.8 | 2.5 | 0.2 |
| [10] Zdravkovich, et al | 1977 | Closed | 13.8 | 9 | 2.5-11 | 0.1 |
| [11] Dalton, et al | 1977 | Closed | 16 | 12.3-18.5 | 2.8 | (?) |
| [16] Gerhardt, et al | 1981 | Closed | 28.6 | (?) | 1000 | (?) |
| [17] Price, et al | 1984 | Closed | 24 | 3.8-8.3 | 5.1-5.8 | 0.5 |
| [18] Eastop, et al | 1982 | Closed | 14.3 | 14-21 | 4.5-11.1 | 0.7 |
| [20] Bardowicks | 1985 | Closed | 10 | (?) | 100 | (?) |

Table 1.1 Comparison of aspect ratio, blockage factor, Reynolds number and turbulence intensity for flow over two and multiple cylinders.

# CHAPTER 2

# POTENTIAL FLOW THEORY

## 2.1 INTRODUCTION

In this chapter, two dimensional steady state potential flow over groups of cylinders is considered and equations for the lift and drag coefficients for any cylinder without separation and wake, comprising the group is determined. The complex potential for flow over a single cylinder is first described, followed by a discussion of the method of images as applied to a doublet exterior to a cylinder. The method of images is then applied to three cylinders in close proximity to each other and equations for the complex potential of three arbitrarily translating cylinders are derived. The three translating cylinders are brought to rest by the superposition of a free stream velocity. Differentiation of this total complex potential yields the velocity at any point in the flow field.

The pressure distribution in the flow field is obtained from the Bernoulli equation in terms of the previously determined velocities, and calculating the pressure distribution around the surface of the cylinder in particular, enables the lift and drag coefficients of the cylinders to be predicted.

## 2.2 FLOW OVER A SINGLE CYLINDER

The complex potential for two-dimensional steady state flow over a single cylinder lying in an infinite flow field is given by Milne-Thomson (1938) [22], as the sum of the complex potentials for rectilinear flow, and a doublet.

$$w(z) = Uze^{-i\delta} + Ua^2e^{i\delta}/z \qquad (2.1)$$

The doublet is at the origin of the Cartesian co-ordinate system shown in Fig. 2.1a, with its axis (sink to source) at angle $\delta$ to the positive x axis. The free stream velocity U is also at angle $\delta$ to the positive x axis, a is the radius of the cylinder, whilst the complex co-ordinate vector, z, of any point in the flow field is the vector sum of the real and imaginary parts (x + iy) of vector z. Putting $\delta = \pi$, gives flow over a cylinder situated in an infinite free stream which is flowing parallel to the x axis from negative to positive x, and

$$w(z) = -U(z + a^2/z) \qquad (2.2)$$

Since $w(z) = \phi + i\psi$, expanding equation (2.2) and solving for the imaginary part leads to the familiar expression for the stream function of this flow. (Appendix A1)

$$\psi = -Uy(1 - a^2/r^2)$$

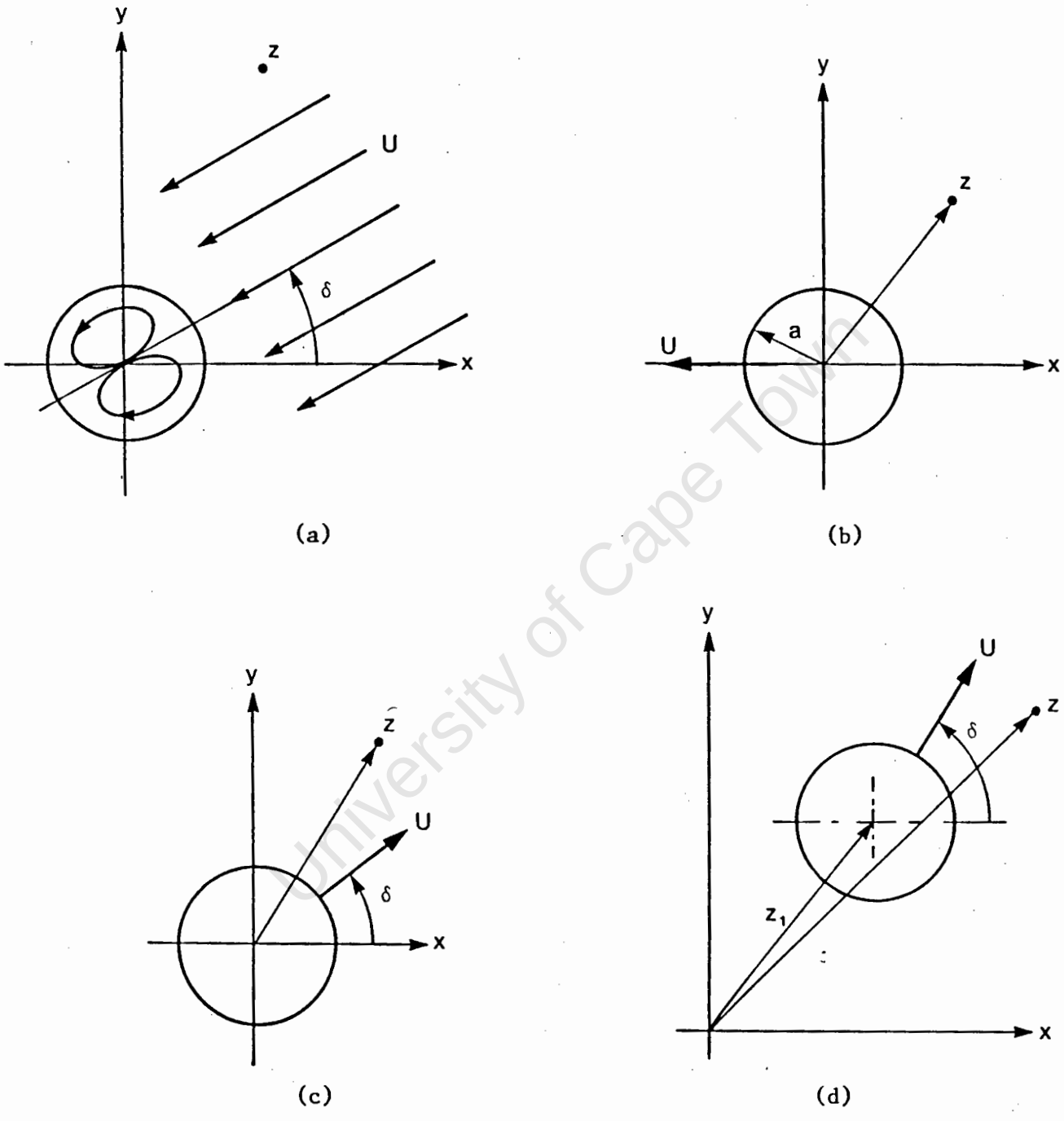




Fig. 2.1 Single cylinder lying in an infinite two dimensional steady state potential flow field

If the complex potential $w(z) = Uz$ is now superimposed on the flow field represented by equation (2.2), then equation (2.3) is obtained,

$$w(z) = -Ua^2/z \qquad (2.3)$$

which is the complex potential for a doublet of strength $Ua^2$ with its axis lying in the negative x direction. This represents the cylinder moving through the fluid in the negative x direction with velocity U, the fluid itself being at rest at infinity as shown in Fig. 2.1b. Now the complex potential for the doublet with its axis inclined at angle $\delta$ to the positive x axis is

$$w(z) = Ua^2 e^{i\delta}/z \qquad (2.4)$$

from which it is evident that with $\delta = \pi$, equation (2.3) is obtained. Thus equation (2.4) describes the motion of the cylinder moving with velocity U at an angle $\delta$ to the x axis, and is shown in Fig. 2.1c.

Finally, for a cylinder placed arbitrarily in the flow field, equation (2.4) becomes

$$w(z) = Ua^2 e^{i\delta}/(z-z_1) \qquad (2.5)$$

where $z_1$ is the complex co-ordinate of the centre of the cylinder as illustrated in Fig. 2.1d.

## 2.3 TRANSLATING MULTIPLE CYLINDERS

Fig. 2.2 shows three cylinders moving in an infinite two-dimensional potential flow field with their respective velocities and directions of motion. When far apart, they behave as if they were single cylinders, their complex potentials for a moving doublet being given by equation (2.5). As their separation decreases, the flow patterns formed by the moving doublets give rise to normal velocities on the cylindrical streamlines representing the surfaces of the cylinders at $r = a$, thereby causing these cylindrical streamlines to deform. Each cylinder will act upon the others in the group in a similar way and a mechanism is therefore required which will restore the deformed cylinder surfaces to their original circular shape.

## 2.4 METHOD OF IMAGES FOR TWO CYLINDERS

Cylinder 1 in Fig. 2.3 has its centre at $z_1$. Its surface streamline, at $r = a_1$, is distorted by an adjacent cylinder denoted by the limit of a sink at A and a source at B which when brought together form a doublet whose axis is at angle $\delta$. If an image of this doublet is now formed in cylinder 1, this has the effect of restoring the distorted circular streamline to its original radius $a_1$. However, this first image now distorts the circular streamline of cylinder 2 and so an image of the image in cylinder 1, must be created in cylinder 2 to restore its circular streamline, which in turn again distorts the surface of cylinder 1, requiring yet another image to correct it, and so on. This image doublet formation is carried

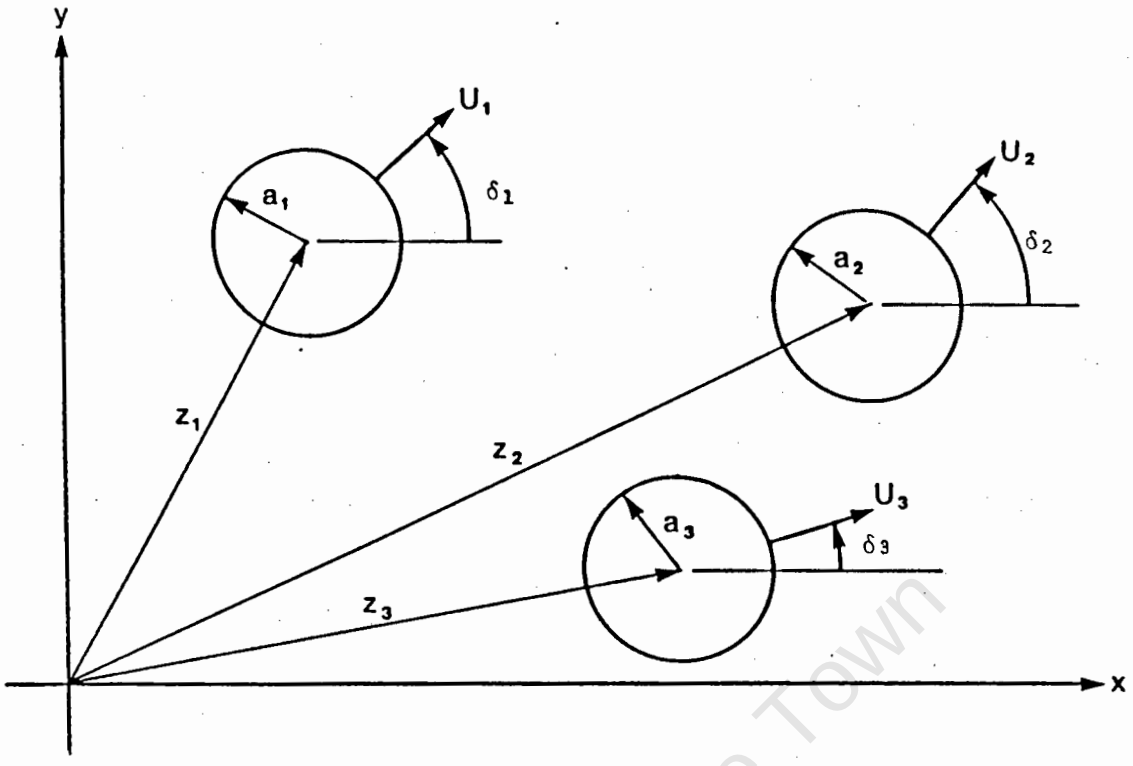


Fig. 2.2 Three cylinders moving randomly through a two dimensional potential flow field

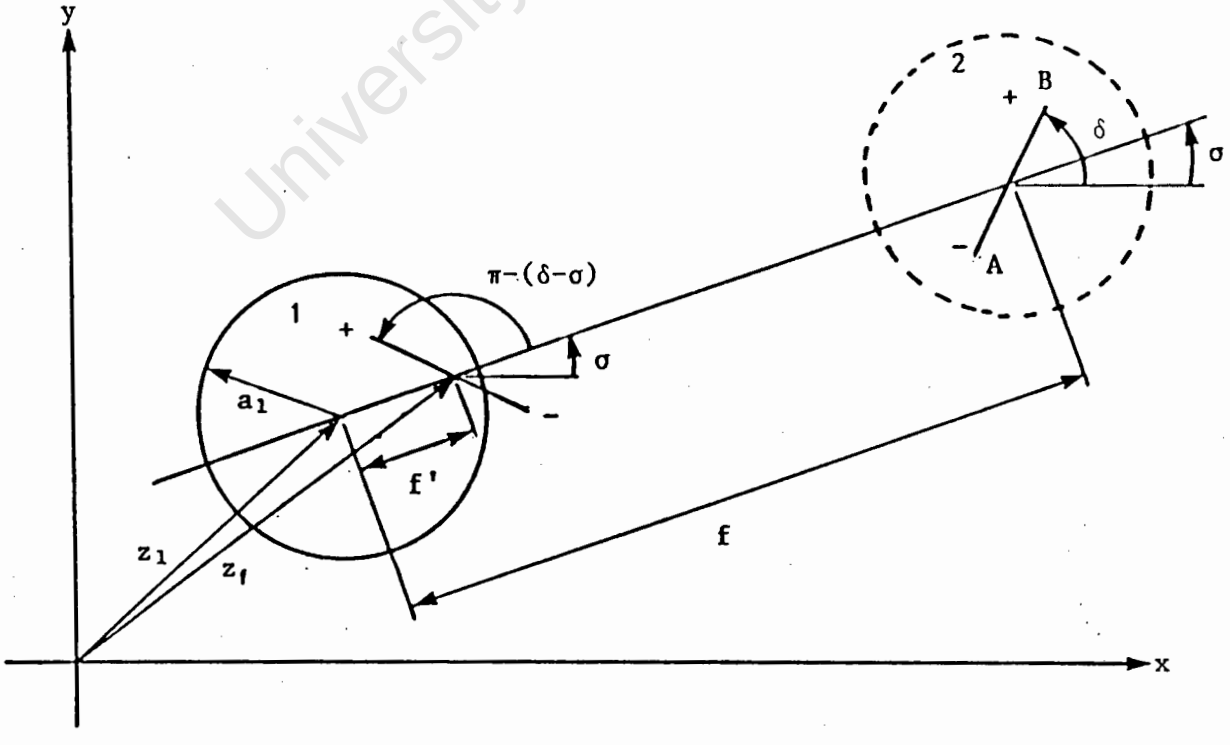


Fig. 2.3 The image of a doublet in a cylinder of radius a

on until an infinite number of doublets and their respective images are formed. The same procedure is followed to correct the distortion of the streamlines of cylinder 2 caused by the doublet originally forming cylinder 1.

It is shown by Milne-Thomson [22] that the image of a doublet of strength $\mu$ situated a distance f from the centre of a cylinder of radius a, and inclined at angle $(\delta-\sigma)$ to the line joining the cylinder centre to the doublet, is a doublet of strength $\mu'$ where

$$\mu' = \mu a^2/f^2 \qquad (2.6)$$

The image doublet is situated at the inverse point, with its axis inclined at angle $(\pi-(\delta-\sigma))$ as shown in Fig. 2.3. The inverse point is at a distance f' from the centre of the cylinder, and is given by

$$f' = a^2/f \qquad (2.7)$$

Thus the complex potential of the image doublet shown in Fig. 2.3 is

$$w(z) = Ua^2(a/|f|)^2(\exp(i(\pi-(\delta-\sigma)+\sigma)))/(z-z_1) \qquad (2.8)$$

where the vector $z_1$ denotes the location of the image doublet and $\sigma$ is the angle subtended by the line connecting the causing doublet and its image.

## 2.5 THREE TRANSLATING CYLINDERS

Consider now Fig. 2.4a where three cylinders of radii $a_1$, $a_2$ and $a_3$ are moving with velocities $U_1, U_2, U_3$ through an infinite stationary fluid in directions $\delta_1, \delta_2, \delta_3$ to the x axis. Each cylinder interferes with the others to distort the circular streamlines. To restore the circular streamlines of cylinders 2 and 3, an image of cylinder 1 must be generated in them at the appropriate inverse points. Similarly, images of the doublets forming cylinders 2 and 3 must be generated in cylinders 1 and 3, and 1 and 2 respectively. The succeeding images of images which then need to be generated are shown in Fig. 2.4b in branch form. The initial doublets which form the moving cylinders are numbered 1 to 3. The first order of generated images are numbered 4 to 9, and each of them generates a further two images to give a total second order image count from 10 to 21, each order doubling the number of images in the previous order. The doublets are referenced by open numbers whilst the numbers in parenthesis refer to the cylinder in which the image doublet is generated.

The complex potentials for the doublets which form cylinders 1, 2 and 3 on their own are, from equation (2.5),

$$w_1 = U_1 a_1^2 (\exp i\delta_1)/(z-z_1) \qquad (a)$$

$$w_2 = U_2 a_2^2 (\exp i\delta_2)/(z-z_2) \qquad (b) \qquad (2.9)$$

$$w_3 = U_3 a_3^2 (\exp i\delta_3)/(z-z_3) \qquad (c)$$

The complex potential for the image of cylinder 1 in cylinder 2, (that is doublet number 4), is designated as follows. The complex potential of doublet number 4 in cylinder 2 is the

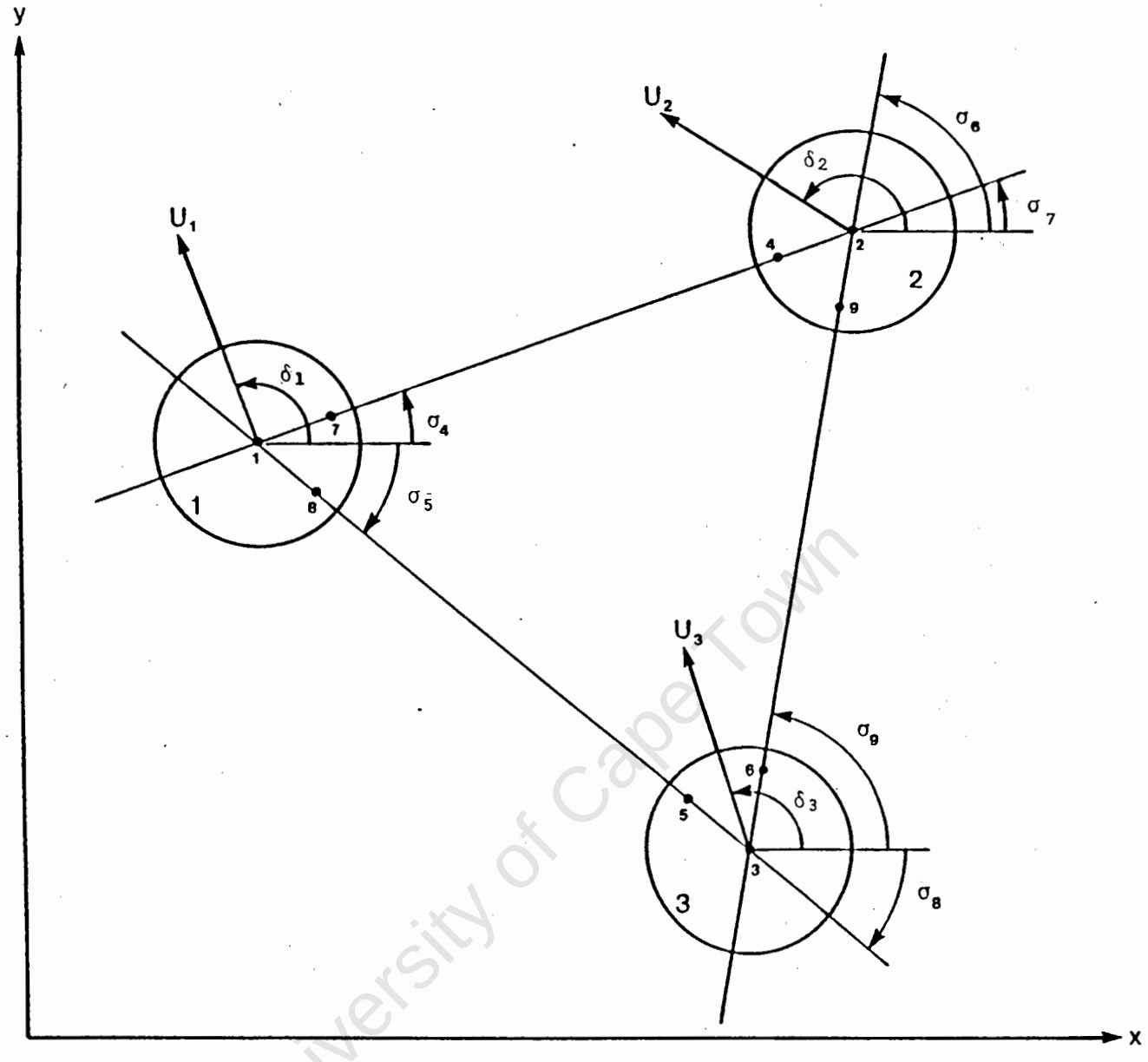


(a) System of image doublets for three translating cylinders

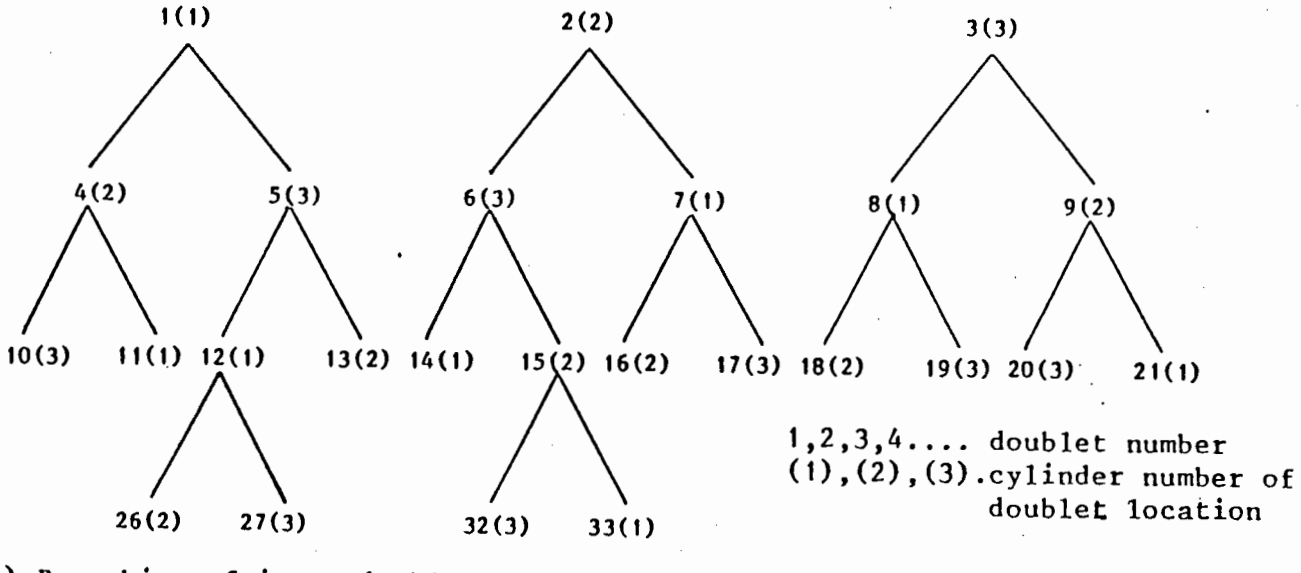


(b) Branching of image doublets

Fig. 2.4 Image doublets in three cylinders

image of doublet number 1 in cylinder 1. This and the complex potentials for doublets 5 to 9 are written, according to equation (2.8), as

$$w_4 = U_1 a_1^2 (a_2^2 / |z_1 - z_2|^2)(\exp i(\pi - (\delta_1 - \sigma_4) + \sigma_4))/(z - z_4) \quad (a)$$

$$w_5 = U_1 a_1^2 (a_3^2 / |z_1 - z_3|^2)(\exp i(\pi - (\delta_1 - \sigma_5) + \sigma_5))/(z - z_5) \quad (b)$$

$$w_6 = U_2 a_2^2 (a_3^2 / |z_2 - z_3|^2)(\exp i(\pi - (\delta_2 - \sigma_6) + \sigma_6))/(z - z_6) \quad (c) \qquad (2.10)$$

$$w_7 = U_2 a_2^2 (a_1^2 / |z_1 - z_2|^2)(\exp i(\pi - (\delta_2 - \sigma_7) + \sigma_7))/(z - z_7) \quad (d)$$

$$w_8 = U_3 a_3^2 (a_1^2 / |z_1 - z_3|^2)(\exp i(\pi - (\delta_3 - \sigma_8) + \sigma_8))/(z - z_8) \quad (e)$$

$$w_9 = U_3 a_3^2 (a_2^2 / |z_2 - z_3|^2)(\exp i(\pi - (\delta_3 - \sigma_9) + \sigma_9))/(z - z_9) \quad (f)$$

Proceeding to the second order images (doublets numbered 10 to 21), doublet number 10 in cylinder 3 is the image of doublet number 4 in cylinder 2 and the complex potential is

$$w_{10} = \mu_4 (a_3^2 / |z_3 - z_2|^2) \ldots\ldots$$
$$\ldots (\exp i((\pi - (\pi - (\delta_1 - \sigma_4) + \sigma_4 - \sigma_{12}) + \sigma_{12})))/(z - z_{12}) \quad (a)$$
$$\vdots \qquad\qquad \vdots \qquad (2.11)$$
$$w_{21} = \mu_9 (a_1^2 / |z_1 - z_2|^2) \ldots\ldots$$
$$\ldots (\exp i((\pi - (\pi - (\delta_3 - \sigma_9) + \sigma_9 - \sigma_{21}) + \sigma_{21})))/(z - z_{21}) \quad (l)$$

where, from equations (2.10a) and (2.10f)

$$\mu_4 = U_1 a_1^2 (a_2^2 / |z_1 - z_2|^2) \text{ and } \mu_9 = U_3 a_3 (a_2^2 / |z_2 - z_3|^2)$$

If the p'th doublet in the q'th cylinder is the image of the r'th doublet in the s'th cylinder, then for any order of images, Table 2.1 may be set up showing the unique relationships that exists between the doublets and their images. This enables general equations to be written in place of the rather long and tedious equations (2.9) to (2.11).

| Doublet p | in cylinder q | is image of doublet r | in cylinder s | |
|---|---|---|---|---|
| 1 | 1 | – | – | originating doublets |
| 2 | 2 | – | – | |
| 3 | 3 | – | – | |
| 4 | 2 | 1 | 1 | 1st order images |
| 5 | 3 | 1 | 1 | |
| 6 | 3 | 2 | 2 | |
| 7 | 1 | 2 | 2 | |
| 8 | 1 | 3 | 3 | |
| 9 | 2 | 3 | 3 | |
| 10 | 3 | 4 | 2 | 2nd order images |
| 11 | 1 | 4 | 2 | |
| 12 | 1 | 5 | 3 | |
| 13 | 2 | 5 | 3 | |
| 14 | 1 | 6 | 3 | |
| 15 | 2 | 6 | 3 | |
| 16 | 2 | 7 | 1 | |
| 17 | 3 | 7 | 1 | |
| 18 | 2 | 8 | 1 | |
| 19 | 3 | 8 | 1 | |
| 20 | 3 | 9 | 2 | |
| 21 | 1 | 9 | 2 | |
| 22 | 1 | 10 | 3 | |
| 23 | 2 | 10 | 3 | |
| 24 | 2 | 11 | 1 | |
| 25 | 3 | 11 | 1 | |
| 26 | 2 | 12 | 1 | |
| 27 | 3 | 12 | 1 | |
| . | . | . | . | |
| . | . | . | . | |
| . | . | . | . | |
| . | . | . | . | |
| 381 | 3 | 189 | 1 | |

Table 2.1 Relationship between doublets and cylinders for three equispaced cylinders

## 2.6 GENERAL COMPLEX POTENTIALS FOR IMAGE DOUBLETS

From equations (2.10) and (2.11) a general equation for the complex potential of any doublet may be written as

$$w_p = \mu_p (\exp i\lambda_p)/(z-z_p) \qquad (2.12)$$

Using the appropriate values of p,q,r and s in Table 2.1, these can be substituted in place of the numbered subscripts in the doublet equations to yield general expressions for $\mu_p$, $\lambda_p$ and $z_p$, as follows.

For $p \leq n$ where n is the number of cylinders, equations (2.9) become

$$\left.\begin{aligned} \mu_p &= U_q a_q^2 && (2.13)\\ \lambda_p &= \delta_q && (2.14)\\ z_p &= z_q && (2.15) \end{aligned}\right\} \; p \leq n$$

For $p > n$ the general expressions are deduced by considering doublet number 4. From Fig. 2.4,

$$z_4 = z_2 - \overline{OA} \qquad (2.16)$$

where $|OA| = f'$.

But from Appendix A2, vector $\overline{OA}$ can be written in complex conjugate form as

$$\overline{OA} = a^2/(\overline{z_A - z_B})$$

and substituting for A = 2 and B = 1, equation (2.16) becomes

$$z_4 = z_2 - a_2^2/(\overline{z_2 - z_1}) \qquad (2.17)$$

From Table 2.1, when p = 4, then q = 2 and r = 1, hence substituting in equation (2.17) for the numbered subscripts,

$$z_p = z_q + a_q^2/(\overline{z_r - z_q})$$

Putting $\Omega_p = z_r - z_q \qquad (2.18)$

then $z_p = z_q + a_q^2/\overline{\Omega}_p \qquad (2.19)$

The strength of the doublet in equation (2.10a) can likewise be written as

$$\begin{aligned} \mu_p &= U_r a_r^2 (a_q^2 / |\Omega_p|^2) \\ &= \mu_r a_q^2 / |\Omega_p|^2 \end{aligned} \qquad (2.20)$$

Again, from equations (2.10a) and (2.12),

$$\begin{aligned} \lambda_4 &= \pi - (\delta_1 - \sigma_4) + \sigma_4 \\ \lambda_p &= \pi - \delta_r + 2\sigma_p \end{aligned} \qquad (2.21)$$

But from Fig. 2.4,

$$\begin{aligned} \sigma_4 &= \tan^{-1}[I(z_2 - z_1)/R(z_2 - z_1)] \\ &= \tan^{-1}[I(z_1 - z_2)/R(z_1 - z_2)] \end{aligned}$$

and substituting for p,q,r and s for doublet 4,

$$\sigma_p = \tan^{-1}[I(z_r - z_q)/R(z_r - z_q)]$$
$$= \tan^{-1}[I(\Omega_p)/R(\Omega_p)] \qquad (2.22)$$

Using equations (2.12) to (2.22), the complex potential for any doublet may be determined provided that the unique relationship between p,q,r and s in Table 2.1 is upheld.

The complex potential for the whole field is obtained by summing the complex potentials of each doublet, so that

$$w(z) = \sum_{p=1}^{m} w_p(z) \qquad (2.23)$$

It is stressed that equation (2.23) is the complex potential for the three cylinders moving randomly in an infinite stationary flow field whereas the problem of interest is that of flow over stationary cylinders lying in a uniform flow field. Modifications to achieve this must therefore be made to equation (2.23) and are addressed in the next section.

The foregoing analysis may be used for any number of cylinders providing the line joining any doublet and its image is not blocked by another doublet. The accuracy of the analysis will improve as the number of images increases but it is shown in section 3.6 for the cases considered in this thesis, that after the third or fourth order of images, there is very little to be gained by considering further orders. Fig. 2.5 shows the cylinders and doublet images for four cylinders whilst Table 2.2 gives the relationships between p,q,r and s

for four cylinders.

## 2.7 STATIONARY CYLINDERS IN A UNIFORM FLOW FIELD

To model the potential flow field for stationary cylinders lying in a uniform flow field, each cylinder is first made to move in the opposite direction to the free stream. The free stream velocity is then superimposed upon the flow field of the moving cylinders thereby bringing them to rest whilst the free stream flows around them.

If the free stream is parallel to the x axis and flows in the positive x direction, then adding the complex potential for the free stream to equation (2.23) gives,

$$w(z) = -Uz + \sum_{p=1}^{m} w_p(z) \qquad (2.24)$$

where m is the total number of doublets. In equation (2.24), $\delta_1$, $\delta_2$, $\delta_3$ in the doublet summation term, are put equal to $\pi$, that is they directly oppose the added free stream velocity. If the free stream velocity were at some general angle $\delta$, equation (2.24) would be written as

$$w(z) = Uze^{-i\delta} + \sum_{p=1}^{m} w_p(z) \qquad (2.25)$$

Now $V(z) = -d(w(z))/dz = u - iv$

where V(z) is the complex velocity of any point in the flow field and u and v are the real and imaginary parts of V(z). Thus differentiating equation (2.25) gives

$$V(z) = -Ue^{-i\delta} + \sum_{p=1}^{m} (-d(w_p(z))/dz)$$

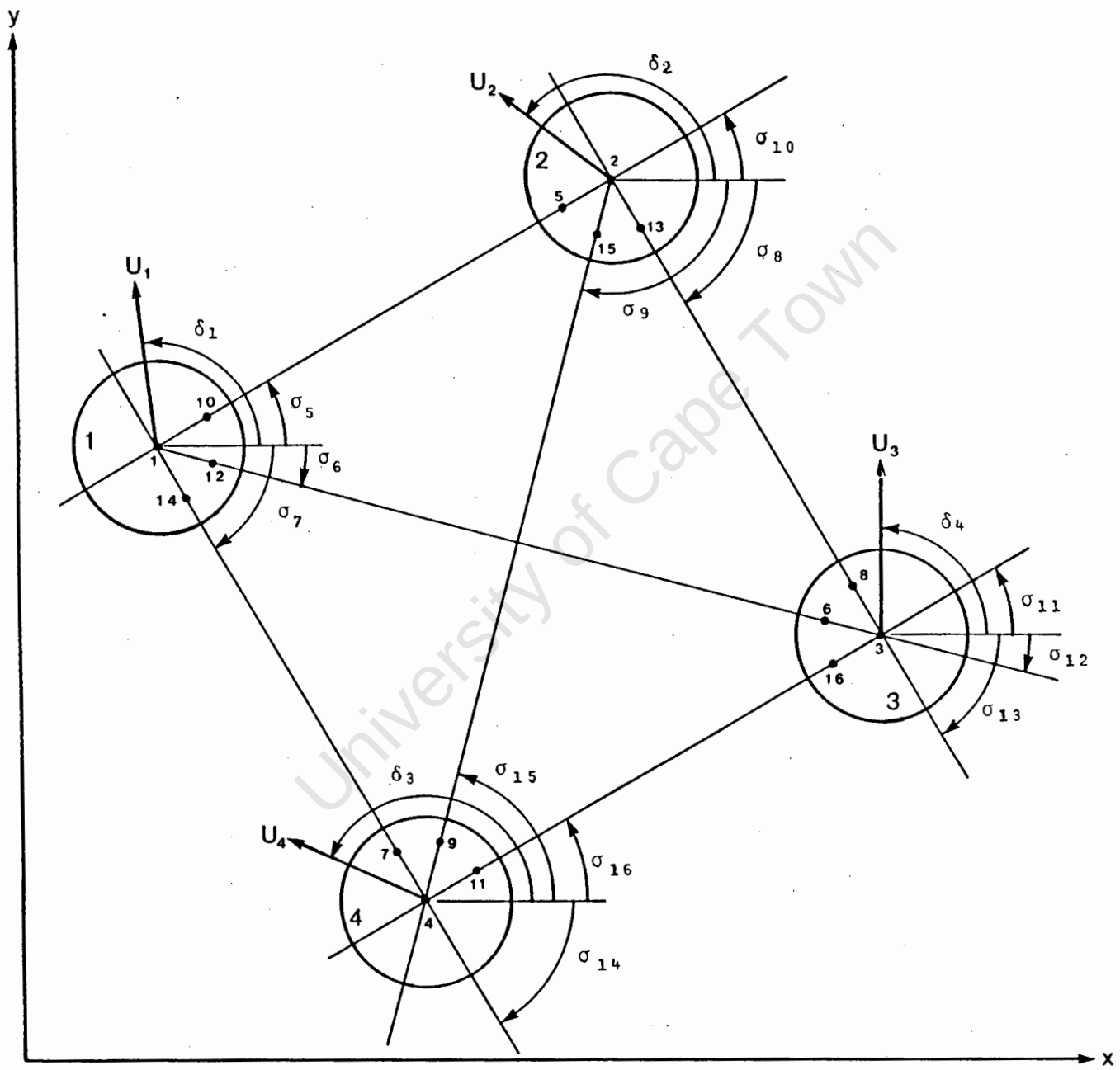




Fig. 2.5 System of image doublets for four translating cylinders

| Doublet p | in cylinder q | is image of doublet r | in cylinder s | |
|---|---|---|---|---|
| 1 | 1 | - | - | originating doublets |
| 2 | 2 | - | - | |
| 3 | 3 | - | - | |
| 4 | 4 | - | - | |
| 5 | 2 | 1 | 1 | 1st order images |
| 6 | 3 | 1 | 1 | |
| 7 | 4 | 1 | 1 | |
| 8 | 3 | 2 | 2 | |
| 9 | 4 | 2 | 2 | |
| 10 | 1 | 2 | 2 | |
| 11 | 4 | 3 | 3 | |
| 12 | 1 | 3 | 3 | |
| 13 | 2 | 3 | 3 | |
| 14 | 1 | 4 | 4 | |
| 15 | 2 | 4 | 4 | |
| 16 | 3 | 4 | 4 | |
| 17 | 3 | 5 | 2 | 2nd order images |
| 18 | 4 | 5 | 2 | |
| 19 | 1 | 5 | 2 | |
| 20 | 4 | 6 | 3 | |
| 21 | 1 | 6 | 3 | |
| 22 | 2 | 6 | 3 | |
| 23 | 1 | 7 | 4 | |
| 24 | 2 | 7 | 4 | |
| 25 | 3 | 7 | 4 | |
| 26 | 4 | 8 | 3 | |
| 27 | 1 | 8 | 3 | |
| 28 | 2 | 8 | 3 | |
| 29 | 1 | 9 | 4 | |
| 30 | 2 | 9 | 4 | |
| 31 | 3 | 9 | 4 | |
| 32 | 2 | 10 | 1 | |
| 33 | 3 | 10 | 1 | |
| 34 | 4 | 10 | 1 | |
| 35 | 1 | 11 | 4 | |
| 36 | 2 | 11 | 4 | |
| 37 | 3 | 11 | 4 | |
| 38 | 2 | 12 | 1 | |
| 39 | 3 | 12 | 1 | |
| 40 | 4 | 12 | 1 | |
| 41 | 3 | 13 | 2 | |
| 42 | 4 | 13 | 2 | |
| 43 | 1 | 13 | 2 | |
| 44 | 2 | 14 | 1 | |
| 45 | 3 | 14 | 1 | |
| 46 | 4 | 14 | 1 | |
| 47 | 3 | 15 | 2 | |
| 48 | 4 | 15 | 2 | |
| 49 | 1 | 15 | 2 | |
| 50 | 4 | 16 | 3 | |
| 51 | 1 | 16 | 3 | |
| 52 | 2 | 16 | 3 | |
| 53 | 4 | 17 | 3 | |
| . | . | . | . | |
| . | . | . | . | |
| . | . | . | . | |
| 484 | 4 | 160 | 1 | |

Table 2.2 Relationship between doublets and cylinders for four equispaced cylinders

$$= -Ue^{-i\delta} + \sum_{p=1}^{m} (\mu_p e^{i\lambda_p}/(z - z_p)^2) \qquad (2.26)$$

The absolute velocity is found by solving for the real and imaginary parts of equation (2.26), then

$$|V(z)| = (u^2 + v^2)^{1/2} \qquad (2.27)$$

The static pressure p at any point in the flow field can now be found from the Bernoulli equation

$$p - p_\infty = \rho(U^2 - |V(z)|^2)/2 \qquad (2.28)$$

where $p_\infty$ is the static pressure in the flow field at infinity.

## 2.8 LIFT AND DRAG FORCES ACTING ON THE CYLINDER

The force per unit length F acting on the cylinder shown in Fig. 2.6 is the integral, around the surface of the cylinder, of the force due to the pressure difference in equation (2.28).

$$F = \int_0^{2\pi} (p - p_\infty) a d\theta \qquad (2.29)$$

where $ad\theta$ is an incremental length along the circumference. The lift and drag components are

$$L = -\int_0^{2\pi} (p - p_\infty) a \sin\theta d\theta \qquad (2.30)$$

and

$$D = -\int_0^{2\pi} (p - p_\infty) a \cos\theta d\theta \qquad (2.31)$$

which two equations are evaluated by numerical integration, in this case Simpson's Rule. Dividing equations (2.30) and (2.31) by $0.5\rho U^2 D$, where D is the cylinder diameter, yields the lift and drag coefficients

$$C_L = -\int_0^{2\pi} (p - p_\infty) a \sin\theta \, d\theta / 0.5\rho U^2 D \qquad (2.32)$$

and

$$C_D = -\int_0^{2\pi} (p - p_\infty) a \cos\theta \, d\theta / 0.5\rho U^2 D \qquad (2.33)$$

Substitution for $(p - p_\infty)$ from equation (2.28) may be made when determining the theoretical coefficients, but when the pressure difference is determined experimentally, equations (2.32) and (2.33) are used directly.

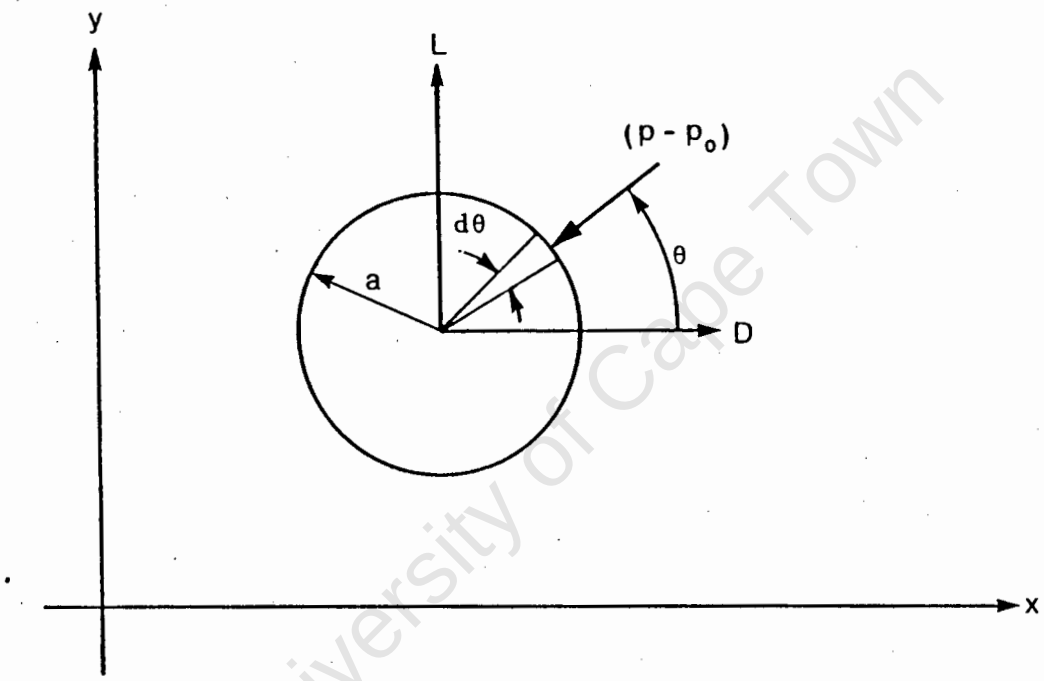


Fig. 2.6 Forces acting on a cylinder

# CHAPTER 3

# THEORETICAL LIFT AND DRAG COEFFICIENTS

## 3.1 INTRODUCTION

The solutions of the equations developed in chapter 2 were carried out on a 640K IBM Personal Computer. The programmes to effect solution are written in Fortran 77 using the packages WATFOR77 and WATFOR87. The former package was used in the development and editing phases of the programmes whilst the latter was used to run the final programme on the IBM P.C. However, the use of Watfor87 requires the P.C. to be fitted with an 8087 math coprocessor. If this is not installed, the time taken to run a group of cylinders with a large number of spacings at different orientations to the free stream was prohibitively long making it necessary to run the programme on a faster (main frame) computer.

The programmes calculate the theoretical potential lift and drag coefficients on any cylinder in a group of three or four equispaced cylinders. From the theoretical results, graphs of lift and drag coefficient on a cylinder are plotted for different orientations of the group to the free stream at their respective centre spacings.

## 3.2 PROGRAMME LISTINGS

The programmes developed for evaluating the potential lift and drag coefficients on a cylinder in a group of three or four equispaced cylinders are titled:

a) TEMO1.FOR - for 3 cylinders

b) FTEST.FOR - for 4 cylinders

In TEMO1.FOR, the three cylinders are equispaced as shown in Fig. 3.1a. Rotation of the group takes place about the centre of cylinder 1 in steps of 7.5 degrees from $\beta$ = 30 to -90 degrees. When $\beta$ is 30, -30 and -90 degrees, two of the cylinders are vertically in line and the angle of the line joining the centres of those cylinders is then 90 degrees measured from the positive x axis. The arctangent of 90 degrees required in equation (2.22) returns the value of infinity thereby causing the programme to terminate. An adjustment to $\beta$ of the order of 0.05 degrees is made to offset the two in line cylinders in these positions.

In FTEST.FOR, the cylinders are arranged in a square formation as in Fig. 3.1b, provision for the vertically in line cases being made when $\beta$ is 45, 0, -45 or -90 degrees.

The complex velocity is calculated at angle $\theta$ on the surface of each cylinder for a given increment of $\beta$. The angle $\theta$ is incremented in 7.5 degree intervals from 0 to $2\pi$ radians. The lift and drag coefficients are then calculated from the summation of the velocity components in the appropriate directions according to equations (2.32) and (2.33).

The structure of each programme follows the flow chart shown in Fig. 3.2. The programmes are listed in Appendix B1, along with explanatory notes on the structure of TEMO1.FOR.

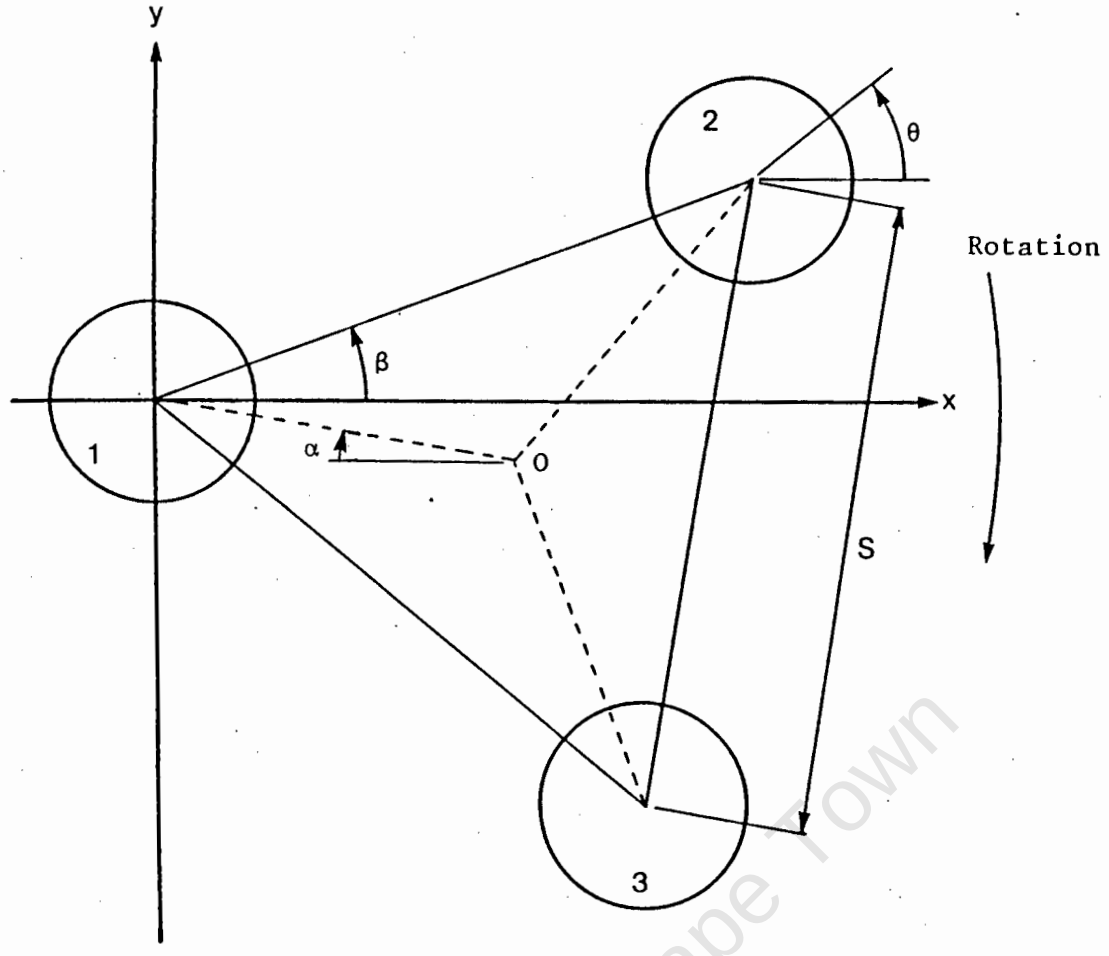


(a) Rotation of cylinders 2 and 3 about centre of cylinder 1 in TEMO.FOR

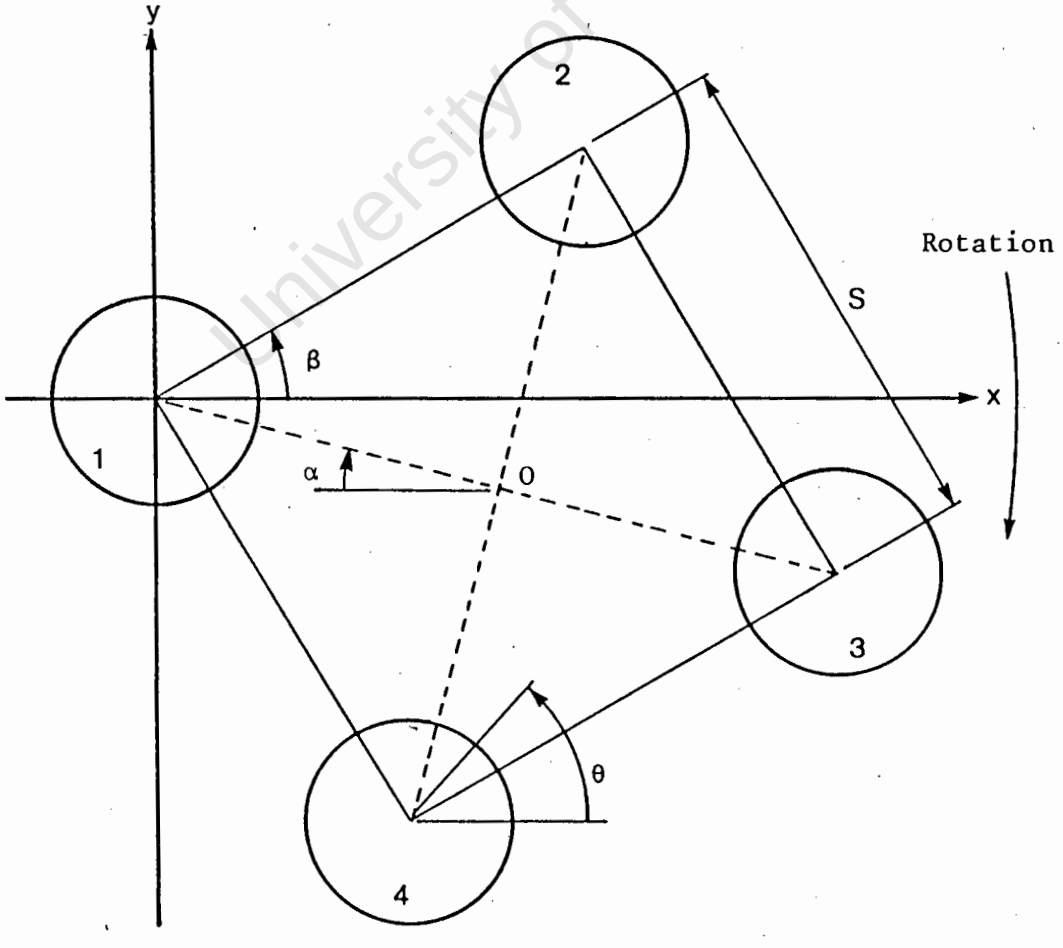


(b) Rotation of cylinders 2,3 and 4 about centre of cylinder 1 in FTEST.FOR

Fig. 3.1 Rotation of cylinder groups in TEMO.FOR and FTEST.FOR

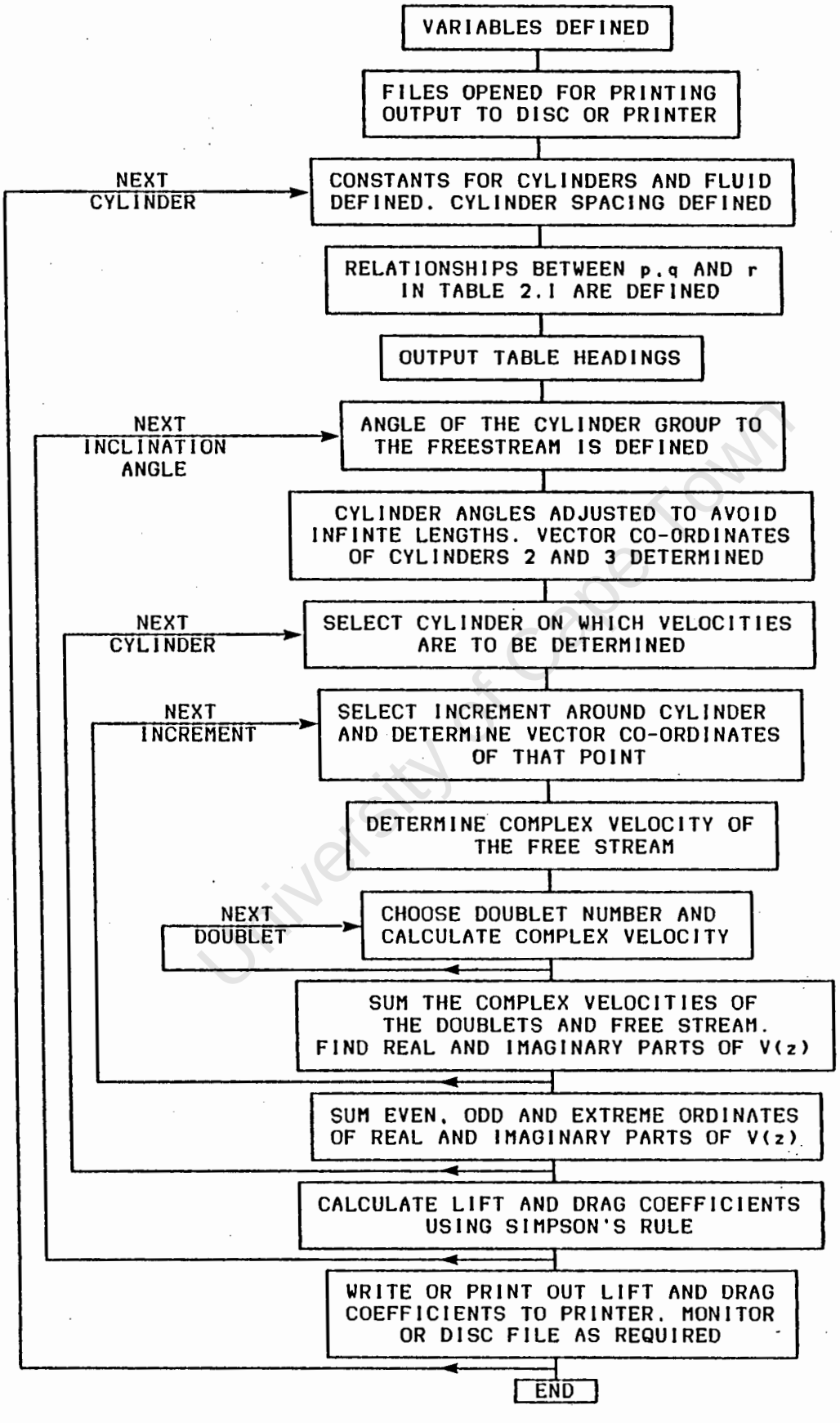


Fig. 3.2 Flow chart for computer programme TEMO1.FOR

## 3.3 POTENTIAL DRAG ON THREE CYLINDERS

The cylinder spacing was first set at the comparatively large value of S/D = 25, when the velocity distribution and force coefficients for each cylinder were obtained. Tables 3.1 and 3.2 show the results for an inclination angle of 7.5 degrees. In these tables and the graphs which follow, the inclination angle is the angle of orientation of the group of cylinders to the free stream as if the group rotated about the point O in Fig. 3.1. Thus when $\beta$ is 30 degrees in the computer programme, this corresponds to a group inclination angle, $\alpha$, of zero degrees, and when $\beta$ is zero (rotating clockwise) the group inclination angle is 30 degrees. This nomenclature is reverted to since the experimental cylinder orientation is about the fixed point O. The velocity distributions around each cylinder are seen to be the same and were repeated at all other angles of inclination. The exact solution for the velocity on the surface of a single cylinder in a potential flow field is also given in Table 3.1 with which, for selected values of $\theta$, the velocities obtained by the doublet image method compare very favourably. In Table 3.2, the drag and lift coefficients are zero (except for some rounding off) as would be expected from a numerical solution. It is therefore concluded that the programme is returning the correct results and that at large spacings each cylinder in the group is behaving as a single and isolated one.

The potential drag at three cylinder spacings, over 180 degrees of rotation, is shown in Fig. 3.3, the corresponding data being displayed in Appendix B2. At inclination angles between 120 and 180 degrees, the force coefficients for

cylinder 1, say, are the same as those on cylinder 2 for the range of inclination angles between 0 and 60 degrees. The error between the drag coefficient for cylinder 1 at 120 degrees and cylinder 2 at 0 degrees is of the order of two percent which considering the numerical techniques used, is most satisfactory. The summation of the drag coefficients on the three cylinders is seen to be zero to within a one or two percent margin of error which is to be expected since the total drag in the potential flow field should be zero, although on individual components within the field, finite values obtain. At $\alpha$ = 90 degrees, the flow pattern on each side of the y axis is symmetrical giving zero drag at all spacings.

The effect of cylinder spacing diminishes rapidly with increase in the spacing ratio, such that at a cylinder spacing of only 2.6, the maximum drag coefficient has a value of 0.006.

## 3.4 POTENTIAL LIFT ON THREE CYLINDERS

The lift coefficients for each cylinder at S/D = 25 are, from Table 3.2 seen to be zero, thus confirming the single cylinder flow regime around the cylinders at large spacing ratios.

Fig. 3.4 shows the lift coefficients corresponding to the drag coefficients of Fig. 3.3. This figure charts the variation in lift coefficient on cylinder 1 whilst the inclination angle changes from 0 to 180 degrees, and indicates that the lift force is directed inwards toward the centre of the group, the lift coefficient being zero at the 0 and 180 degree positions. At these two positions the flow pattern on either side of the x axis is symmetrical. In Table 3.2, although the

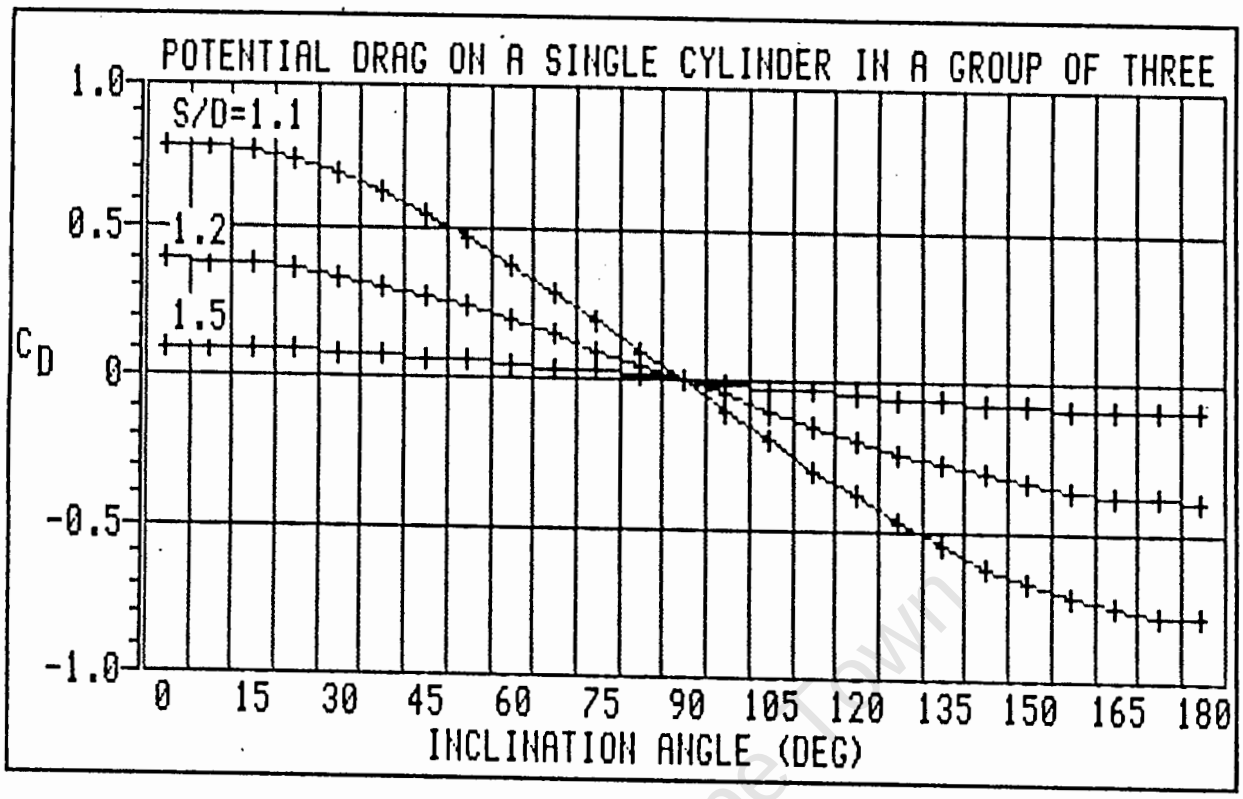


Fig. 3.3 Potential drag coefficient on cylinder 1 in the group of three cylinders versus group inclination angle α

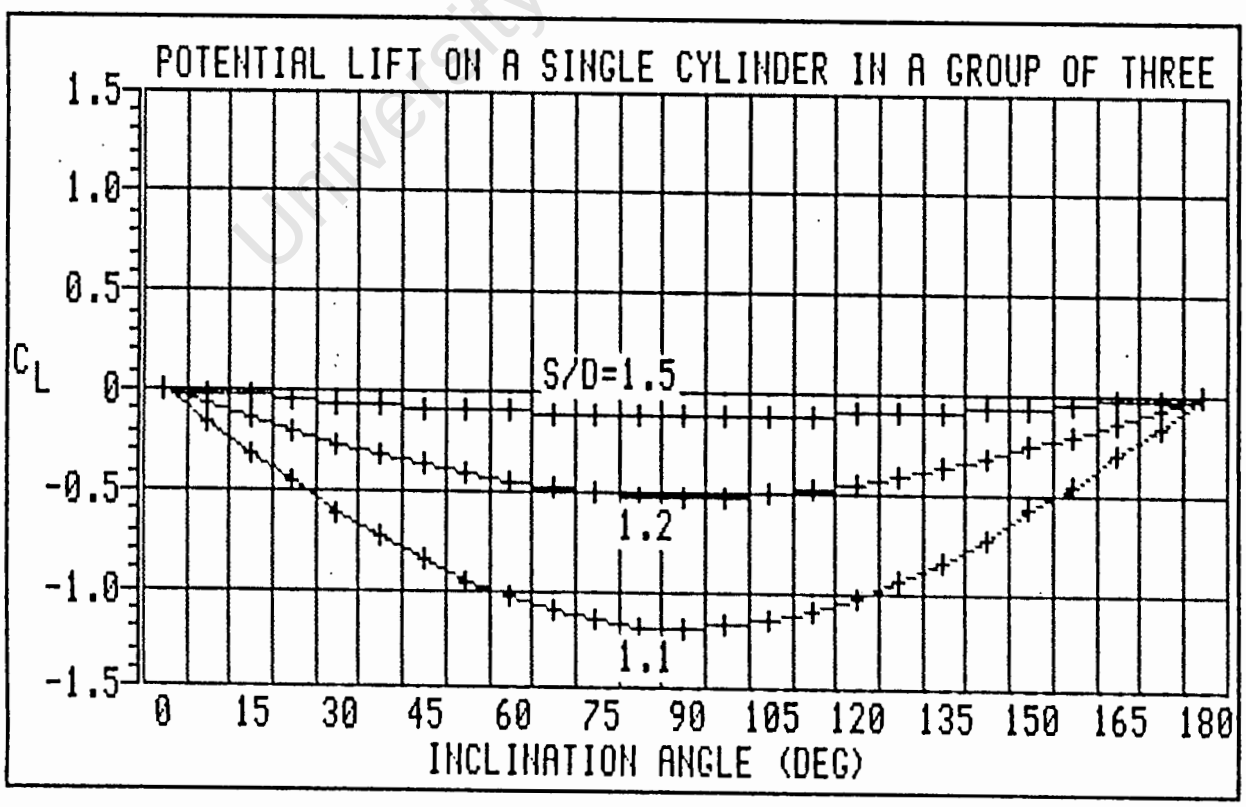


Fig. 3.4 Potential lift coefficient on cylinder 1 in the group of three cylinders versus group inclination angle α

individual cylinders in the potential flow field do experience a lift coefficient, the summation of those coefficients at any given inclination angle is seen to be zero. This is expected over the whole potential flow field and is further corrobaration that the potential flow programme is running correctly.

## 3.5 POTENTIAL LIFT AND DRAG ON FOUR CYLINDERS

The potential drag curves for four equispaced cylinders are illustrated in Fig. 3.5. They show that at zero inclination, the two vertically in line cylinders (2 and 4) have zero drag, whilst the horizontally in line upstream and downstream cylinders (1 and 3), have positive and negative drag coefficients respectively thereby being attracted towards each other due to the low pressure region lying between them. As the inclination angle of the group increases, the drag on cylinder 1 decreases and becomes negative at 37.5 degrees, the drag on cylinder 3 becomes positive at 217.5 degrees. Minimum and maximun drags are found at 60 and 120 degrees, the magnitudes of the drags increasing with decreasing spacing ratio.

The corresponding lift variation for a single cylinder in the group is shown in Fig. 3.6. Here, the lift coefficient is zero at inclination angles of 0 and 180 degrees, as would be expected due to the symmetry of the flow. At $\alpha$ = 90 degrees a positive lift coefficient is seen to occur and the data shows that the lift coefficient increases with decreasing S/D until the spacing ratio of 1.2 is reached, when $C_L$ decreases. The increasing lift coefficient is due to the velocity on the outer surface of cylinder 2 being, in general, higher than that in the gap between the cylinders, and this difference in

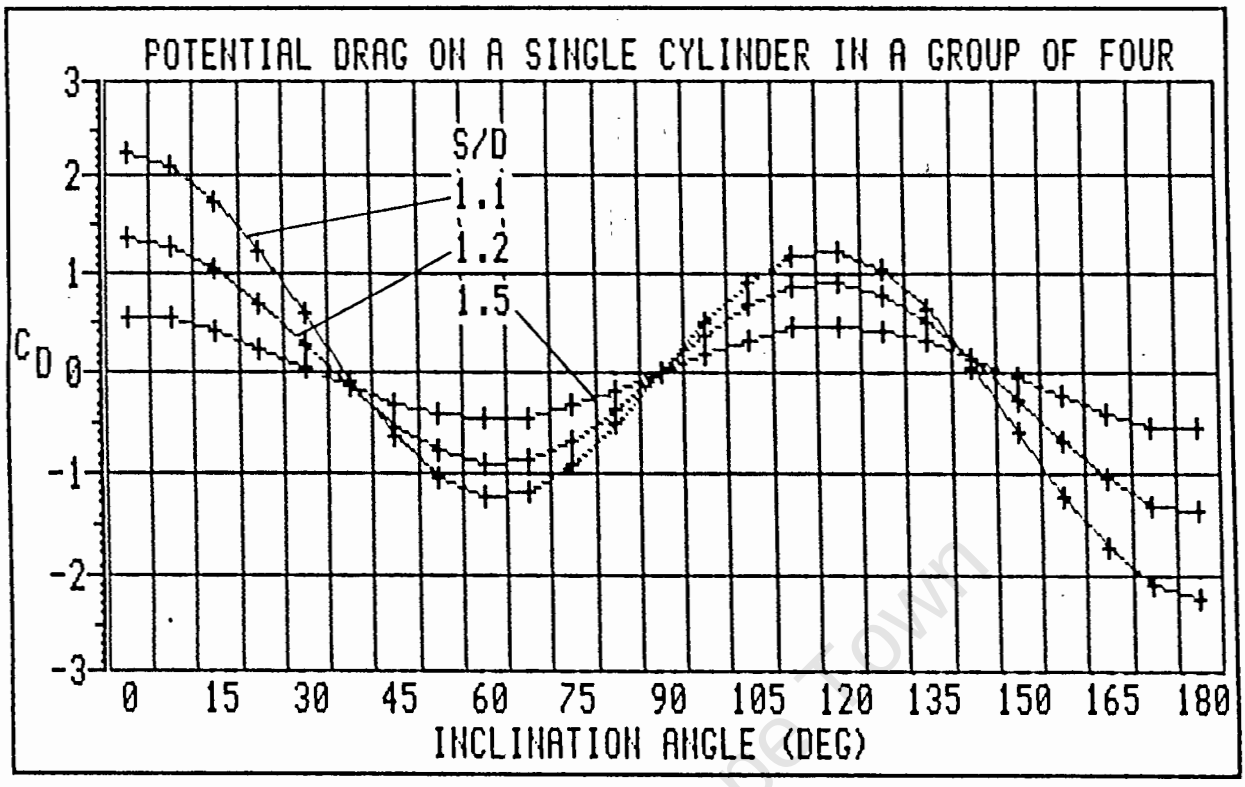


Fig. 3.5 Potential drag coefficient on cylinder 1 in the group of four cylinders versus group inclination angle α

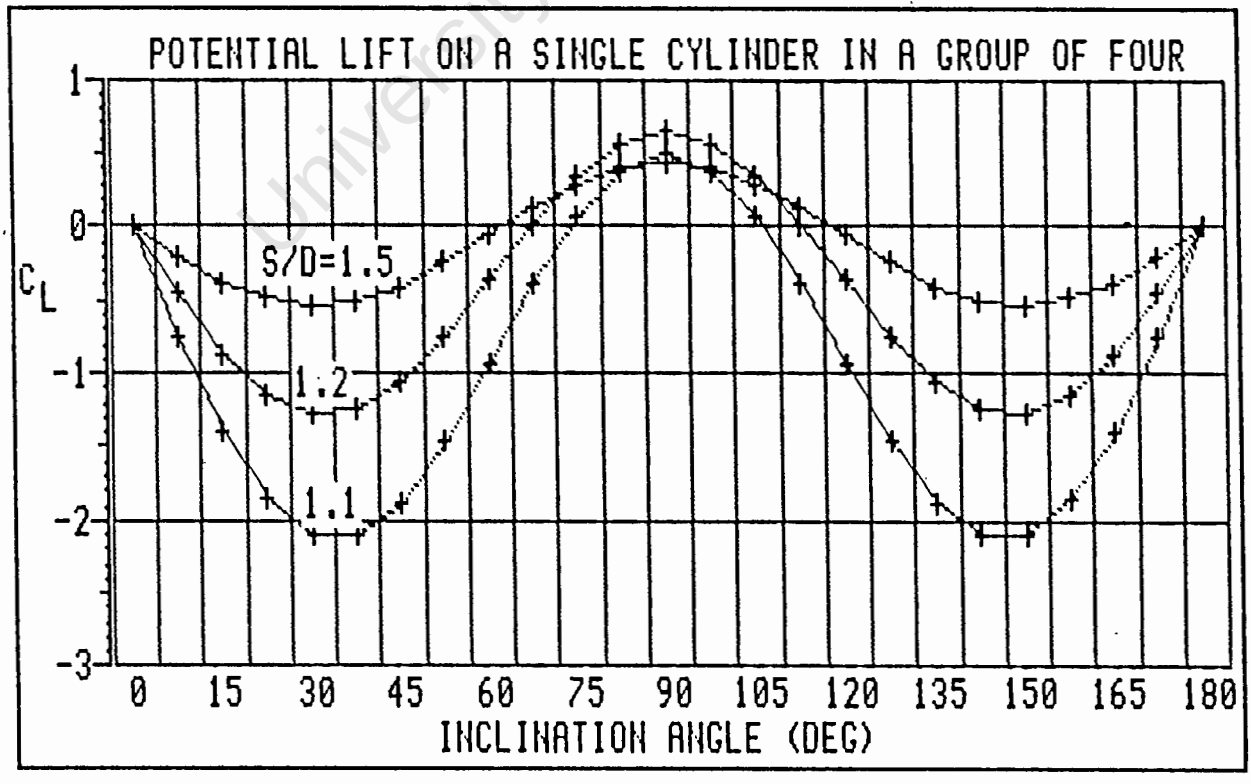


Fig. 3.6 Potential lift coefficient on cylinder 1 in the group of four cylinders versus group inclination angle α

velocities increases as the cylinders approach each other. At a spacing ratio of approximately 1.2, the cylinders are so close that the rate of increase of the gap velocity exceeds that over the outer surface of cylinder 2, and the lift coefficient starts to decrease. Fig. 3.7a traces the increase and subsequent decrease in lift coefficient on cylinder 1 at the 90 degree inclination angle, when the spacing ratio is decreased. Except at spacing ratios less than 1.05, cylinders 2 and 4 at an inclination angle of zero are attracted towards each other. Fig 3.7b describes the lift coefficient variation on cylinder 1 at the 45 degree inclination angle. Here it is seen that a negative lift coefficient pertains throughout with cylinders 1 and 4, and 3 and 2 being attracted towards each other.

## 3.6 EFFECT OF DOUBLET NUMBER

The greater the number of doublets used in the numerical solution of equation (2.24), so the smaller should be the error. It was also expected that the magnitude of the errors would increase as the cylinder spacing became smaller, so that to maintain a given constant error, (say that pertaining at an S/D ratio of 25), the number of doublets employed in the solution would need to be increased. This notion was investigated by examining the velocity distribution on the surface of two adjacent cylinders lying with their centres on the y axis.

The choice of two cylinders was made firstly because of the speed of execution of the modified computer programme for two cylinder flow, and secondly an exact solution for the velocity on the surface of a single cylinder in contact with a solid

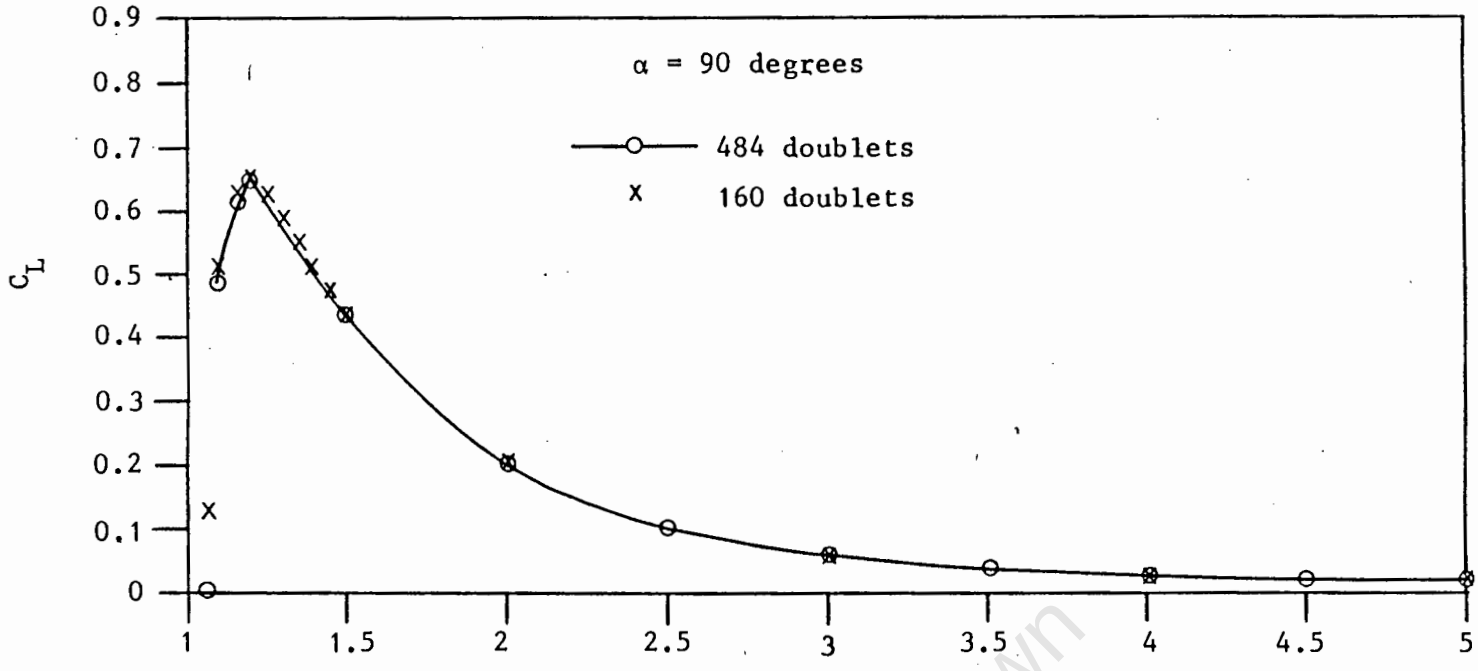


(a) α = 90 degrees

Spacing ratio (S/D)

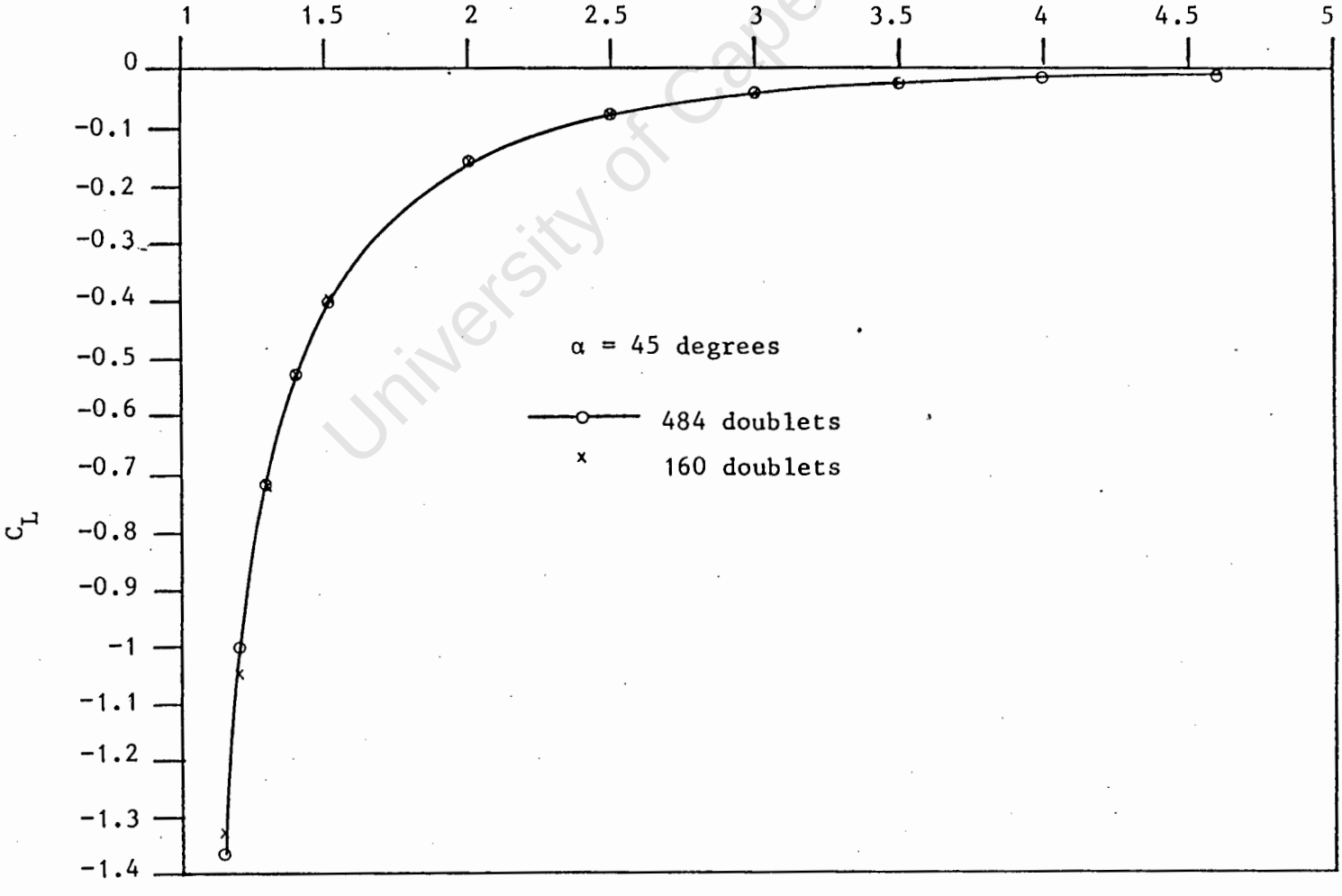


(b) α = 45 degrees

Fig. 3.7 Lift coefficient on cylinder 1 in a group of four at various spacing ratios

wall was developed from a complex potential given by Milne-Thomson [22] for that flow regime. This exact solution provided a basis with which to compare the values of velocity calculated in the numerical solution of equation (2.27). Equation (3.1) gives the exact solution for the magnitude of the velocity on the surface of the cylinder lying on the horizontal boundary shown in Fig. 3.8a and is developed in Appendix B3.

$$q = |V(z)| = |(a^2\pi^2 U/z^2)(1 + \cot^2(i\pi a/z))| \qquad (3.1)$$

The twin cylinder configuration of Fig. 3.8b will also solve the same problem since one of the streamlines between the two cylinders will be horizontal and may be taken as the horizontal solid boundary. The velocities generated on the surfaces of the cylinders using the method of doublet images are compared with those generated from equation (3.1) and are tabulated in Appendix B4.

Appendix B4 first shows the velocity distribution around cylinder 2 at S/D = 100, where the values are seen to be the same as those for the three cylinder grouping at S/D = 25 (Table 3.1). This verified the correct running of the modified three cylinder programme to a two cylinder programme. When the two cylinders were touching at S/D = 1, and with 24 and 48 doublets respectively, the image doublet method of solution departs drastically from the exact solution of equation (3.1) in the range $205.5 < \theta < 337.5$ degrees, otherwise the numerical solution returns values that lie within 13 per cent of the exact solution. At $\theta$ = 270 degrees, which is the point of contact of the cylinders, extremely high velocities are in

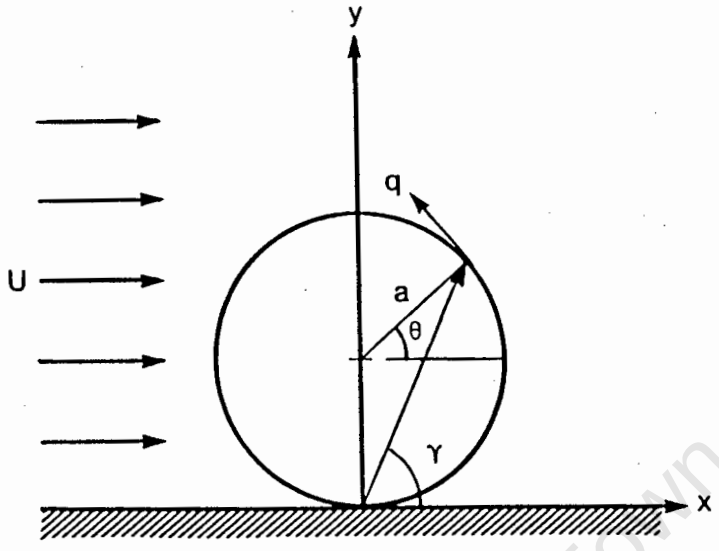


(a) Cylinder in contact with boundary

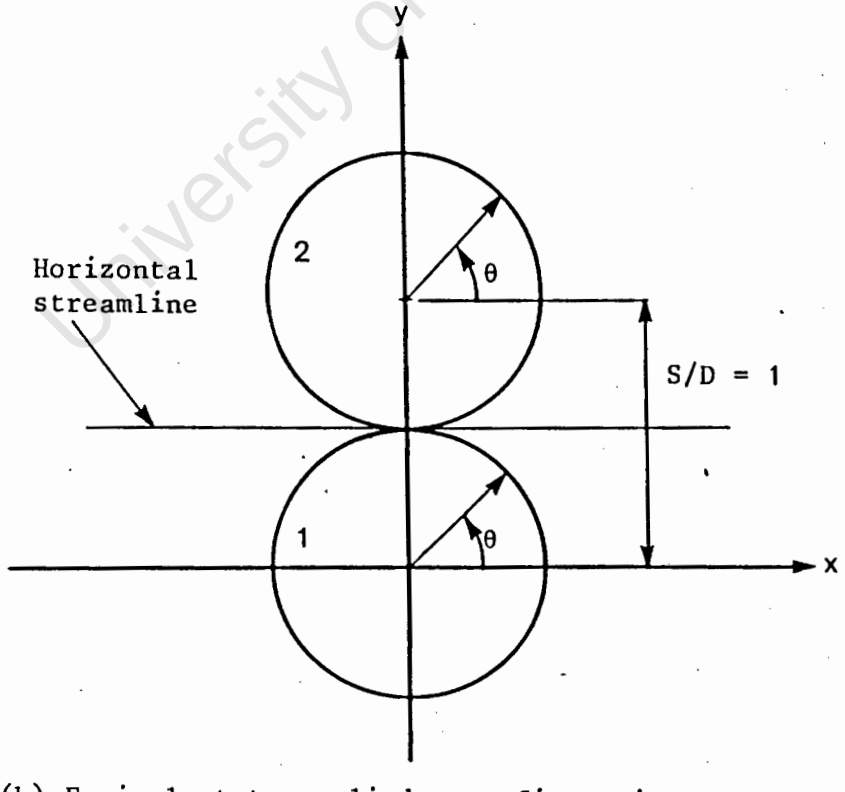


(b) Equivalent two cylinder configuration

Fig. 3.8 Potential flow over a cylinder in contact with a boundary

evidence which are clearly not feasible. The exact solution tends towards zero velocity at the point of contact and also for a range of angles on either side of the 270 degree contact point. Fig. 3.9 summarises the data of Appendix B4, and clearly shows the excessive error range.

The high velocities near the contact points of the two cylinders are due to distortion of the cylinder surfaces in this region. It must be remembered that although the centre spacing of the cylinders is set at 1, the surface distortion causes a small gap to exist through which the velocities are necessarily high. Increasing the number of doublets from 24 to 48 also increases the velocity, since although an increase in the number of doublets makes the cylinders more circular, the width of the gap in the near contact region decreases. An infinite number of doublets would give rise to an infinite velocity in the region of contact. Corrections were made by forcing values of zero velocity onto the surfaces of cylinders 1 and 2 in the error band range and these results are shown in the last column of Appendix B4, where the lift coefficient has the value 4.41 compared to 4.49 for the exact solution.

When two cylinders are spaced at S/D = 1.1 with 24 and 48 doublets, the lift coefficients for cylinder 2 were -3.6 (and 3.6 for cylinder 1) thus indicating that for two cylinders 24 doublets representing 11 orders of images were sufficient to solve the problem, there being no further gain in accuracy by increasing the number of doublets. At a spacing of S/D = 1.5 and using 12 and 48 doublets, lift coefficients of -0.65 were obtained on cylinder 2 in each case.

Considering the four cylinder grouping, the number of doublets was reduced to 160 (3 orders of images) and Fig. 3.7

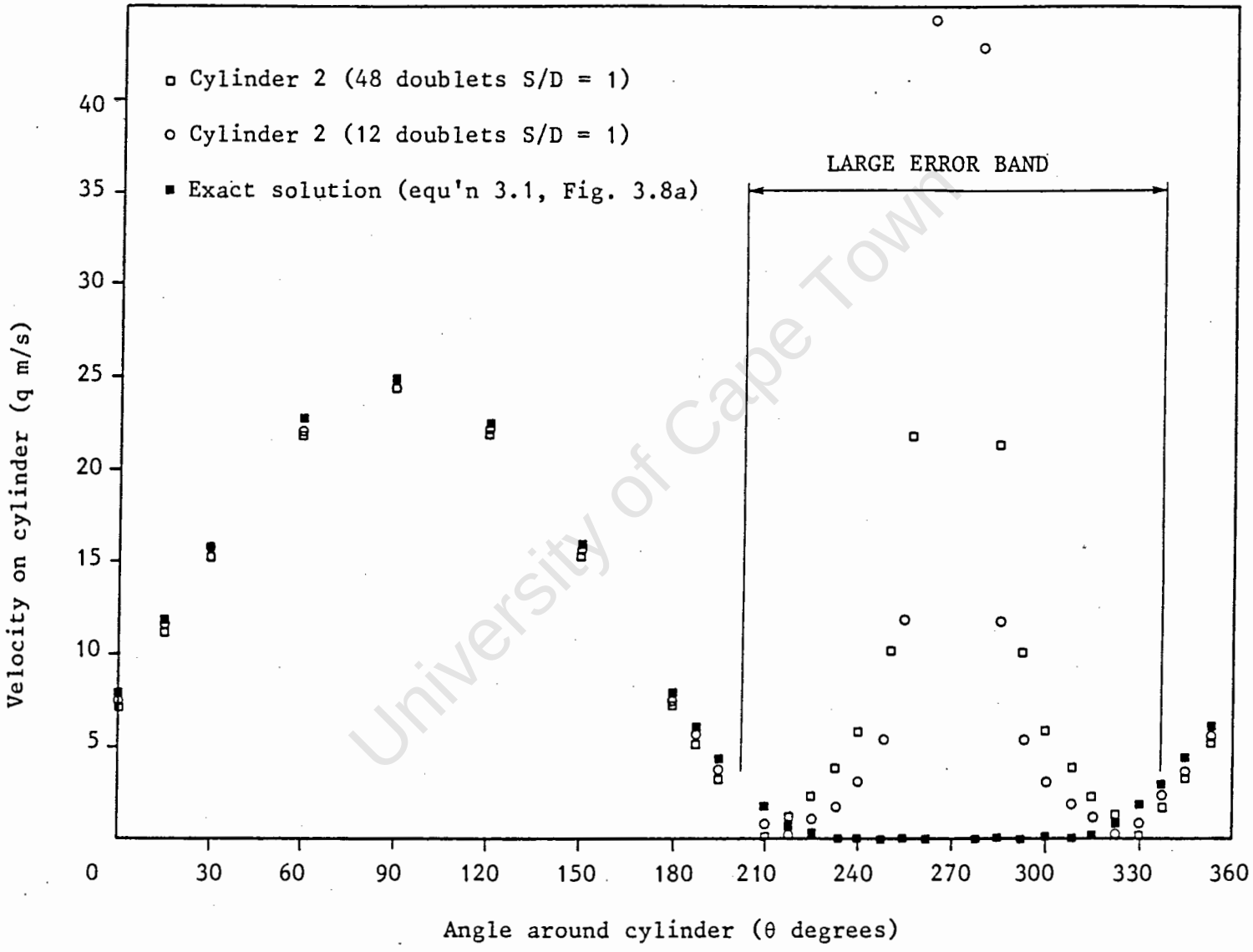


Fig. 3.9 Velocity on the surface of a cylinder lying on a solid boundary in a potential flow field

also shows the data points for this regime. At a spacing ratio of S/D = 1.1 in Fig. 3.7a, the difference in lift coefficient is only 5 percent but the error increases rapidly for smaller spacing ratios. In Fig. 3.7b a 4.5 percent error at S/D = 2 occurs. The 45 degree and 90 degree inclination angles represent the limits of the maximum errors, and it is therefore concluded that the numerical solution requires at least three orders of image doublets and may be used with confidence at spacing ratios greater than 1.2.

# CHAPTER 4

# WIND TUNNEL BLOCKAGE

## 4.1 INTRODUCTION

When any model is tested in a wind tunnel, blockage effects, due to the presence of the model, cause the air velocity in the vicinity of the model to be different from the air velocity in the vicinity of the same model placed in an unlimited free air stream, the upstream velocity being the same in both cases. A velocity correction factor must therefore be applied to the wind tunnel upstream velocity that is used in the calculation of lift, drag and pressure coefficients.

In the case of flow past streamlined bodies (aerofoils), blockage corrections are fairly well established for closed jet wind tunnels and are discussed in general terms by Pankhurst et al (1952) [23] and Pope et al (1966) [24]. However, for flow over bluff or semi-bluff bodies such as groups of cylinders, blockage corrections for streamlined bodies are not relevant. The wind tunnel available to the author, and in which the cylinder group studies were to be performed, was of the open jet type, and no information relating to bluff body blockage correction for this type of tunnel could be found in the literature. It was therefore necessary to study the effects of wind tunnel blockage in the open jet wind tunnel so as to account for, or eliminate it,

and this chapter is devoted to a description of that work.

## 4.2 THEORY

Maskell (1965) [9] found that for bluff bodies, the blockage corrections required were much larger than for streamlined bodies, and since they require a detailed understanding of the wake properties and wake distortion effects, they are also far more difficult to treat theoretically. Maskell [9] theoretically considered the bluff body blockage problem for closed jet test sections and found that for low aspect ratio bluff bodies placed normal to the flow, the corrected velocity could be expressed in terms of equation (4.1),

$$U_c/U = [1 + 2.5C_D(a/A)]^{0.5} \qquad (4.1)$$

He verified this expression by comparison with existing data for square plates with up to a 4.5% blockage ratio. Subsequently, Awbi (1972) [25], Fackrell (1975) [26] and Alexander (1978) [27] validated Maskell's theory at higher blockage ratios.

West et al (1981) [28] specifically studied the blockage caused by a single cylinder in a closed test section wind tunnel. The experiments covered a range of blockage ratios from 2% to 16%, and of aspect ratios from 4 to 10. They found that for blockage ratios less than 6%, the effects of blockage on pressure distribution and the drag coefficient, were small. For blockage ratios in the range 6-16%, there is considerable distortion of the flow due to blockage, and the effects are complex, the pressure distribution around the cylinder in

particular being of a different form to that in an unlimited free stream. However, conflicting influences resulted in a blocked drag coefficient which was not very different from that at no blockage.

Consider the two cases shown in Fig. 4.1, where a body is placed in an unlimited (free air) and a limited wind tunnel flow field. In Fig. 4.1a, the correct value of drag coefficient is given by,

$$C_{Dc} = D_1 / 0.5\rho U^2 a \qquad (4.2)$$

where $D_1$ is the measured drag and a is the projected area of the body.

In Fig. 4.1b, the uncorrected drag coefficient is given by,

$$C_D = D_2 / 0.5\rho U^2 a \qquad (4.3)$$

but whilst the free stream velocity, U, is the same in both cases, $D_1$ and $D_2$ are not equal. This is because the velocity at the body in each case is not the same due to the constraining effects of the tunnel walls in Fig. 4.1a. Therefore $C_D$ and $C_{Dc}$ are not equal.

To obtain the correct value for the drag coefficient in Fig. 4.1a, the value of free stream velocity used in equation (4.3) must be modified by a velocity correction factor $U_c/U$ so that the correct value of drag coefficient is calculated from,

$$C_{Dc} = D_2 / 0.5\rho [U(U_c/U)]^2 a \qquad (4.4)$$

Combining equations (4.2) and (4.4) gives $(U_c/U)^2 = D_2/D_1$ and

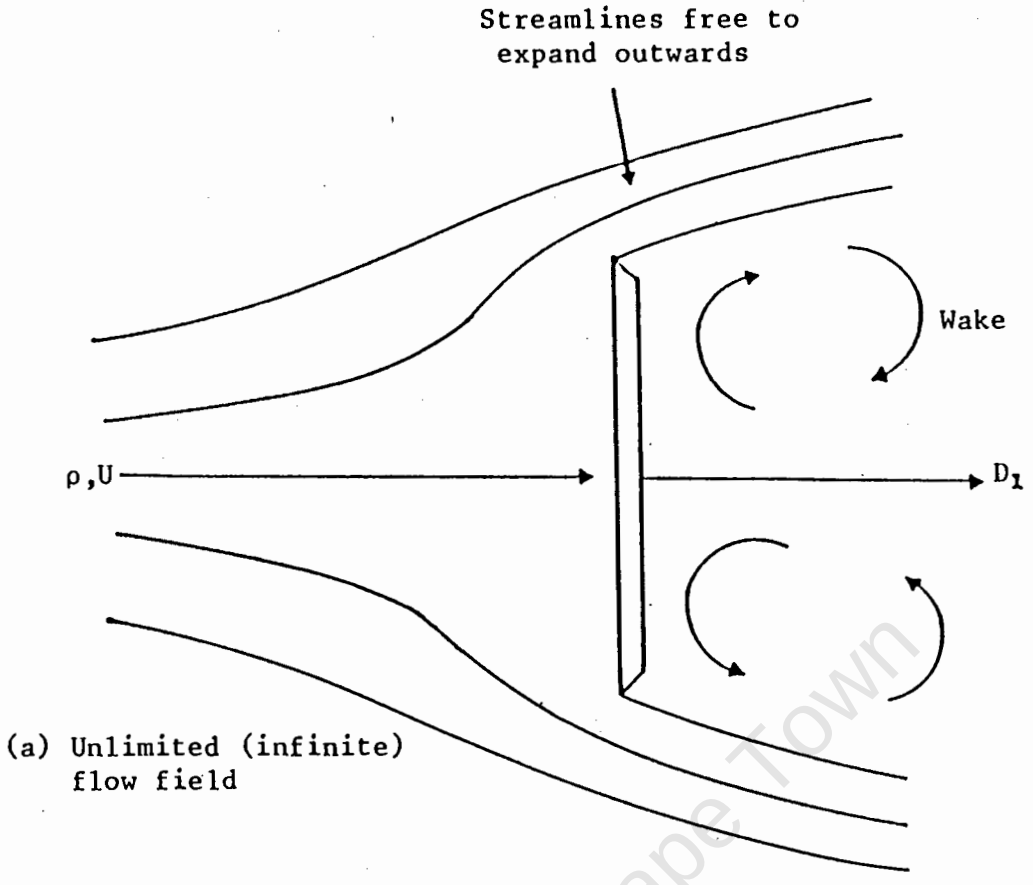


(a) Unlimited (infinite)
flow field

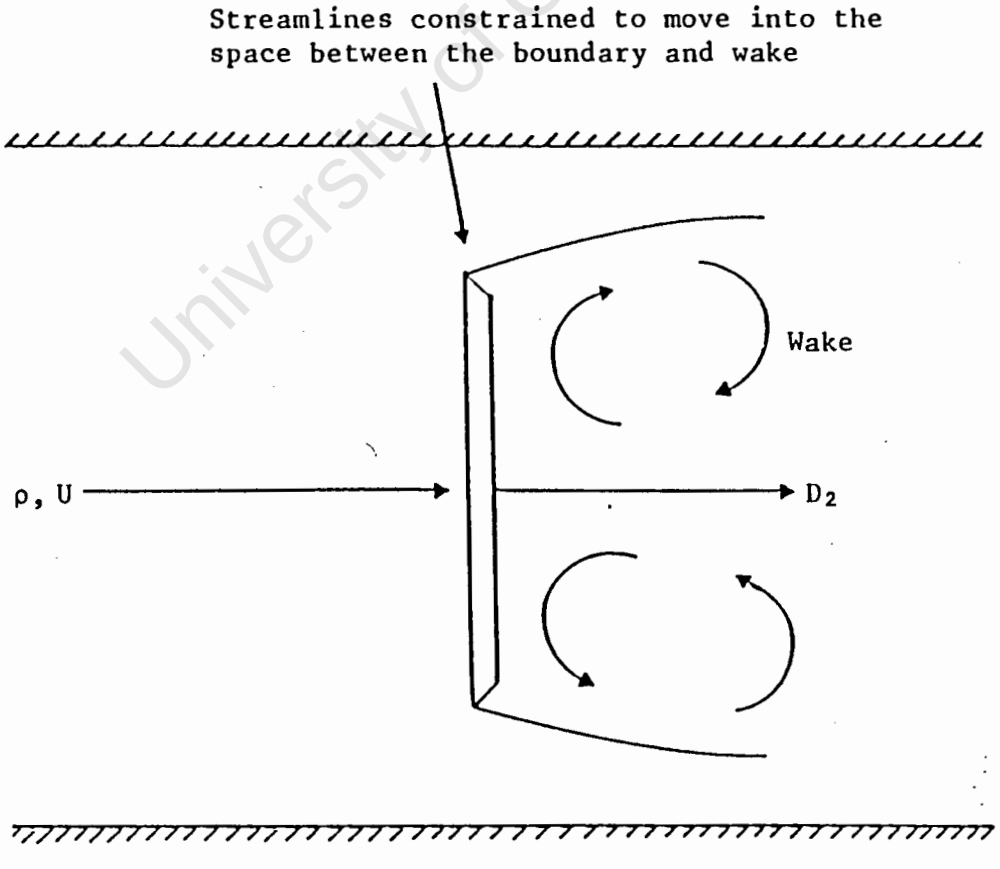


(b) Limited flow field

Fig. 4.1 Flow over a body with sharp edge flow separation

substituting for $D_1$ and $D_2$ from equations (4.2) and (4.3) gives,

$$U_c/U = (C_D/C_{Dc})^{0.5} \qquad (4.5)$$

For a bluff body with sharp edge flow separation, the effect of Reynolds number is expected to be small and therefore $C_{Dc}$ is unaffected by changes in the upstream nominal flow velocity. The value of $C_{Dc}$ is determined experimentally by plotting the drag coefficients of progressively smaller bluff bodies against area ratio (a/A), and then extrapolating the resultant curve to zero area ratio. This corresponds to the infinitely wide free stream, when the value of $C_{Dc}$ will be obtained. Hence for a measured $C_D$ on the model in the wind tunnel, and knowing $C_{Dc}$ and U, the corrected velocity $U_c$ may be determined and used in equation (4.4) for the calculation of the corrected drag coefficient.

# CHAPTER 5

# EXPERIMENTAL APPARATUS AND PROCEDURE FOR THE DETERMINATION OF OPEN JET WIND TUNNEL BLOCKAGE CORRECTION

## 5.1 WIND TUNNEL

The wind tunnel that was employed for the flow interference investigations was of the return circuit open jet type shown in Fig. 5.1. The open jet test section measured 870 x 580 mm with corner fillets at the throat and a working length of 1.6 m. The static pressure in the test section was atmospheric. A velocity traverse across the test section showed a 1% velocity variation and a turbulence intensity of 0.4%. The maximum velocity attainable in the test section was 36 m/s whilst the area ratio between the settling chamber and test section was 10:1. Measurements taken along the horizontal axis of the empty test section showed a velocity variation of 2.6% over the 1.6 m jet length. The tunnel was driven by a twelve bladed variable pitch axial flow fan which was powered by a two speed 380 V three phase motor.



## 5.2 WIND TUNNEL BALANCE

Drag and lift forces were measured through a T.E.M. three component strain gauge wind tunnel balance having lift and drag force ranges of 0 to 89 N and 0 to 36 N respectively. A

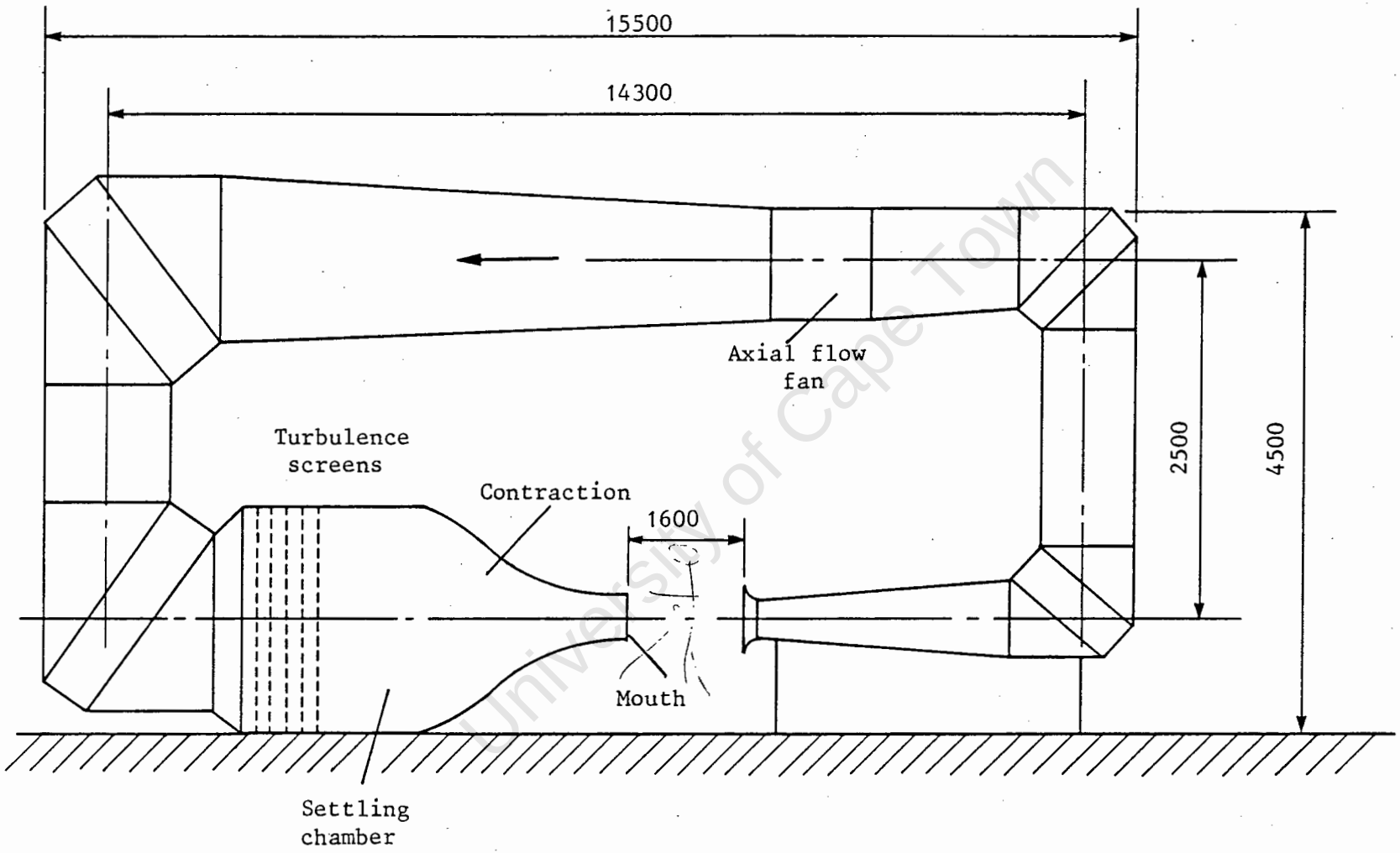


Fig. 5.1 Open jet wind tunnel

digital voltmeter gave a direct reading of the lift and drag force accurate to within 0.005 and 0.02 N respectively. The balance was floor mounted on levelling pads below the open jet test section as illustrated in Fig. 5.2. A collar which was fitted to the balance support plate enabled a horizontal steel beam, drilled with locating holes along its length, to be secured on the balance. The balance and bar were both low enough to be unaffected by the open jet air stream. Calibration of the balance was checked by loading it with known horizontal (drag) and vertical (lift) deadweights.

## 5.3 BLUFF BODIES

The worst blockage occurs when a vertical flat plate is held in the test section perpendicular to the air stream. When three or four cylinders are likewise held, the worst case of blockage occurs when the upstream projected area of the cylinders is four cylinder diameters for a given span and thereby resembling bluff body flow. However, it should be noted that because of flow through the cylinder gaps, the blockage would not be expected to be as high as for a flat plate. For the bluff bodies, 5 mm thick rectangular plywood plates, of the dimensions given in Table 5.1, were therefore chosen, the area ratio ranging from 0.005 to 0.3. A 3 mm hole was drilled through at the centre of each plate, for mounting the plates on the balance sting, and later for suspension of the plates in the air stream. The plates were mounted at their geometric centres on a 'T' bar sting which was bolted to the horizontal bar on top of the balance. Slight vertical adjustment of the horizontal bar was then made to ensure that the centre of each

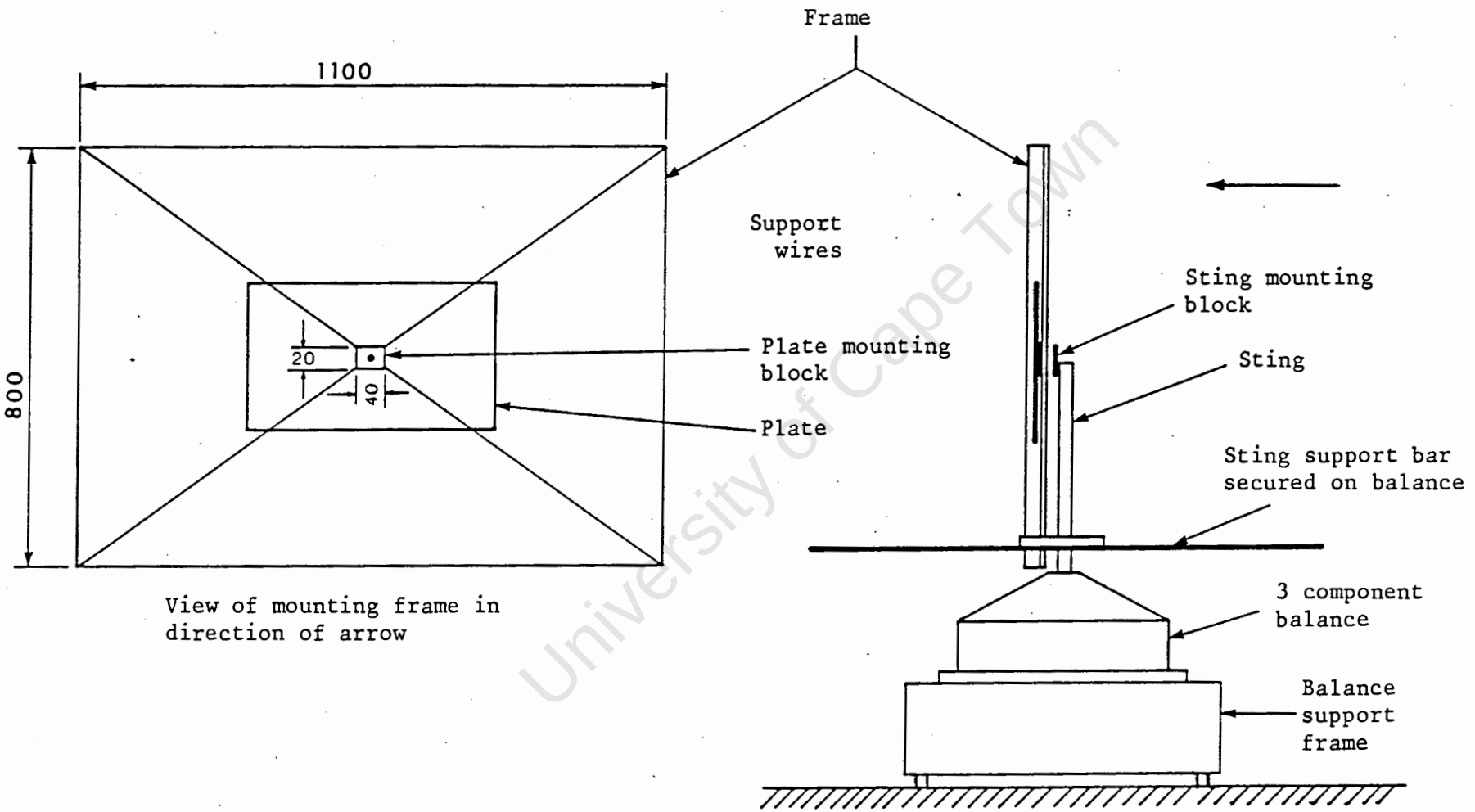


Fig. 5.2 Mounting of plates and suspension frame on the drag balance

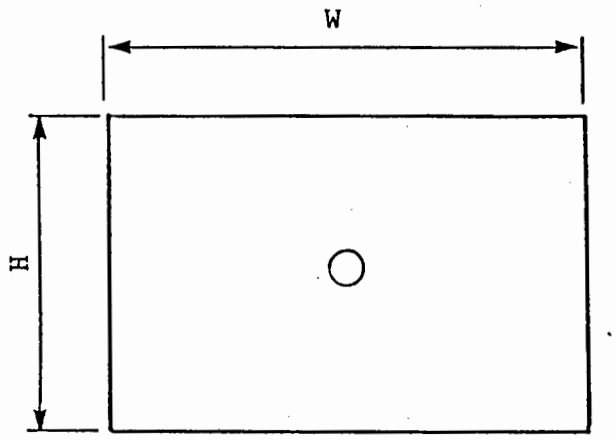


| Width W mm | 60 | 105 | 150 | 195 | 240 | 285 | 330 | 375 | 420 | 465 |
|---|---|---|---|---|---|---|---|---|---|---|
| Heigth H mm | 40 | 70 | 100 | 130 | 160 | 190 | 220 | 250 | 280 | 310 |

Table 5.1 Dimensions of plates. Exact cross sectional area of tunnel mouth = 0.48 $m^2$

plate coincided with the longitudinal axis of the test section. To facilitate a comparison with the closed wind tunnel blockage tests of Maskell [9], a separate sting was used to mount the plates in the closed contracting section of the wind tunnel just before the start of the free jet.

A rectangular frame 800 x 1100 mm was constructed from flat rectangular bar. A steel plate 40 x 20 mm was suspended at the centre of the frame by four taut wires 0.5 mm in diameter, the wires being secured at the four corners of the frame. The plywood plates could then be screwed onto the steel plate at the centre of the frame and hence be positioned centrally in the test section air stream. With this arrangement it was possible to remove a plate from its sting, and with the sting remaining in position, suspend the plate in front of it, but unattached to it. The arrangement is shown in Fig. 5.2. Thus the drag on the sting alone ($D_o$) could be determined under the conditions prevailing when the plate was attached. The frame size was such that when being used, it lay outside of the test section air stream. It was not possible to use this method of plate suspension in the closed section of the tunnel, but since the test in that section was for approximate comparative purposes only, the drag on the sting alone with no plate attached or suspended in front of it was the only sting drag measured.

## 5.4 FREE STREAM VELOCITY MEASUREMENT

Velocity heads were measured with a Prandtl type pitot-static tube connected to an inclined alcohol manometer which permitted velocities to be determined to within 0.25 m/s.

Preliminary tests showed that the flat plates influenced the free stream velocity for a distance of 600 mm upstream of them, and that this distance decreased as the plate area was reduced. The nominal free stream velocity, U, was set at the proposed plate position in the empty test section by adjusting the velocity head of the pitot-static tube to the required value. The pitot-static tube was then moved 700 mm upstream from the proposed plate position. When the plate was placed in the air stream, the wind speed was adjusted until the previously noted velocity head at the 700 mm upstream position was again obtained.

The difference between the velocity heads at the plate location and the 700 mm upstream position when measured in the empty test section, lay within the 2.6% longitudinal velocity variation noted previously. As the plate position moved progressively upstream towards the beginning of the open jet, and on into the contraction section, the velocity head at the 700 mm upstream position was substantially below that at the proposed plate location, this being due to the larger cross sectional area in the contraction section. However, by ensuring that the plate again had no effect on the upstream pitot-static tube at the 700 mm position, velocity head measurement was not affected by the plate in the contraction section and the nominal free stream velocity could be maintained for all plate positions.

## 5.5 EXPERIMENTAL METHOD

For a selected axial distance downstream from the mouth of the test section, each plate and sting assembly was in turn

mounted on the drag balance, the plate being normal to the air stream. The free stream velocity 700 mm upstream of the plate was set at 10 m/s for each of the plates and the drag force $D_3$, acting on the sting and plate together was recorded. The plates were then removed from the sting and suspended centrally by the four wires of the suspension frame. The frame was positioned such that, with the sting still mounted on the drag balance, the plate was in the same position as when mounted on the sting but detached from it. The drag force $D_0$, on the sting alone was now recorded, and the drag force on the plate $D_2$, was calculated from the difference ($D_3 - D_0$). This was repeated for five longitudinal settings of the plate, one position being in the contracting section of the tunnel.

At a position 750 mm downstream from the test section mouth, the procedure was repeated for upstream nominal velocities of 5 and 15 m/s to check the effects of varying Reynolds number.

# CHAPTER 6

## RESULTS OF INVESTIGATION OF WIND TUNNEL BLOCKAGE

### 6.1 EXPERIMENTAL RESULTS

The experimental results recorded in chapter 5 are tabulated in Appendix C1. Using the measured values U, $D_o$ and $D_j$, the uncorrected drag coefficient $C_D$, was calculated from equation (5.3) and plotted against the area ratio for each plate position as shown in Fig. 6.1. The curve labelled -125 mm refers to plates situated 125 mm upstream from the tunnel mouth in the closed section of the tunnel. Each curve is extrapolated to the vertical axis where (a/A) is zero and at which point the value of $C_D$ tends towards $C_{Dc}$, the corrected drag coefficient. For those plates which were situated in both the open jet and contraction section of the wind tunnel, $C_D$ (that is $C_{Dc}$), tended towards 1.1. This value of $C_{Dc}$ was used in equation (4.5) for the calculation of the velocity ratio $U_c/U$.

This velocity ratio is plotted against area ratio in Fig. 6.2 for all plates tested, along with Alexander's [27] results. $C_D$ was also substituted into Maskell's [9] equation (4.1) and this has been plotted up to an area ratio of 0.3.

The effect of changing the nominal wind speed is shown in Fig. 6.3 where $C_D$ is plotted against (a/A), some of the data points falling on top of each other.

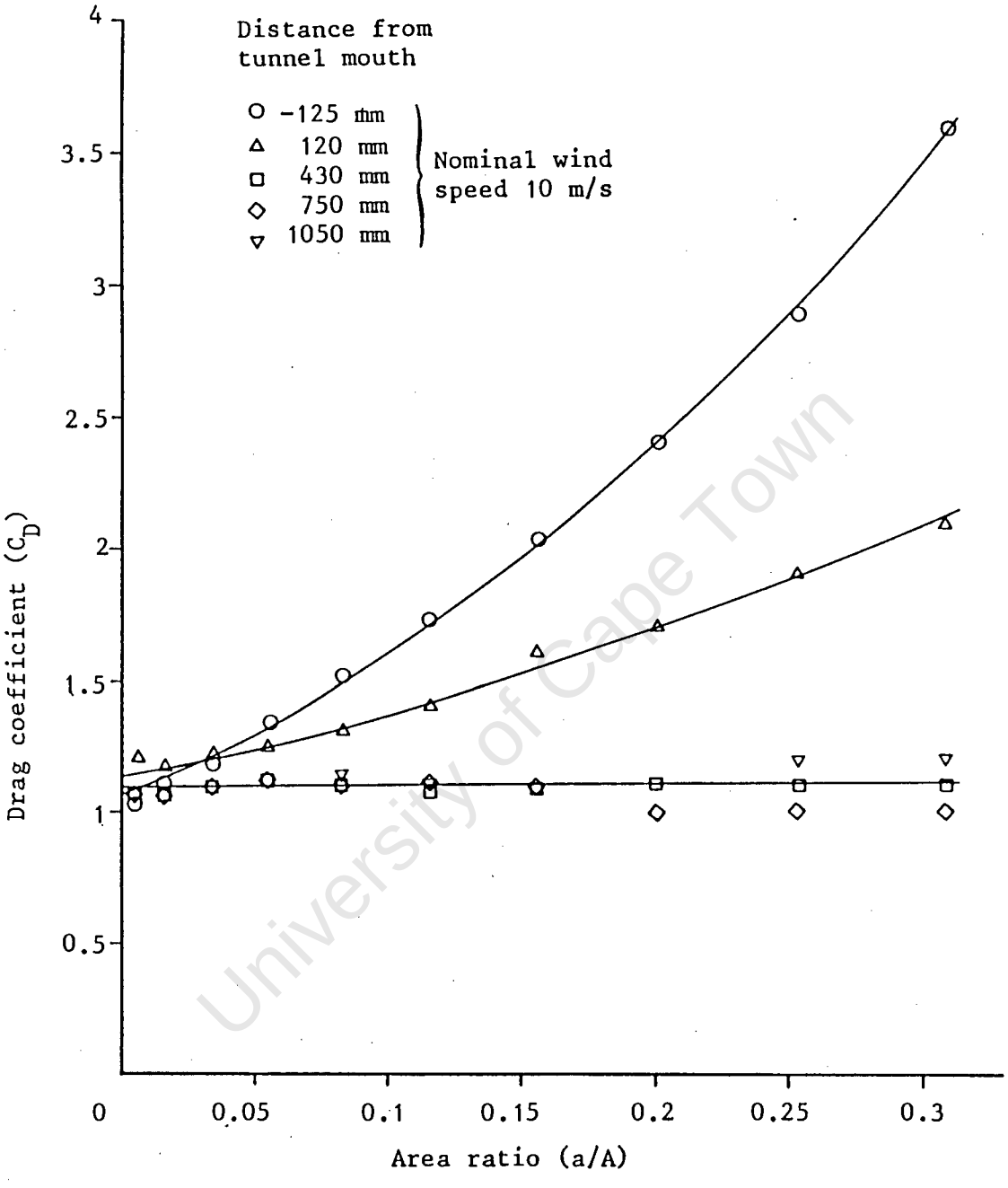




Fig. 6.1 Drag coefficient versus area ratio for varying distances of the plate from the tunnel mouth

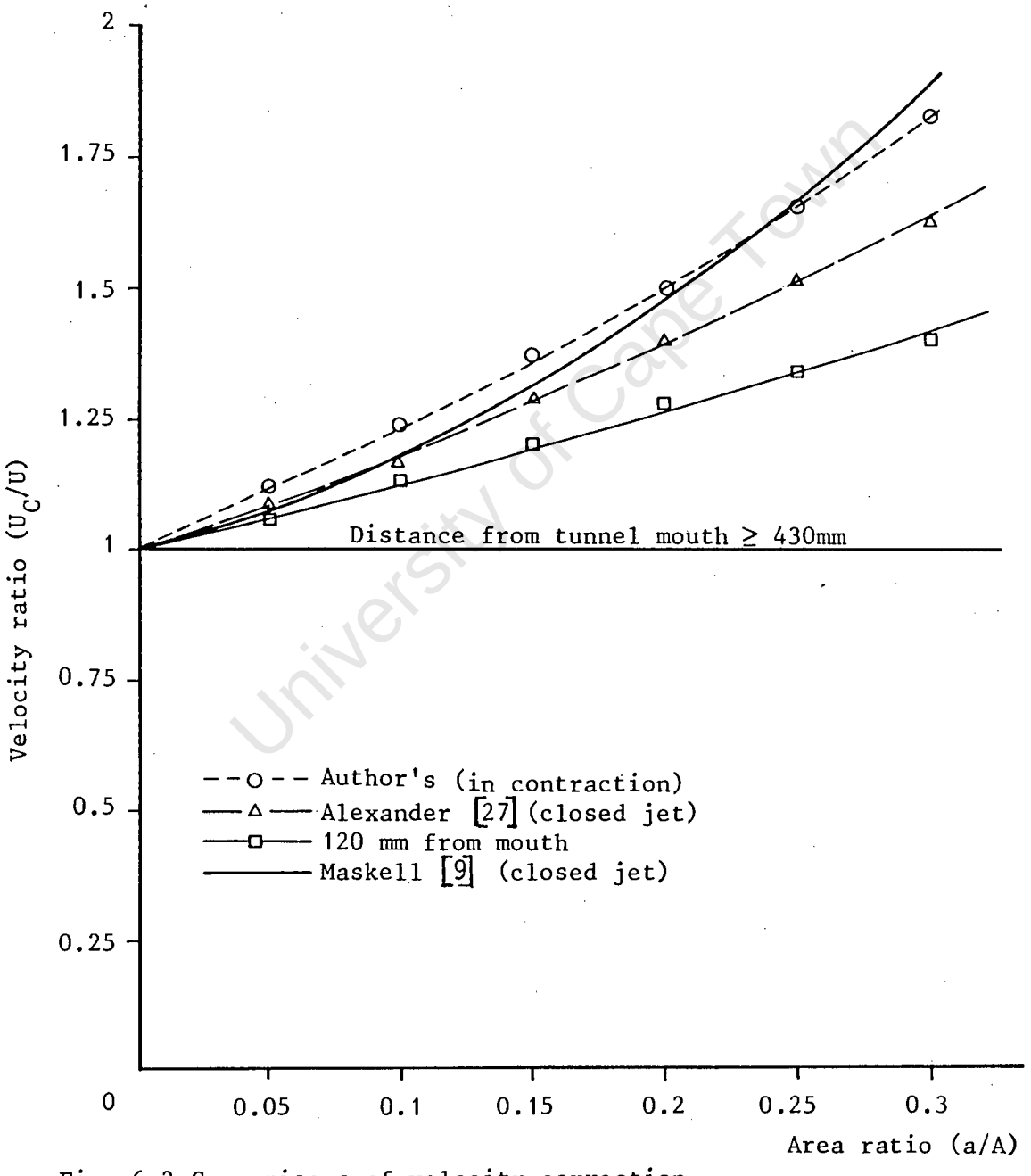


Fig. 6.2 Comparisons of velocity correction

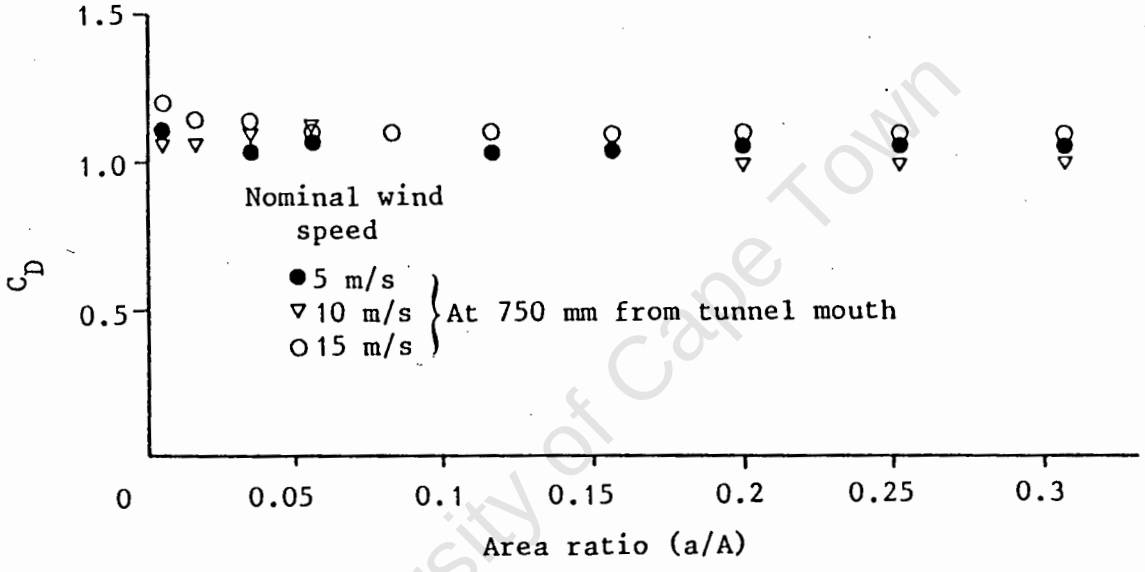


Fig. 6.3 Effect of Reynolds number on the drag coefficient at 750 mm downstream of the tunnel mouth

## 6.2 DISCUSSION

The value of $C_{Dc}$ at zero area ratio would be expected to be the same for both an open and closed jet wind tunnel and the value of 1.1 compares favourably with Alexander's [27] value of 1.15, the difference being 4.5 per cent. As the plate was moved away from the mouth of the tunnel, the drag coefficient was seen to steadily decrease until at 430 mm downstream from the tunnel mouth, there was no perceived change in the drag coefficient with increase in area ratio. Only the curves for the 120, 430, 750 and 1050 mm positions are shown in Fig. 6.1 since the reason for plotting the figure was to determine the value of $C_{Dc}$ at zero area ratio.

The velocity ratios for flat plates in the open jet test section are compared with those in a closed wind tunel in Fig. 6.2, where it is seen that the corrected velocity $U_c$, is always greater than or equal to U. As the plate was moved away from the tunnel mouth, the velocity ratio decreased to unity at a distance of 430 mm downstream from the tunnel mouth, and remained at that value for even greater distances downstream, indicating that $U_c$ does not fall below the free stream velocity of the wind tunnel. Pankhurst et al [23] expressed the view that the velocity correction would be less than unity in flow past a streamlined body in an open jet wind tunnel. Although they agreed that their argument for that reasoning was not rigorous, these results prove conclusively that in the case of bluff body flow, the velocity in the region of the model is always increased.

When the air exits from the mouth of the tunnel and becomes the open jet, a certain distance is required for the jet

bounding streamlines to adjust to the new boundary conditions of surrounding atmospheric pressure. If a plate is placed within this adjustment length, the bounding streamlines are unable to adjust rapidly enough to their natural fully expanded state. The velocity at the plane of the plate between the bounding streamlines and those forming the edge of the wake at the separation point on the plate will therefore have a value between that for the plate in the closed section and that in the fully adjusted open jet. This intermediate velocity decreases as the plate is moved downstream in the open jet until the velocity at the plate attains its naturally fully expanded streamline value, when $U_c/U$ becomes unity. The ratio of distance downstream from the tunnel mouth for no correction, to the cross-sectional area of the test section is the adjustment length ratio. For this particular tunnel the adjustment length ratio was 0.845.

The velocity ratios for the position 125 mm upstream from the tunnel mouth are seen to correspond closely to Maskell's [9] equation but are higher than those of Alexander [27], particularly at high area ratios where the difference is in the order of 8.7 per cent at an approximate area ratio of 0.3. If, for a given area ratio, the drag coefficients of Alexander were the same as those obtained in this thesis, the difference of 0.05 in the value of $C_{Dc}$ previously noted, would result in a velocity ratio difference of only 2 per cent, and therefore no explanation can be attributed to the relatively large difference of 8.7 per cent. Although Maskell's curve is based on an equation derived from results obtained using flat plates of area ratio up to 0.045, the present results tend to confirm that Maskell's equation (4.1) may also be used at higher

blockage ratios.

## 6.3 CONCLUSIONS

Closed wind tunnel blockage corrections can not be used for open jet test section flows. The open jet blockage corrections that must be applied to the force coefficients of a bluff body decrease in magnitude the further the body is placed downstream of the tunnel mouth. For this particular tunnel, the adjustment length ratio is 0.845, and provided the body was placed in the test section with its adjustment length ratio greater than 0.845, then no blockage correction was required. This finding lends confidence to the placement of the cylinder groups and the subsequent accuracy of the measurements described in chapter 7.

# CHAPTER 7

# EXPERIMENTAL APPARATUS AND PROCEDURE FOR THE DETERMINATION OF THE FORCE COEFFICIENTS ACTING ON GROUPS OF CYLINDERS

## 7.1 GROUPS OF THREE AND FOUR CYLINDERS

The experimental determination of the force coefficients acting on groups of three and four cylinders was carried out in the open jet wind tunnel described in section 5.1.

Figs. 7.1, 7.2 and 7.3 illustrate the general experimental arrangement. Each cylinder of the group was a 1 m long hollow steel tube of 48 mm internal diameter, and 50 mm external diameter, this outer surface being machined to a smooth finish. One of the tubes was cut in half and a brass ring, 20 mm wide with 24 equispaced (15 degree) 1 mm diameter static pressure tapping holes drilled through it, was inserted between the two halves (Fig. 7.4). The wall thickness of the brass ring was 5 mm and into each of the 1 mm holes was inserted a 19 gauge hypodermic needle which protruded slightly above the external surface of the ring. The needles were a push fit into the holes and were held rigid by epoxy glue on the inside of the cylinder. This particular cylinder (the measuring cylinder) was finish machined after insertion of the ring to ensure that there were no burrs or sharp edges on the surface. A plug with a centrally located stud was pressed into one end of each cylinder following which they were screwed vertically into

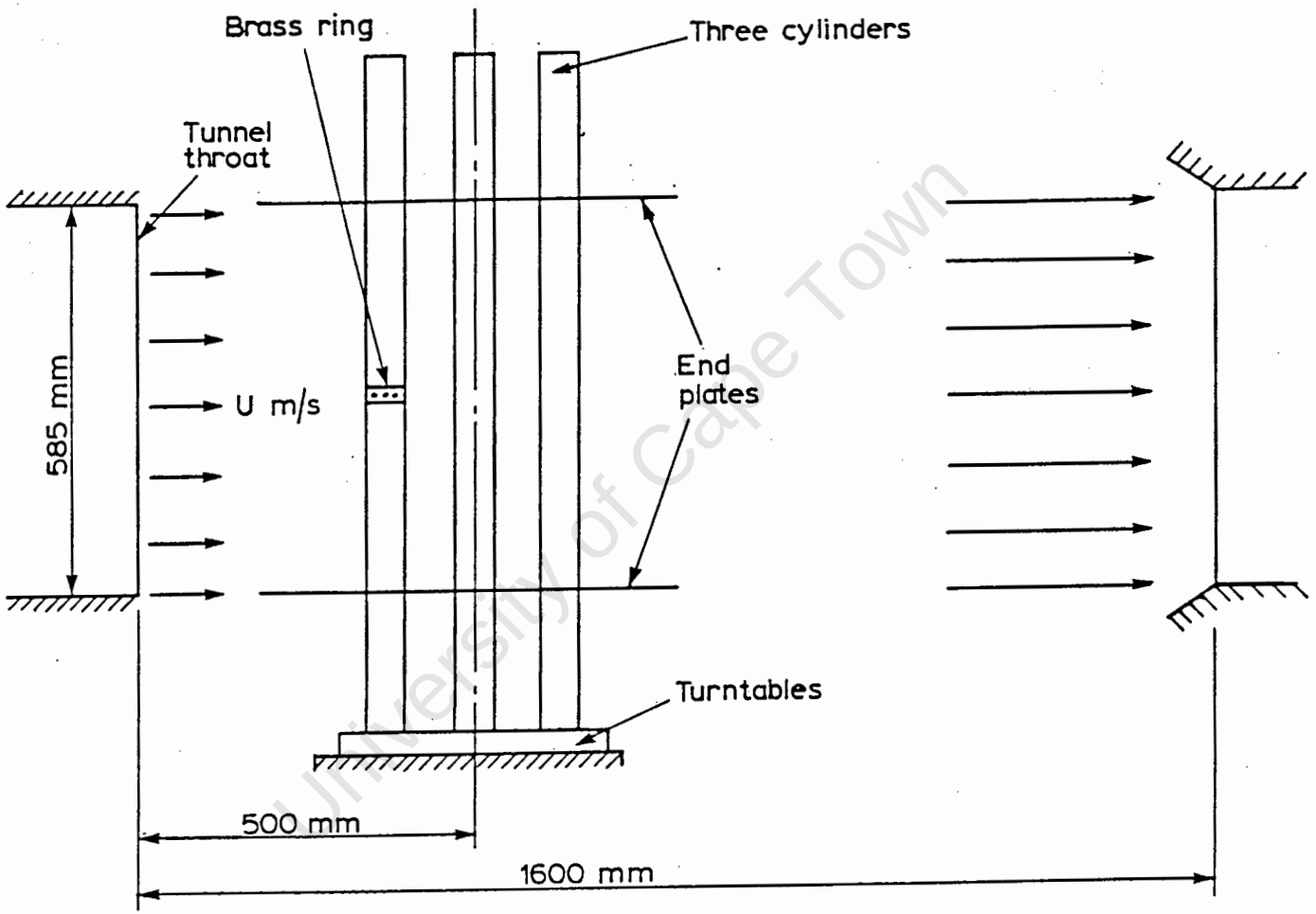


Fig. 7.1 Location of cylinder group in the open jet test section

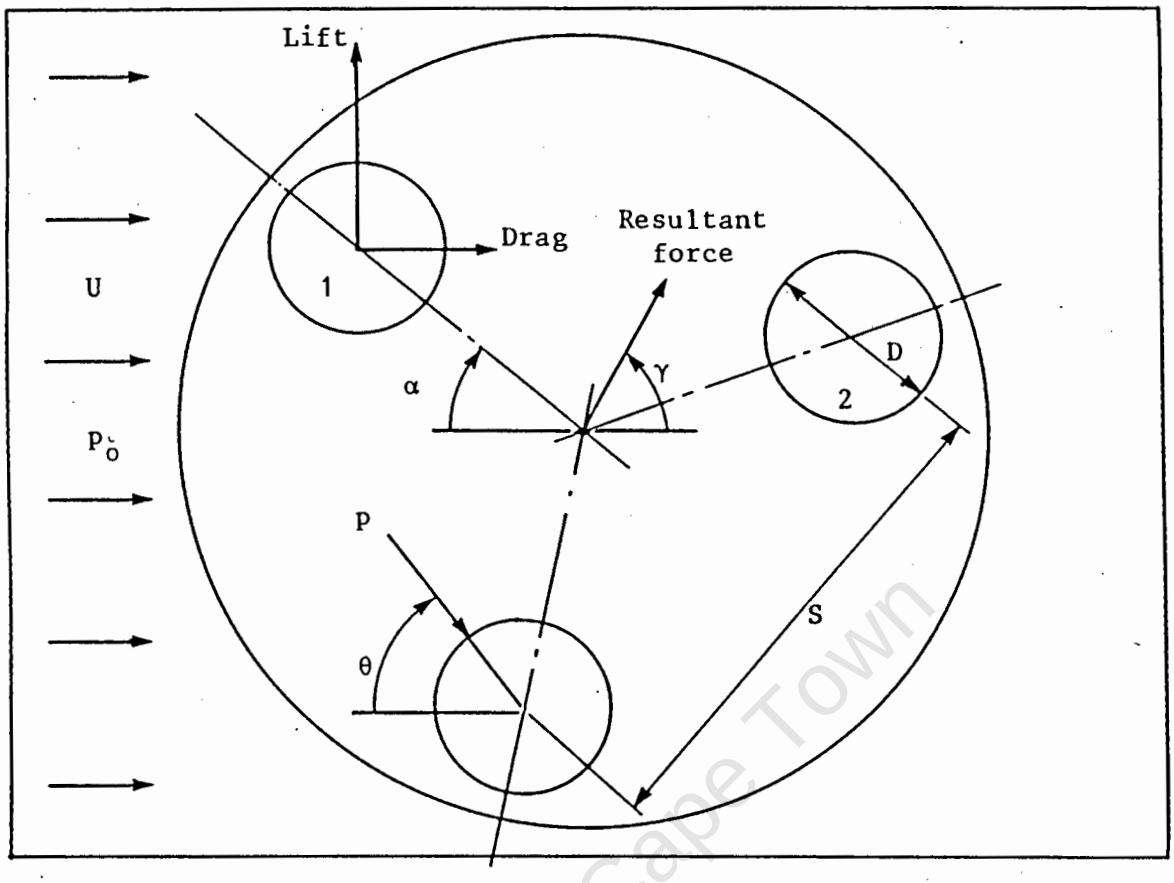


Fig. 7.2 Three equispaced cylinders

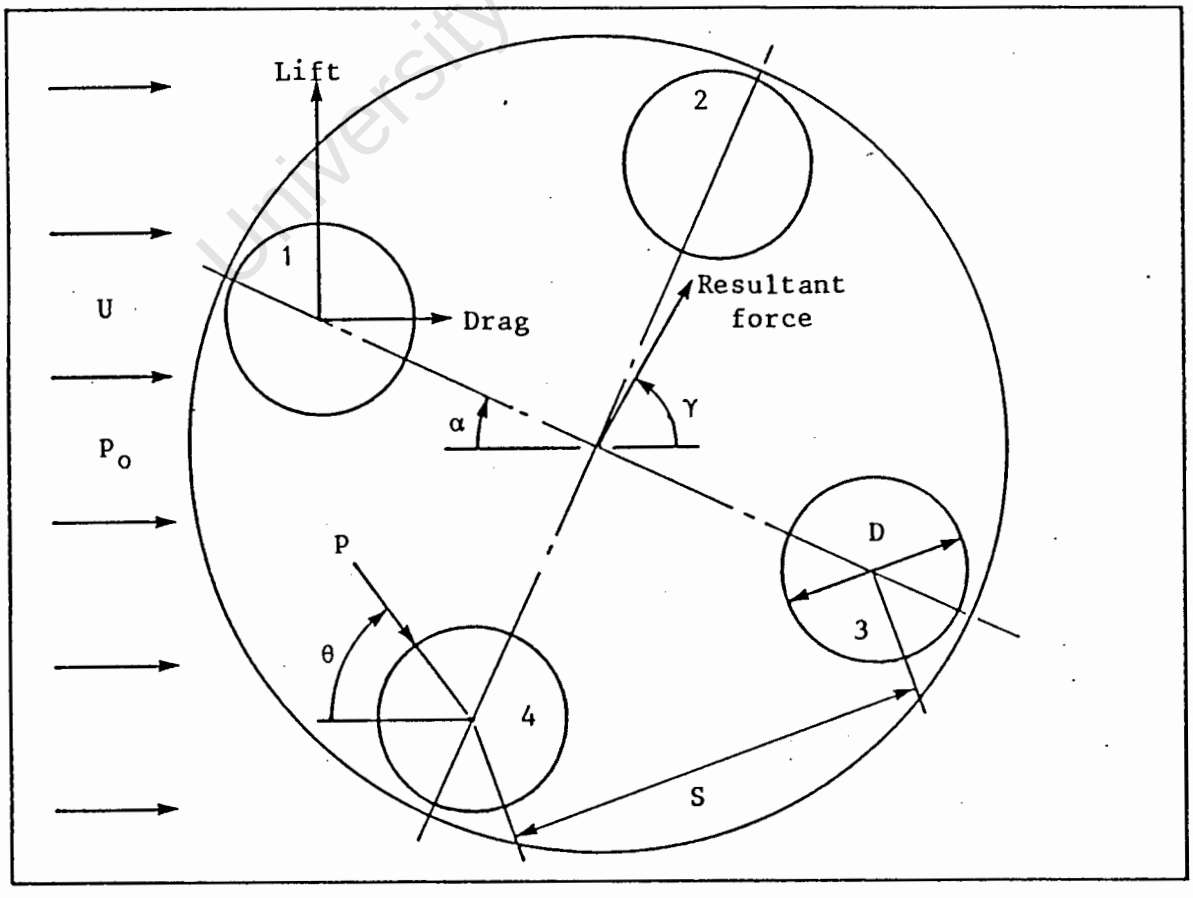


Fig. 7.3 Four equispaced cylinders

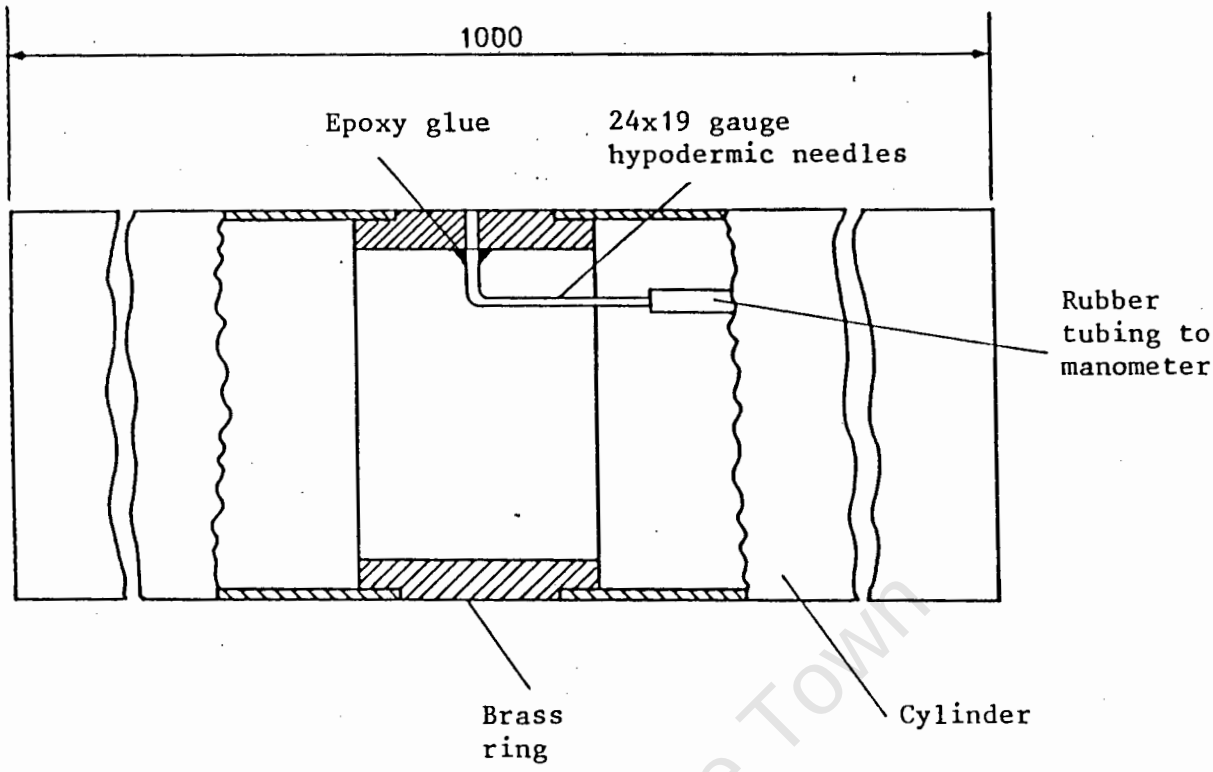


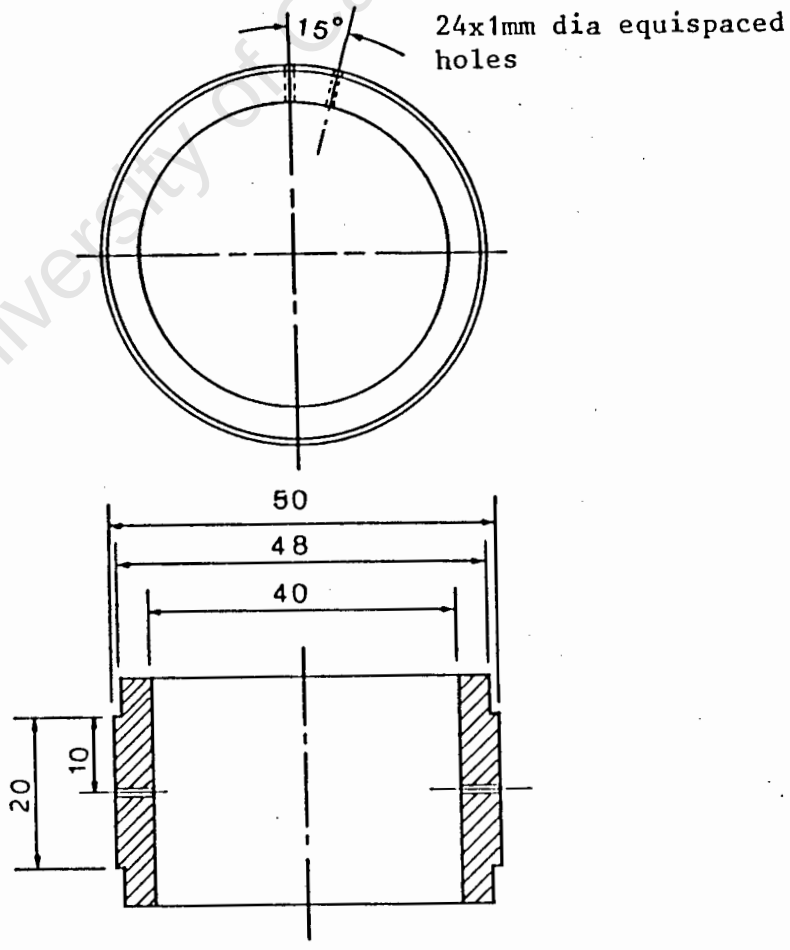




Fig. 7.4 Detail of measuring cylinder ring

their respective holes on a 340 mm diameter wooden turntable graduated in divisions of 7.5 degrees. The turntable was clamped to a base plate situated below the open jet test section, and the whole assembly was located in the test section at a distance 500 mm downstream from the tunnel throat so as to eliminate the effects of blockage as discussed in section 6.2.

The height and lateral position of the platform was adjusted until the 24 pressure tappings lay along the horizontal axis of the test section, while the vertical axis through the centre of rotation of the platform also intersected the test section axis. In this position the ends of the cylinders protruded approximately 65 mm outside the upper and lower jet boundary.

Flexible tubing was connected to each pressure tapping of the measuring cylinder and led up through the inside of the cylinder to a pressure selector switch which permitted each tapping to be connected in turn to one side of an inclined alcohol manometer, the other side of the manometer being connected to the static pressure tapping of a pitot-static tube. The pitot-static tube was located at the tunnel throat for the measurement of free stream velocity. Pressure differences were determined to within 0.025 mm of water and free stream velocity to within 0.25 m/s.

At all times, great care was taken to ensure that the cylinder separation remained constant along the span and that the axes of the cylinders remained perpendicular to the free stream flow. Rotation of the turntable was about the point O. The angle $\theta$, around the circumference of the cylinder, at which the static pressures were recorded, is measured clock-

wise from the negative x axis. The angle of inclination of the cylinder group to the free stream is $\alpha$, and is likewise incremented clockwise from the negative x axis. The resultant force acting on the group is inclined at angle $\gamma$ to the positive x axis.

## 7.2 FLOW UNIFORMITY

To check the uniformity of flow along the span of a cylinder, another cylinder was provided with static pressure tappings in line along the span, at the positions shown in Fig. 7.5. From pressure readings taken along the span of this single cylinder with the pressure tappings facing directly downstream, it was deemed necessary to attach end plates to the cylinders, and these took the form of 3 mm thick boards 620 mm in diameter with 50 mm holes drilled at the positions corresponding to the cylinder spacings. These end plates were changed depending on the cylinder spacing under test. The end plates were a tight push fit over the cylinders, but as a precaution against any leakage flow through small gaps between the cylinder wall and the plates, a layer of masking tape was wound over the joint.



## 7.3 CHECKING FLOW UNIFORMITY

The cylinders were made 1 m long so that they would protrude well outside the boundaries of the open jet and thus obviate any end effects which would otherwise occur were the cylinders of finite length in the free stream. To confirm that uniform flow over the cylinders was being achieved in this way, the single cylinder with the spanwise pressure tappings was first

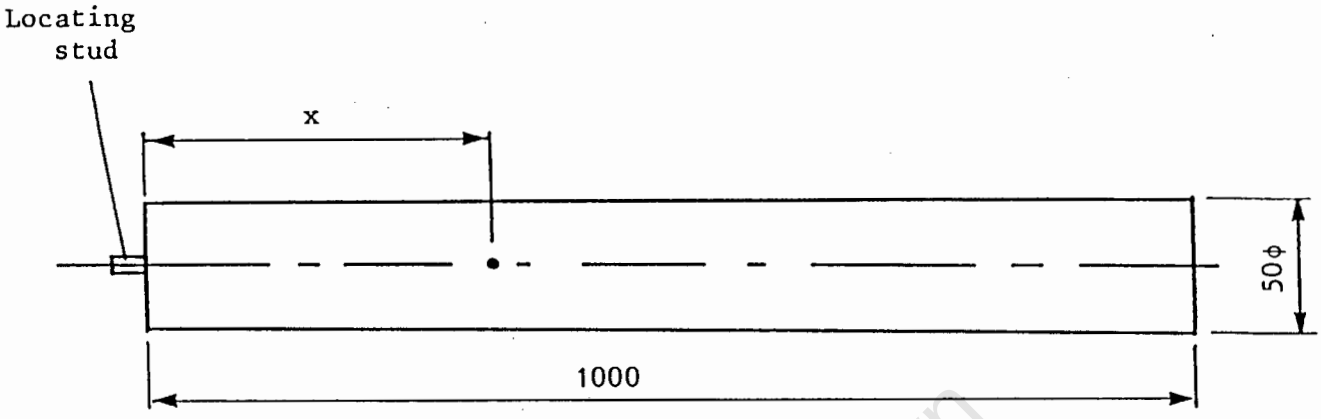


| Hole No. | 1 | 2 | 3 | 4 | 5 |
|---|---|---|---|---|---|
| x (mm) | 231 | 372 | 511 | 581 | 721 |

Fig. 7.5 Location of base pressure tapping holes along span of cylinder

placed in the test section with the static pressure holes facing directly downstream. The base pressure coefficient $C_{p_b}$, at $\theta$ = 180 degrees, was then measured along the span. The resulting pressure distribution is shown in Fig. 8.1, where it is evident that the flow around the cylinder at the jet boundaries affects the pressure distribution along the span through the flow being three dimensional.

In order to achieve two dimensional flow over the cylinder, the 620 mm diameter end plates were attached to the cylinder just inside the jet boundaries such that the effective span of the cylinder was 575 mm. The new spanwise base pressure distribution was measured.

The cylinder with the twenty four mid-span pressure tappings was then placed in the test section with one of the tappings facing directly upstream, and, at a free stream velocity of 10 m/s, the twenty four circumferential static pressures were recorded both with and without the end plates in position. The results of the foregoing experiments confirmed the need for end plates to be fitted to the cylinders.



## 7.4 PRESSURE DISTRIBUTION AROUND A SINGLE CYLINDER IN A GROUP OF THREE AND FOUR

Having satisfied the requirement of two dimensional flow over the single cylinder, three cylinders were located on the turntable forming an equilateral triangle at a chosen spacing ratio. The 620 mm end plates were attached to give an effective span of 575 mm. The turntable was initially set at $\alpha$ = 0 degrees, when the measurement cylinder was rotated until one of the mid-span pressure tappings pointed directly up-

stream. Twenty four static pressure readings were then taken, via the pressure selector switch, around the circumference of the cylinder in increments of 15 degrees. Without further adjustment of the measurement cylinder, the turntable was incremented from 0 to 180 degrees in steps of 7.5 degrees, sets of pressure readings being taken at each increment. The above procedure was repeated for the range $1.25 < S/D < 5$ at the nominal free stream velocity of 10 m/s.

Tests similar to those just described were also repeated for four cylinders arranged as a square for the spacing ratios $1.1 < S/D < 5$.

# CHAPTER 8

## RESULTS AND DISCUSSION CONCERNING THE PRESSURE DISTRIBUTION AROUND A SINGLE CYLINDER IN A GROUP OF THREE

### 8.1 SPANWISE PRESSURE DISTRIBUTION FOR THE SINGLE CYLINDER

All the experimental results are expressed in terms of dimensionless pressure, drag and lift coefficients. The pressure coefficient is defined as

$$C_p = (p-p_o)/0.5\rho U^2 \qquad (8.1)$$

The drag coefficient is given by equation (2.33) with the negative sign removed since $\theta$ is now measured from the negative x axis whilst the lift coefficient is given by equation (2.32), and remains unchanged. The integrals of the pressure distributions were carried out using Simpson's rule.

The base pressure distribution along the span of the cylinder with and without end plates fitted are shown in Fig. 8.1. When no end plates are fitted, the pressure increases gradually towards mid span. When end plates are fitted, a constant uniform spanwise pressure distribution is achieved and it is noted that the pressures at the jet/atmosphere interface are the same in each case. Since, upon the removal of the end plates, the only additional factor affecting the flow is the

atmosphere bounding the jet, it is concluded that the increase in pressure towards mid-span is due to intense vortex formation starting at the jet/atmosphere interface and then joining with the other shed vortices along the span to form a free vortex with a central atmospheric core extending along the span. The imposition of the end plates effectively prohibits the ingress of the atmosphere since the plates are themselves submerged in the jet, thus severing connection with the atmosphere.

The pressure distribution around the single cylinder at centre span with the end plates in position is shown in Fig. 8.2 and is in agreement with well established data [29] for two dimensional flow over an infinitely long cylinder, as also is the value of drag coefficient of 1.14 at a Reynolds number of $3x10^4$. This agreement vindicates the numerical integration of the pressure distribution in equation (8.1) using Simpson's rule. It was considered most important for this single cylinder flow regime to be established since it is the same as the flow conditions, pertaining to two dimensional flow over an infinitely long cylinder, and therefore forms a basis for the determination and comparison of flows over groups of cylinders.



## 8.2 DRAG COEFFICIENTS ON A SINGLE CYLINDER IN A GROUP OF THREE

Figs. 8.3 and 8.4 show the drag and lift coefficients acting on cylinder number 1 as the group of cylinders is rotated through 180 degrees about its axis. It is assumed that symmetry of flow occurs for the range $180<\alpha<360$ degrees and this

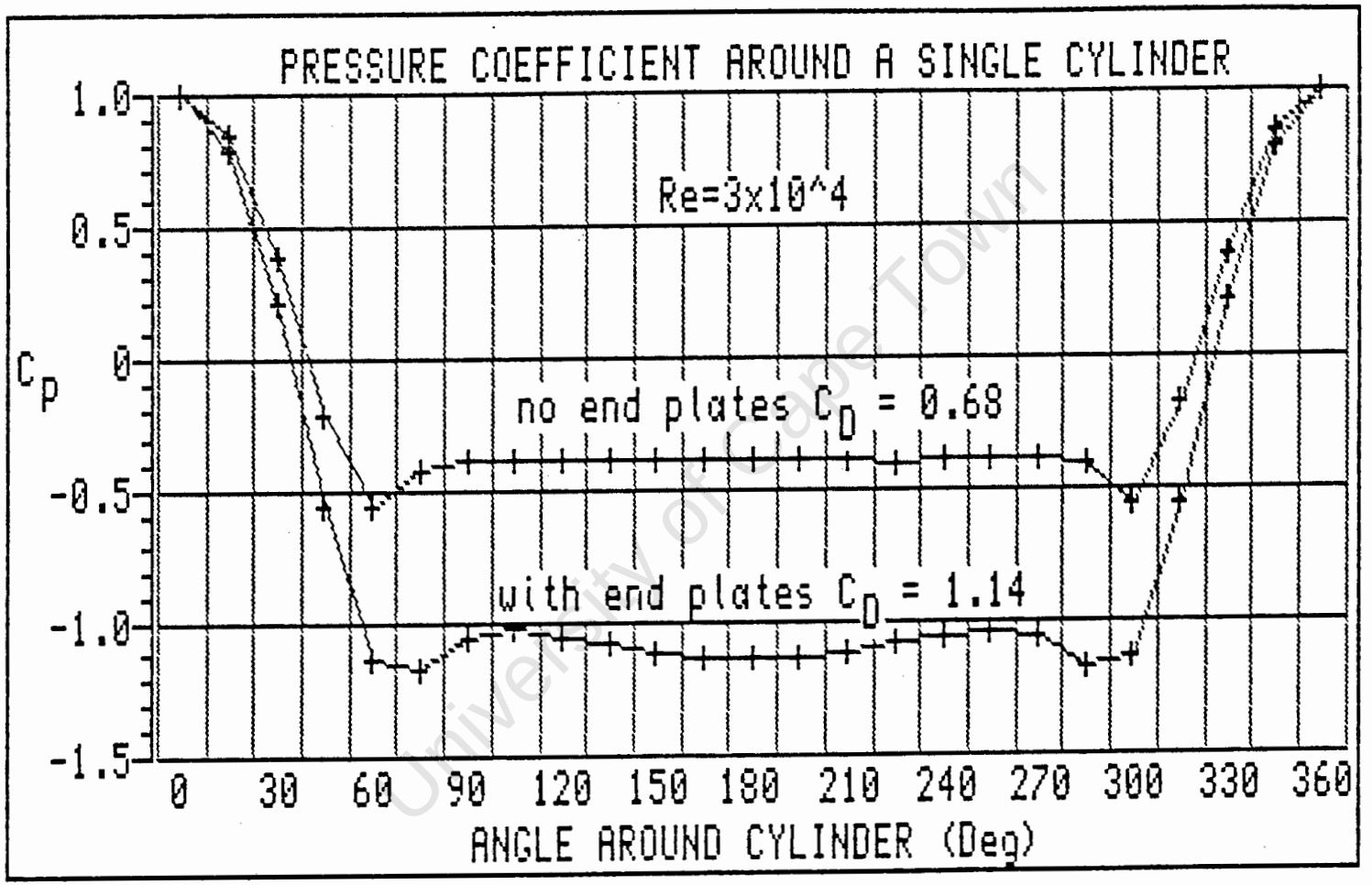


Fig. 8.2 Pressure coefficient versus angle θ around a single cylinder with and without end plates

was verified by random pressure measurements during the course of experimentation. For a given spacing ratio, the lift and drag coefficients acting on each cylinder of the group at any inclination may be obtained. For example, in Figs. 8.3a and 8.4a for an inclination to the free stream of 90 degrees, the drag and lift coefficients of each cylinder are

| Cylinder No. | 1 | 2 | 3 |
|---|---|---|---|
| $\alpha$ (degrees) | 90 | 210 | 330 |
| Equivalent angle | 90 | 150 | 30 |
| $C_D$ | 0.67 | -0.18 | 1.3 |
| $C_L$ | -0.04 | - 0.23 | - 0.61 |

By summing these three values of lift and drag coefficients taking into account their signs and noting that the projected cross sectional area of the cylinders is now 3D, the total lift and drag coefficients $C_{LT}$ and $C_{DT}$ are obtained from equations (8.2) and (8.3).

$$C_{LT} = (C_{L1} + C_{L2} + C_{L3})/1.5\rho U^2 D \qquad (8.2)$$

$$C_{DT} = (C_{D1} + C_{D2} + C_{D3})/1.5\rho U^2 D \qquad (8.3)$$

These results are shown in Figs. 8.5 and 8.6 where it will be noted that the total coefficients repeat themselves every 120 degrees. From the total lift and drag coefficients, the direction of the resultant force acting on the group as a whole is determined from equation (8.4)

$$\gamma = \text{atan}(C_{LT}/C_{DT}) \qquad (8.4)$$

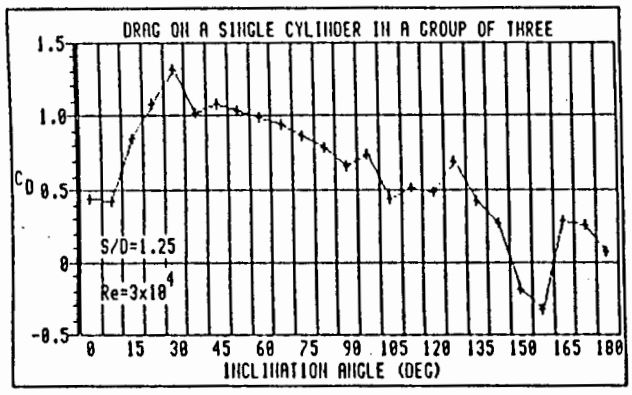


(a)

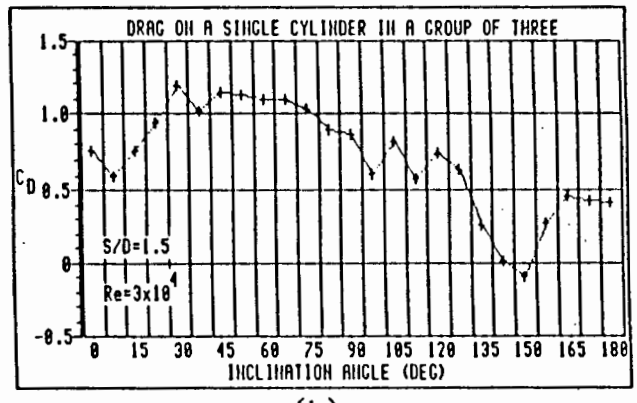


(b)

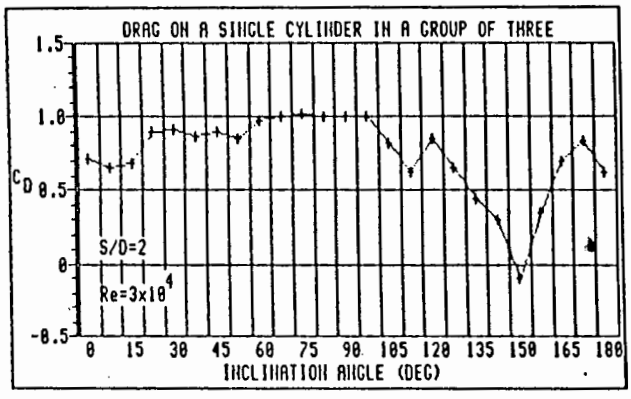


(c)

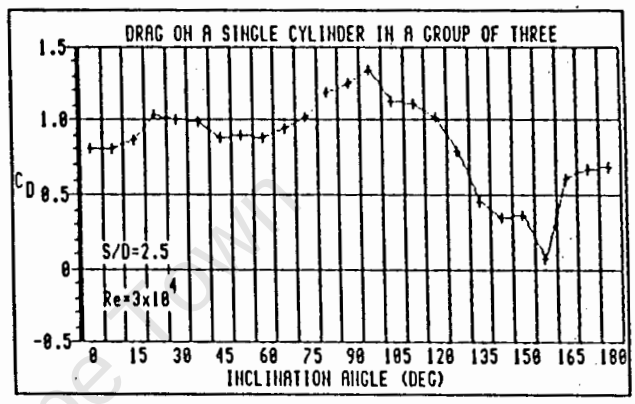


(d)

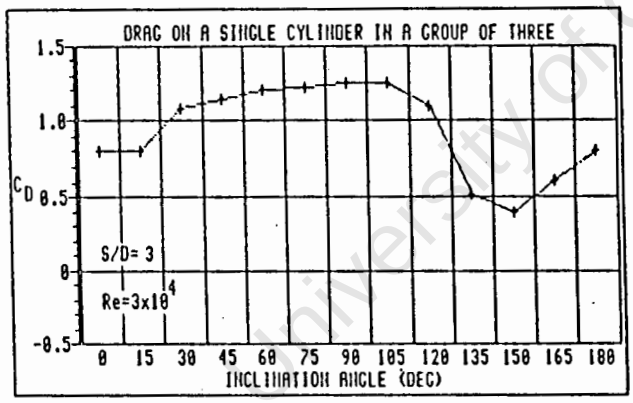


(e)

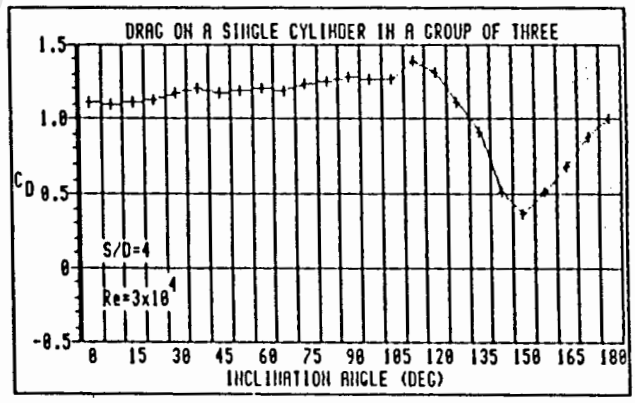


(f)

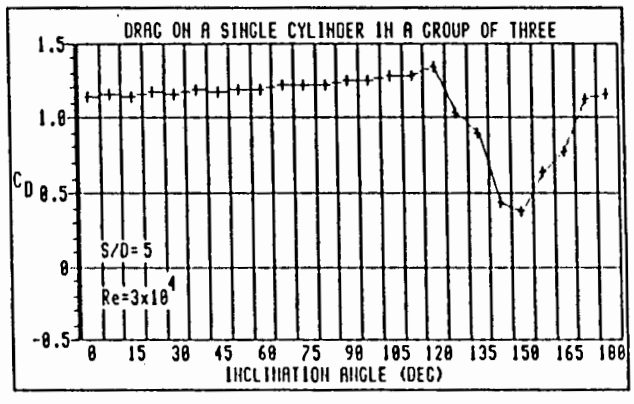


(g)

Fig. 8.3 Drag coefficient on cylinder 1 in the group of three cylinders versus group inclination angle α

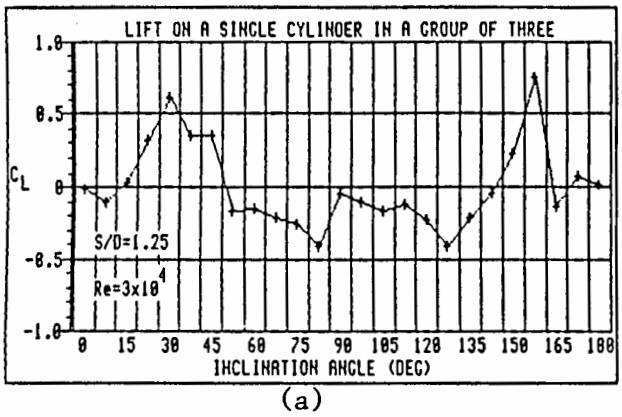


(a)

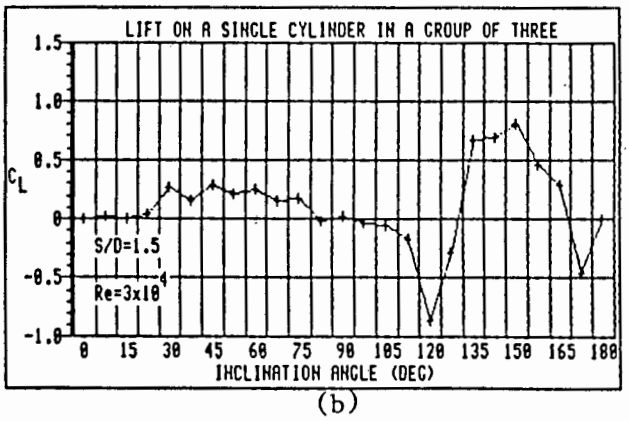


(b)

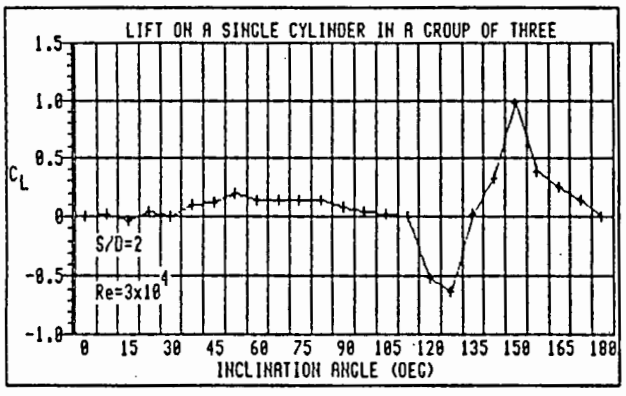


(c)

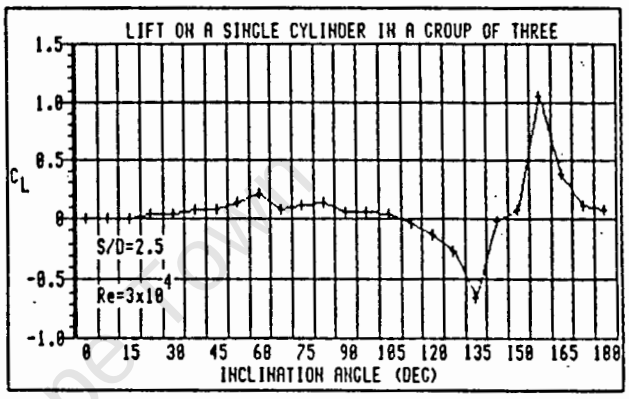


(d)

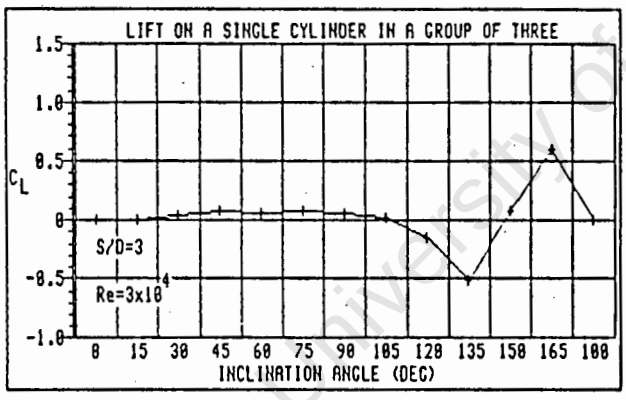


(e)

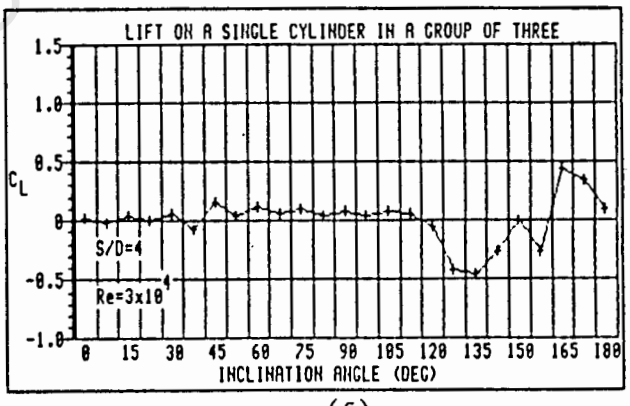


(f)

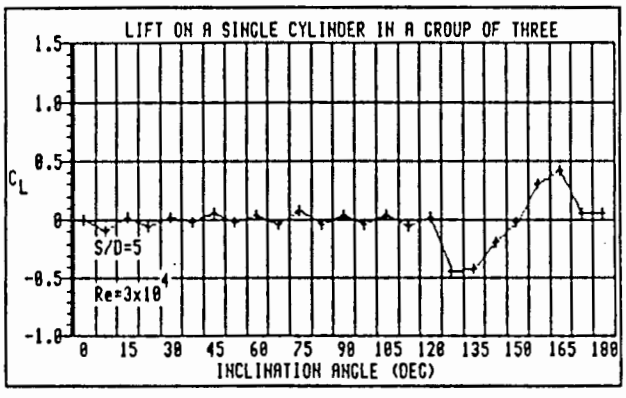


(g)

Fig. 8.4 Lift coefficient on cylinder 1 in the group of three cylinders versus group inclination angle α

and this variation is shown in Fig. 8.7.

For S/D of 4 and 5 at $\alpha$ = 0 degrees (Fig. 8.3), cylinder 1 behaves as if it were isolated, the drag coefficients of 1.1 being the same as for the single cylinder. As S/D decreases, the downstream cylinders 2 and 3 begin to affect the flow over cylinder 1, its drag coefficient dropping to 0.44 at a spacing of 1.25D. The reason for the decrease is clearly shown in Fig. 8.8 where the negative pressure coefficient on the downstream part of the cylinder becomes positive, while the front positive pressure coefficient between $30>\theta>270$ degrees remains virtually unchanged. When the cylinders are rotated, for S/D of 4 and 5, cylinder 1 exhibits a steadily increasing drag coefficient rising to 1.4 at about 120 degrees although there is some evidence of fluctuating pressures for S/D of 4. It is concluded that the lower cylinder 2 is affecting the flow around cylinder 1, and is of the proximity type interference. For S/D between 3 and 1.25, Fig. 8.3 shows the maximum $C_D$ on cylinder 1 occurring at decreasing angles of inclination, this being due to increasing combined proximity and wake interference. From the maximum $C_D$ attained, all spacings show a steep drop to a minimum $C_D$ at an inclination of about 150 degrees, when cylinder 1 is directly in line with cylinder 3 as if in a two cylinder tandem arrangement. At $\alpha$ = 180 degrees, the drag coefficient returns to the isolated cylinder value for the large spacing but is increasingly affected by proximity and wake interference as the spacing decreases. The general trend of the drag curves in Fig. 8.3 show similar features to those obtained by Bardowicks (1985) [20]. However, nowhere did he obtain negative drag coefficients at small spacings as obtained in these experiments and

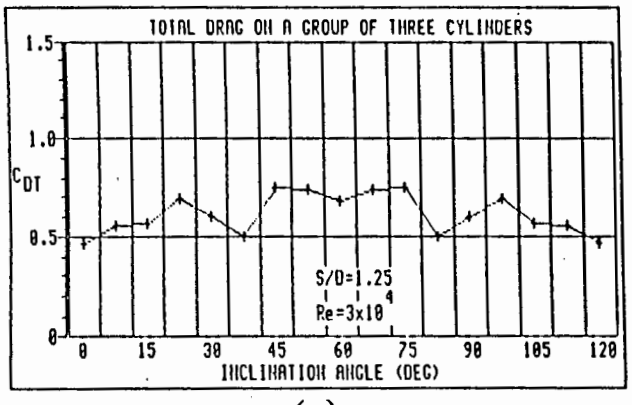


(a)

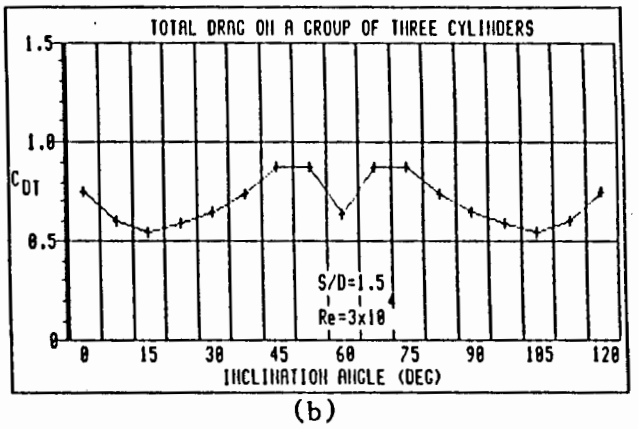


(b)

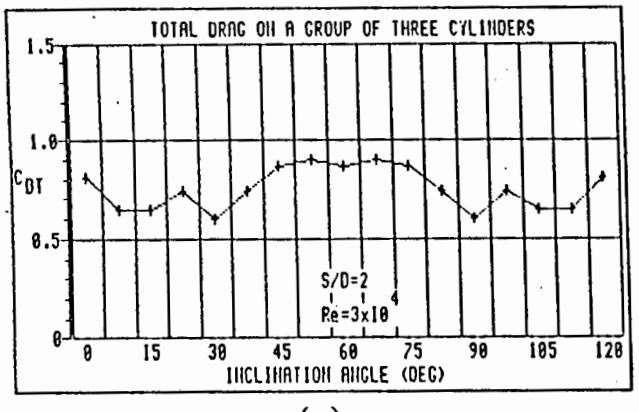


(c)

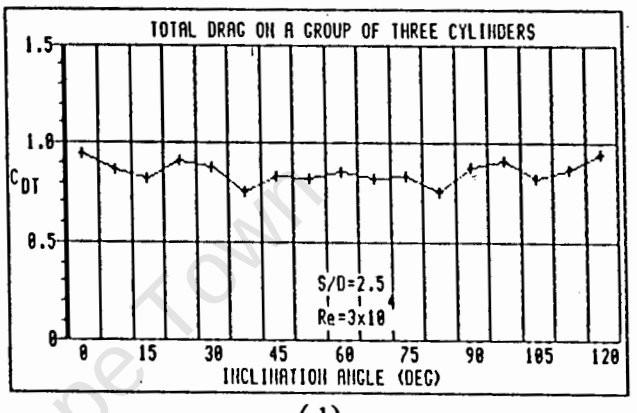


(d)

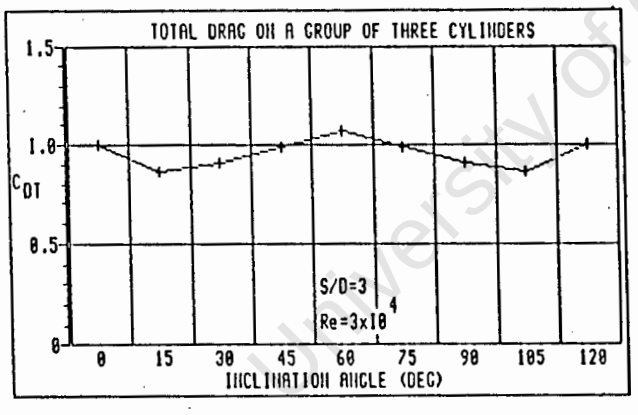


(e)

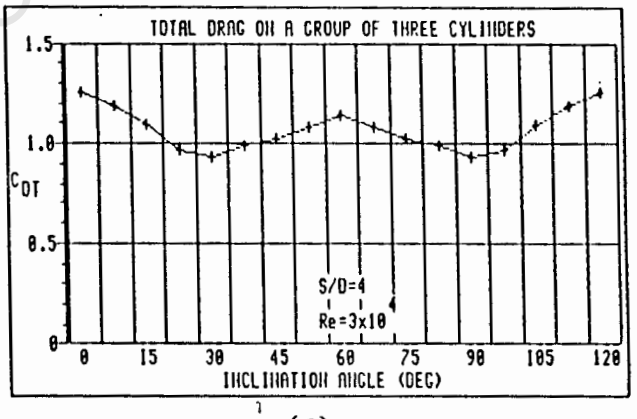


(f)

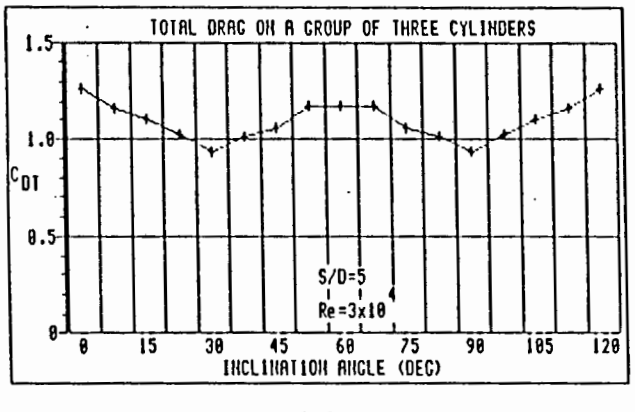


(g)

Fig. 8.5 Total drag coefficient for the group of three cylinders versus group inclination angle $\alpha$

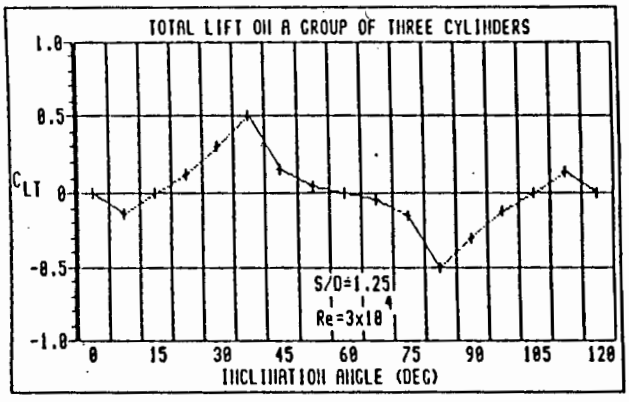


(a)

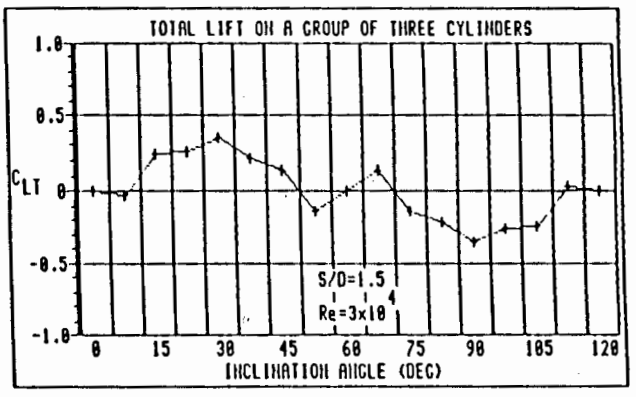


(b)

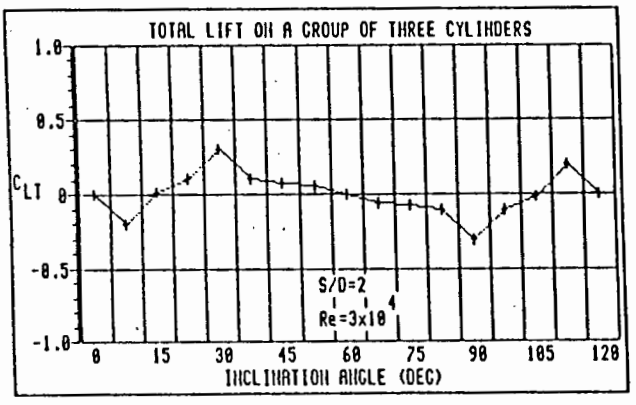


(c)

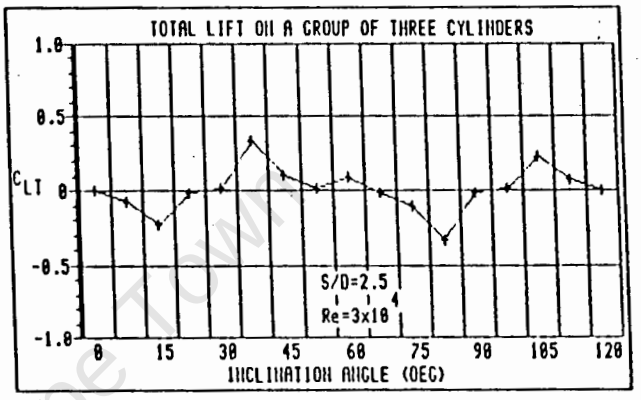


(d)

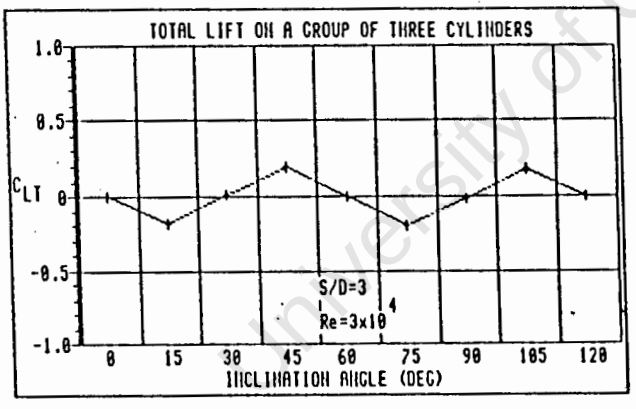


(e)

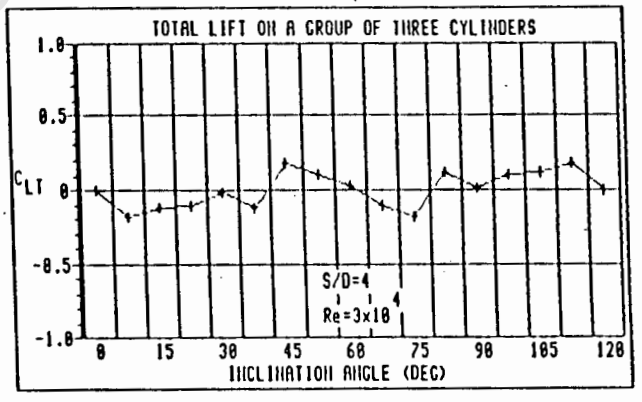


(f)

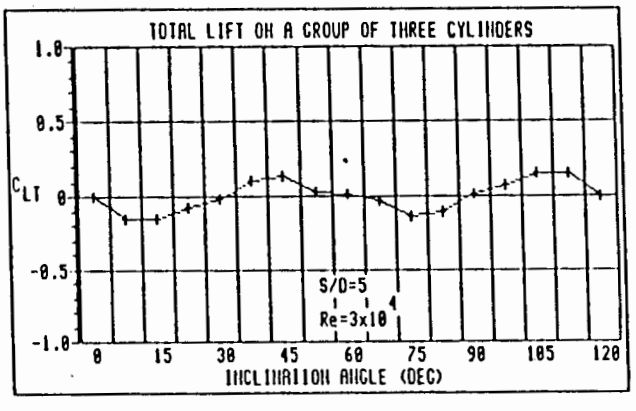


(g)

Fig. 8.6 Total lift coefficient for the group of three cylinders versus group inclination angle α

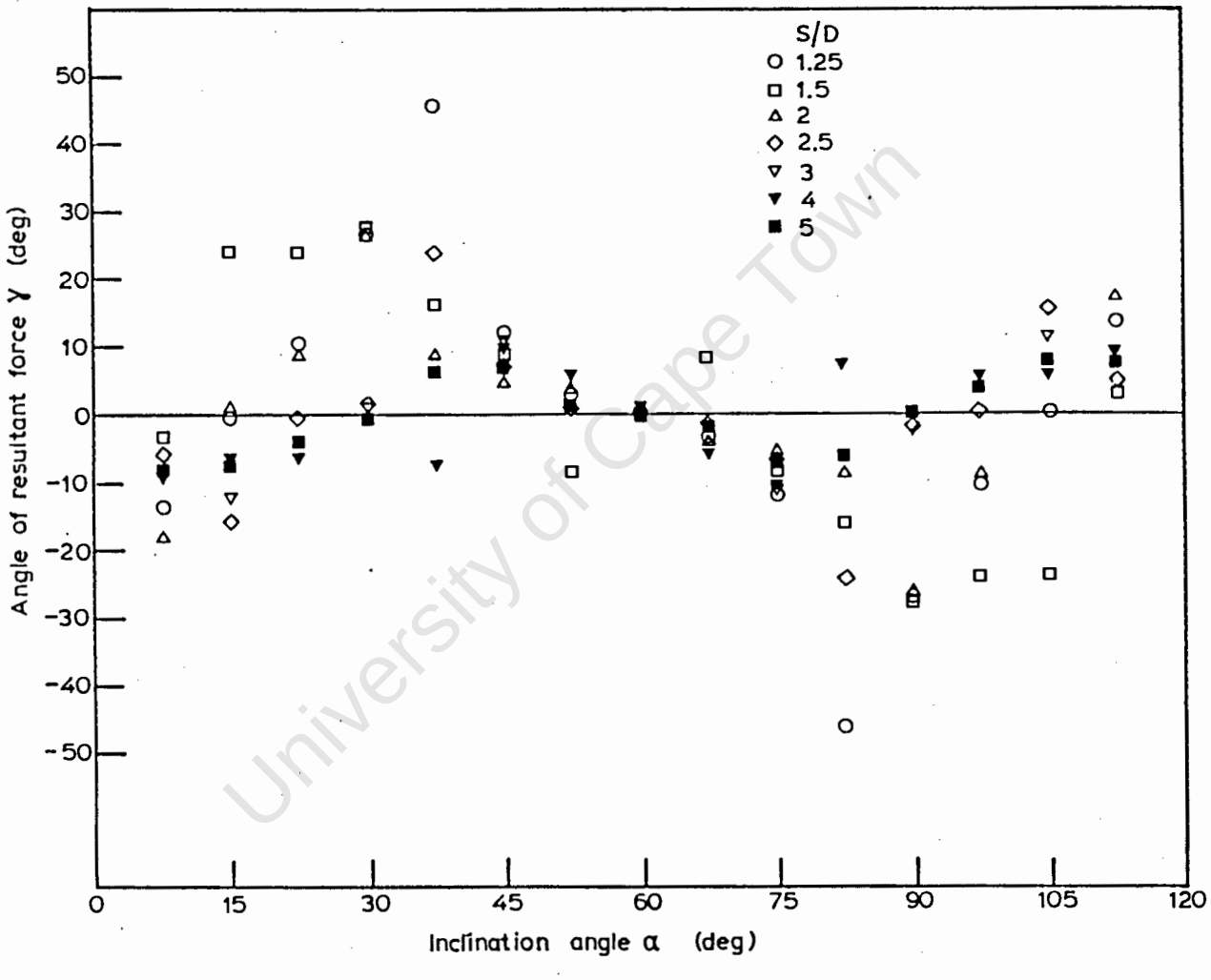




Fig. 8.7 Variation of the direction of the resultant force acting on the group of three cylinders

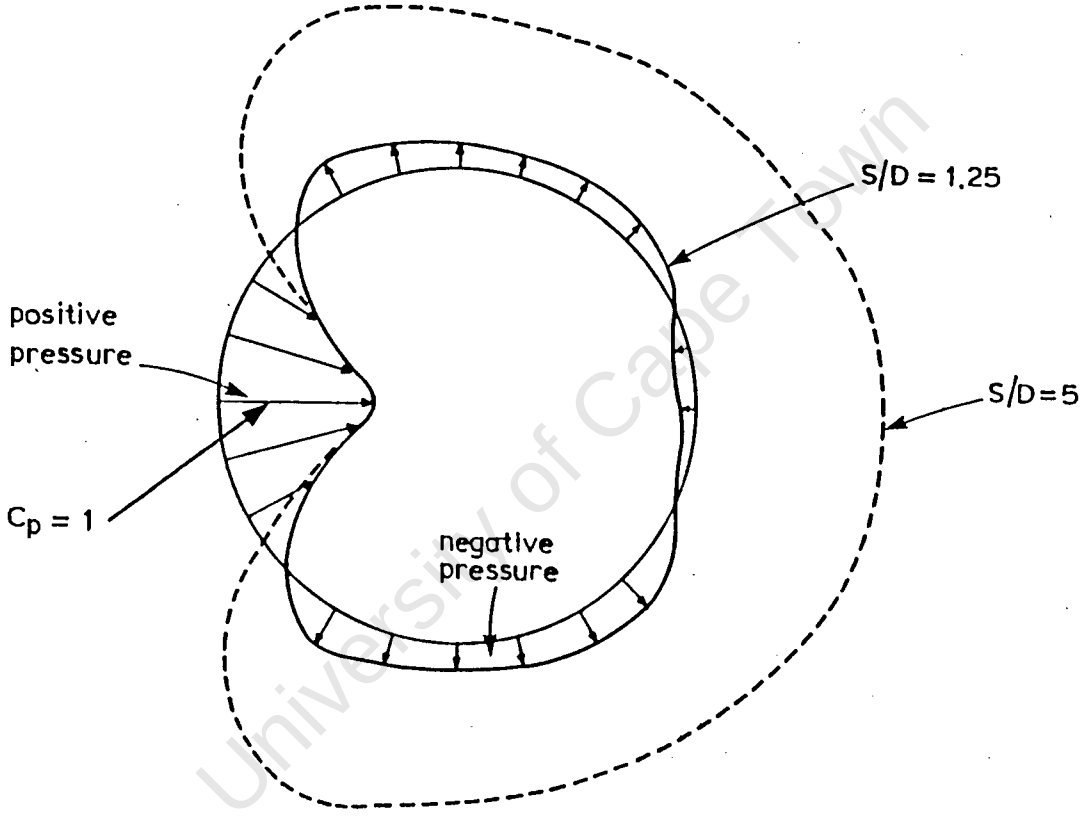




Fig. 8.8 Polar plots of pressure coefficient around cylinder 1 at $\alpha$ = 0 degrees. ($C_p$ measured radially from surface)

this is attributed to flow along the span of the cylinder caused by flow over the ends of his finite length cylinders.

## 8.3 LIFT COEFFICIENTS ON A SINGLE CYLINDER IN A GROUP OF THREE

In Fig. 8.4, negative lift forces are those directed towards the axis of the test section. At S/D = 5, Fig. 8.4g shows almost zero lift in the range $0<\alpha<120$ degrees indicating symmetry of flow about the horizontal axis of the cylinder. At 127.5 degrees, cylinder 1 experiences a sudden inward lift force due to wake interference from cylinder 3 which is now at the 7.5 degree position. In effect, the edge of the wake generated by cylinder 3 acts as a boundary and prevents the streamlines on the underside of cylinder 1 from diverging as much as they would were the wake not present. This causes an increase in velocity on the underside of cylinder 1 and a consequent reduction in pressure. The situation persists to 135 degrees at which point the pressure starts to recover to give a positive lift coefficient at $\alpha$ = 165 degrees when cylinder 3 is lying above cylinder 1, its wake now acting on the opposite side of cylinder 1. Cylinder 2 has no effect on the flow around cylinder 1.

As the spacing decreases, a bias towards a positive lift force develops for $\alpha>30$ degrees whilst the change to the negative lift force become less severe. There is also a tendency for the magnitude of the negative lift to increase as also does the magnitude of the recovery on the positive side. For $2< S/D <5$, maximum and minimum lift occur at more or less the same inclination angle and the curves in general exhibit the

same characteristics. In contrast, at S/D = 1.25, rapid changes in lift force are noted at inclination angles of 7.5, 30 and 82.5 degrees, and it would appear that at S/D = 1.5 a transient state exists between the two types of flow regimes. In the case of two cylinders in tandem, Zdravkovich et al (1977) [10] found that for 2.7< S/D <4 the lift coefficient on the downstream cylinder was positive or very close to zero. This is confirmed here by examining the lift at $\alpha$ = 150 degrees since in this position cylinders 3 and 1 are situated in tandem with the lift being measured on the effective downstream cylinder 1. However, Zdravkovich et al [10] also inferred a negative lift coefficient in tandem arrangement for S/D <2.7 but for the three cylinder case at similar spacings, Figs. 8.4a to 8.4c show that the lift is clearly positive indicating a strong interference from the lower cylinder 2. The upstream cylinder 3 at S/D = 1.25 also shows a high positive lift at $\alpha$ = 30 degrees indicating proximity interference from the lower cylinder 2.

Cylinders 1 and 3 are in a transverse arrangement at $\alpha$ = 60 degrees and Figs. 8.4b to 8.4g show positive lift forces the order of which are in agreement with the results of Zdravkovich et al (1977) [10] for the two cylinder case. As the spacing decreases the velocity of the flow in the gap between the cylinders increases, with the interference being of the proximity type.

## 8.4 TOTAL FORCE COEFFICIENTS ON THE GROUP OF THREE CYLINDERS

The total lift and drag data points shown in Figs. 8.5 and 8.6, and the angle of the resultant force acting on the group shown in Fig. 8.7, indicate how rapidly the total force components can change with relatively small changes in flow direction. In general, the total drag is greater as the spacing ratio increases due to each of the individual cylinders behaving more as an isolated one. Conversely, the total lift coefficient tends towards zero with increasing S/D but shows wide positive to negative changes as the cylinders move towards each other. Although the magnitude of the resultant force might be low, rapid changes in its direction could present important design problems in situations where the flow direction is constantly changing.

## 8.5 CONCLUSIONS

It has been shown that for a standard equispaced group of three cylinders arranged with centres forming an equilateral triangle, the angle of orientation of the group to the free stream will strongly influence the force coefficients acting on any one of the cylinders. Large reversals in lift magnitude and direction occur at inclination angles lying between 120 degrees and 165 degrees for all cylinder spacings tested, whilst a minimum drag is found at about 150 degrees. At some spacings the force coefficients were similar to those for flow interference between two cylinders. The total force coefficients for the three cylinder structure as a unit can

also exhibit large variations in magnitude and direction and care should be taken in the design of such structures especially when a variable direction free stream flow is present.

# CHAPTER 9

## RESULTS AND DISCUSSION CONCERNING THE PRESSURE DISTRIBUTION AROUND A SINGLE CYLINDER IN A GROUP OF FOUR

### 9.1 DRAG COEFFICIENTS ON A SINGLE CYLINDER IN A GROUP OF FOUR

Equations (8.1), (2.33) and (2.32) are again used to determine the pressure, drag and lift coefficients, the latter two being shown in Figs. 9.1 and 9.2. The total force coefficients are similarly determined by the summation of the individual drag and lift coefficients of the four cylinders as described below. Considering a spacing ratio of 1.1, from Figs. 9.1a and 9.2a, at an inclination angle of 15 degrees, the drag and lift coefficients of each cylinder are

| Cylinder No. | 1 | 2 | 3 | 4 |
|---|---|---|---|---|
| $\alpha$ (degrees) | 15 | 105 | 195 | 285 |
| Equivalent angle | 15 | 105 | 165 | 75 |
| $C_D$ | 0.85 | 0.39 | 0.09 | 0.91 |
| $C_L$ | 0.49 | -0.34 | 0.08 | -0.15 |

The negative sign indicates a lift force directed towards the axis of the wind tunnel test section. When these coefficients are summed, noting that the total cross sectional area is now

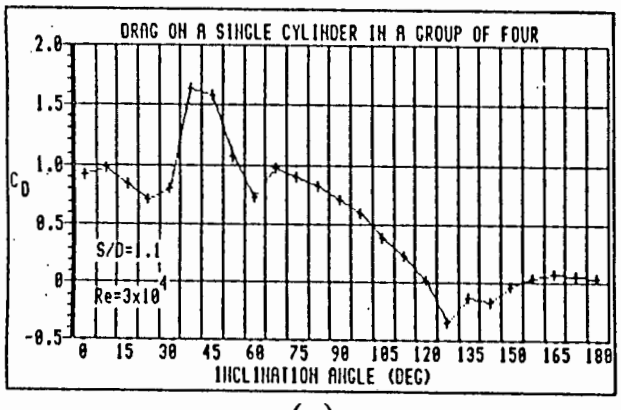


(a)

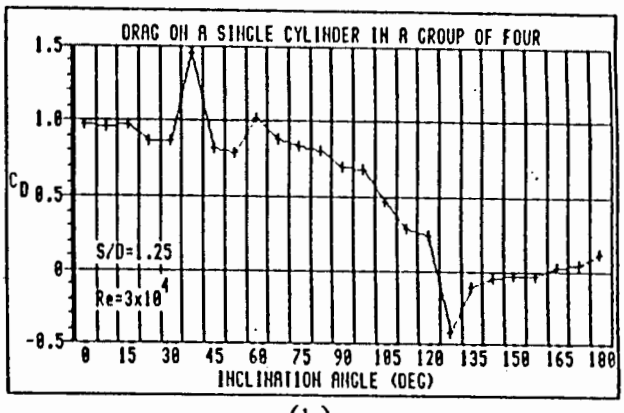


(b)

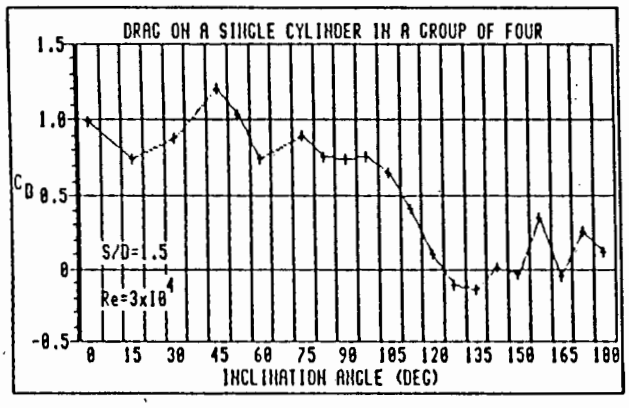


(c)

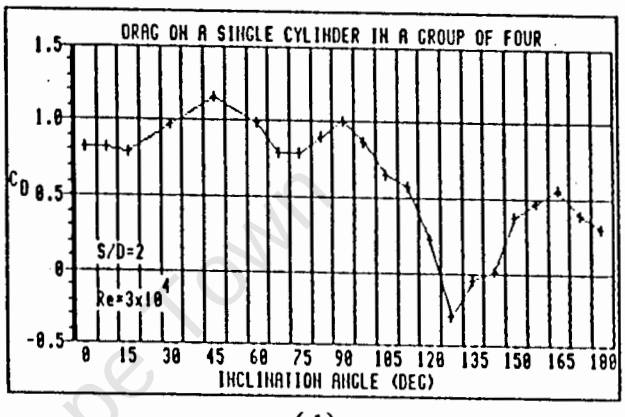


(d)

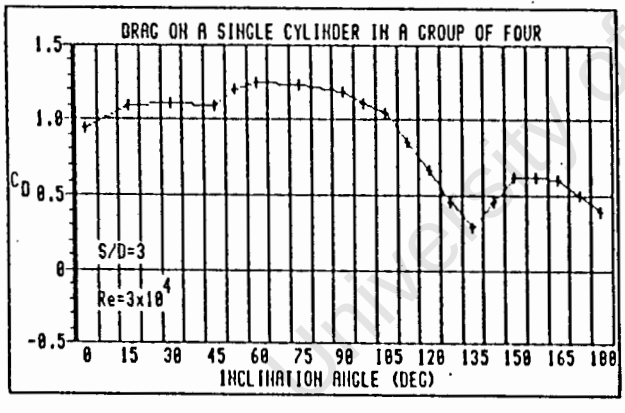


(e)

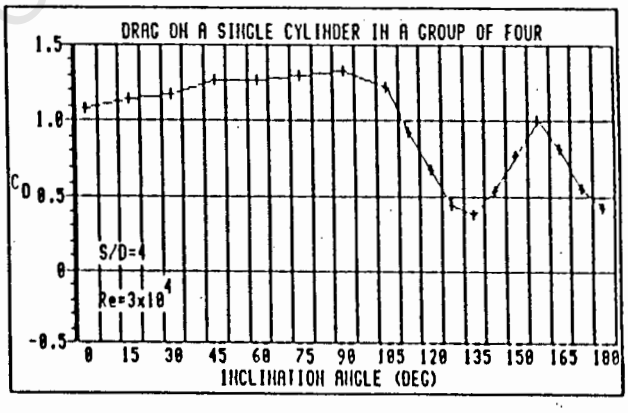


(f)

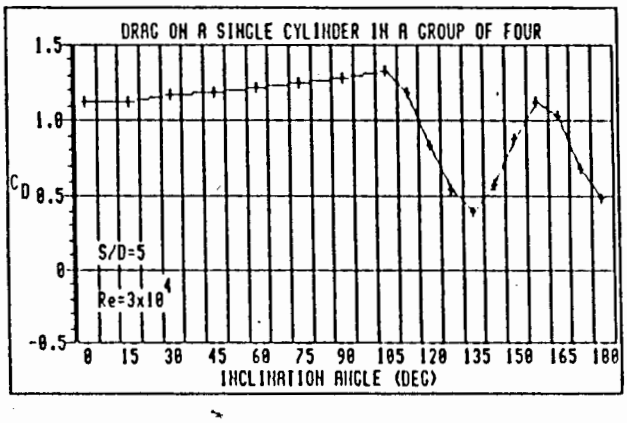


(g)

Fig. 9.1 Drag coefficient on cylinder 1 in the group of four cylinders versus group inclination angle α

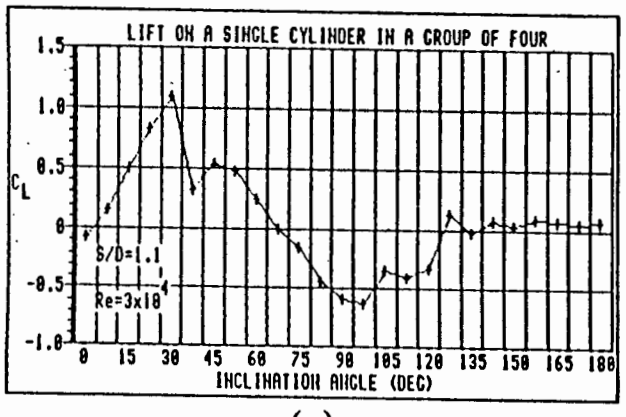


(a)

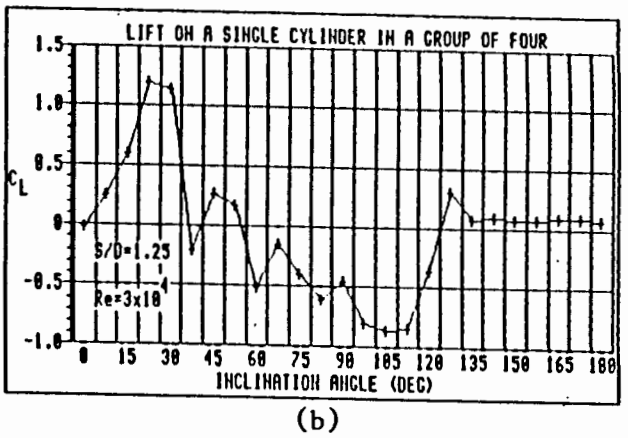


(b)

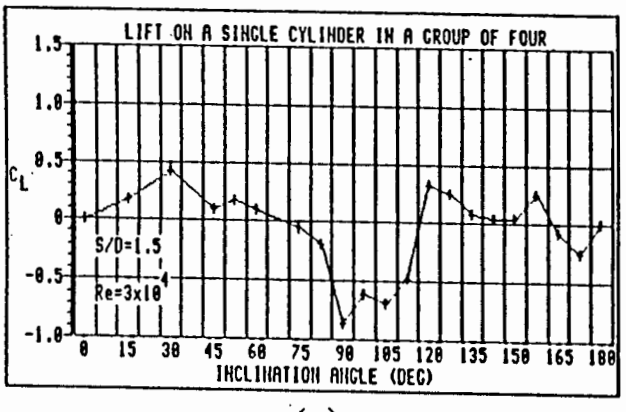


(c)

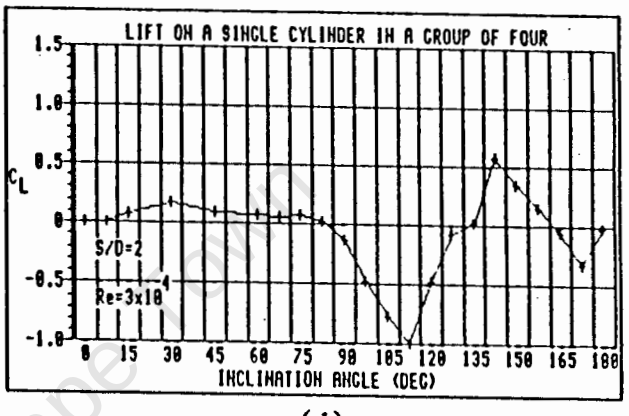


(d)

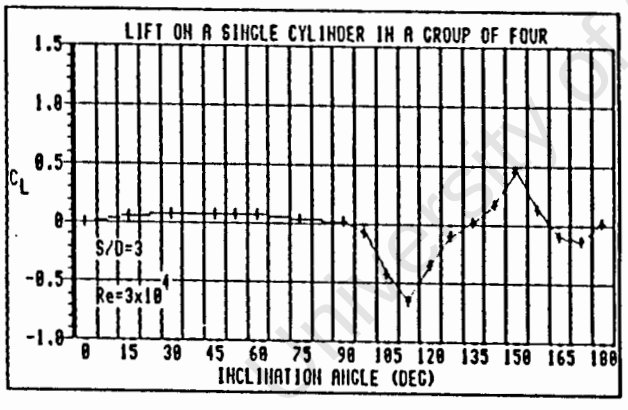


(e)

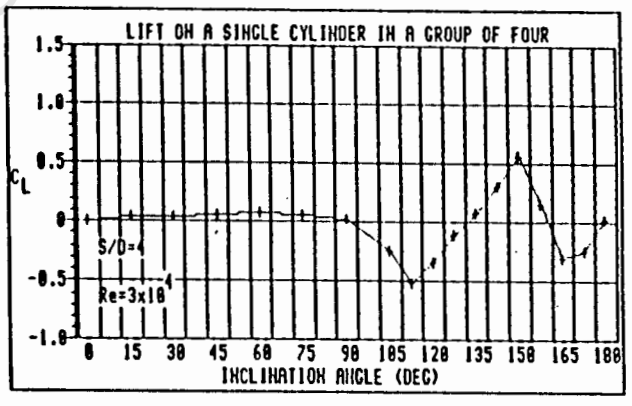


(f)

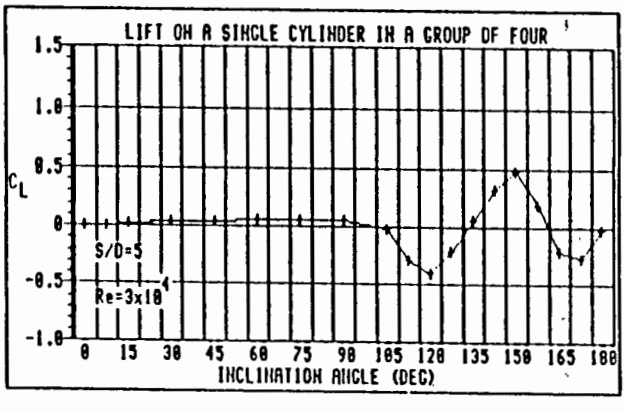


(g)

Fig. 9.2 Lift coefficient on cylinder 1 in the group of four cylinders versus group inclination angle α

4D, the total drag and lift coefficients $C_{D_T}$ and $C_{L_T}$ are obtained from equations (9.1) and (9.2).

$$C_{D_T} = (C_{D_1} + C_{D_2} + C_{D_3} + C_{D_4})/2\rho U^2 D \qquad (9.1)$$

$$C_{L_T} = (C_{L_1} + C_{L_2} + C_{L_3} + C_{L_4})/2\rho U^2 D \qquad (9.2)$$

The total force coefficients are shown in Figs. 9.6 and 9.7 where they repeat themselves every 90 degrees. The direction of the resultant force acting on the group of four cylinders as a whole is calculated from equation (8.4), and its variation with inclination angle is displayed in Fig. 9.8.

At $\alpha$ = 0 degrees and spacing ratios of 4 and 5, cylinder 1 behaves as a single isolated cylinder in a two dimensional flow field, the drag coefficient of 1.1 being the same as that determined for the isolated cylinder in section 8.1. At a spacing ratio of 2, the drag coefficient has dropped to 0.82, but for a further decrease in spacing ratio, the drag coefficient recovers to remain steady at approximately 0.95. This is due to the presence of the adjacent cylinders affecting the pressure distribution around cylinder 1. Unlike the three cylinder case, the negative pressure coefficient does not become positive on the downstream part of cylinder 1, but as shown in Fig. 9.3, increases from -1.1 to only -0.49 as the cylinder spacing decreases. Also, the positive pressure coefficient acts over a much wider total angle at the smaller spacings than was the case for three cylinders, where it remained virtually unchanged. This spreading of the positive pressure coefficient on the upstream side of cylinder 1 negates the increase in pressure on the downstream side.

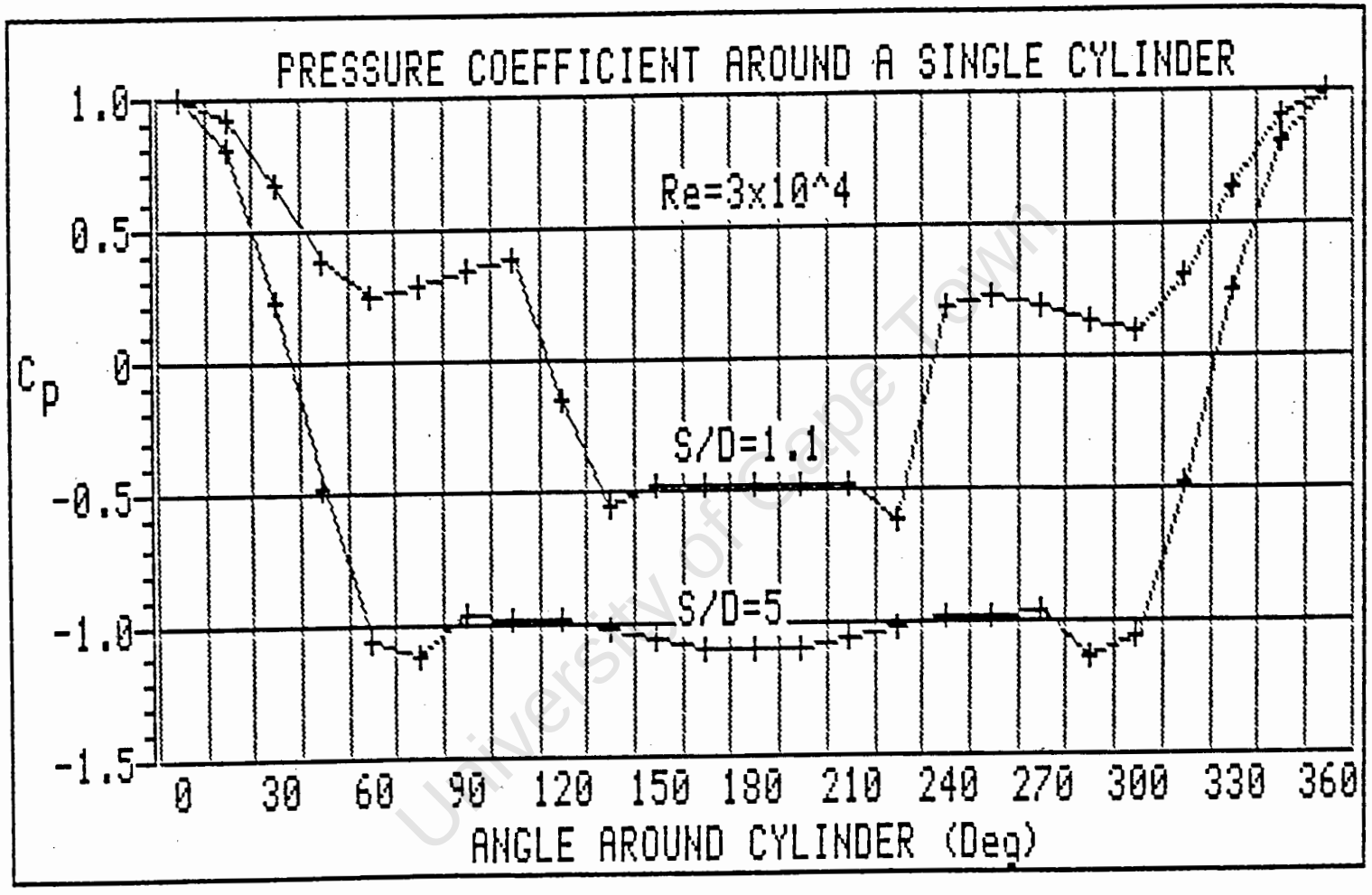


Fig. 9.3 Pressure coefficient around cylinder 1 in the group of four at $\alpha$ = 0 degrees

resulting in only a small change in drag coefficient.

As the group of cylinders is rotated, between 0 and 180 degrees, the shape of the drag coefficient curves for the different spacing ratios are similar in form to those for the three cylinder grouping but the inclination angles for maximum and minimum $C_D$ of cylinder 1 have changed. At spacing ratios of 1.1 and 1.25, the drag coefficient rises steeply over 7.5 degrees to a maximum value at an inclination angle of 37.5 degrees. For further increases in spacing, the position of maximum $C_D$ occurs at increasing inclination angles although its rate of change and magnitude become less severe.

$C_D$ drops steeply to a negative value at an inclination angle of 127.5 degrees for $1.1 < S/D < 2$. A similar trend is observed for the range $3 < S/D < 5$ but the minimum $C_D$ occurs at $\alpha$ = 135 degrees and it remains positive. For the latter spacings, cylinder 1 (at $\alpha$ = 135 degrees) is directly behind cylinder 4 (at $\alpha$ = 45 degrees) and flow interference is of the wake type only since the cylinders are now far enough apart not to affect the flow appreciably. With the lower spacings, both proximity and wake interference are of importance, the adjacent cylinders deflecting the flow and as a result causing the minimum $C_D$ to occur when the cylinders 1 and 4 are not in line. The changes in $C_D$ are closely mirrored by the variation in base pressure coefficient shown in Fig. 9.4, and it may therefore be concluded that the drag coefficient is highly dependent on the base pressure coefficient $C_{p_b}$.

For all spacings, $C_D$ recovers from its minimum value and except for spacings of 1.1 and 1.25, it peaks again at an inclination of 157.5 degrees this being due to the displacement

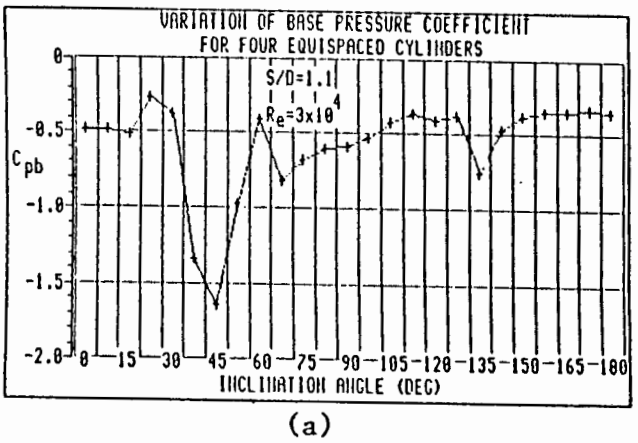


(a)

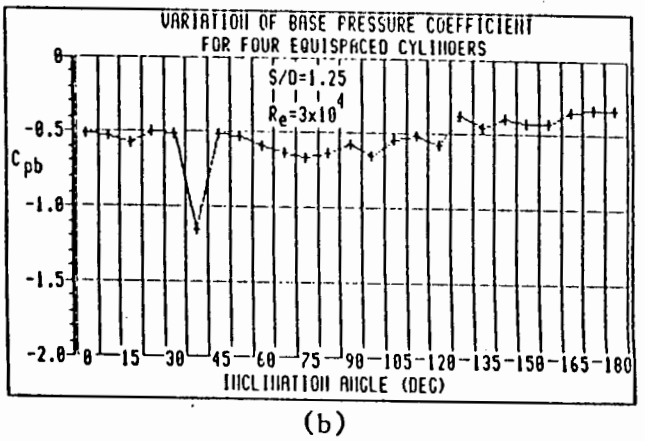


(b)

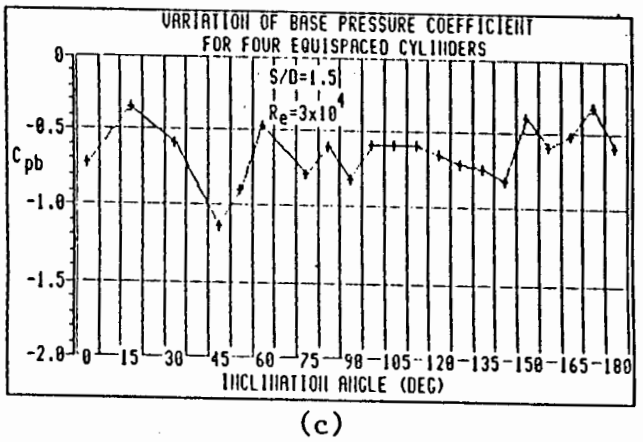


(c)

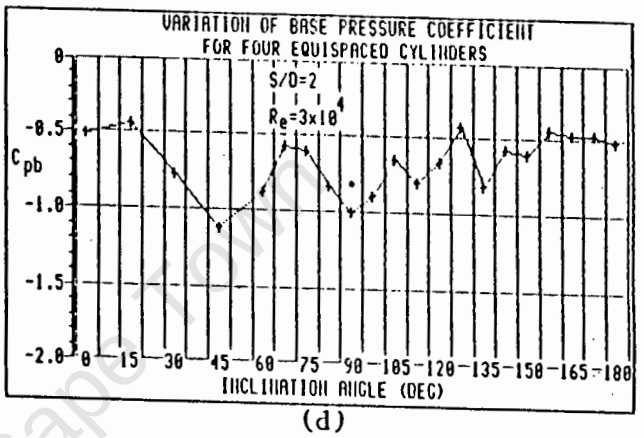


(d)

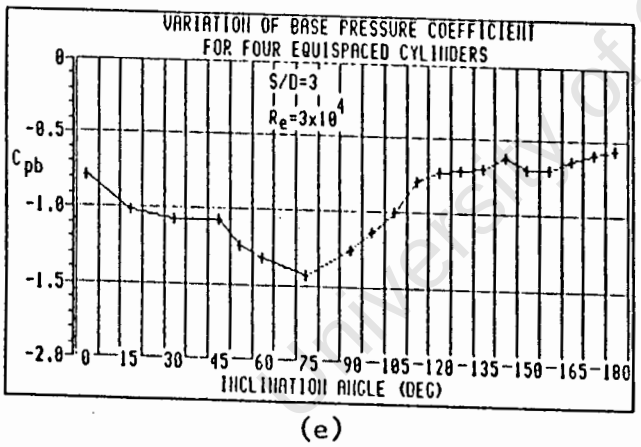


(e)

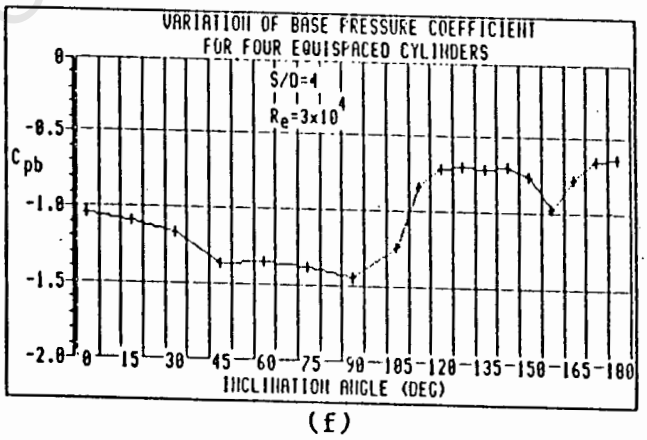


(f)

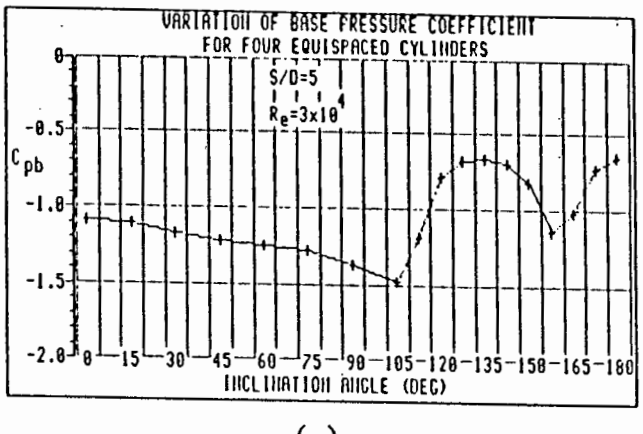


(g)

Fig. 9.4 Variation of base pressure on cylinder 1 with inclination angle α

of the wake from cylinder 4 (at 67.5 degrees) affecting the flow around cylinder 1. This effect diminishes as cylinder 1 moves out of the wake of cylinder 4 for further increases in inclination angle. The drag coefficient also gradually decreases to a value of half that for cylinder 3 (at the 0 degree position), the flow about cylinder 1 now being strongly affected by the wake shed from cylinder 3. At spacings of 1.1 and 1.25, proximity and wake interference reduce the drag coefficient to about zero.

## 9.2 LIFT COEFFICIENTS ON A SINGLE CYLINDER IN A GROUP OF FOUR

All spacing ratios in Fig. 9.2 show a zero lift coefficient for cylinder 1 at $\alpha$ = 0 degrees, indicating symmetry of flow about that cylinder. Considering first the range $2 < S/D < 5$ of Figs. 9.2(d-g), a bias towards a positive outwardly directed lift coefficient occurs for $0 < \alpha < 90$ degrees. At $\alpha$ = 90 degrees, the lift coefficient increases rapidly in the negative direction (i.e. inwards) where it reaches its maximum negative value at approximately 112.5 degrees, the magnitude of this value increasing as the cylinder spacing decreases. With cylinder 1 at 112.5 degrees, cylinder 4 is at an inclination angle of 22.5 degrees and therefore lies closer to the axis of symmetry. The edge of the wake of cylinder 4 extends past the lower side of cylinder 1 thereby creating an effective boundary. The flow passing around the lower side of cylinder 1 has a reduced cross sectional area and consequently a higher velocity and lower pressure than that on the upper side. This is clearly shown by the pressure distribution in Fig. 9.5. A

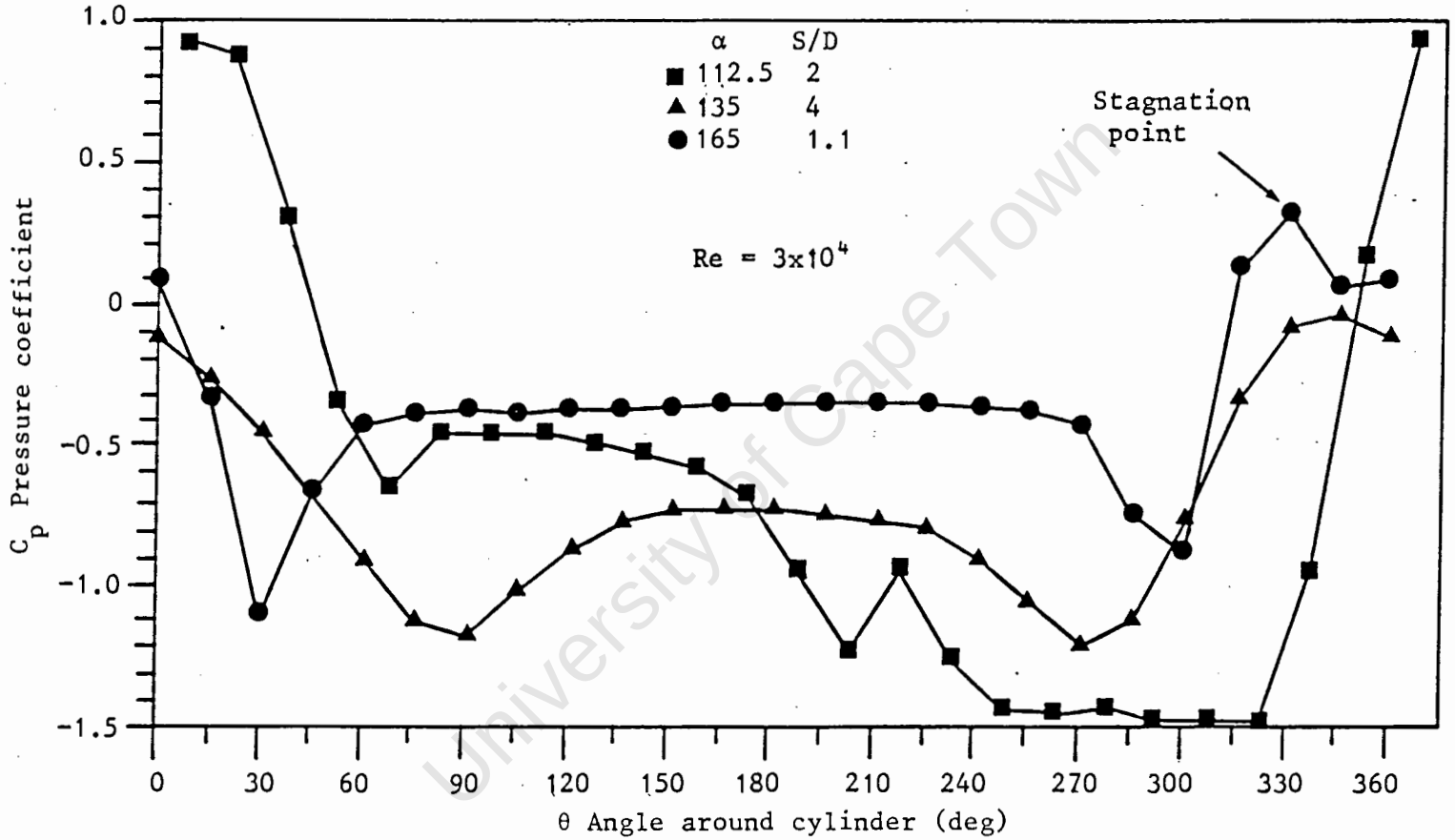


Fig. 9.5 Pressure distributions around cylinder 1 at various orientations and spacings

further increase in $\alpha$ causes part of the wake of cylinder 4 to stagnate on cylinder 1 and then to partially flow around it. At $\alpha$ = 135 degrees, the cylinders are in line with respect to the free stream, the flow around cylinder 4 being symmetrical as demonstrated by the zero lift coefficients and typical pressure distribution shown in Fig. 9.5. Increasing $\alpha$ still further now moves cylinder 4 above cylinder 1 and the reverse pressure distribution occurs to give a positive peaking lift coefficient at $\alpha$ = 150 degrees. Between 150 and 180 degrees, cylinder 1 becomes increasingly influenced by the wake of cylinder 2 which is moving towards the $\alpha$ = 0 degrees position.

In the range 1.1< S/D <1.5, Figs. 9.2a to 9.2c show that the lift coefficient increases from zero to peak at $\alpha$ = 30 degrees although there is evidence that this phenomenon is already underway at S/D = 2 (Fig. 9.2d). This is due to proximity interference of the lower cylinder 4 before cylinders 1 and 4 are in a transverse arrangement, when it might be expected that the greatest proximity interference would occur. However, the close proximity of all cylinders causes intense interaction of the wakes and makes any conclusions based on the two cylinder results of Zdravkovich and Pridden (1977) [10], of little value. At spacing ratios of 1.5 and 1.25, rapid fluctuations in $C_L$ indicate a transitory phase before stability is again established at S/D = 1.1. During this transitory phase, the magnitude of the change from a positive to negative lift coefficient with change in inclination angle becomes greater but less severe whilst the inclination angle at which maximum negative $C_L$ occurs, changes to 90 degrees when cylinder 1 is at its outermost position. This movement

from the 112.5 degree position at the wide spacing ratios indicates strong proximity interference as opposed to wake interference and gives rise to high velocities in the gaps between the cylinders and subsequently high negative pressure coefficients in the range $210<\alpha<315$ degrees. Increasing from 90 to 180 degrees sees a return to an almost zero lift coefficient at $\alpha$ = 135 degrees when cylinder 1 is in tandem behind cylinder 4. In the range $135<\alpha<180$ degrees, the lift coefficient is slightly positive biased and this is due to a stagnation point occurring at $\alpha$ = 330 degrees as shown in Fig. 9.5.

## 9.3 TOTAL FORCE COEFFICIENTS ON THE GROUP OF FOUR CYLINDERS

In comparing Figs. 9.6 and 9.7 with Figs. 8.5 and 8.6, for the three cylinder grouping, it is seen that the variation in $C_{D_T}$ with $\alpha$ is of the same order, and that at high spacing ratios $C_{D_T}$ approaches unity due to the flow about the cylinders approaching that about a single isolated cylinder. Changes in $C_{L_T}$ are less extreme than for the three cylinder case but these changes increase with decreasing spacing ratio whilst the absolute values of $C_{L_T}$ are lower on either side of zero than in the three cylinder case. Fig. 9.8 shows that the greatest change in $\gamma$ occurs for low values of S/D. For spacing ratios of 4 and 5 the change in $\gamma$ is negligible, and therefore in variable direction flow fields, structures of this type should be designed with cylinder spacings of at least four diameters.

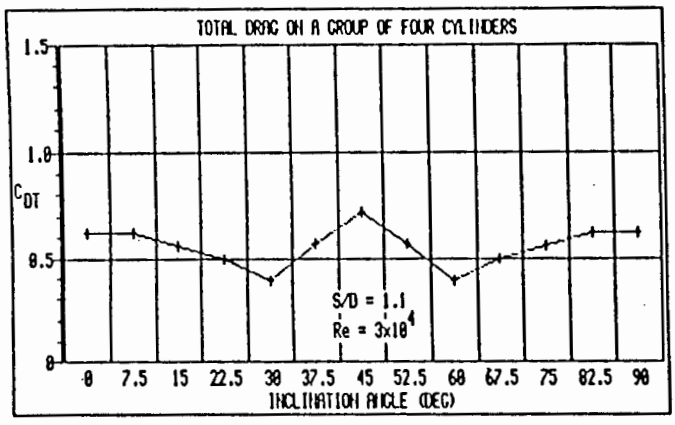


(a)

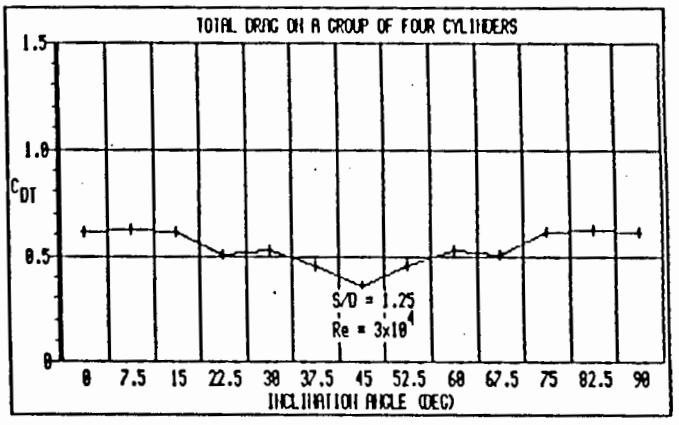


(b)

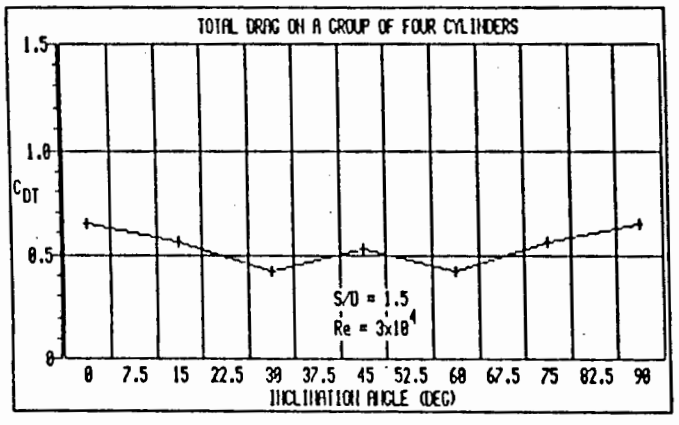


(c)

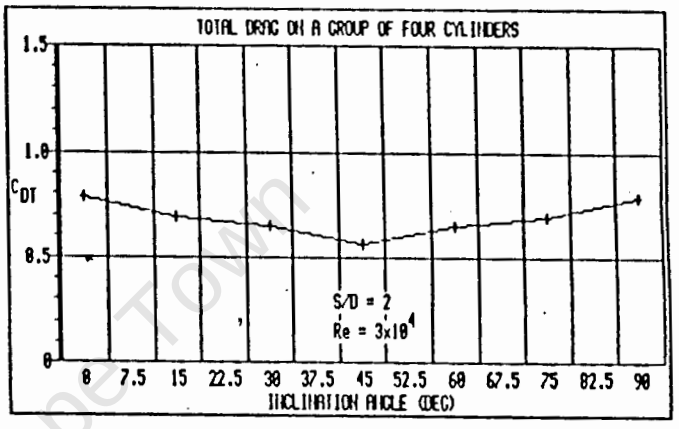


(d)

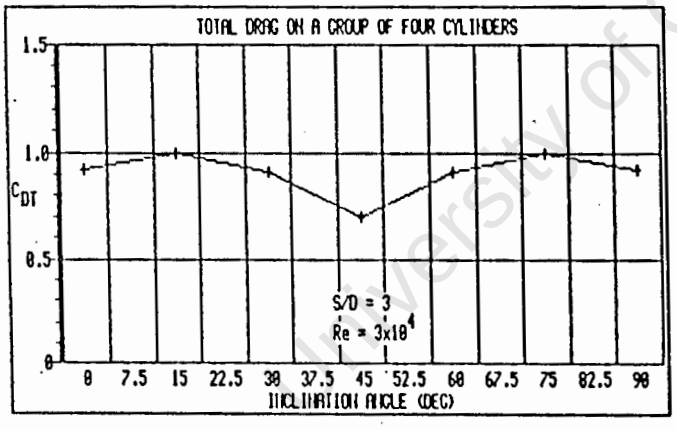


(e)

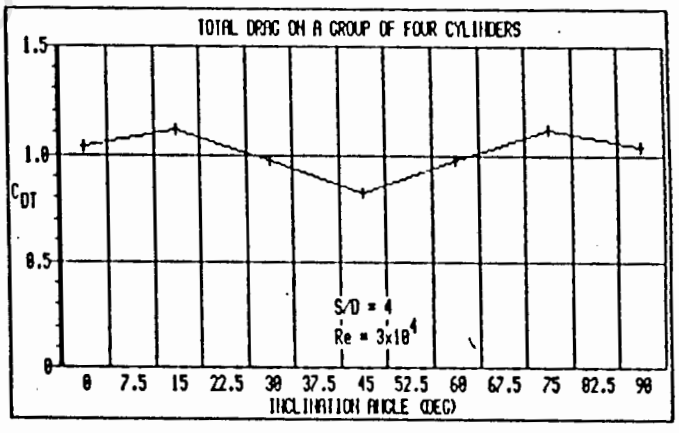


(f)

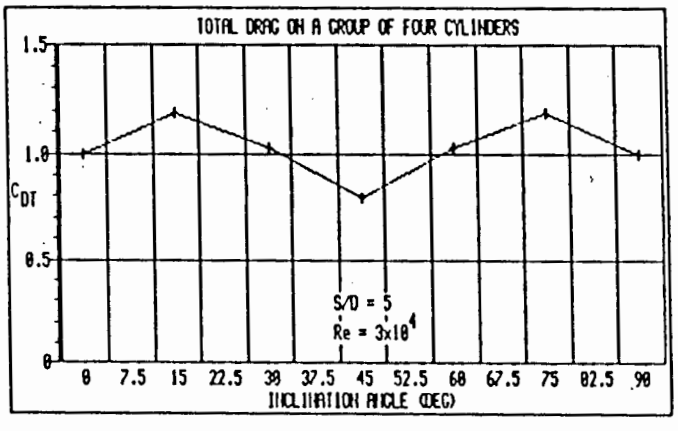


(g)

Fig. 9.6 Total drag coefficient for the group of four cylinders versus group inclination angle $\alpha$

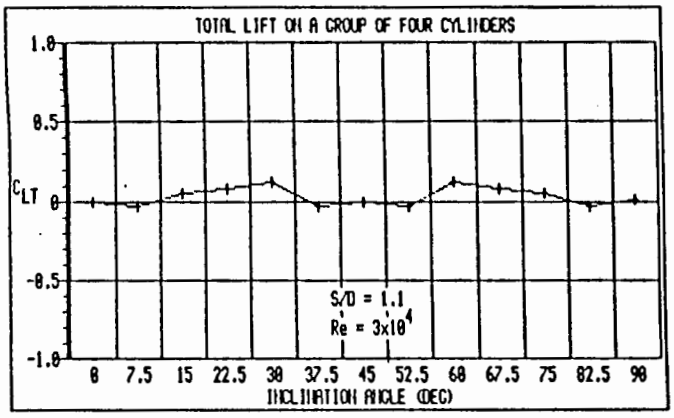


(a)

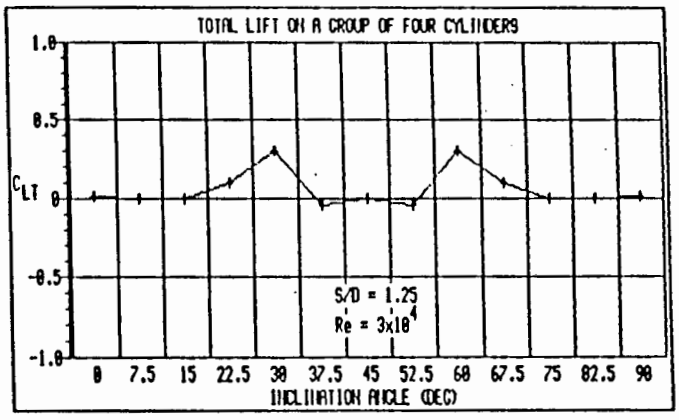


(b)

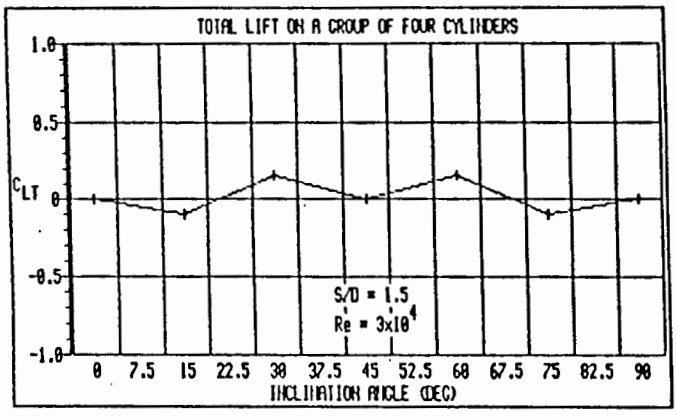


(c)

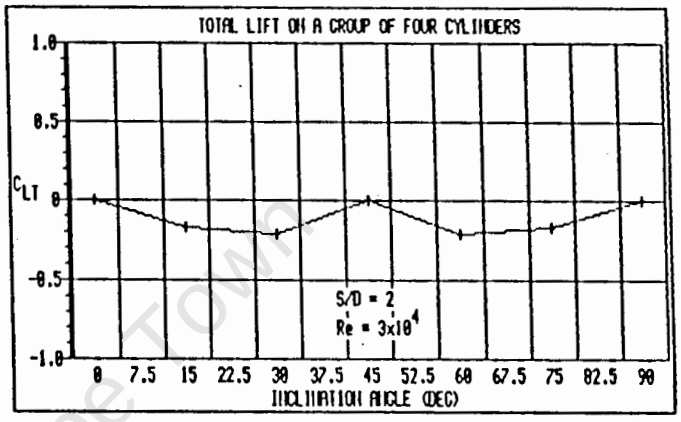


(d)

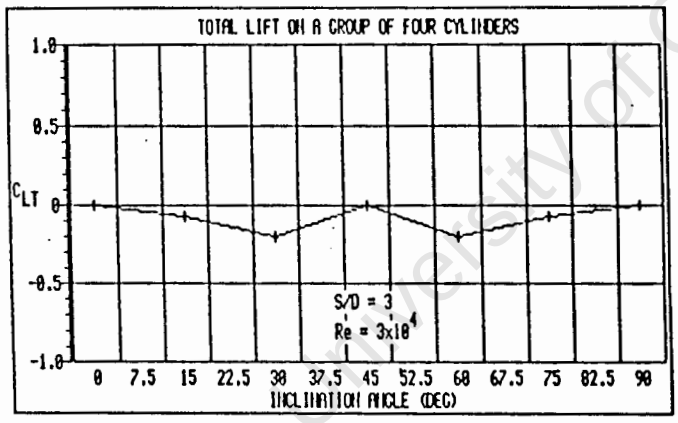


(e)

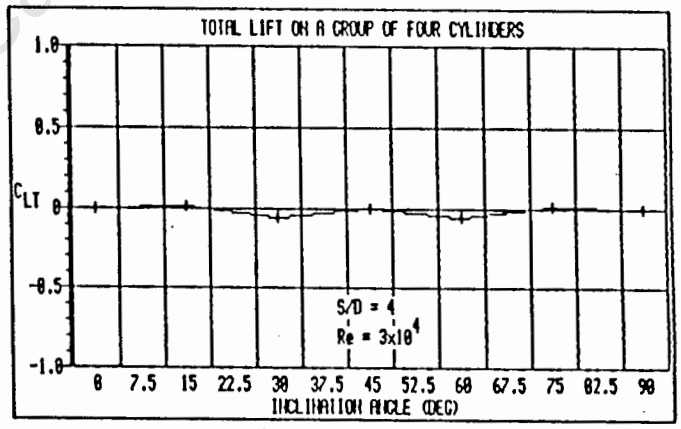


(f)

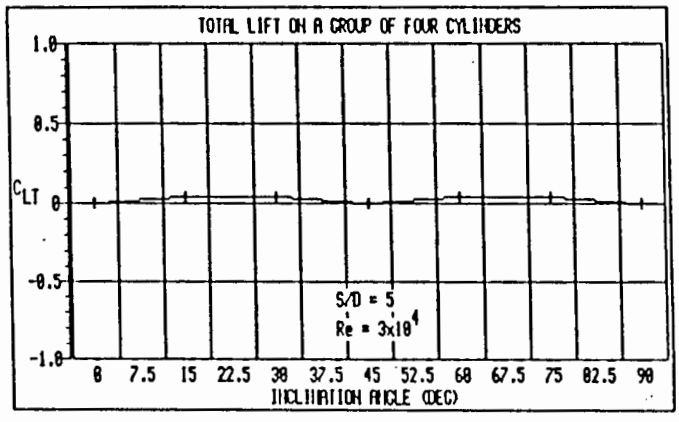


(g)

Fig. 9.7 Total lift coefficient for the group of four cylinders versus group inclination angle α

## 9.4 CONCLUSIONS

The lift and drag coefficients acting on a single cylinder in a group of four situated in a uniform free stream flow have been determined and they show that the forces acting on each cylinder of the group can vary widely. The magnitude of the coefficients is strongly influenced by the orientation of the group to the free stream with minimum drags occurring at inclination angles between 127.5 and 135 degrees. For all spacing ratios, rapid reversals in both lift and drag occur but greatest stability is achieved with higher spacing ratios, when large and rapid changes only take place between inclination angles of 90 and 180 degrees.

These results may be regarded as basic force coefficient data to be included with two and three cylinder data in a design code of practice.

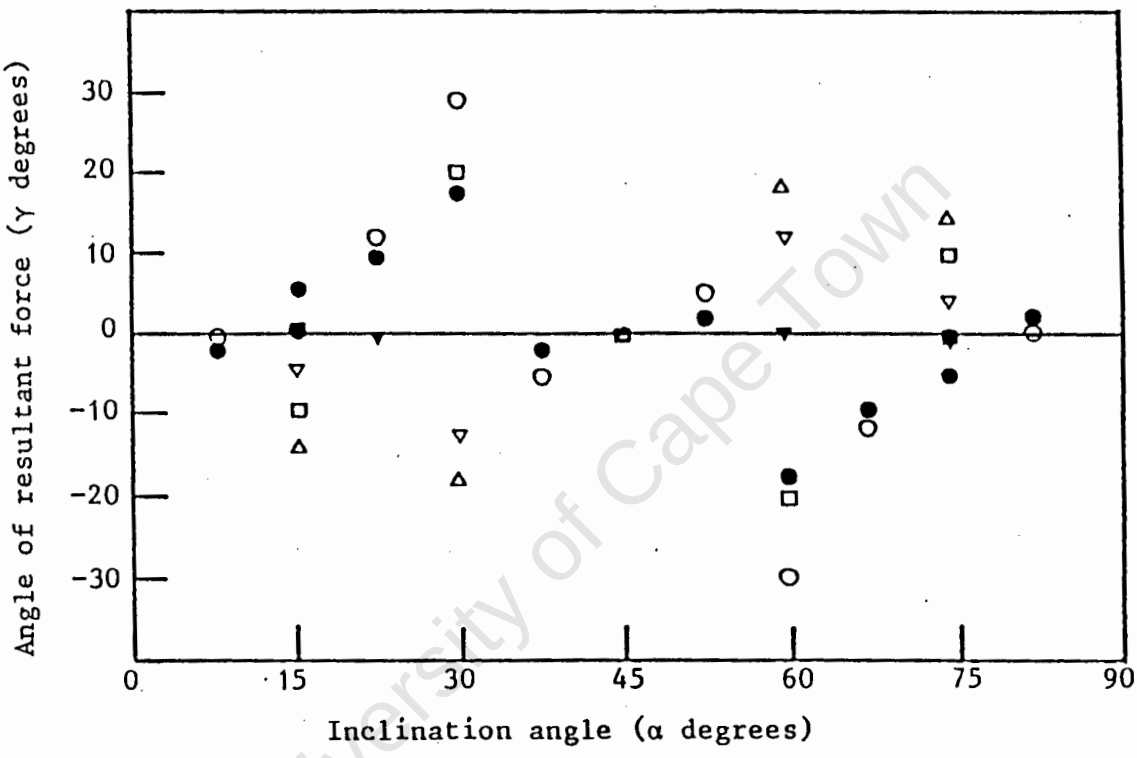


Fig. 9.8 Variation in the direction of the resultant force acting on the group of four cylinders. (S/D: ●1.1, ○1.25, □1.5, △2, ▽3, ▼4, ■5)

# CHAPTER 10

# COMPARISON BETWEEN POTENTIAL AND ACTUAL FORCE COEFFICIENTS

## 10.1 DRAG COEFFICIENTS ON A SINGLE CYLINDER IN A GROUP OF THREE

For cylinder spacing ratios greater than 1.5, and at all inclination angles of the group, Fig. 10.1a shows that cylinder 1 experiences almost no potential drag force. At $\alpha$ = 0 degrees and S/D = 1.5, the potential drag coefficient is only 0.1 compared to an actual drag coefficient of 0.76 as found in Fig. 10.1b.

When $\alpha$ = 90 degrees, the potential drag coefficient of cylinder 1 is zero at all spacings indicating symmetry of flow on either side of the cylinder's vertical axis. Further increases in $\alpha$ give the same drag coefficients in the negative upstream direction and the general form of this curve is repeated for all other spacing ratios. This flow symmetry is not attained in practice due to cylinder proximity, spacing ratio, viscous effects boundary layer formation and separation. Indeed, as Figs. 10.2 and 8.3 illustrate, in the real flow situation negative drag coefficients occur only briefly when $\alpha$ = 150 degrees. When $\alpha$ = 90 degrees the actual drag coefficients are always positive.

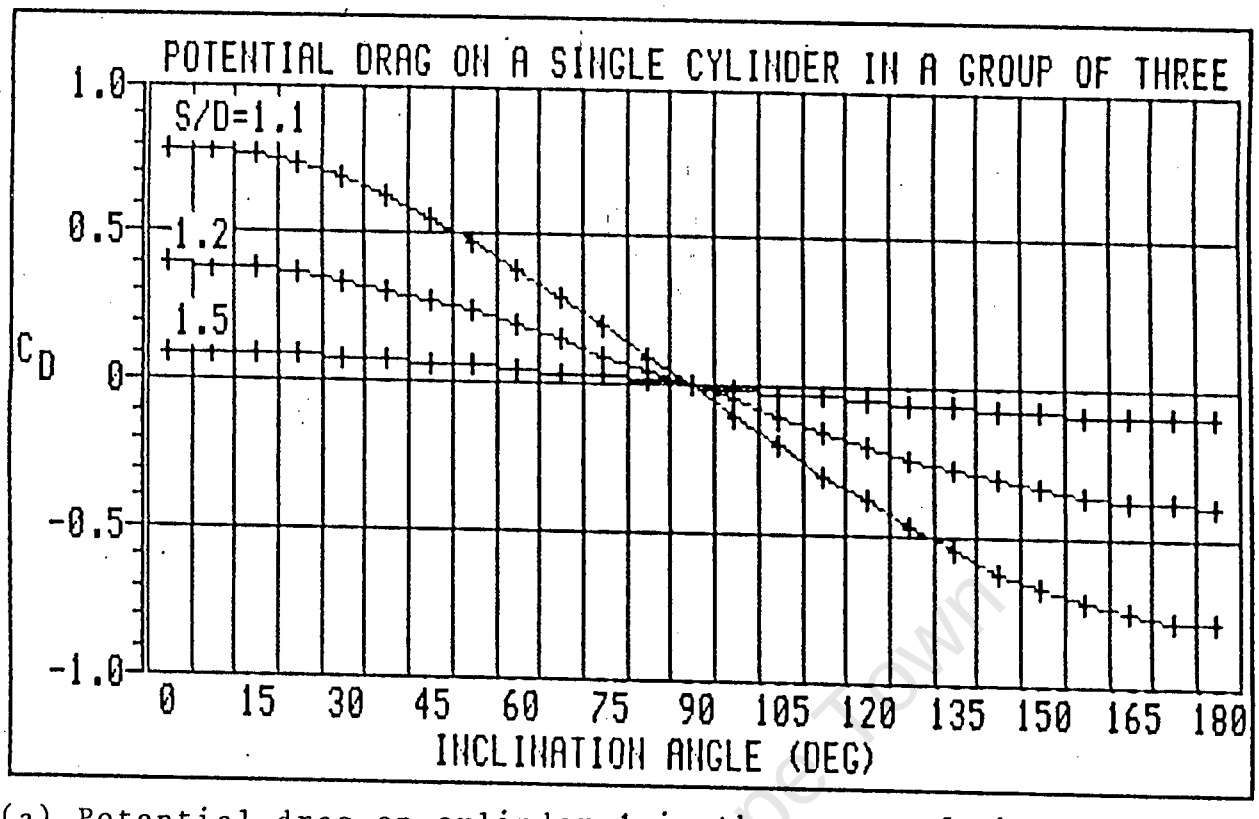


(a) Potential drag on cylinder 1 in the group of three

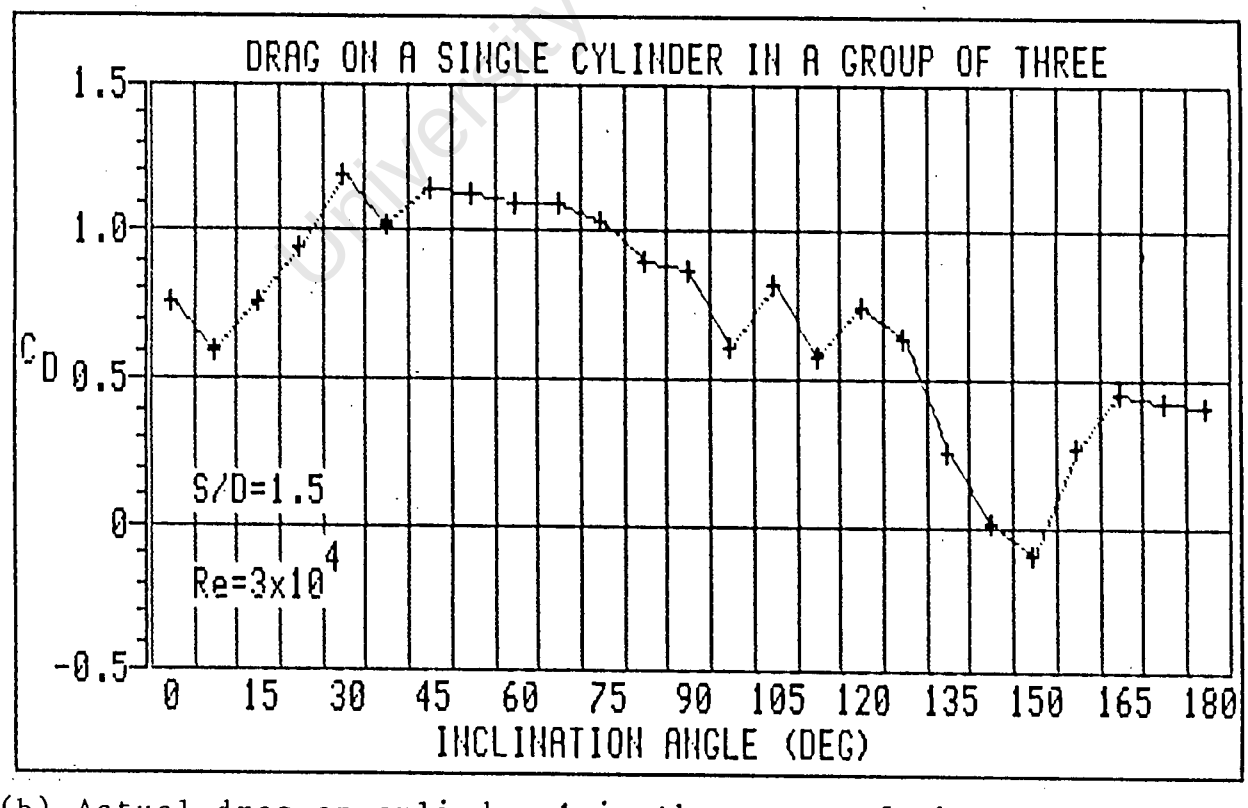


(b) Actual drag on cylinder 1 in the group of three

Fig. 10.1 Comparison between potential and actual drag coefficients for cylinder 1 in the group of three

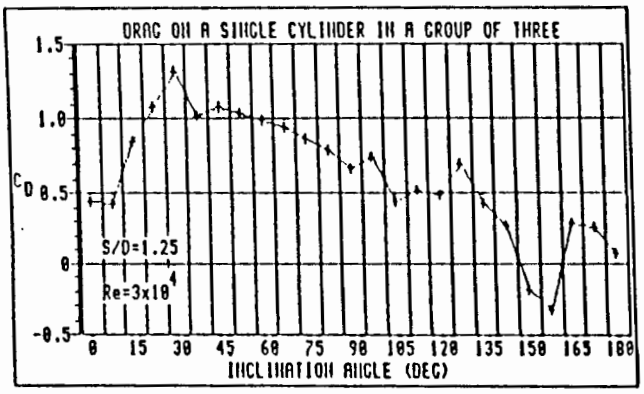


(a)

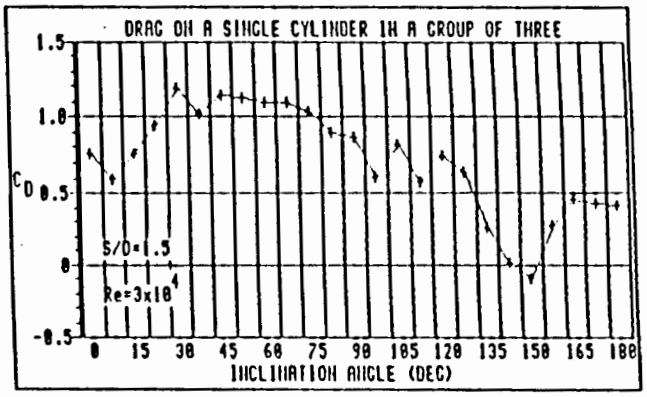


(b)

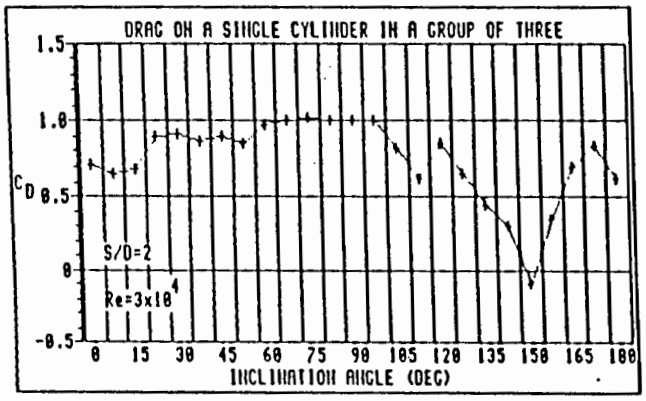


(c)

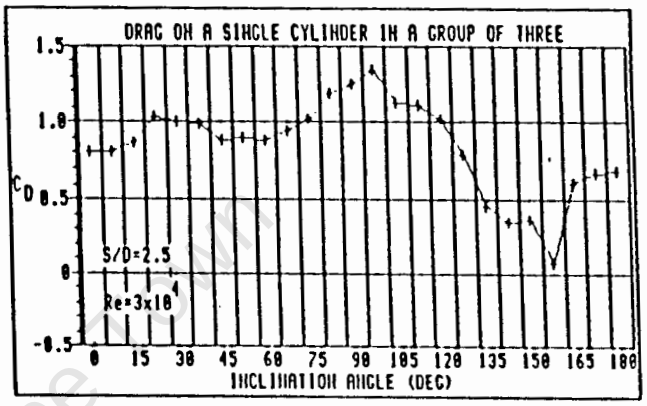


(d)

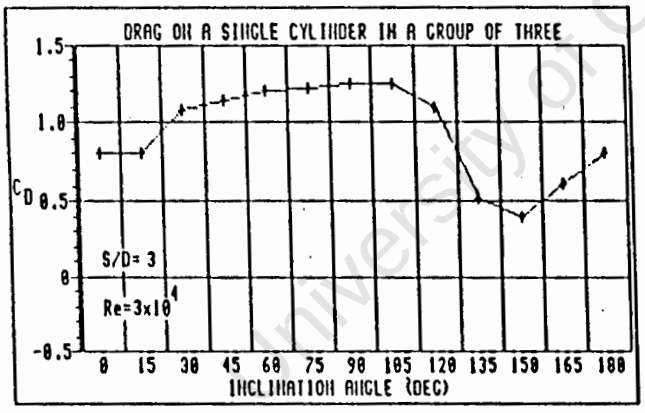


(e)

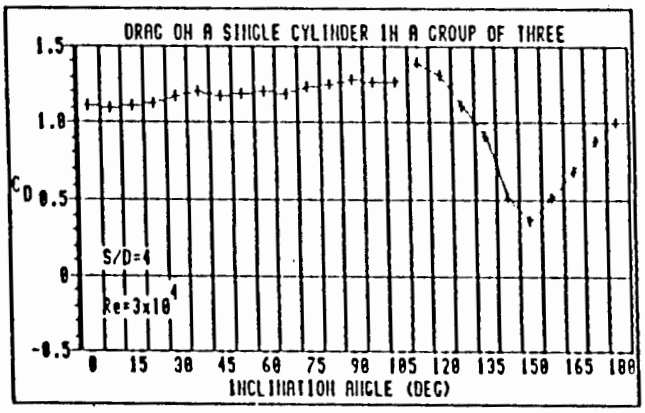


(f)

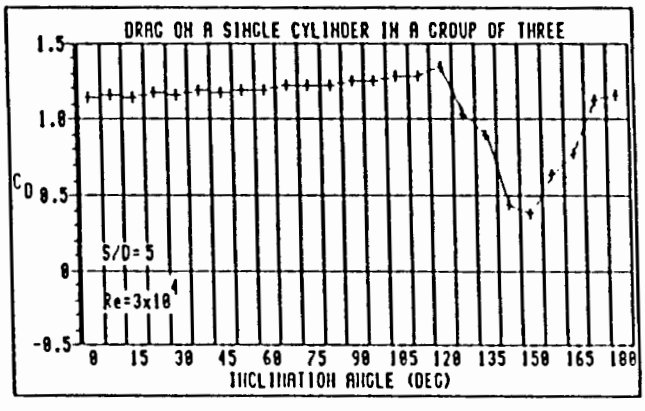


(g)

Fig. 10.2 Actual drag coefficient on cylinder 1 in the group of three versus group inclination angle α

## 10.2 LIFT COEFFICIENTS ON A SINGLE CYLINDER IN A GROUP OF THREE

Fig. 10.3 shows zero potential lift coefficients for cylinder 1 at $\alpha$ = 0 degrees and 180 degrees for all cylinder spacings. This is so because of the symmetry of the cylinders and the consequent streamline flow patterns at those orientations, the cylinder 1 being situated on the central flow axis in each case. Maximum potential lift occurs at $\alpha$ = 90 degrees and is directed towards the free stream flow axis, but it decreases rapidly towards zero as the cylinder spacing increases.

With real flow (Fig. 10.4) in the range $1.5<S/D<5$, the lift coefficient is approximately zero for $0<\alpha<105$ degrees after which it oscillates between a negative and positive lift coefficient. The rate of change of lift coefficient with respect to the inclination angle is extremely high and is due to wake interference. For $S/D<1.5$, the combination of wake and proximity interference gives rise to lift coefficients which depart totally from the potential lift curves.

## 10.3 TOTAL FORCE COEFFICIENTS FOR THREE CYLINDERS

When the potential lift and drag coefficients for each cylinder given in Appendix B2 are summed, the resulting total potential force coefficients are zero. This is clearly not so in the real flow situation (Figs. 10.5 and 10.6) where real and fluctuating force coefficients exist.

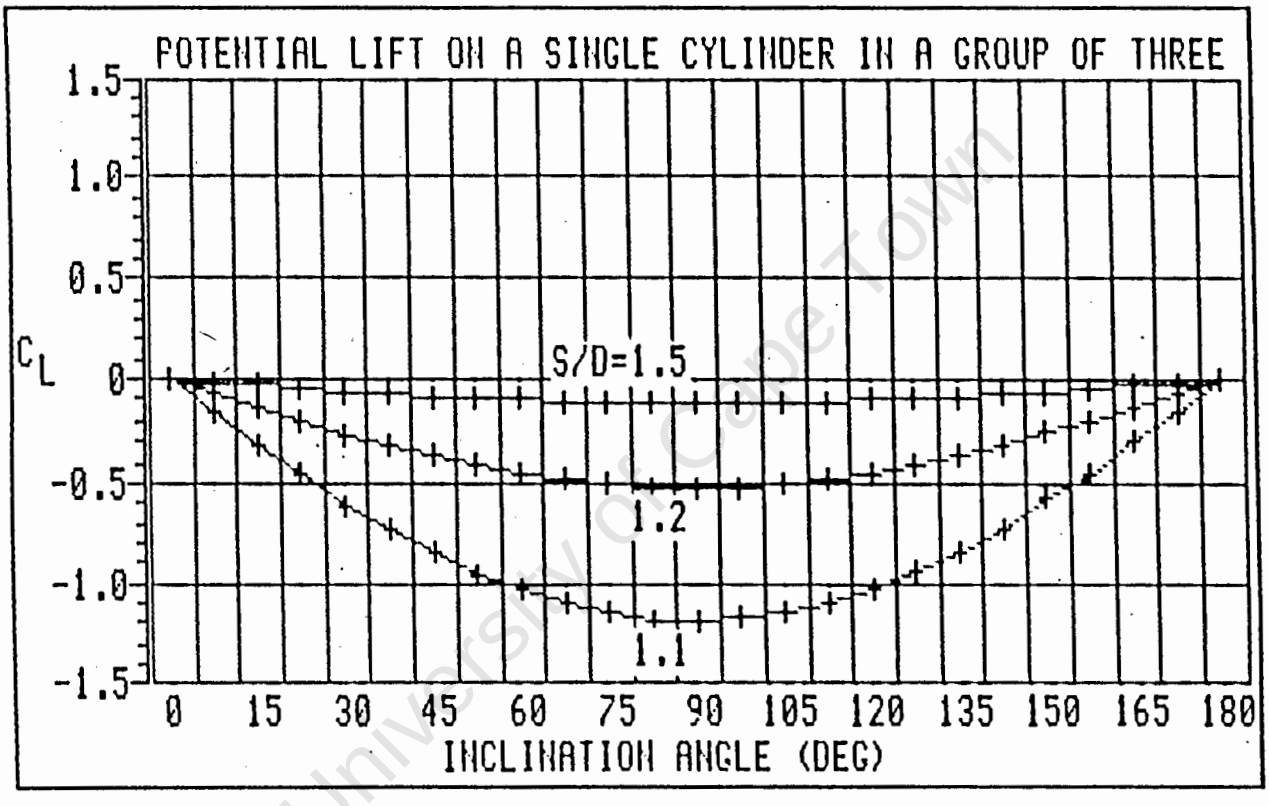




Fig. 10.3 Variation of potential lift coefficient on cylinder 1 in the group of three with group inclination angle $\alpha$

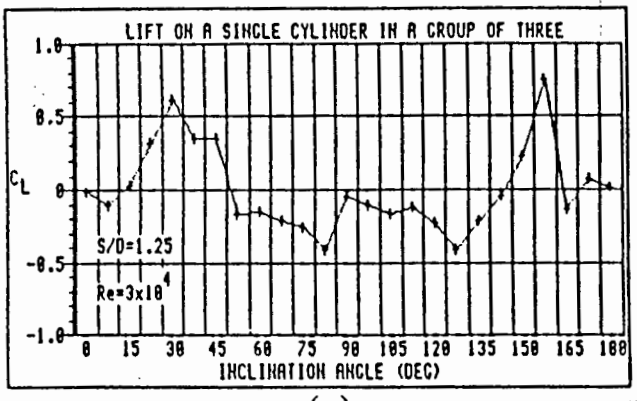


(a)

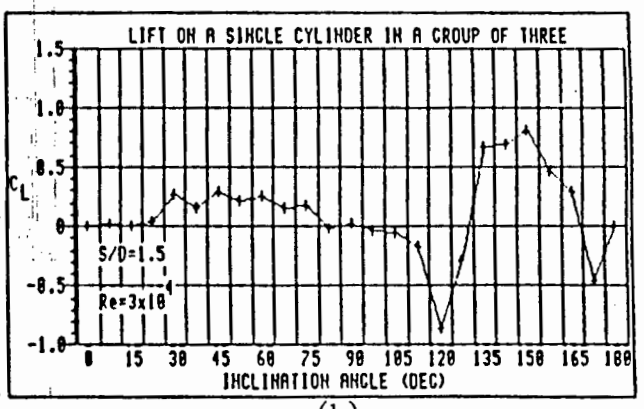


(b)

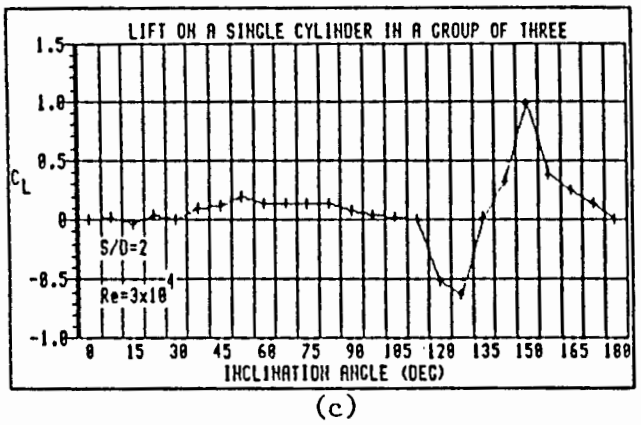


(c)

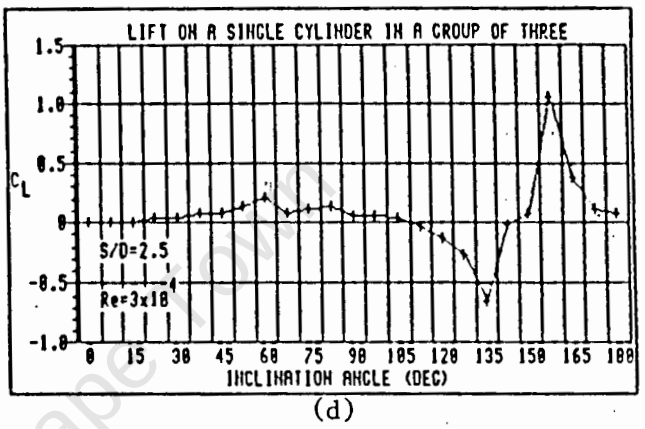


(d)

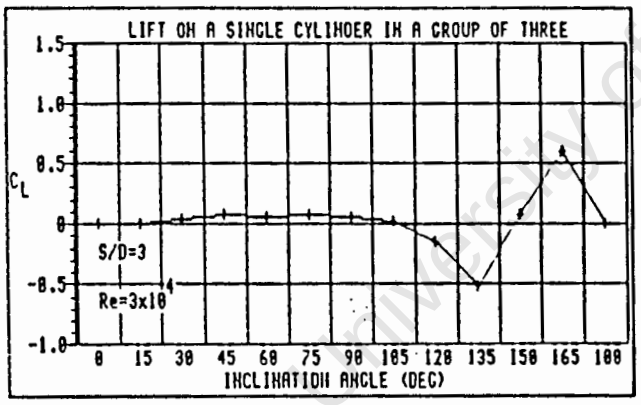


(e)

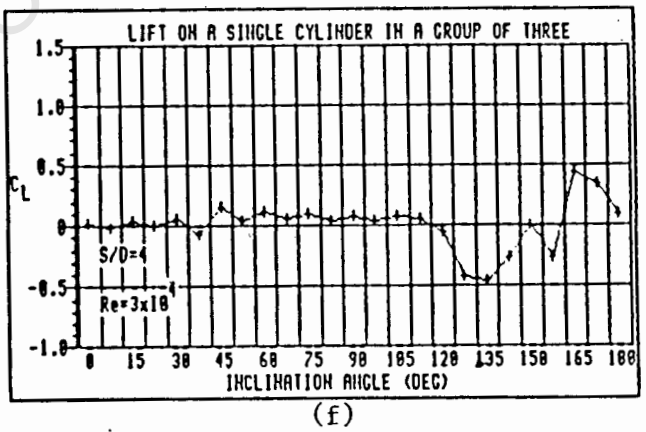


(f)

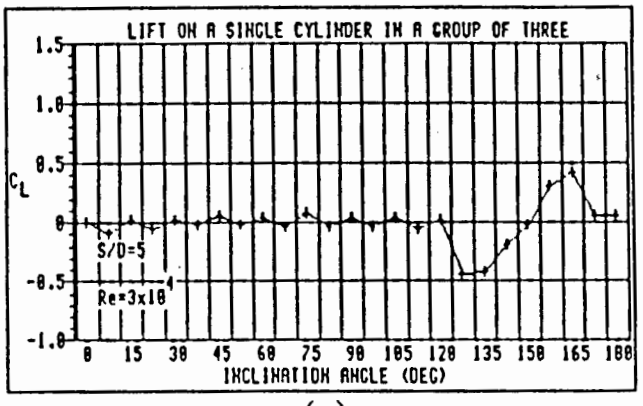


(g)

Fig. 10.4 Actual lift coefficent on cylinder 1 in the group of three versus group inclination angle α

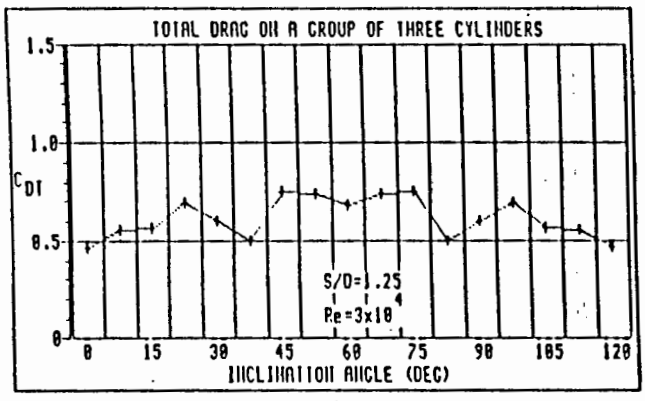


(a)

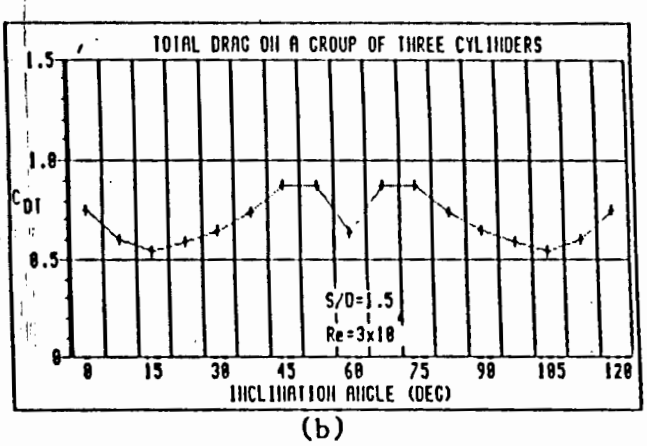


(b)

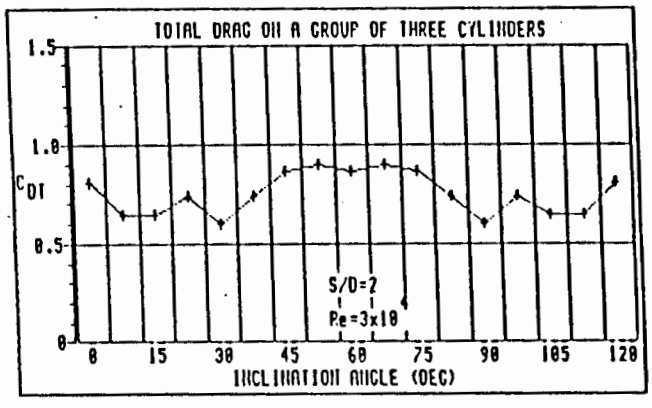


(c)

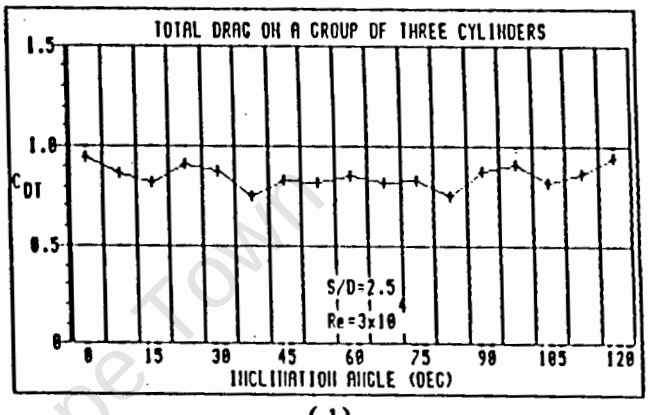


(d)

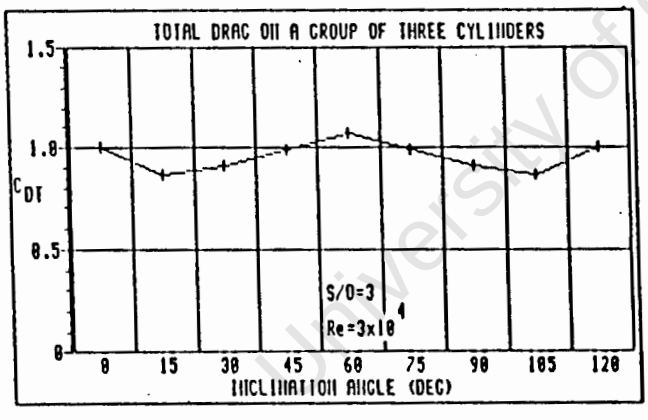


(e)

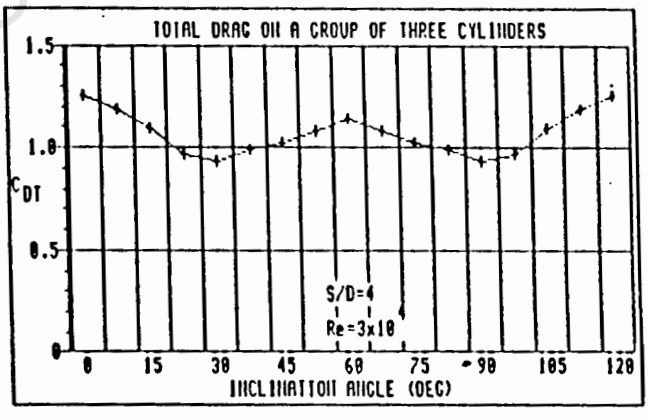


(f)

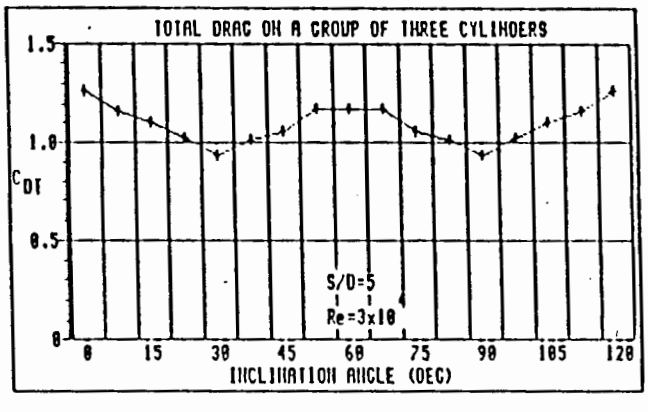


(g)

Fig. 10.5 Actual total drag coefficient for the group of three cylinders versus group inclination angle α

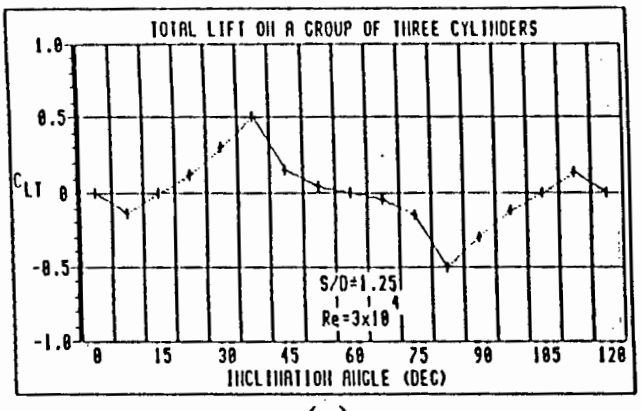


(a)

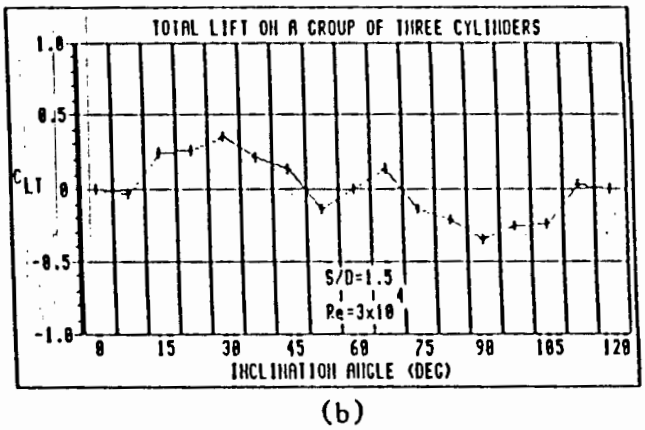


(b)

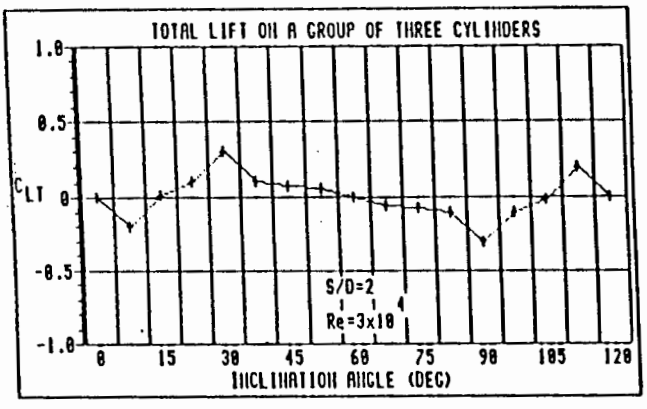


(c)

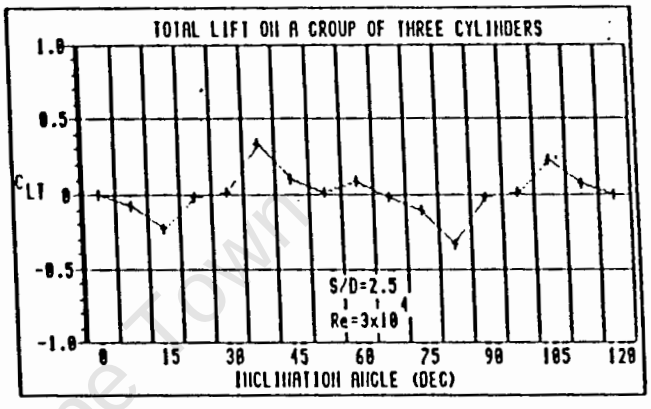


(d)

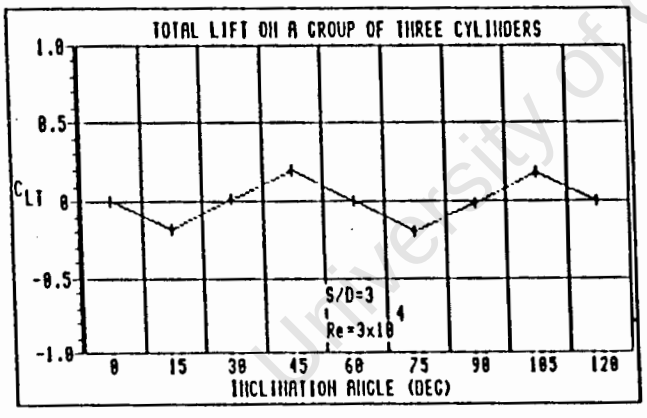


(e)

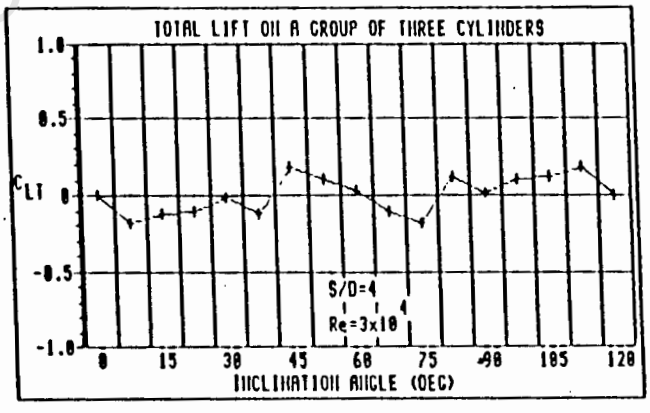


(f)

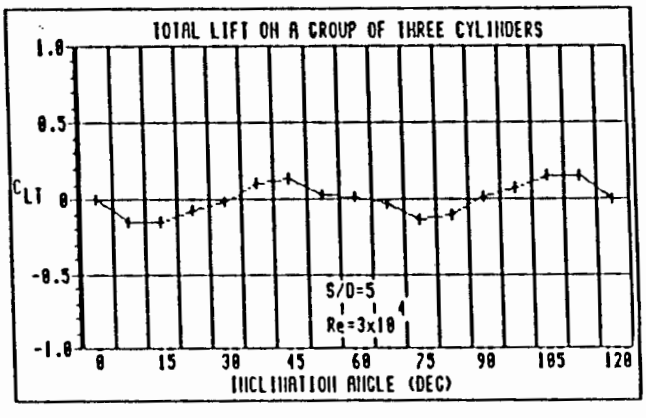


(g)

Fig. 10.6 Actual total lift coefficient for the group of three cylinders versus group inclination angle α

## 10.4 FORCE COEFFICIENTS ON A GROUP OF FOUR CYLINDERS

Similar comparisons between Figs. 3.5 and 9.1 and Figs. 3.6 and 9.2 respectively, show that the potential lift and drag coefficients do not in any way approximate the real flow situation in respect of absolute values or trends. The potential total force coefficients are again zero which is obviously not so in the real flow situation.

## 10.5 CONCLUSIONS

Whilst the potential flow analysis provided a theoretical basis on which to predict the force coefficients acting on a group of cylinders, the results do not correspond to the force coefficients in the real flow case. The reasons for the differences are to be found in the large number of variables involved in the real flow situation, and the author considers it doubtful that a satisfactory theoretical analysis will adequately describe the real flow situation. This makes it even more important to establish a standard data base of real flow data for designers as presented in this thesis.

## REFERENCES


1. Zdravkovich, M.M. 1977. Review of flow interference between two circular cylinders in various arrangements, J. Fluids Eng., ASME, 618-633.
2. Pannell, J.R., Griffiths, E.A. and Coales, J.D., 1915. Experiments on the interference between pairs of aeroplane wires of circular and lenticular cross section, (British) Advisory Committee for Aeronautics, Reports and Memoranda No.208, 1915, Annual Reports for 1915-1916, Vol.7, 219-221.
3. Biermann, D and Herrnstein, W.H. 1933. The interference between struts in various combinations, NACA, Tech. Report No.468.
4. Spivak, H.M. 1946. Vortex frequency and flow pattern in the wake of two parallel cylinders at various spacing normal to an air stream, J. Aero. Sci., 13, 289-301.
5. Hori, E. 1959. Experiments on flow around a pair of parallel circular cylinders, Proc. 9th Japan National Congress for Applied Mech, Tokyo, 231-234.
6. Zdravkovich, M.M. and Stanhope, D.J. 1972. Flow pattern in the gap between two cylinders in tandem, University of Salford, Internal Report FM 5/72.
7. Ishigai, S., Nishikawa, E., Nishimura, K. and Cho, K. 1972. Experimental study on structure of gas flow in tube banks with tube axis normal to flow (part 1, Karmen vortex flow around two tubes at various spacings), Bull. Japan Soc. Mech. Engs., 15, No.86, 949-956.

8. Bearman, P.W. and Wadcock, A.J. 1973. The interaction between a pair of circular cylinders normal to a stream, J. Fluid Mech., 61, 499-511.

9. Maskell, E.C. 1965. A theory of the blockage effects on bluff bodies and stalled wings in a closed wind tunnel, Aero. Research Council, Reports and Memoranda, 3400, 1-22.

10. Zdravkovich, M.M. and Pridden, D.L. 1977. Interference between two circular cylinders; Series of unexpected discontinuities, J. Ind. Aerodynamics, 2, 255-270.

11. Dalton, C. and Szabo, J.M. 1977. Drag on a group of cylinders, J. Pressure Vessel Technology, ASME, 99, 152-157.

12. Allen, H.J. and Vincenti, W.G. 1944. Wall interference in a two dimensional flow wind tunnel, with consideration of the effect of compressibility, NACA, Report No.782.

13. Dalton, C. 1971. Allen and Vincenti blockage correction in a wind tunnel, AIAA Journal, 9, 1864-1865.

14. Roberts, B.W. 1966. Low frequency aeroelastic vibrations in a cascade of circular cylinders, Inst. Mech. Eng., Mech. Eng. Sci. Monograph No.4.

15. Mair, W.A. and Maull, D.J. 1971. Aerodynamic behaviour of bodies in the wake of other bodies, Roy. Soc., Phil. Trans, 269A, 425-437.

16. Gerhardt, H.J. and Kramer, C. 1982. Interference effects for groups of stacks, J. Wind Eng. and Ind. Aero., 8, 195-202.

17. Price, S.J. and Paidoussis, M.P. 1984. The aerodynamic forces acting on groups of two and three circular cylinders when subjected to a cross flow, J. Wind Eng. and Ind.Aero., 17, 329-347.

18. Eastop, T.D. and Turner, J.B. 1982. Air flow around three cylinders at various pitch to diameter ratios for both a longitudinal and transverse arrangement, Trans. Inst. Chem. Eng., 60, 359-363.

19. Zdravkovich, M.M. 1985. Forces on pipe clusters, Proc. of Conf. on Separated Flow Around Marine Structures, Norwegian Inst. of Technology, Trondheim, 201-226.

20. Bardowicks, H. 1985. A new six-component balance and applications on wind tunnel models of slender structure, Private communication with Zdravkovich ref [19].

21. Pearcey, H.H., Cash, R.F., Salter, I.J. and Boribond, A. 1982. Interference effects on the drag loading for groups of cylinders in uni-directional flow, National Maritime Institute, NMI R 130.

22. Milne-Thomson, L.M. 1938. Theoretical hydrodynamics, Mac-Millan, London.

23. Pankhurst, R.C. and Holder, D.W. 1952. Wind tunnel technique, Pitman, London.

24. Pope, A. and Harper, J.J. 1966. Low-speed wind tunnel testing, Wiley, New York.

25. Awbi, H.B. 1972. Wind tunnel wall constraint on two dimensional rectangular prisms, J. Indust. Aero., 3, 285-306.

26. Fackrell, J.E. 1975. Blockage effects on two-dimensional bluff body flow, Aero. Quart., 26, 243-253.

27. Alexander, A.J. 1978. Wind tunnel corrections for Savonius rotors, 2nd Int. Symp. on Wind Energy Systems, Amsterdam.

28. West, G.S. and Apelt, C.J. 1982. The effects of tunnel blockage and aspect ratio on the mean flow past a circular cylinder with Reynolds number between 104 and 105, J. Fluid Mech., 114, 361-377.

29. Douglas, J.F., Gasiorek, J.M. and Swaffield, J.A. 1979. Fluid mechanics, Pitman, London, 318-319.

# BIBLIOGRAPHY

Achenbach, E. 1968. Distribution of local pressure and skin friction around a circular cylinder in cross-flow up to $Re=5x10^6$, Journal Fluid Mechanics, 34, 625-639.

Arie, M., Kiya, M. Tamura, H. and Mori, H. 1983. Pressure fluctuations on two circular cylinders in tandem arrangements, Journal Fluids Engineering, ASME, 105, 161-167.

Ball, D.J. and Hall, C.D. 1980. Drag of yawed pole groups at low Reynolds numbers, Journal of the Waterway etc, Proc. ASCE, 106, 229-238.

Barnes, F.H., Baxendale, A.J. and Grant, I. 1985. The flow past two cylinders having different diameters, Aeronautical Journal, April, 125-134.

Barnes, F.H., Baxendale, A.J. and Grant, I. 1986. A lock-in effect in the flow over two cylinders, Aeronautical Journal, April, 128-138.

Carpenter, L.H. 1958. On the motion of two cylinders in an ideal fluid, Journal of Research of the National Bureau of Standards, 61, No. 2, 83-87.

Chen, Y.N. 1972. Fluctuating lift forces of the Karmen vortex streets on single circular cylinders and in tube bundles, Journal Engineering for Industry, ASME, 94, 601-628.

Dayoub, A.H. 1982. Aerodynamic forces on a cylindrical structure, Applied Scientific Research, 39, 3-20.

Farell, C., Carrasquel, S., Guven, O. and Patel, O.C. 1977. Effect of wind tunnel walls on the flow past circular cylinders and cooling tower models, Journal Fluid Mechanics, 22, 187-196.

Glauert, H. 1933. Wind tunnel interference on wings, bodies and airscrews, A.R.C., R. and M. 1566.

Hiwada, M., Mabuchi, I. and Yanagihara, H. 1982. Fluid flow and heat transfer around two circular cylinders, Bull. Japanese Society of Mechanical Engineers, 25, 1737-1745.

Igarashi, T. 1984. Characteristics of the flow around two circular cylinders arranged in tandem, Bull. Japanese Society of Mechanical Engineers, Report 1, 24, 323-331, Report 2, 27, 2380-2387.

Igarashi, T. and Suzuki, K. 1984. Characteristics of the flow around three circular cylinders arranged in-line, Bull. Japanese Society of Mechanical Engineers, 27, 2397-2404.

Jendrzejczyk, J.A. and Chen, S.S. 1982. Fluid forces acting on circular cylinders in liquid cross flow, Flow induced vibration of circular cylindrical structures, Ed. S.S. Chen, et al, ASME, 63, 31-44.

Kiya, M., Arie, M., Tamura, H. and Mori, H. 1980. Vortex shedding from two circular cylinders in staggered arrangement, Journal Fluids Engineering, ASME, 102, 166-173.

Kreyszig, E. 1967. Advanced engineering mathematics, Wiley, London.

Lamb, H.L. 1932. Hydrodynamics, Cambridge University Press.

Mujumdar, A.S. and Douglas, W.J.M. 1970. The unsteady wake behind a group of three parallel cylinders, ASME, Winter Annual Meeting, paper 70-Pet-8.

Okajima, A. 1979. Flow around two tandem cylinders at very high Reynolds numbers, Bull. Japanese Society Mechanical Engineers, 22, 504-511.

Price, S.J. 1976. The origin and nature of the lift force on two bluff bodies, Aeronautical Quarterly, 26, 154-168.

Schlichting, H. 1960. Boundary layer theory, 4th Edition, McGraw-Hill, New York.

Stansby, P.K. 1974. The effects of end plates on the base pressure coefficient of a circular cylinder, Aeronautical Journal, 78, 36-37.

Streeter, V.L. 1948. Fluid dynamics, McGraw-Hill, New York.

Weaver, D.S. and Grover, L.K. 1978. Cross flow induced vibrations in a tube bank, Journal of Sound and Vibration, 59, 263-294.

Yeung, H.C. and Weaver, D.S. 1983. The effect of approach flow direction on the flow induced vibrations of a triangular tube array, Journal of Vibration, Acoustics, Stress and Reliability in Design, ASME, 105, 76-82.

Zdravkovich, M.M. 1968. Smoke observations of the wake of a group of three cylinders at low Reynolds number, Journal Fluid Mechanics, 32, 339-351.

Zdravkovich, M.M. 1972. Smoke observations of wakes of tandem cylinders at low Reynolds numbers, The Aeronautical Journal, 76, 108-114.

Zdravkovich, M.M., Singh, S., Nuttall, J.A. and Causon, D.M. 1976. Flow induced vibrations in staggered tube banks, 6th Thermo. and Fluid Mech. Convention, Inst. Mech. Eng., 237-243.

Zdravkovich, M.M. 1980. Aerodynamics of two parallel circular cylinders of finite height at simulated high Reynolds numbers, Journal of Wind Engineering and Industrial Aerodynamics, 6, 59-71.

Zdravkovich, M.M. and Namork, J.E. 1979. Structure of interstitial flow between closely spaced tubes in staggered array, Flow induced vibration, Ed. S.S. Chen et al, ASME, 41-46.

## PUBLISHED PAPERS

Sayers, A.T. and Ball, D.R. 1983. Blockage corrections for rectangular flat plates mounted in an open jet wind tunnel, Proc. Instn. Mech. Engrs, 197C, 259-263.

Sayers, A.T. 1987. Flow interference between three equispaced cylinders when subjected to a cross flow, Journal of Wind Engineering and Industrial Aerodynamics, 26, 1-19.

Sayers, A.T. 1988. Flow interference between four equispaced cylinders when subjected to a cross flow, Journal of Wind Engineering and Industrial Aerodynamics, 31, 9-28.

# APPENDIX A

## A1 STREAM FUNCTION FOR FLOW OVER A CYLINDER

Referring to the flow field of Fig. 2.1a, the complex potential may be written as [22]

$$w(z) = U(ze^{-i\delta} + a^2 e^{i\delta}/z) \qquad (i)$$

Putting $\delta = \pi$ so that the flow field of Fig. 2.1b is obtained, equation (i) becomes

$$w(z) = -U(z + a^2/z)$$

and substituting for $z = (x + iy)$, gives

$$w(z) = -U[(x + iy) + a^2(x - iy)/(x + iy)(x - iy)]$$
$$= -U[(x + iy) + a^2(x - iy)/(x^2 + y^2)]$$

Noting that $r^2 = x^2 + y^2$, then collecting real and imaginary parts

$$w(z) = -U[x + a^2 x/r^2) + i(y - a^2 y/r^2)]$$

But $w(z) = \phi + i\psi$, therefore

$$\psi = -Uy(1 - a^2/r^2)$$

## A2 VECTOR $\overline{OA}$ IN COMPLEX CONJUGATE FORM

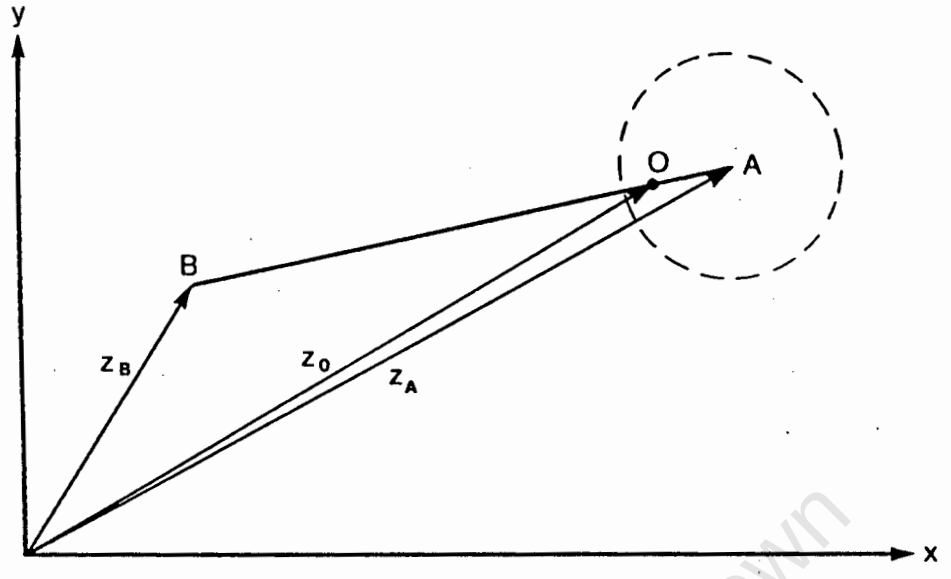


Fig. A1

Consider a doublet at point B exterior to a cylinder of radius a which has a centre at A as in Fig. A1. The image of the doublet is situated at the inverse point O, where from equation (2.7)

$$|OA| = a^2/|AB|$$

The vector $\overline{OA} = a^2/\overline{AB}$

$$= a^2(\cos\theta + i\sin\theta)/|z_A - z_B|$$

but $\cos\theta = (x_A - x_B)/|z_A - z_B|$

and $\sin\theta = (y_A - y_B)/|z_A - z_B|$

therefore $\overline{OA} = a^2[(x_A - x_B) + i(y_A - y_B)]/|z_A - z_B|^2$

$$= a^2(z_A - z_B)/|z_A - z_B|^2$$

Now in general, $|z| = (z\bar{z})^{1/2}$, but $|z| = |z_A - z_B|$

therefore substituting for $|z_A - z_B|^2$

$$\overline{OA} = a^2(z_A - z_B)/(z_A - z_B)(\overline{z_A - z_B})$$

$$= a^2/(\overline{z_A - z_B})$$

# APPENDIX B

## B1 Computer programme listings for potential lift and drag

```
*                          FILE: TEMO1.FOR
*
*                  ***************************************
*                  *POTENTIAL FLOW OVER THREE CYLINDERS*
*                  ***************************************
*
*
*       THIS PROGRAMME CALCULATES THE LIFT AND DRAG COEFFICIENTS
*       ON EACH CYLINDER IN A GROUP OF THREE LYING IN A POTENTIAL
*       FLOW FIELD. THE ANGULAR INCLINATION OF THE CYLINDERS IS
*       VARIED IN THE RANGE 0 TO 120 DEGREES
*
*       INPUT VARIABLES ARE DEFINED
*
*       A(1)        RADIUS OF CYLINDER 1                        (m/s)
*       A(2)        RADIUS OF CYLINDER 2                        (m/s)
*       A(3)        RADIUS OF CYLINDER 3                        (m/s)
*       DELTA(1)    ANGLE OF DOUBLET AXIS FOR CYLINDER 1        (radians)
*       DELTA(2)    ANGLE OF DOUBLET AXIS FOR CYLINDER 2        (radians)
*       DELTA(3)    ANGLE OF DOUBLET AXIS FOR CYLINDER 3        (radians)
*       ANG         ANGLE OF FREE STREAM VELOCITY VECTOR        (radians)
*       INC         NUMBER OF INCREMENTS AROUND EACH
*                   CYLINDER AT WHICH THE VELOCITIES AND
*                   FORCES ARE CALCULATED
*       NCYL        NUMBER OF CYLINDERS
*       ND          NUMBER OF DOUBLETS
*       U(1)        VELOCITY OF CYLINDER 1                      (m/s)
*       U(2)        VELOCITY OF CYLINDER 2                      (m/s)
*       U(3)        VELOCITY OF CYLINDER 3                      (m/s)
*       U(5)        FREE STREAM VELOCITY                        (m/s)
*       Z(1)        VECTOR CO-ORDINATES OF CYLINDER 1           (m)
*       Z(2)        VECTOR CO-ORDINATES OF CYLINDER 2           (m)
*       Z(3)        VECTOR CO-ORDINATES OF CYLINDER 3           (m)
*
*
*       DEFINE VARIABLES
*
1       COMPLEX Z(400),ZED,BLAM(400),VZED,VEE(400),ZZ(400),V1,
       1VTOT(48),SUM,FIRST
2       REAL A(4),U(5),ANG,DELTA(4),THETA(48),G,H,AMU(400),ALAM
       1(400),VEL(48),C,D,DTHETA(48),ANGLE,XVEL(48),YVEL(48),
       2DRAG(4),ALIFT(4)
3       INTEGER NCYL,NCHO(4),X(400),Y(400)
*
*       OPEN FILES FOR DATA OUTPUT
*
*       OPEN(UNIT=1, FILE='(C)PRINTER')
4       OPEN(UNIT=9, FILE='MANY')
*
*       PUT IN CONSTANTS
*
5       DO 505 IR = 11,15
6       RO = IR/10.0
7       INC = 48
8       A(1) = 0.025
9       A(2) = 0.025
```

```
10        A(3) = 0.025
11        U(5) = 10.
12        ANG = 3.14159
13        NCYL = 3
14        DELTA(1) = 3.14159
15        DELTA(2) = 3.14159
16        DELTA(3) = 3.14159
17        ND =381
18        Z(1) = (0,0)
19        U(1) = 10.0
20        U(2) = 10.0
21        U(3) = 10.0
      *
      *       PUT IN DOUBLET AND CYLINDER RELATIONSHIPS
      *
22        Y(1) = 0.0
23        Y(2) = 0.0
24        Y(3) = 0.0
25        TY1 = 0.0
26        DO 100 JY = 4,380,2
27        TY1 = TY1+1
28        Y(JY) = TY1
29   100  CONTINUE
30        TY2 = 0.0
31        DO 110 JZ = 5,381,2
32        TY2 = TY2+1
33        Y(JZ) = TY2
34   110  CONTINUE
      *
      *       SET TABLE HEADINGS
      *
      *       WRITE(1,510)RO
      *       WRITE(1,520)
      *       WRITE(1,530)
35        WRITE(9,515)RO
36        PRINT *, RO
      *
      *       CALCULATE THE VECTOR CO-ORDINATES OF CYLINDERS 2 AND 3
      *
37        DO 500 KA = 1,17
38        IF(KA.EQ.1)GO TO 190
39        IF(KA.EQ.5)GO TO 195
40        IF(KA.EQ.9)GO TO 190
41        IF(KA.EQ.17)GO TO 196
42        ANGL1 = (30-(7.5*(KA-1)))*3.142/180.
43        ANGL2 = (-30-(7.5*(KA-1)))*3.142/180.
44   180  DANG1 =(7.5*(KA-1))
45        WRITE(9,570)DANG1
46        PRINT *, DANG1
47        S = 0.05*RO
48        RS1 = S*COS(ANGL1)
49        RI1 = S*SIN(ANGL1)
50        RS2 = S*COS(ANGL2)
51        RI2 = S*SIN(ANGL2)
52        Z(2) = CMPLX(RS1,RI1)
53        Z(3) = CMPLX(RS2,RI2)
54        GO TO 210
55   190  ANGL1 = (29.95-(7.5*(KA-1)))*3.142/180.
56        ANGL2 = (-30.05-(7.5*(KA-1)))*3.142/180.
57        GO TO 180
```

```
 195  ANGL1 = (30.05-(7.5*(KA-1)))*3.142/180.
      ANGL2 = (-30-(7.5*(KA-1)))*3.142/180.
      GO TO 180
 196  ANGL1 = (30.05-(7.5*(KA-1)))*3.142/180.
      ANGL2 = (-30-(7.5*(KA-1)))*3.142/180.
      GO TO 180
*
*     CHOOSE CYLINDER ON WHICH VELOCITIES ARE TO BE DETERMINED
*
 210  DO 490 IN = 1,NCYL
      WRITE(9,560)IN
      PRINT *, IN
*
*     DETERMINE ANGLE AROUND CYLINDER AND THE VECTOR CO-ORDINATES
*     (VZED) OF THAT POINT ON ITS SURFACE AT WHICH THE VELOCITIES
*     ARE TO BE DETERMINED
*
      DO 450 I = 1,INC
      DTHETA(I) = 7.5*(I-1)
      THETA(1) = 7.5*3.142*(I-1)/180.
      C = A(IN)*COS(THETA(I))
      D = A(IN)*SIN(THETA(I))
      SUM = CMPLX(C,D)
      VZED =(SUM+Z(IN))
*
*     CALCULATE COMPLEX VELOCITY FOR THE FREE STREAM
*
      G = COS(ANG)
      H = SIN(ANG)
      ZED = CMPLX(G,H)
      FIRST = -U(5)/(ZED)
*
*     CALCULATE V(Z) FOR THE DOUBLETS IN THE RANGE P
*     LESS THAN OR EQUAL TO THE NUMBER OF CYLINDERS
*
 250  DO 380 JP = 1,ND
      JQ = X(JP)
      JR = Y(JP)
      IF(JP.GT.NCYL)GO TO 330
      AMU(JP) =U(JQ)*A(JQ)**2
      ALAM(JP) = DELTA(JQ)
      BLAM(JP) =CMPLX(COS(ALAM(JP)),SIN(ALAM(JP)))
      Z(JP) = Z(JQ)
      VEE(JP) =AMU(JP)*BLAM(JP)/(VZED-Z(JP))**2
      GO TO 380
*
*     CALCULATE V(Z) FOR THE DOUBLETS IN THE RANGE P
*     GREATER THAN THE NUMBER OF CYLINDERS
*
 330  ZZ(JP) = Z(JR)-Z(JQ)
 335  Z(JP) = Z(JQ)+CONJG(A(JQ)**2/(ZZ(JP)))
      AMU(JP) = AMU(JR)*(A(JQ)**2/(CABS(ZZ(JP)))**2)
      ALAM(JP) = 3.14159+(2*ATAN(AIMAG(ZZ(JP))/REAL(ZZ(JP))))
     1-ALAM(JR)
      BLAM(JP)= CMPLX(COS(ALAM(JP)),SIN(ALAM(JP)))
      VEE(JP) =AMU(JP)*BLAM(JP)/(VZED-Z(JP))**2
 380  CONTINUE
*
*     SUM THE V(Z)'S OF THE DIPOLES AND ADD FREE STREAM VELOCITY
*     POTENTIAL
```

```
      *
 95         V1 = (0.,0.)
 96         DO 420 J = 1,ND
 97         V1 = V1+VEE(J)
 98   420   CONTINUE
 99         VTOT(I) = FIRST+V1
100         VEL(I) = CABS(VTOT(I))
101         XVEL(I) = REAL(VTOT(I))
102         YVEL(I) = -AIMAG(VTOT(I))
103         PRINT *, DANG1,IN,DTHETA(I),VTOT(I),VEL(I)
104         WRITE(9,550)DTHETA(I),VTOT(I),VEL(I)
105   450   CONTINUE
      *
      *     FIND ODD EVEN AND EXTREME ORDINATES OF COMPONENT FORCES
      *     ON CYLINDER AND SUM THEM
      *
106         SUMED = 0.0
107         SUMEL = 0.0
108         DO 460 J = 2,INC,2
109         TOTED = 4*A(IN)*(VEL(J)**2-U(5)**2)*COS(THETA(J))
110         TOTEL = 4*A(IN)*(VEL(J)**2-U(5)**2)*SIN(THETA(J))
111         SUMED = SUMED + TOTED
112         SUMEL = SUMEL + TOTEL
113   460   CONTINUE
114         SUMOD = 0.0
115         SUMOL = 0.0
116         DO 470 J = 3,(INC-1),2
117         TOTOD = 2*A(IN)*(VEL(J)**2-U(5)**2)*COS(THETA(J))
118         TOTOL = 2*A(IN)*(VEL(J)**2-U(5)**2)*SIN(THETA(J))
119         SUMOD = SUMOD+TOTOD
120         SUMOL = SUMOL+TOTOL
121   470   CONTINUE
122         EXTRD = 2*A(IN)*(VEL(1)**2-U(5)**2)*COS(THETA(1))
123         EXTRL = 2*A(IN)*(VEL(1)**2-U(5)**2)*SIN(THETA(1))
      *
      *     CALCULATE DRAG AND LIFT COEFFICIENT USING SIMPSON'S
      *     RULE
      *
124         DRAG(IN) =  (EXTRD+SUMOD+SUMED)*7.5*3.142/180/3/U(5)**2
           1/A(IN)/2
125         ALIFT(IN) = (EXTRL+SUMOL+SUMEL)*7.5*3.142/3/180/U(5)**2
           2/A(IN)/2
126   490   CONTINUE
      *
      *     WRITE OR PRINT THE LIFT AND DRAG COEFFICIENTS
      *
      *     WRITE(1,540)DANG1,DRAG(1),ALIFT(1),DRAG(2),ALIFT(2),
      *    1DRAG(3),ALIFT(3)
127   *     WRITE(9,580)DRAG(1),ALIFT(1),DRAG(2),ALIFT(2),DRAG(3),
      *    1ALIFT(3)
128         PRINT *, DRAG(1),ALIFT(1),DRAG(2),ALIFT(2),DRAG(3),ALIFT(3)
129   500   CONTINUE
130   505   CONTINUE
131   510   FORMAT(27X,'S/D = ',F6.2,/)
132   515   FORMAT(F6.2)
133   520   FORMAT(1X,'INCLINATION ANGLE',6X,'D1',8X,'L1',8X,'D2',
           18X,'L2',8X,'D3',8X,'L3')
134   530   FORMAT(6X,'Degrees')
135   540   FORMAT(6X,F6.2,5X,F10.2,F10.2,F10.2,F10.2,F10.2,F10.2,
           1/////)
```

blockage ratios.

## 6.3 CONCLUSIONS

Closed wind tunnel blockage corrections can not be used for open jet test section flows. The open jet blockage corrections that must be applied to the force coefficients of a bluff body decrease in magnitude the further the body is placed downstream of the tunnel mouth. For this particular tunnel, the adjustment length ratio is 0.845, and provided the body was placed in the test section with its adjustment length ratio greater than 0.845, then no blockage correction was required. This finding lends confidence to the placement of the cylinder groups and the subsequent accuracy of the measurements described in chapter 7.

```
136   550  FORMAT(F10.3,F10.3,F10.3,F10.3)
137   560  FORMAT(I2)
138   570  FORMAT(F10.3)
139   580  FORMAT(F10.4,F10.4,F10.4,F10.4,F10.4,F10.4)
140        DATA (X(I), I = 1,3     )/1,2,3/
141        DATA (X(I), I = 4,9     )/2,3,3,1,1,2/
142        DATA (X(I), I = 10,21   )/3,1,1,2,1,2,2,3,2,3,3,1/
143        DATA (X(I), I = 22,45   )/1,2,2,3,2,3,3,1,2,3,3,1,3,1,
          11,2,3,1,1,2,1,2,2,3/
144        DATA (X(I), I = 46,93   )/2,3,3,1,3,1,1,2,3,1,1,2,1,2,
          12,3,3,1,1,2,1,2,2,3,1,2,2,3,2,3,3,1,1,2,2,3,2,3,3,
          21,2,3,3,1,3,1,1,2/
145        DATA (X(I), I = 94,189 )/3,1,1,2,1,2,2,3,1,2,2,3,2,3,3,
          11,1,2,2,3,2,3,3,1,2,3,3,1,3,1,1,2,1,2,2,3,2,3,3,1,2,3,
          23,1,3,1,1,2,2,3,3,1,3,1,1,2,3,1,1,2,1,2,2,3,2,3,3,1,3,
          31,1,2,3,1,1,2,1,2,2,3,3,1,1,2,1,2,2,3,1,2,2,3,2,3,3,1/
146        DATA (X(I), I = 190,381)/1,2,2,3,2,3,3,1,2,3,3,1,3,1,1,
          12,2,3,3,1,3,1,1,2,3,1,1,2,1,2,2,3,2,3,3,1,3,1,1,2,3,1,
          21,2,1,2,2,3,3,1,1,2,1,2,2,3,1,2,2,3,2,3,3,1,2,3,3,1,3,
          31,1,2,3,1,1,2,1,2,2,3,3,1,1,2,1,2,2,3,1,2,2,3,2,3,3,1,
          43,1,1,2,1,2,2,3,1,2,2,3,2,3,3,1,1,2,2,3,2,3,3,1,2,3,3,
          51,3,1,1,2,3,1,1,2,1,2,2,3,1,2,2,3,2,3,3,1,1,2,2,3,2,3,
          63,1,2,3,3,1,3,1,1,2,1,2,2,3,2,3,3,1,2,3,3,1,3,1,1,2,2,
          73,3,1,3,1,1,2,3,1,1,2,1,2,2,3/
147        STOP
148        END
```

```
*                          FILE: FTEST.FOR
*
*                  ************************************
*                  *POTENTIAL FLOW OVER FOUR CYLINDERS*
*                  ************************************
*
*
*      THIS PROGRAMME CALCULATES THE LIFT AND DRAG COFFICIENTS
*      ON EACH CYLINDER IN A GROUP OF FOUR LYING IN A POTENTIAL
*      FLOW FIELD. THE ANGULAR INCLINATION OF THE CYLINDERS IS
*      VARIED IN THE RANGE 0 TO 90 DEGREES.
*
*      INPUT VARIABLES ARE DEFINED
*
*      A(1)       RADIUS OF CYLINDER 1                        (m)
*      A(2)       RADIUS OF CYLINDER 2                        (m)
*      A(3)       RADIUS OF CYLINDER 3                        (m)
*      A(4)       RADIUS OF CYLINDER 4                        (m)
*      DELTA(1)   ANGLE OF DOUBLET AXIS FOR CYLINDER 1        (radians)
*      DELTA(2)   ANGLE OF DOUBLET AXIS FOR CYLINDER 2        (radians)
*      DELTA(3)   ANGLE OF DOUBLET AXIS FOR CYLINDER 3        (radians)
*      DELTA(4)   ANGLE OF DOUBLET AXIS FOR CYLINDER 4        (radians)
*      ANG        ANGLE OF FREE STREAM VELOCITY VECTOR        (radians)
*      INC        NUMBER OF INCREMENTS AROUND EACH
*                 CYLINDER AT WHICH THE VELOCITIES AND
*                 FORCES ARE CALCULATED
*      NCYL       NUMBER OF CYLINDERS
*      ND         NUMBER OF DOUBLETS
*      U(1)       VELOCITY OF CYLINDER 1                      (m/s)
*      U(2)       VELOCITY OF CYLINDER 2                      (m/s)
*      U(3)       VELOCITY OF CYLINDER 3                      (m/s)
*      U(4)       VELOCITY OF CYLINDER 4                      (m/s)
*      U(5)       FREE STREAM VELOCITY                        (m/s)
*      Z(1)       VECTOR CO-ORDINATES OF CYLINDER 1           (m)
*      Z(2)       VECTOR CO-ORDINATES OF CYLINDER 2           (m)
*      Z(3)       VECTOR CO-ORDINATES OF CYLINDER 3           (m)
*      Z(4)       VECTOR CO-ORDINATES OF CYLINDER 4           (m)
*
*
*      DEFINE VARIABLES
*
1      COMPLEX Z(500),ZED,BLAM(500),VZED,VEE(500),ZZ(500),V1,
      1VTOT(48),SUM,FIRST
2      REAL A(4),U(5),ANG,DELTA(4),THETA(48),G,H,AMU(500),ALAM
      1(500),VEL(48),C,D,DTHETA(48),ANGLE,XVEL(48),YVEL(48),
      2DRAG(4),ALIFT(4)
3      INTEGER NCYL,NCHO(4),X(500),Y(500)
*
*      OPEN FILES FOR DATA OUTPUT
*
*      OPEN(UNIT=1, FILE='(C)PRINTER')
*      OPEN(UNIT=9, FILE='FOUR2')
*
*      PUT IN CONSTANTS
*
4      DO 505 IR = 20,20
5      RO = IR/10.
6      INC = 48
7      A(1) = 0.025
8      A(2) = 0.025
```

```
 9        A(3) = 0.025
10        A(4) = 0.025
11        U(5) = 10.
12        ANG = 3.14159
13        NCYL = 4
14        DELTA(1) = 3.14159
15        DELTA(2) = 3.14159
16        DELTA(3) = 3.14159
17        DELTA(4) = 3.14159
18        ND =484
19        Z(1) = (0,0)
20        U(1) = 10.0
21        U(2) = 10.0
22        U(3) = 10.0
23        U(4) = 10.0
    *
    *     PUT IN DOUBLET AND CYLINDER RELATIONSHIPS
    *
24        Y(1) = 0.0
25        Y(2) = 0.0
26        Y(3) = 0.0
27        Y(4) = 0.0
28        TY1 = 0.0
29        DO 100 JY=5,482,3
30        TY1 = TY1+1
31        Y(JY) = TY1
32   100  CONTINUE
33        TY2 = 0.0
34        DO 110 JZ = 6,483,3
35        TY2 = TY2+1
36        Y(JZ) = TY2
37   110  CONTINUE
38        TY3 = 0.0
39        DO 111 JX = 7,484,3
40        TY3 = TY3+1
41        Y(JX) = TY3
42   111  CONTINUE
    *
    *     SET TABLE HEADINGS
    *
    *     WRITE(1,510)RO
    *     WRITE(1,520)
    *     WRITE(1,530)
    *     WRITE(9,515)RO
43        PRINT *, RO
    *
    *     CALCULATE THE VECTOR CO-ORDINATES OF CYLINDERS 2,3 AND 4
    *
44        DO 500 KA = 5,5
45        IF(KA.EQ.1)GO TO 190
46        IF(KA.EQ.7)GO TO 195
47        IF(KA.EQ.13)GO TO 196
48        ANGL1 = (45-(7.5*(KA-1)))*3.142/180.
49        ANGL2 = (0.0 -(7.5*(KA-1)))*3.142/180.
50        ANGL3 = (-45-(7.5*(KA-1)))*3.142/180.
51   180  DANG1 =(7.5*(KA-1))
    *     WRITE(9,570)DANG1
52        S = 0.05*RO
53        RS1 = S*COS(ANGL1)
54        RI1 = S*SIN(ANGL1)
```

```
55        RS2 = S*1.414*COS(ANGL2)
56        RI2 = S*1.414*SIN(ANGL2)
57        RS3 = S*COS(ANGL3)
58        RI3 = S*SIN(ANGL3)
59        Z(2) = CMPLX(RS1,RI1)
60        Z(3) = CMPLX(RS2,RI2)
61        Z(4) = CMPLX(RS3,RI3)
62        GO TO 210
63   190  ANGL1 = (45.00-(7.5*(KA-1)))*3.142/180.
64        ANGL2 = (-00.05-(7.5*(KA-1)))*3.142/180.
65        ANGL3 = (-44.95-(7.5*(KA-1)))*3.142/180.
66        GO TO 180
67   195  ANGL1 = (44.95-(7.5*(KA-1)))*3.142/180.
68        ANGL2 = (-0.0-(7.5*(KA-1)))*3.142/180.
69        ANGL3 = (-44.95-(7.5*(KA-1)))*3.142/180.
70        GO TO 180
71   196  ANGL1 = (44.95-(7.5*(KA-1)))*3.142/180.
72        ANGL2 = (-0.05-(7.5*(KA-1)))*3.142/180.
73        ANGL3 = (-45.0-(7.5*(KA-1)))*3.142/180.
74        GO TO 180
     *
     *    CHOOSE CYLINDER ON WHICH VELOCITIES ARE TO BE DETERMINED
     *
75    210 DO 490 IN = 1,NCYL
     *    WRITE(9,560)IN
76        PRINT *, IN
     *
     *    DETERMINE ANGLE AROUND CYLINDER AND THE VECTOR CO-ORDINATES
     *    (VZED) OF THAT POINT ON ITS SURFACE AT WHICH THE VELOCITIES
     *    ARE TO BE DETERMINED
     *
77        DO 450 I = 1,INC
78        DTHETA(I) = 7.5*(I-1)
79        THETA(I) = 7.5*3.142*(I-1)/180.
80        C = A(IN)*COS(THETA(I))
81        D = A(IN)*SIN(THETA(I))
82        SUM = CMPLX(C,D)
83        VZED =(SUM+Z(IN))
     *
     *    CALCULATE COMPLEX VELOCITY FOR FREE STREAM
     *
84        G = COS(ANG)
85        H = SIN(ANG)
86        ZED = CMPLX(G,H)
87        FIRST = -U(5)/ZED
     *
     *    CALCULATE V(Z) FOR THE DOUBLETS IN THE RANGE P
     *    LESS THAN OR EQUAL TO THE NUMBER OF CYLINDERS
     *
87   250  DO 380 JP = 1,ND
88        JQ = X(JP)
89        JR = Y(JP)
90        IF(JP.GT.NCYL)GO TO 330
91        AMU(JP) =U(JQ)*A(JQ)**2
92        ALAM(JP) = DELTA(JQ)
93        BLAM(JP) =CMPLX(COS(ALAM(JP)),SIN(ALAM(JP)))
94        Z(JP) = Z(JQ)
95        VEE(JP) =AMU(JP)*BLAM(JP)/(VZED-Z(JP))**2
96        GO TO 380
     *
```

```
*     CALCULATE V(Z) FOR THE DOUBLETS IN THE RANGE P
*     GREATER THAN THE NUMBER OF CYLINDERS
*
 97  330  ZZ(JP) = Z(JR)-Z(JQ)
 98  335  Z(JP) = Z(JQ)+CONJG(A(JQ)**2/(ZZ(JP)))
 99       AMU(JP) = AMU(JR)*(A(JQ)**2/(CABS(ZZ(JP)))**2)
100       ALAM(JP) = 3.14159+(2*ATAN(AIMAG(ZZ(JP))/REAL(ZZ(JP))))
     1-ALAM(JR)
101       BLAM(JP)= CMPLX(COS(ALAM(JP)),SIN(ALAM(JP)))
102       VEE(JP) =AMU(JP)*BLAM(JP)/(VZED-Z(JP))**2
103  380  CONTINUE
*
*     SUM THE V(Z)'S OF THE DIPOLES AND ADD FREE STREAM VELOCITY
*     POTENTIAL
*
104       V1 = (0.,0.)
105       DO 420 J = 1,ND
106       V1 = V1+VEE(J)
107  420  CONTINUE
108       VTOT(I) = FIRST+V1
109       VEL(I) = CABS(VTOT(I))
110       XVEL(I) = REAL(VTOT(I))
111       YVEL(I) = -AIMAG(VTOT(I))
*     PRINT *,R,DANG1,IN,DTHETA(1),VTOT(I),VEL(1)
*     WRITE(9,550)DTHETA(I),VTOT(I),VEL(I)
112  450  CONTINUE
*
*     FIND ODD, EVEN AND EXTREME ORDINATES OF COMPONENT FORCES
*     ON CYLINDER AND SUM THEM
*
113       SUMED = 0.0
114       SUMEL = 0.0
115       DO 460 J = 2,INC,2
116       TOTED = 4*A(IN)*(VEL(J)**2-U(5)**2)*COS(THETA(J))
117       TOTEL = 4*A(IN)*(VEL(J)**2-U(5)**2)*SIN(THETA(J))
118       SUMED = SUMED + TOTED
119       SUMEL = SUMEL + TOTEL
120  460  CONTINUE
121       SUMOD = 0.0
122       SUMOL = 0.0
123       DO 470 J = 3,(INC-1),2
124       TOTOD = 2*A(IN)*(VEL(J)**2-U(5)**2)*COS(THETA(J))
125       TOTOL = 2*A(IN)*(VEL(J)**2-U(5)**2)*SIN(THETA(J))
126       SUMOD = SUMOD+TOTOD
127       SUMOL = SUMOL+TOTOL
128  470  CONTINUE
129       EXTRD = 2*A(IN)*(VEL(1)**2-U(5)**2)*COS(THETA(1))
130       EXTRL = 2*A(IN)*(VEL(1)**2-U(5)**2)*SIN(THETA(1))
*
*     CALCULATE DRAG AND LIFT COEFFICIENT USING SIMPSON'S
*     RULE
*
131       DRAG(IN) =  (EXTRD+SUMOD+SUMED)*7.5*3.142/180/3/U(5)**2
     1/A(IN)/2
132       ALIFT(IN) = (EXTRL+SUMOL+SUMEL)*7.5*3.142/3/180/U(5)**2
     1/A(IN)/2
133  490  CONTINUE
*
*     WRITE OR PRINT THE LIFT AND DRAG COEFFICIENTS
*
```

```
*      WRITE(1,540)DANG1,DRAG(1),ALIFT(1),DRAG(2),ALIFT(2),
*     1DRAG(3),ALIFT(3),DRAG(4),ALIFT(4)
*      WRITE(9,580)DRAG(1),ALIFT(1),DRAG(2),ALIFT(2),DRAG(3),
*     1ALIFT(3),DRAG(4),ALIFT(4)
134    PRINT *,DRAG(1),ALIFT(1),DRAG(2),ALIFT(2),DRAG(3),ALIFT(3),
      1DRAG(4),ALIFT(4)
135  500 CONTINUE
136  505 CONTINUE
137  510 FORMAT(27X,'S/D = ',F6.2,/)
138  515 FORMAT(F6.2)
139  520 FORMAT(2X,'DANG1',6X,'D1',8X,'L1',8X,'D2',8X,'L2',
      18X,'D3',8X,'L3')
140  530 FORMAT(6X,'Degrees')
141  550 FORMAT(F10.3,F10.3,F10.3,F10.3)
142  560 FORMAT(I2)
143  570 FORMAT(F10.3)
144  580 FORMAT(F10.4,F10.4,F10.4,F10.4,F10.4,F10.4,F10.4,F10.4)
145    DATA (X(I), I = 1,4     )/1,2,3,4/
146    DATA (X(I), I = 5,16    )/2,3,4,3,4,1,4,1,2,1,2,3/
147    DATA (X(I), I = 17,52   )/3,4,1,4,1,2,1,2,3,4,1,2,1,2,3,2,
      13,4,1,2,3,2,3,4,3,4,1,2,3,4,3,4,1,4,1,2/
148    DATA (X(I), I = 53,160 )/4,1,2,1,2,3,2,3,4,1,2,3,2,3,4,3,
      14,1,2,3,4,3,4,1,4,1,2,1,2,3,2,3,4,3,4,1,2,3,4,3,4,1,4,1,
      22,3,4,1,4,1,2,1,2,3,2,3,4,3,4,1,4,1,2,3,4,1,4,1,2,1,2,3,
      34,1,2,1,2,3,2,3,4,3,4,1,4,1,2,1,2,3,4,1,2,1,2,3,2,3,4,1,
      42,3,2,3,4,3,4,1/
149    DATA (X(I), I =161,428 )/1,2,3,2,3,4,3,4,1,2,3,4,3,4,1,4,
      11,2,3,4,1,4,1,2,1,2,3,2,3,4,3,4,1,4,1,2,3,4,1,4,1,2,1,2,
      23,4,1,2,1,2,3,2,3,4,3,4,1,4,1,2,1,2,3,4,1,2,1,2,3,2,3,4,
      31,2,3,2,3,4,3,4,1,2,3,4,3,4,1,4,1,2,3,4,1,4,1,2,1,2,3,4,
      41,2,1,2,3,2,3,4,3,4,1,4,1,2,1,2,3,4,1,2,1,2,3,2,3,4,1,2,
      53,2,3,4,3,4,1,4,1,2,1,2,3,2,3,4,1,2,3,2,3,4,3,4,1,2,3,4,
      63,4,1,4,1,2,3,4,1,4,1,2,1,2,3,4,1,2,1,2,3,2,3,4,1,2,3,2,
      73,4,3,4,1,4,1,2,1,2,3,2,3,4,1,2,3,2,3,4,3,4,1,2,3,4,3,4,
      81,4,1,2,1,2,3,2,3,4,3,4,1,2,3,4,3,4,1,4,1,2,3,4,1,4,1,2,
      91,2,3,4,1,2,1,2,3,2,3,4,1,2,3,2,3,4,3,4,1,2,3,4,3,4,1,4/
150    DATA (X(I), I = 429,484)/1,2,1,2,3,2,3,4,3,4,1,2,3,4,3,4,
      11,4,1,2,3,4,1,4,1,2,1,2,3,2,3,4,3,4,1,4,1,2,3,4,1,4,1,2,
      21,2,3,4,1,2,1,2,3,2,3,4/
151    STOP
152    END
```

## DISCUSSION OF PROGRAMME STRUCTURE

Although the following discussion refers to TEMO1.FOR, each programme has essentially the same form.

Lines 1-3

The complex, real and integer variables are defined along with the number of values expected in the respective arrays. The variables listed here are used later in the programme.

Line 4

The OPEN statements are to open a disc or printer file for the recording of the output data. For output only to the monitor screen, each OPEN statement was preceded by an asterisk thus making it a comment line. For TEMO1.FOR, output data is written to the disc file called MANY.

Lines 5-21

Cylinder centre spacing is set. Constants pertaining to the fluid and cylinder geometry are defined. The number of cylinders, their diameters, speed and direction of travel are stipulated. In this case, each cylinder has a speed of 10 m/s in the negative x direction: that is the axis of the doublet forming the cylinder lies at $\delta$ (DELTA) = $\pi$. The free stream velocity is 10 m/s at an angle $\pi$ to the positive x axis : that is it flows from negative to positive x as depicted in Fig. 2.1b. Five orders of images have been chosen which together with the three originating doublets gives a total of 381 doublets. The number of increments around the surface of each cylinder for the numerical integration of the pressure distribution is set at 48; that is every 7.5 degrees. The centre of cylinder 1 is located at the origin of the co-ordinate axes

and the other cylinders revolve as a fixed body about this point.

Lines 22-34

The unique relationship between p and r given in Tables 2.1 and 2.2 is established. The corresponding values of q are entered via the data statements in lines 139-145.

Lines 34-37

Output table headings may be selected as required by deleting the appropriate asterisks.

Lines 37-63

Cylinder 1 has been previously located at the origin. The vector co-ordinates of the remaining cylinders are now calculated at the different angles of inclination of the group to the free stream, for the previously chosen center spacing ratio. The group is rotated in increments of 7.5 degrees about the centre of cylinder 1. For the three cylinder group, 17 increments are required whilst for the four cylinder group, 13 increments are required, since after these numbers of increments the relative positions of the cylinders are once again the same. Special provisions are made for cases where two cylinders are vertically in line with each other. In line 91, the inverse tangent of 90 degrees is required, which being equal to infinity, causes the programme to terminate. This is overcome by deliberately offsetting the cylinders by 0.05 degrees as shown in lines 55-63.

Lines 64-73

The cylinder on which the velocities are to be determined is chosen and the co-ordinates of the increments around the cylinder are calculated, refered to the origin of the co-ordinate axes in cylinder 1. The total number of increments around

each cylinder is 48.

Lines 74-77

Calculation of the complex velocity of the free stream. This is the first term in equation (2.26).

Lines 78-94

These lines solve the second term in equation (2.26) for the first three doublets then for the remaining image doublets. The p'th doublet is represented by JP. The q'th cylinder is represented by JQ, which is read from the data statements, (lines 140-146), via X(JP), whilst the r'th doublet is represented by JR which is obtained from lines 28 and 38.

Lines 95-105

The separate complex velocities for the image doublets are summed to give the total complex velocity of the doublets. In line 99, the free stream velocity from line 77 is added to give VTOT(I), the complex velocity at an increment KA around cylinder I, where I is the cylinder under consideration. Lines 101 and 102 select the velocity components u and v of equation (2.27). These are printed to a monitor screen in line 103 or to a data disc in line 104 if desired.

Lines 106-122

These lines set the ordinates of the component forces at the 48 increments around the cylinder and sums them. Line 108 starts the loop for the even ordinates and line 116 starts the loop for the odd ordinates, the x and y components being separated out by the SIN and COS terms. Lines 111,112,119 and 120 sum the odd and even ordinates whilst lines 122 and 123 sum the extreme ordinates.

Lines 124-126

Calculation of the drag and lift coefficients according to

equations (2.32) and (2.33).

Lines 126-139

These lines define the output mode and format statements for the data output.

Lines 140-146

Here are listed the data statements defining the relationship between p and q in Table 2.1. For example, in line 141, the fifth doublet (I=5) occurs in the third cylinder, that is X(5)=3. This correlates with Table 2.1, where, when p=5, then q=3.

## B2 POTENTIAL LIFT AND DRAG ON CYLINDER 1 IN THE GROUP OF THREE

SPACING RATIO S/D = 1.10

| α | D1 | L1 | D2 | L2 | D3 | L3 |
|---|---|---|---|---|---|---|
| 0.000 | 0.784 | 0.001 | -0.391 | -1.036 | -0.396 | 1.050 |
| 7.500 | 0.779 | -0.154 | -0.478 | -0.950 | -0.303 | 1.118 |
| 15.000 | 0.759 | -0.309 | -0.556 | -0.844 | -0.206 | 1.164 |
| 22.500 | 0.727 | -0.459 | -0.624 | -0.726 | -0.106 | 1.195 |
| 30.000 | 0.683 | -0.607 | -0.671 | -0.582 | -0.017 | 1.198 |
| 37.500 | 0.622 | -0.732 | -0.724 | -0.453 | 0.097 | 1.194 |
| 45.000 | 0.552 | -0.848 | -0.754 | -0.304 | 0.196 | 1.162 |
| 52.500 | 0.474 | -0.952 | -0.773 | -0.152 | 0.294 | 1.115 |
| 60.000 | 0.385 | -1.036 | -0.777 | 0.004 | 0.387 | 1.045 |
| 67.500 | 0.293 | -1.104 | -0.769 | 0.156 | 0.475 | 0.962 |
| 75.000 | 0.195 | -1.150 | -0.748 | 0.306 | 0.554 | 0.858 |
| 82.500 | 0.095 | -1.180 | -0.716 | 0.452 | 0.627 | 0.742 |
| 90.000 | -0.007 | -1.186 | -0.671 | 0.588 | 0.688 | 0.610 |
| 97.500 | -0.107 | -1.176 | -0.617 | 0.717 | 0.738 | 0.469 |
| 105.000 | -0.205 | -1.142 | -0.552 | 0.832 | 0.775 | 0.316 |
| 112.500 | -0.300 | -1.094 | -0.478 | 0.936 | 0.798 | 0.159 |
| 120.000 | -0.384 | -1.027 | -0.393 | 1.026 | 0.798 | -0.003 |

SPACING RATIO S/D = 1.20

| α | D1 | L1 | D2 | L2 | D3 | L3 |
|---|---|---|---|---|---|---|
| 0.000 | 0.391 | 0.001 | -0.196 | -0.456 | -0.198 | 0.462 |
| 7.500 | 0.388 | -0.068 | -0.239 | -0.417 | -0.152 | 0.493 |
| 15.000 | 0.379 | -0.136 | -0.278 | -0.372 | -0.103 | 0.514 |
| 22.500 | 0.362 | -0.201 | -0.312 | -0.319 | -0.052 | 0.528 |
| 30.000 | 0.340 | -0.268 | -0.336 | -0.257 | -0.006 | 0.532 |
| 37.500 | 0.311 | -0.321 | -0.362 | -0.200 | 0.051 | 0.527 |
| 45.000 | 0.276 | -0.373 | -0.378 | -0.134 | 0.101 | 0.514 |
| 52.500 | 0.237 | -0.418 | -0.387 | -0.067 | 0.150 | 0.492 |
| 60.000 | 0.194 | -0.457 | -0.390 | 0.001 | 0.197 | 0.461 |
| 67.500 | 0.148 | -0.486 | -0.386 | 0.069 | 0.240 | 0.423 |
| 75.000 | 0.099 | -0.508 | -0.376 | 0.135 | 0.279 | 0.377 |
| 82.500 | 0.049 | -0.521 | -0.359 | 0.200 | 0.314 | 0.325 |
| 90.000 | -0.002 | -0.524 | -0.337 | 0.261 | 0.343 | 0.267 |
| 97.500 | -0.053 | -0.519 | -0.309 | 0.317 | 0.367 | 0.204 |
| 105.000 | -0.102 | -0.506 | -0.276 | 0.369 | 0.384 | 0.138 |
| 112.500 | -0.150 | -0.483 | -0.239 | 0.414 | 0.394 | 0.069 |
| 120.000 | -0.192 | -0.454 | -0.197 | 0.455 | 0.394 | -0.002 |

SPACING RATIO S/D = 1.50

| α | D1 | L1 | D2 | L2 | D3 | L3 |
|---|---|---|---|---|---|---|
| 0.000 | 0.096 | 0.000 | -0.049 | -0.100 | -0.049 | 0.101 |
| 7.500 | 0.095 | -0.015 | -0.059 | -0.092 | -0.037 | 0.108 |
| 15.000 | 0.093 | -0.030 | -0.068 | -0.082 | -0.025 | 0.113 |
| 22.500 | 0.088 | -0.045 | -0.076 | -0.071 | -0.013 | 0.116 |
| 30.000 | 0.083 | -0.060 | -0.082 | -0.057 | -0.002 | 0.117 |
| 37.500 | 0.076 | -0.071 | -0.089 | -0.044 | 0.012 | 0.116 |
| 45.000 | 0.067 | -0.082 | -0.093 | -0.030 | 0.025 | 0.113 |
| 52.500 | 0.058 | -0.092 | -0.095 | -0.015 | 0.037 | 0.108 |
| 60.000 | 0.047 | -0.101 | -0.096 | 0.000 | 0.048 | 0.101 |
| 67.500 | 0.036 | -0.107 | -0.095 | 0.015 | 0.059 | 0.093 |
| 75.000 | 0.024 | -0.112 | -0.093 | 0.030 | 0.068 | 0.083 |
| 82.500 | 0.012 | -0.115 | -0.089 | 0.044 | 0.076 | 0.071 |
| 90.000 | -0.001 | -0.116 | -0.083 | 0.058 | 0.083 | 0.058 |
| 97.500 | -0.013 | -0.115 | -0.077 | 0.071 | 0.089 | 0.045 |
| 105.000 | -0.025 | -0.112 | -0.068 | 0.082 | 0.093 | 0.030 |
| 112.500 | -0.037 | -0.107 | -0.059 | 0.092 | 0.095 | 0.015 |
| 120.000 | -0.047 | -0.101 | -0.049 | 0.102 | 0.095 | -0.001 |

## B3 VELOCITY ON THE SURFACE OF A CYLINDER LYING NEAR TO A SOLID BOUNDARY

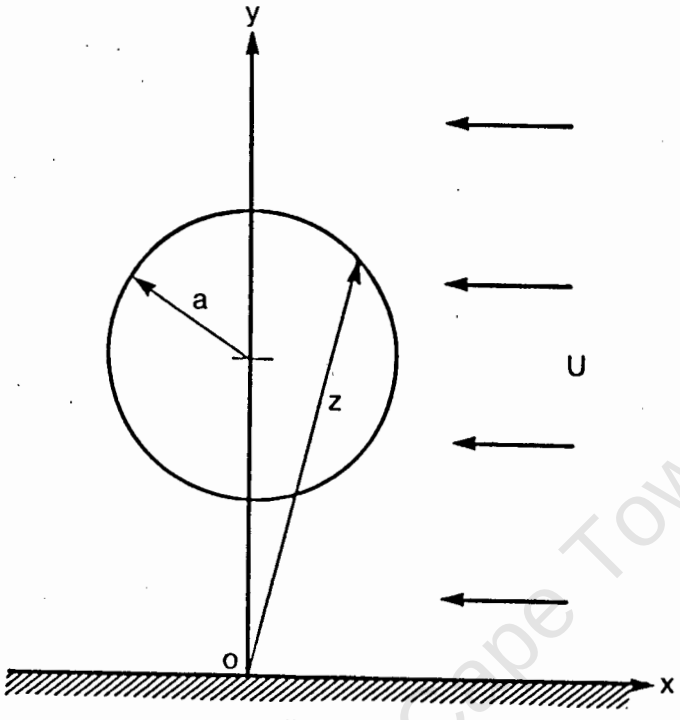


Fig. B1

The complex potential for flow over a cylinder lying near to a solid boundary is given by [22] as

$$w(z) = a\pi U \coth(a\pi/z) \qquad (B1)$$

Putting $\coth(a\pi/z) = (\cosh(a\pi/z))/(\sinh(a\pi/z))$

and noting that $\cosh(a\pi/z) = \cos(ia\pi/z)$

and $\sinh(a\pi/z) = -i\sin(ia\pi/z)$,

the equation (B1) becomes

$$w(z) = -(a\pi U/i)(\cos(ia\pi/z))/\sin(ia\pi/z) \qquad (B2)$$

Differentiating equation (B2) w.r.t.z gives

$$dw(z)/dz = V(z) = -(a\pi U/i)[(\cos(ia\pi/z))(-\sin(ia\pi/z))^{-2}\,..$$
$$..(\cos(ia\pi/z))(-ia\pi/z^2) + (\sin(ia\pi/z))^{-1}\,..$$
$$..(-\sin(ia\pi/z))(-ia\pi/z^2)]$$
$$= -(a\pi U/i)(-ia\pi/z^2)[-\cot^2(ia\pi/z) - 1]$$
$$= -(a^2\pi^2 U/z^2)(1 + \cot^2(ia\pi/z))$$

$$\text{Velocity } q = |V(z)| = |(a^2\pi^2 U/z^2)(1 + \cot^2(ia\pi/z))| \qquad (B3)$$

## B4 A COMPARISON OF THE IMAGE DOUBLET METHOD WITH THE EXACT SOLUTION OF MILNE-THOMSON [22] FOR A CYLINDER IN CONTACT WITH A SOLID BOUNDARY

| | | TWO CYLINDERS | | | | | |
|---|---|---|---|---|---|---|---|
| CYLINDER ANGLE $\theta$ | EXACT SOLUTION EQU'N (3.1) | CYLINDER 2 S/D = 100 | CYLINDER 2 S/D = 1 | | | | |
| | | | 24 DOUBLETS | ERROR (%) | 48 DOUBLETS | ERROR (%) | CORRECTED |
| 0.00 deg. | 7.837 m/s | 0.00 m/s | 7.04 m/s | -10.1 | 7.43 | - 5.2 | 7.43 m/s |
| 7.50 | 9.816 | 2.61 | 9.11 | - 7.2 | 9.45 | - 3.7 | 9.45 |
| 15.00 | 11.852 | 5.18 | 11.22 | - 5.33 | 11.53 | - 2.7 | 11.53 |
| 22.50 | 13.886 | 7.65 | 13.31 | | 13.59 | | 13.59 |
| 30.00 | 15.863 | 10.00 | 15.33 | - 3.3 | 15.59 | - 1.7 | 15.59 |
| 37.50 | 17.733 | 12.18 | 17.23 | | 17.48 | | 17.48 |
| 45.00 | 19.450 | 14.14 | 18.98 | - 2.4 | 19.21 | - 1.23 | 19.21 |
| 52.50 | 20.974 | 15.87 | 20.52 | | 20.74 | | 20.74 |
| 60.00 | 22.269 | 17.32 | 21.83 | - 2.0 | 22.05 | - 1.12 | 22.05 |
| 67.50 | 23.307 | 18.48 | 22.89 | - | 23.09 | | 23.09 |
| 75.00 | 24.065 | 19.32 | 23.65 | - 1.7 | 23.85 | - 0.89 | 23.85 |
| 82.50 | 24.526 | 19.83 | 24.12 | | 24.31 | | 24.31 |
| 90.00 | 24.680 | 20.00 | 24.27 | - 1.6 | 24.47 | - 0.85 | 24.47 |
| 97.50 | 24.525 | 19.83 | 24.12 | | 24.31 | | 24.31 |
| 105.00 | 24.063 | 19.32 | 23.65 | - 1.7 | 23.85 | - 0.89 | 23.85 |
| 112.50 | 23.304 | 18.48 | 22.88 | | 23.09 | | 23.09 |
| 120.00 | 22.266 | 17.32 | 21.83 | - 2.1 | 22.04 | - 0.99 | 22.04 |
| 127.50 | 20.970 | 15.86 | 20.52 | | 20.74 | | 20.74 |
| 135.00 | 19.445 | 14.14 | 18.97 | - 2.3 | 19.20 | - 1.3 | 19.20 |
| 142.50 | 17.728 | 12.17 | 17.23 | | 17.47 | | 17.47 |
| 150.00 | 15.857 | 9.99 | 15.32 | - 3.1 | 15.58 | - 1.7 | 15.58 |
| 157.50 | 13.880 | 7.65 | 13.30 | | 13.59 | | 13.59 |
| 165.00 | 11.846 | 5.17 | 11.21 | - 5.4 | 11.52 | - 2.8 | 11.52 |
| 172.50 | 9.810 | 2.60 | 9.10 | | 9.45 | | 9.45 |
| 180.00 | 7.831 | 0.01 | 7.03 | -10.2 | 7.43 | - 5.1 | 7.43 |
| 187.50 | 5.970 | 2.62 | 5.05 | | 5.50 | | 5.50 |
| 195.00 | 4.289 | 5.18 | 3.21 | -25.1 | 3.74 | -12.8 | 3.74 |
| 202.50 | 2.846 | 7.66 | 1.56 | | 2.19 | | 0.00 |
| 210.00 | 1.692 | 10.01 | 0.10 | -94.0 | 0.88 | -48.0 | 0.00 |
| 217.50 | 0.857 | 12.18 | 1.18 | | 0.18 | | 0.00 |
| 225.00 | 0.341 | 14.15 | 2.37 | -595.0 | 1.05 | +208.0 | 0.00 |
| 232.50 | 0.091 | 15.87 | 3.74 | | 1.88 | | 0.00 |
| 240.00 | 0.012 | 17.33 | 5.86 | +48733 | 3.03 | +25150 | 0.00 |
| 247.50 | 0.000 | 18.48 | 10.17 | | 5.34 | | 0.00 |
| 255.00 | 0.000 | 19.32 | 21.70 | | 11.81 | | 0.00 |
| 262.50 | 0.000 | 19.83 | 69.14 | | 44.28 | | 0.00 |
| 270.00 | 0.000 | 20.00 | 249.94 | | 489.52 | | 0.00 |
| 277.50 | 0.000 | 19.83 | 67.20 | | 42.73 | | 0.00 |
| 285.00 | 0.000 | 19.32 | 21.32 | | 11.59 | | 0.00 |
| 292.50 | 0.001 | 18.47 | 10.05 | | 5.27 | | 0.00 |
| 300.00 | 0.012 | 17.31 | 5.81 | | 3.00 | | 0.00 |
| 307.50 | 0.092 | 15.86 | 3.72 | +3943 | 1.87 | +1932 | 0.00 |
| 315.00 | 0.344 | 14.13 | 2.36 | | 1.04 | | 0.00 |
| 322.50 | 0.864 | 12.16 | 1.17 | +35.4 | 0.18 | -79.0 | 0.00 |
| 330.00 | 1.701 | 9.99 | 0.11 | | 0.88 | | 0.00 |
| 337.50 | 2.858 | 7.64 | 1.57 | -45 | 2.20 | -23.0 | 0.00 |
| 345.00 | 4.303 | 5.16 | 3.23 | | 3.75 | | 3.75 |
| 352.50 | 5.987 | 2.59 | 5.07 | -15.3 | 5.52 | - 7.8 | 5.52 |
| $C_L$ | 4.494 | 0.000 | -31.59 | 803 | -103.63 | 2406 | 4.41 |
| $C_0$ | 0.000 | 0.000 | 0.000 | 0.000 | 0.000 | 0.000 | 0.000 |

# APPENDIX C

## C1 DRAG DATA FOR OPEN JET BLOCKAGE EXPERIMENTS NOMINAL FREE STREAM VELOCITY 10 m/s.

| Distance from Tunnel Mouth | Area Ratio (a/A) | Drag $D_s$ | Drag $D_o$ | Drag Coeff. $C_D$ |
|---|---|---|---|---|
| -125 mm | $5.1 \times 10^{-3}$ | 0.46N | 0.38N | 1.03 |
| | 16.1 | 0.65 | 0.38 | 1.11 |
| | 32.5 | 0.97 | 0.38 | 1.20 |
| | 55.0 | 1.49 | 0.38 | 1.34 |
| | 82.2 | 2.28 | 0.39 | 1.52 |
| | 115.2 | 3.40 | 0.40 | 1.73 |
| | 156.3 | 5.23 | 0.42 | 2.04 |
| | 200.8 | 7.77 | 0.45 | 2.41 |
| | 252.6 | 11.6 | 0.49 | 2.9 |
| | 308.7 | 17.3 | 0.54 | 3.6 |
| 120 mm | $5.1 \times 10^{-3}$ | 0.48 | 0.39 | 1.21 |
| | 16.1 | 0.66 | 0.39 | 1.16 |
| | 32.5 | 0.96 | 0.39 | 1.21 |
| | 55.0 | 1.39 | 0.39 | 1.25 |
| | 82.2 | 2.0 | 0.39 | 1.3 |
| | 115.2 | 2.8 | 0.41 | 1.4 |
| | 156.2 | 4.0 | 0.46 | 1.6 |
| | 200.8 | 5.5 | 0.52 | 1.7 |
| | 252.6 | 7.4 | 0.58 | 1.9 |
| | 308.7 | 10.0 | 0.66 | 2.1 |
| 430 mm | $5.1 \times 10^{-3}$ | 0.47 | 0.39 | 1.07 |
| | 16.1 | 0.64 | 0.39 | 1.07 |
| | 32.5 | 0.91 | 0.39 | 1.10 |
| | 55.0 | 1.28 | 0.39 | 1.12 |
| | 82.2 | 1.70 | 0.39 | 1.10 |
| | 115.2 | 2.20 | 0.39 | 1.08 |
| | 156.2 | 2.85 | 0.39 | 1.09 |
| | 200.8 | 3.6 | 0.39 | 1.1 |
| | 252.6 | 4.5 | 0.39 | 1.1 |
| | 308.7 | 5.5 | 0.39 | 1.1 |
| 750 mm | $5.1 \times 10^{-3}$ | 0.47 | 0.39 | 1.07 |
| | 16.1 | 0.64 | 0.39 | 1.07 |
| | 32.5 | 0.91 | 0.39 | 1.10 |
| | 55.0 | 1.28 | 0.39 | 1.12 |
| | 82.2 | 1.7 | 0.39 | 1.1 |
| | 115.2 | 2.2 | 0.39 | 1.1 |
| | 156.3 | 2.8 | 0.39 | 1.1 |
| | 200.8 | 3.4 | 0.39 | 1.0 |
| | 252.6 | 4.2 | 0.39 | 1.0 |
| | 308.7 | 5.1 | 0.39 | 1.0 |
| 1050 mm | $5.1 \times 10^{-3}$ | 0.47 | 0.39 | 1.07 |
| | 16.1 | 0.64 | 0.39 | 1.07 |
| | 32.5 | 0.92 | 0.39 | 1.12 |
| | 55.0 | 1.28 | 0.39 | 1.12 |
| | 82.2 | 1.75 | 0.39 | 1.14 |
| | 115.1 | 2.25 | 0.39 | 1.11 |
| | 156.3 | 2.9 | 0.39 | 1.1 |
| | 200.8 | 3.7 | 0.39 | 1.1 |
| | 252.6 | 4.6 | 0.39 | 1.2 |
| | 308.7 | 5.6 | 0.39 | 1.2 |

# APPENDIX D

D1 PRESSURE COEFFICIENT VERSUS ANGLE $\theta$ AROUND CYLINDER 1 IN THE GROUP OF THREE CYLINDERS AT VARIOUS INCLINATION ANGLES $\alpha$

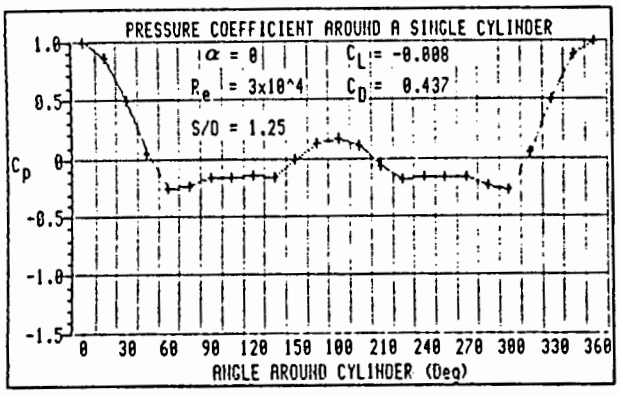


(a)

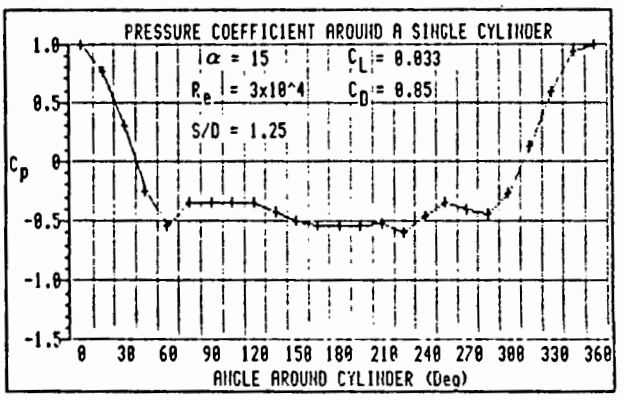


(b)

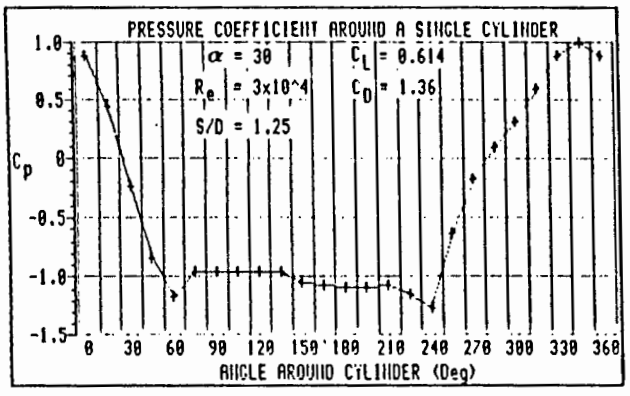


(c)

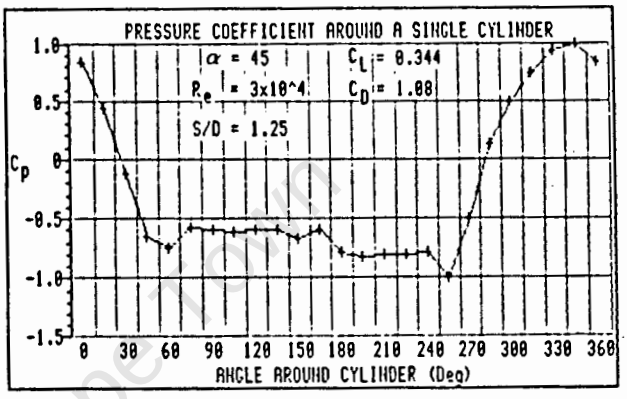


(d)

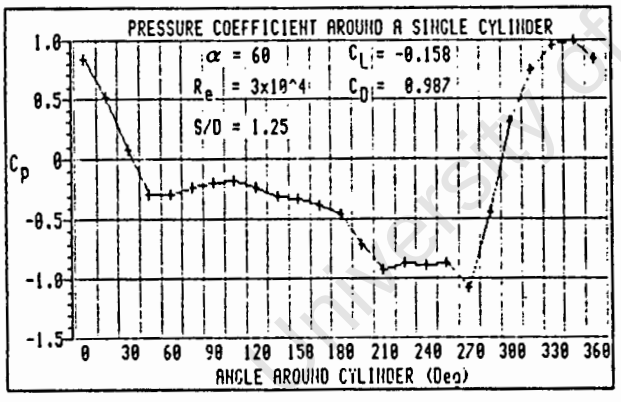


(e)

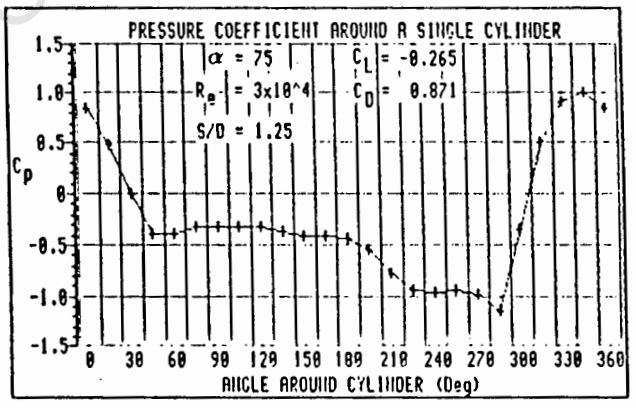


(f)

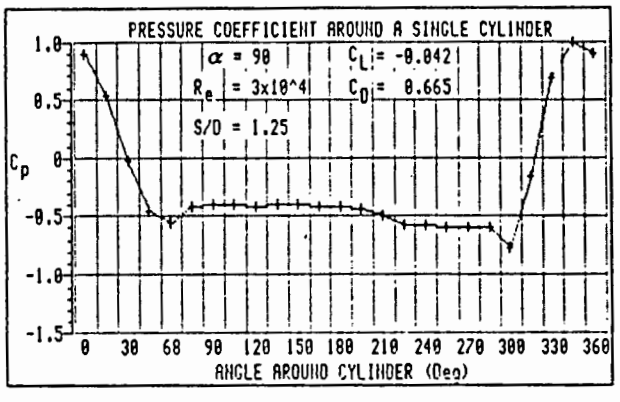


(g)

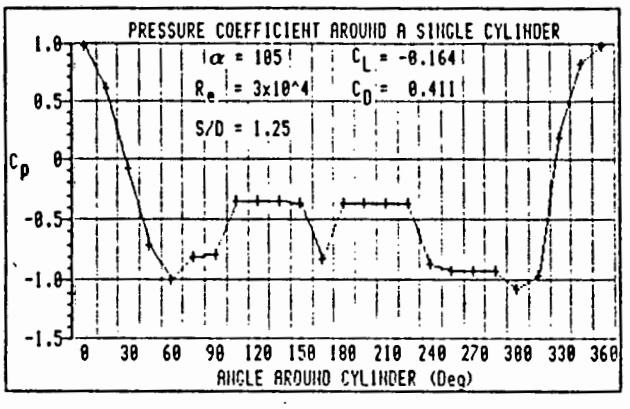


(h)

Fig. D1.1 Pressure coefficient around cylinder 1 in the group of three for various inclination angles. S/D = 1.25

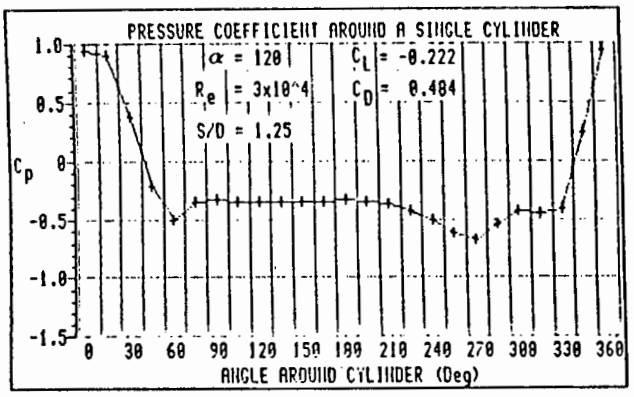


(i)

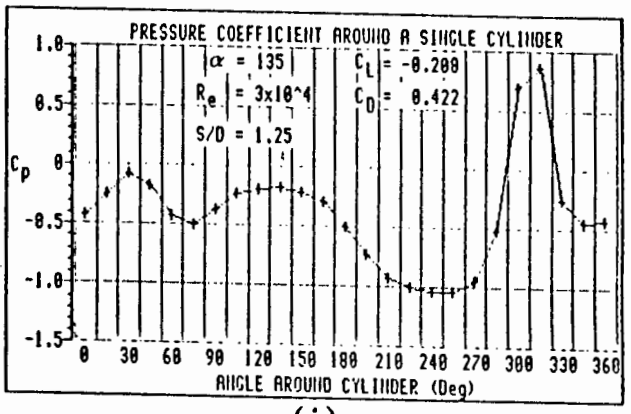


(j)

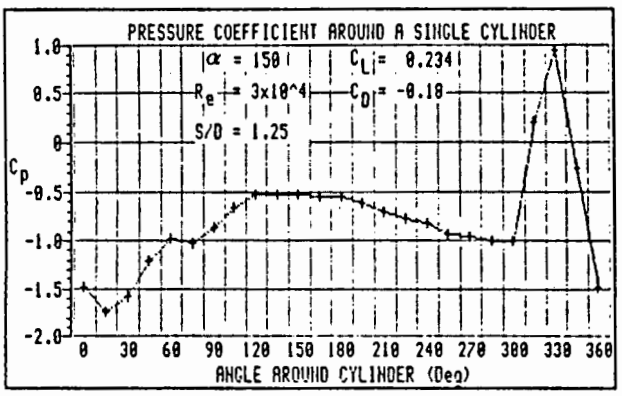


(k)

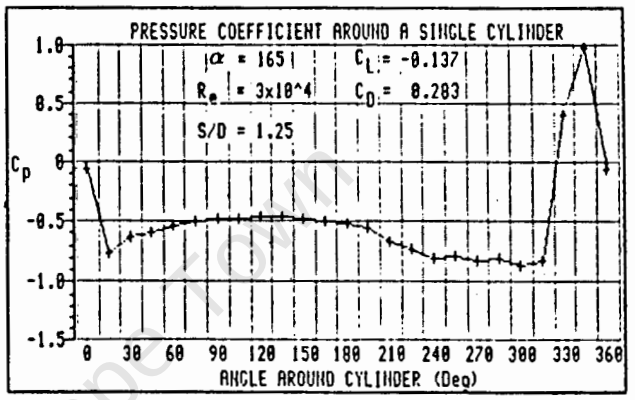


(l)

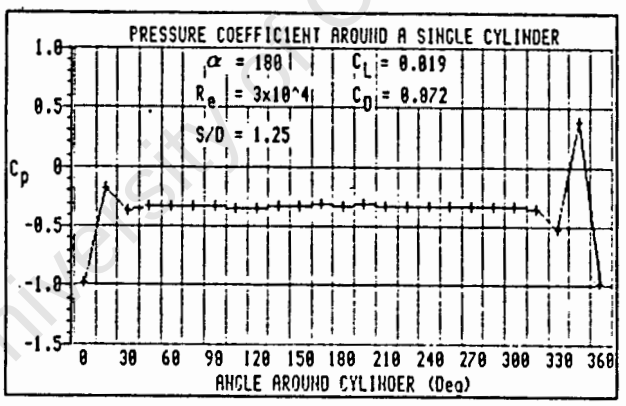


(m)



Fig. D1.1 Pressure coefficient around cylinder 1 in the group of three for various inclination angles. S/D = 1.25

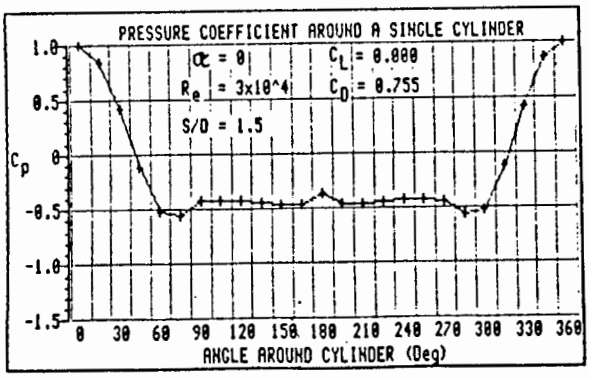


(a)

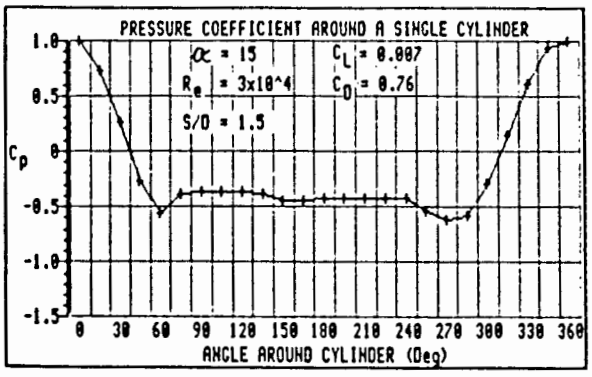


(b)

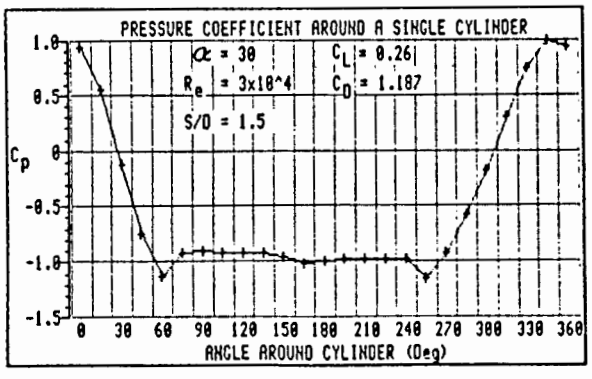


(c)

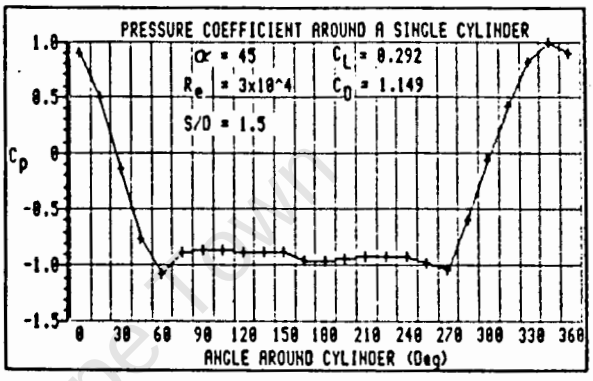


(d)

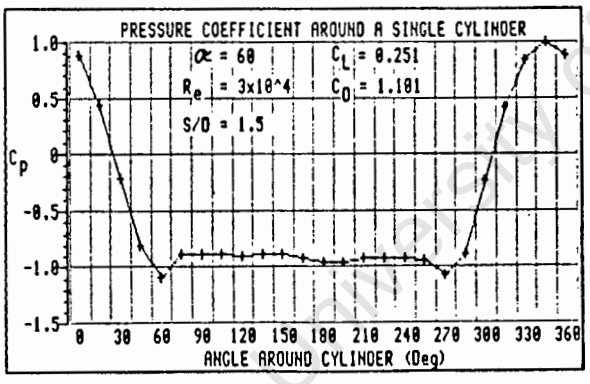


(e)

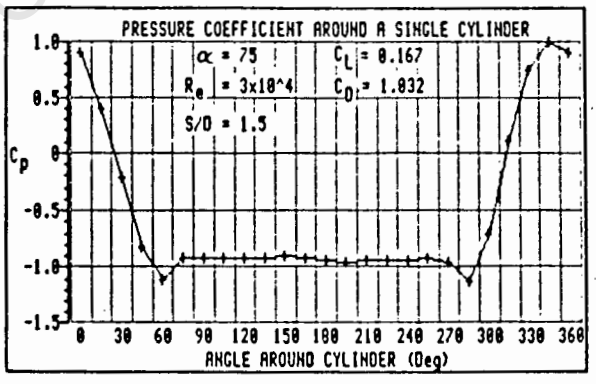


(f)

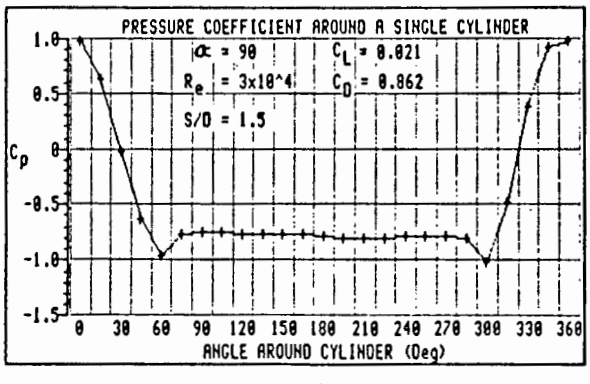


(g)

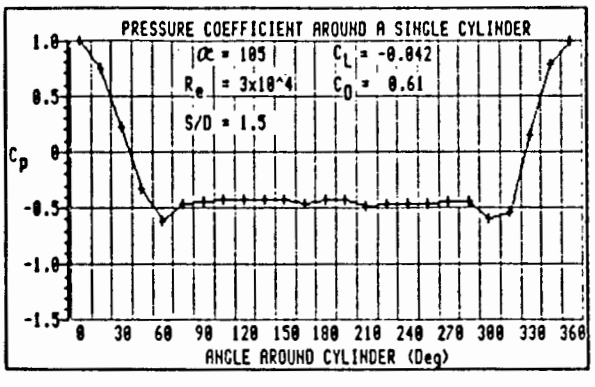


(h)

Fig. D1.2 Pressure coefficient around cylinder 1 in the group of three for various inclination angles. S/D = 1.5

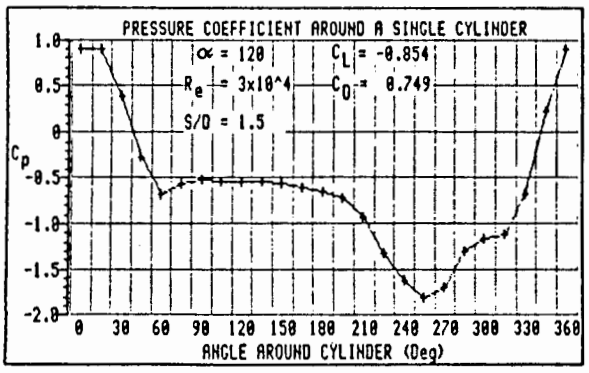


(i)

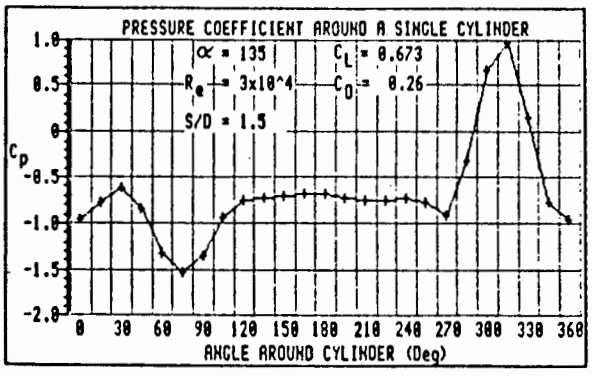


(j)

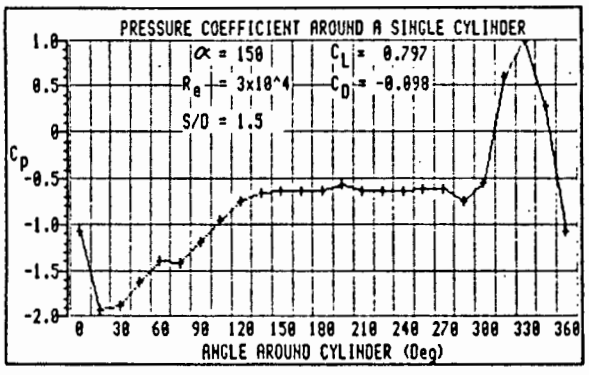


(k)

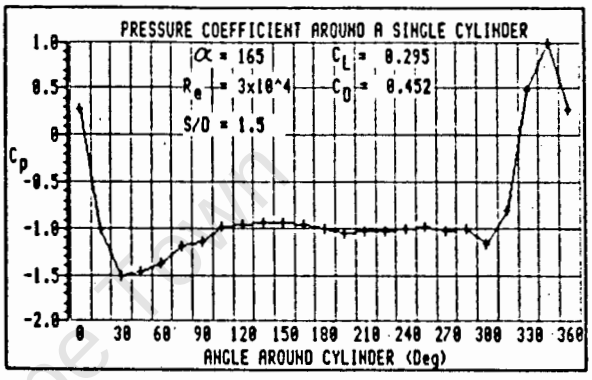


(l)

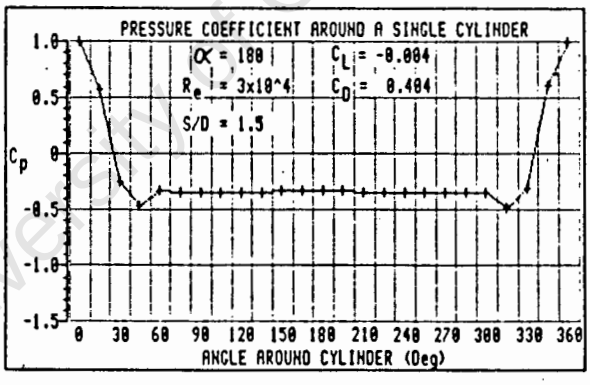


(m)



Fig. D1.2 Pressure coefficient around cylinder 1 in the group of three for various inclination angles. S/D = 1.5

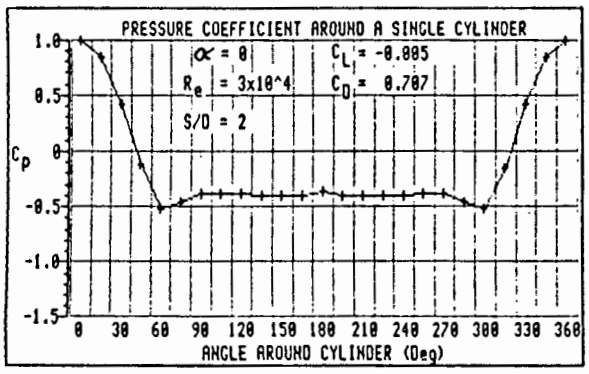


(a)

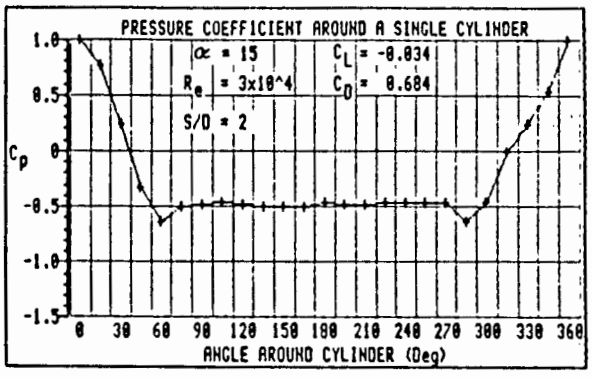


(b)

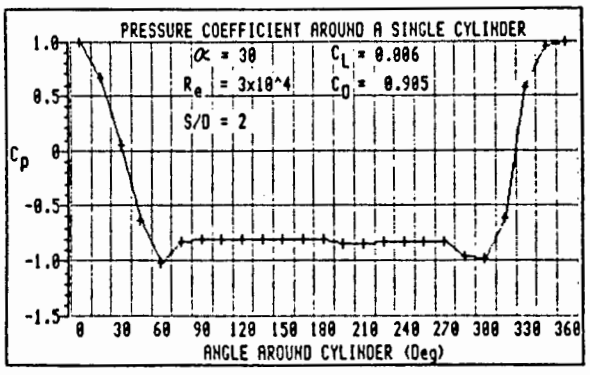


(c)

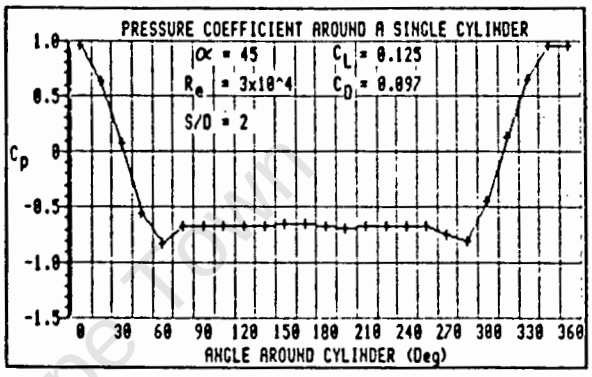


(d)

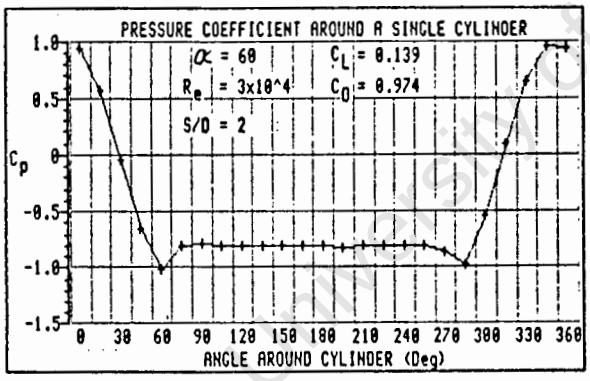


(e)

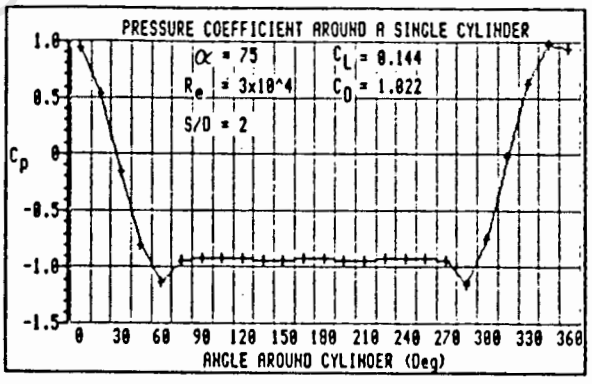


(f)

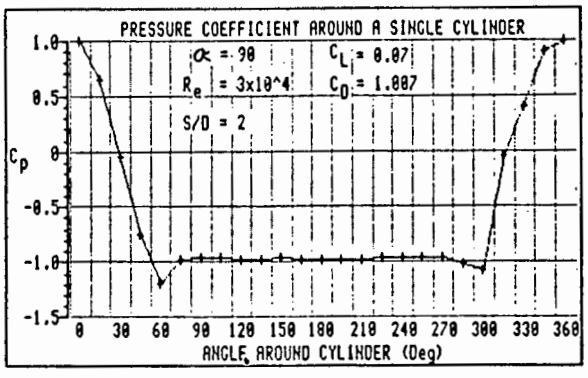


(g)

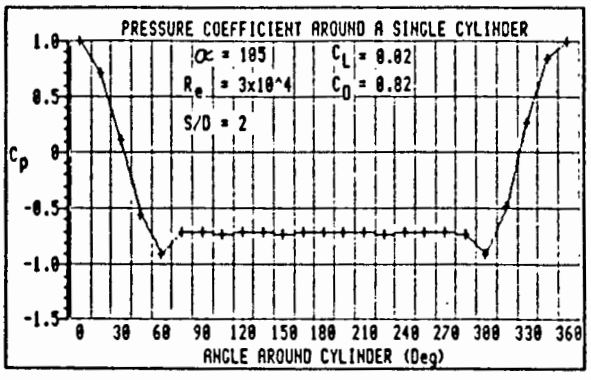


(h)

Fig. D1.3 Pressure coefficient around cylinder 1 in the group of three for various inclination angles. S/D = 2.

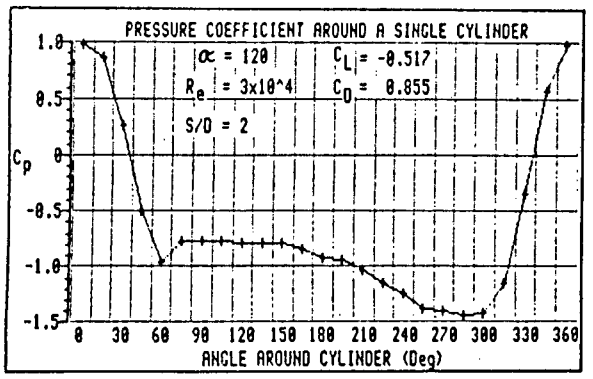


(i)

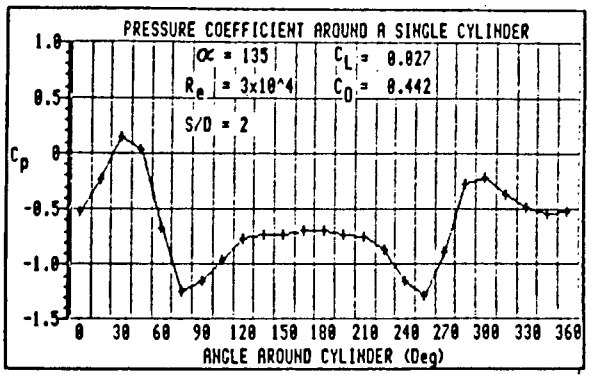


(j)

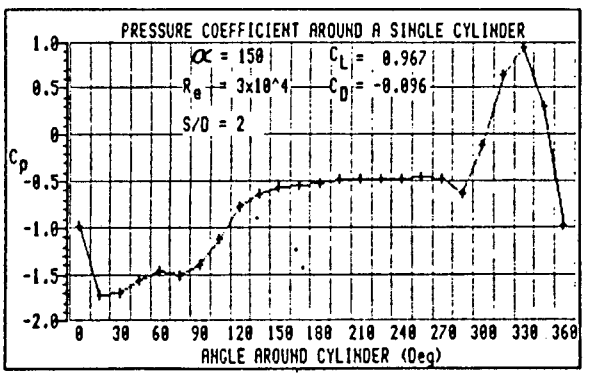


(k)

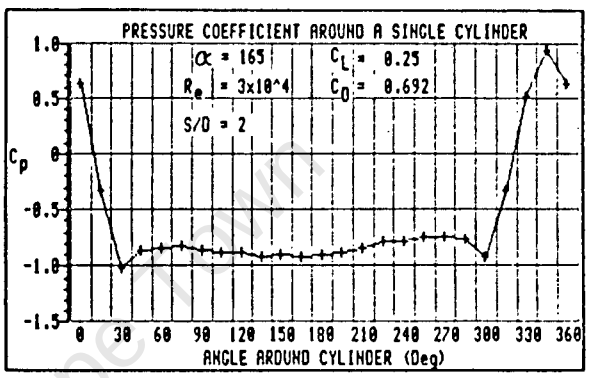


(l)

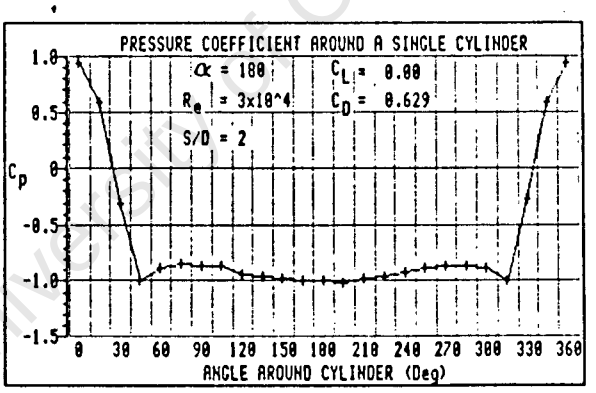


(m)



Fig. D1.3 Pressure coefficient around cylinder 1 in the group of three for various inclination angles. S/D = 2.

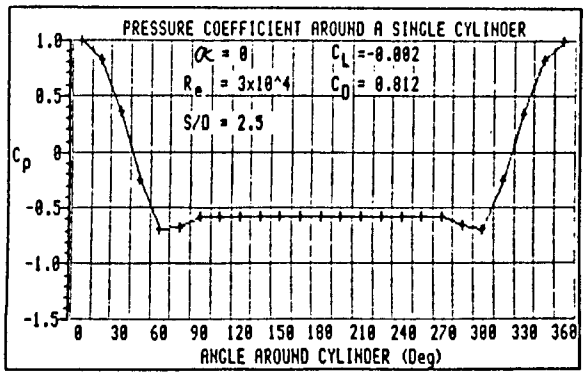


(a)

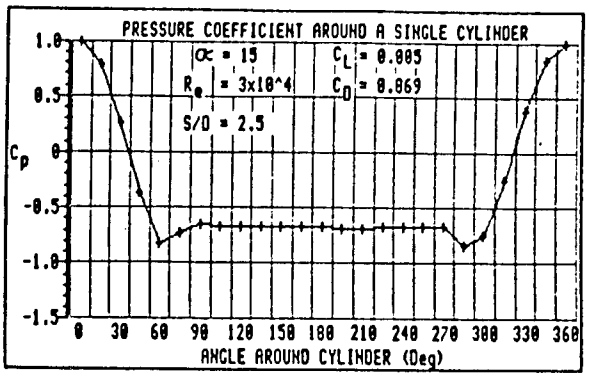


(b)

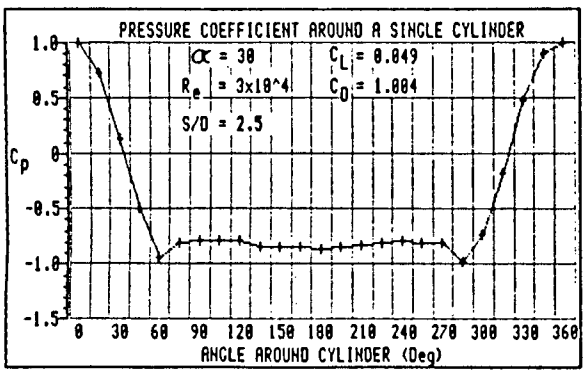


(c)

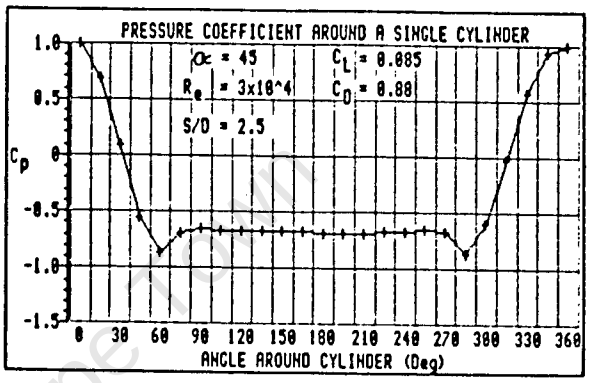


(d)

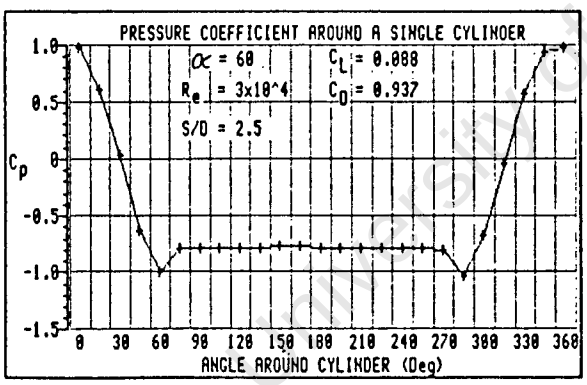


(e)

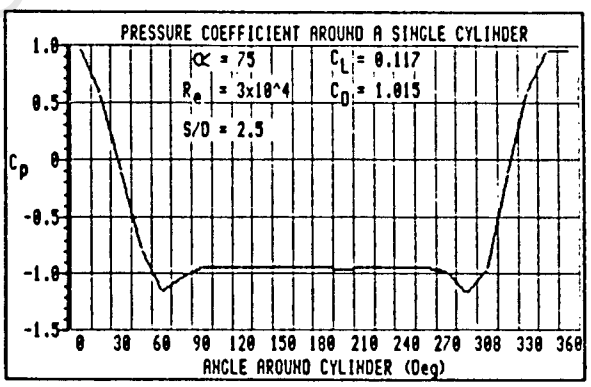


(f)

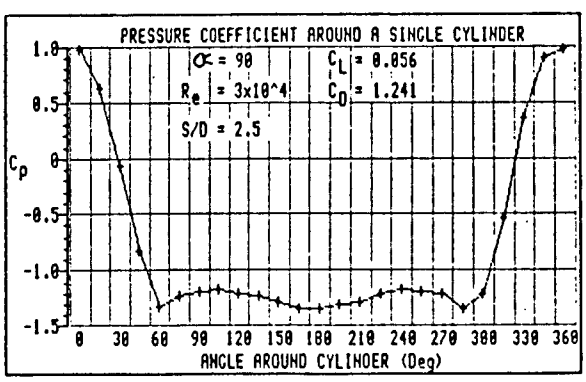


(g)

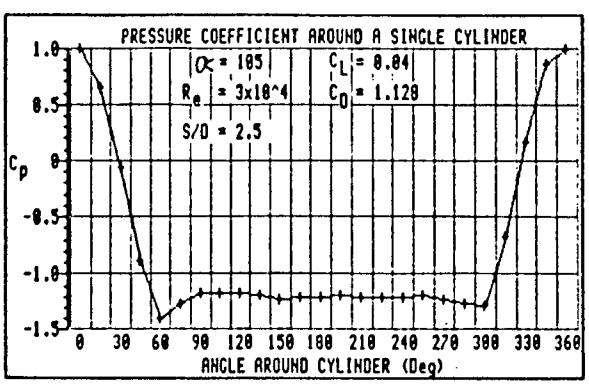


(h)

Fig. D1.4 Pressure coefficient around cylinder 1 in the group of three for various inclination angles. S/D =2.5.

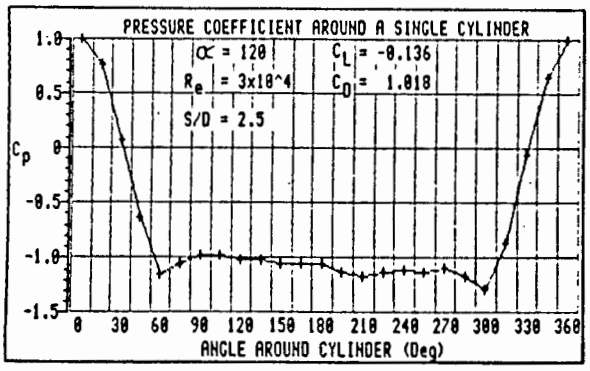


(i)

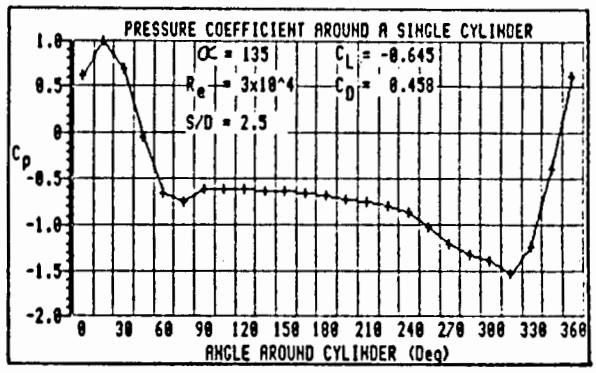


(j)

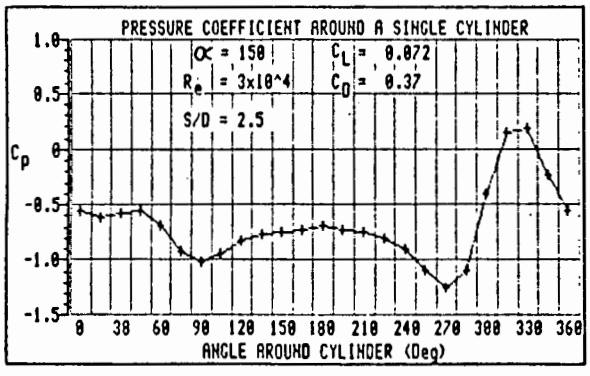


(k)

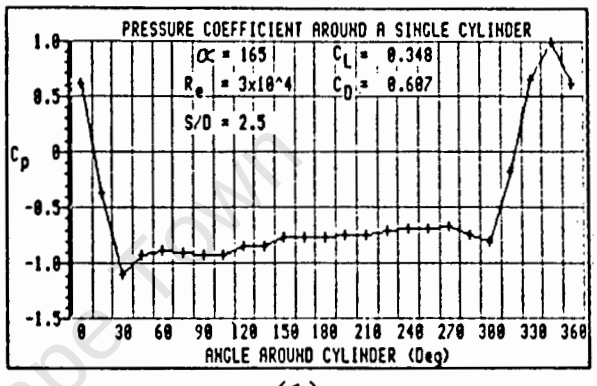


(l)

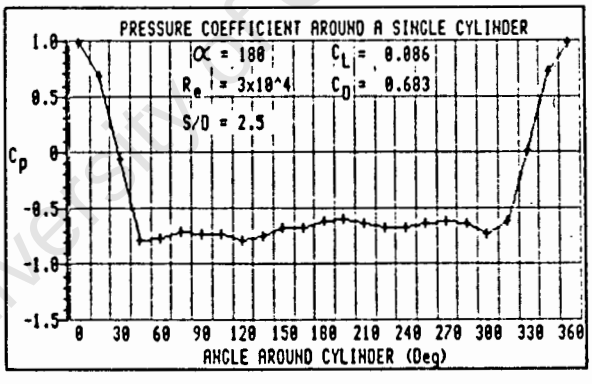


(m)



Fig. D1.4 Pressure coefficient around cylinder 1 in the group of three for various inclination angles. S/D = 2.5.

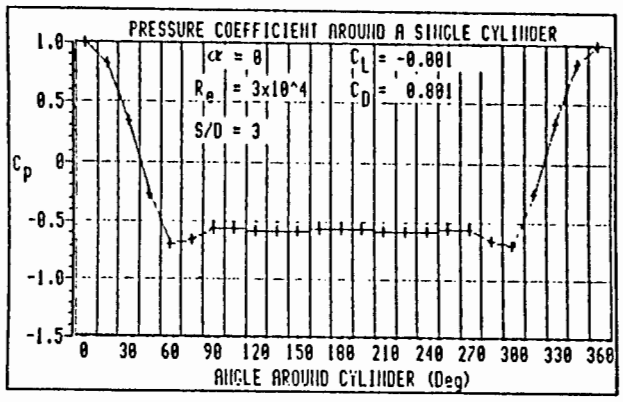


(a)

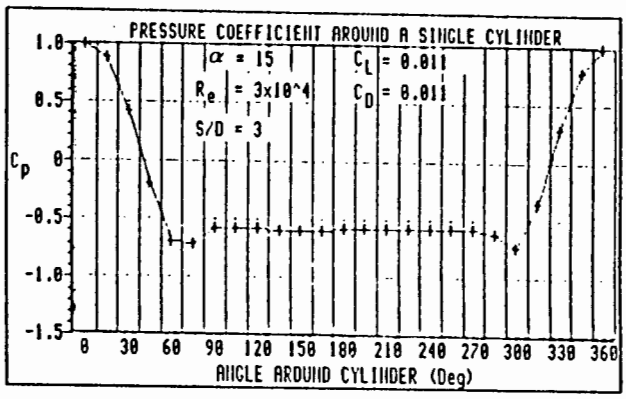


(b)

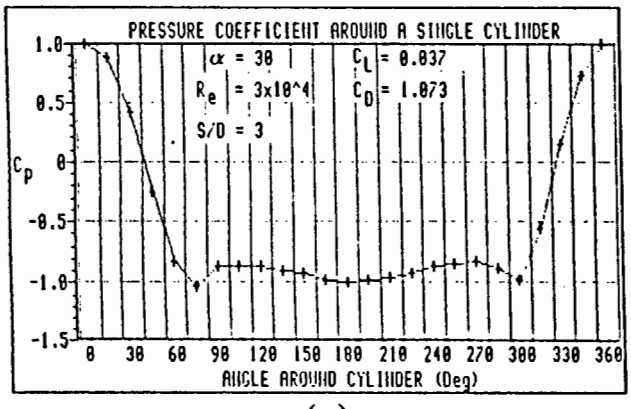


(c)

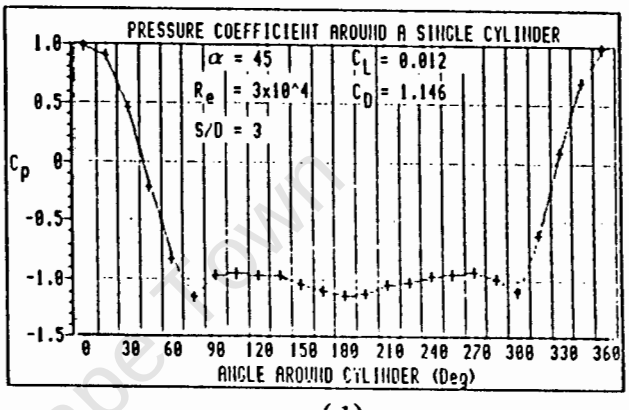


(d)

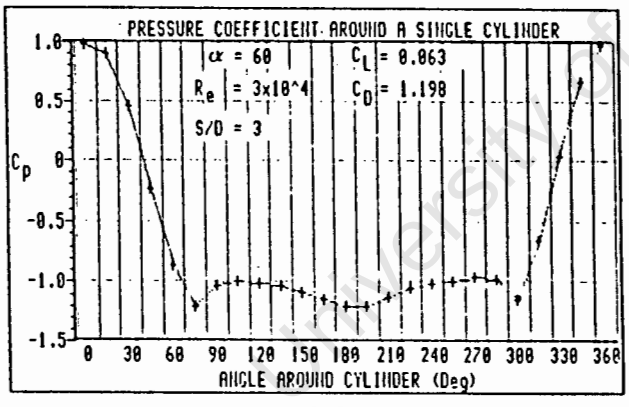


(e)

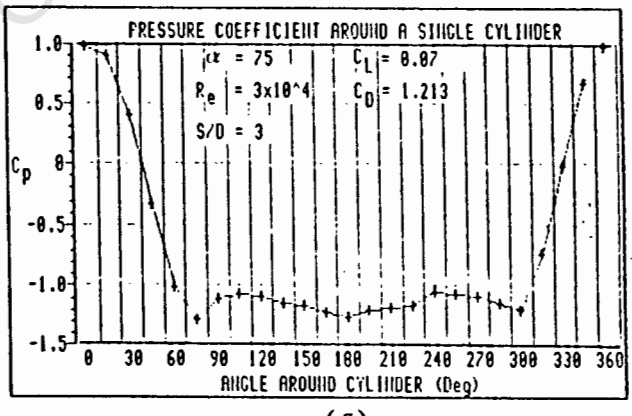


(f)

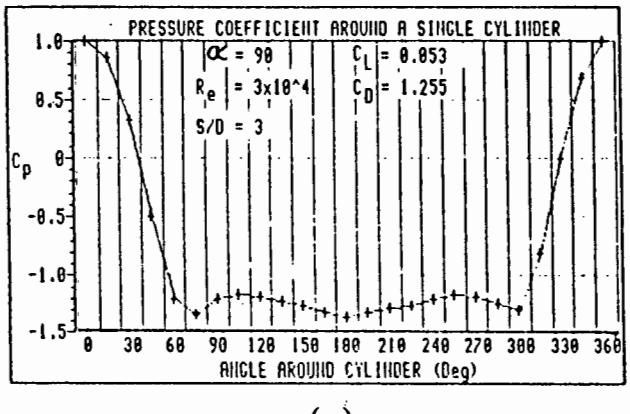


(g)

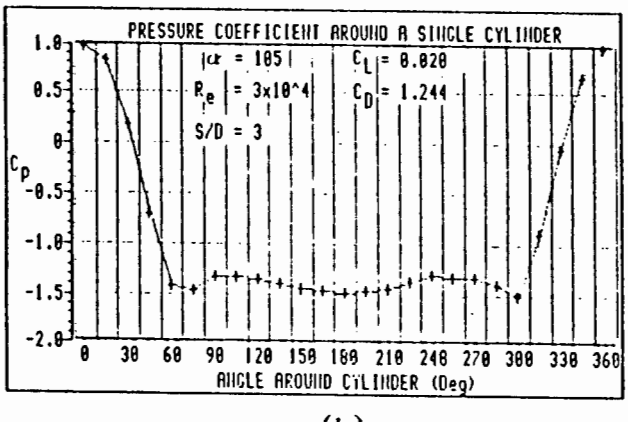


(h)

Fig. D1.5 Pressure coefficient around cylinder 1 in the group of three for various inclination angles. S/D = 3.

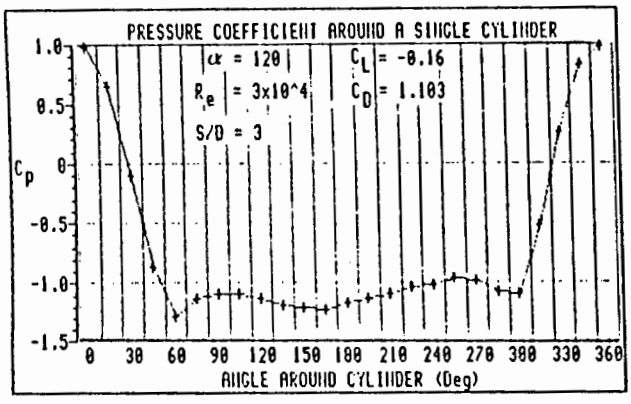


(i)

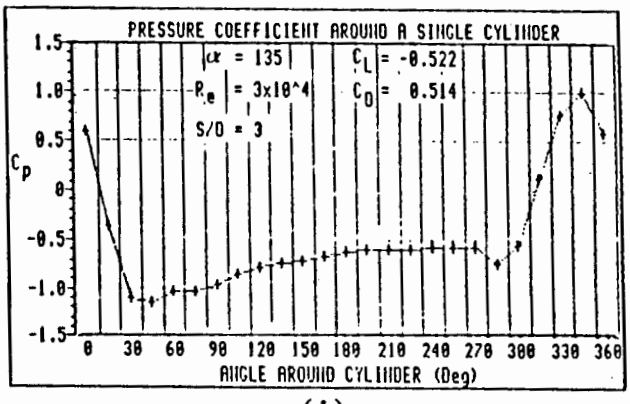


(j)

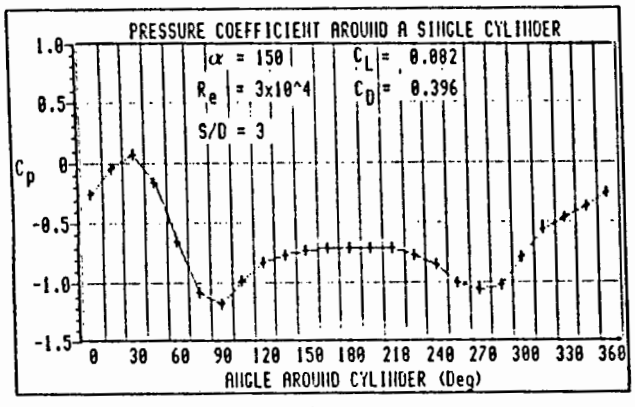


(k)

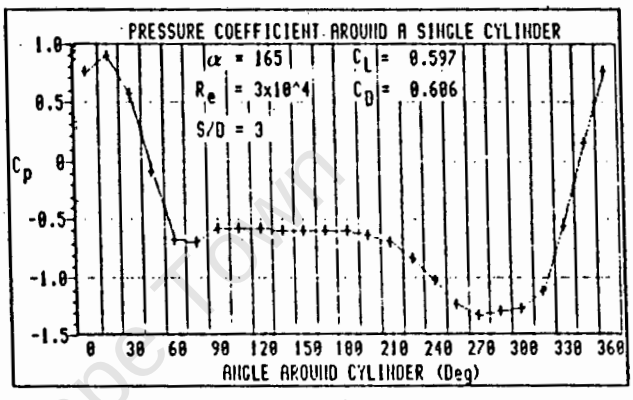


(l)

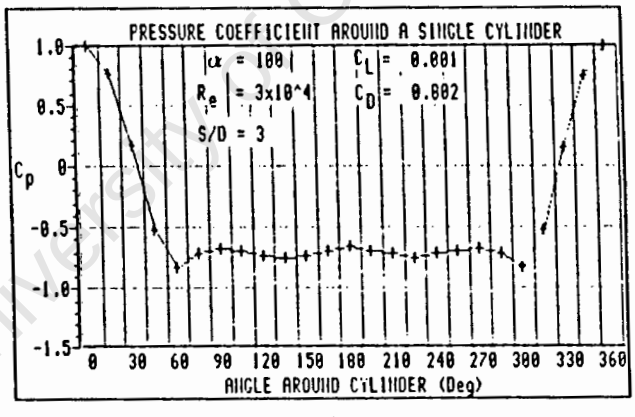


(m)



Fig. D1.5 Pressure coefficient around cylinder 1 in the group of three for various inclination angles. S/D = 5.

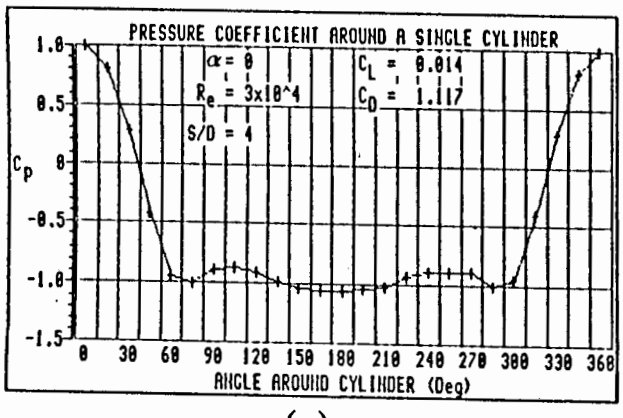


(a)

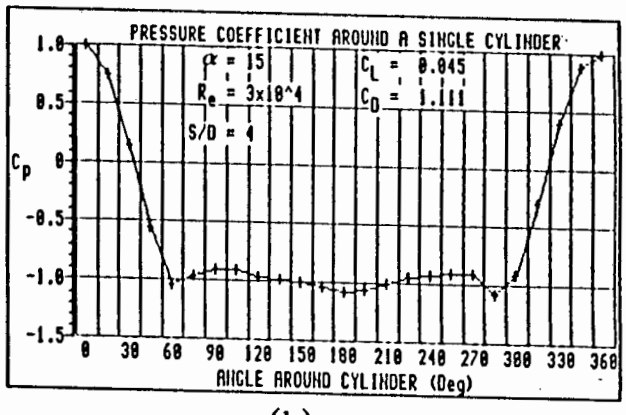


(b)

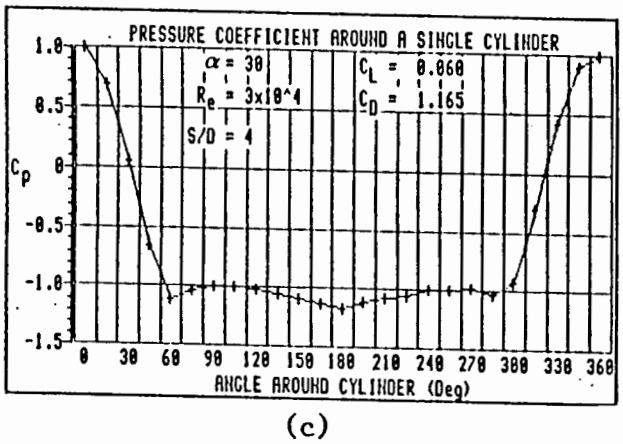


(c)

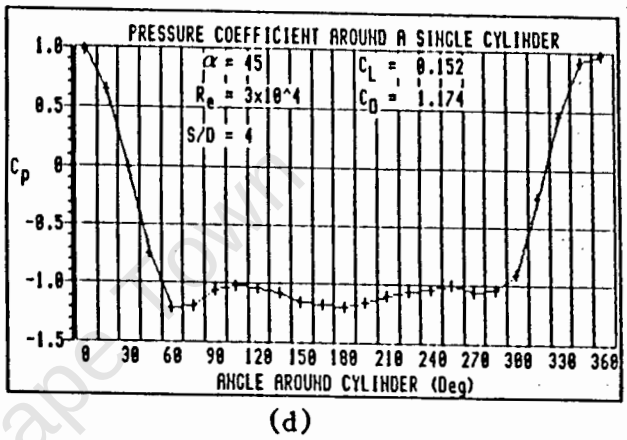


(d)

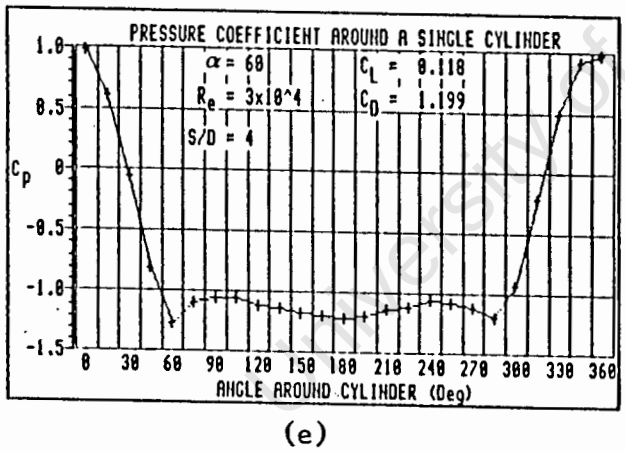


(e)

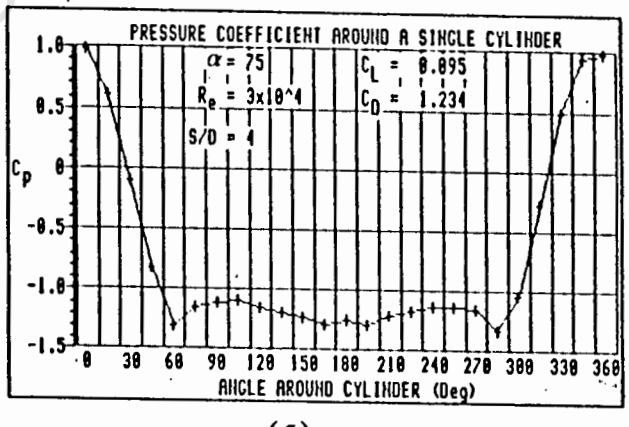


(f)

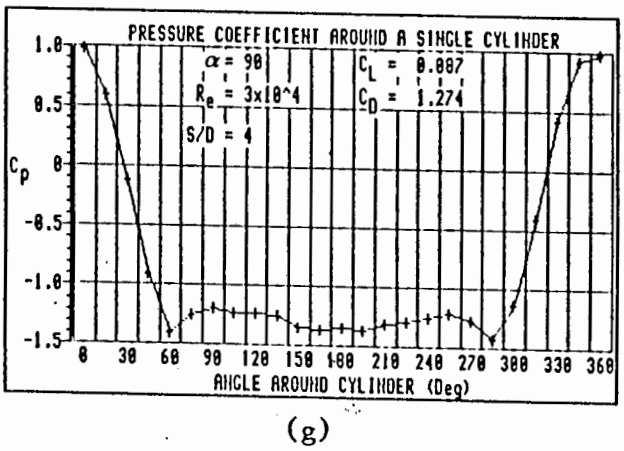


(g)

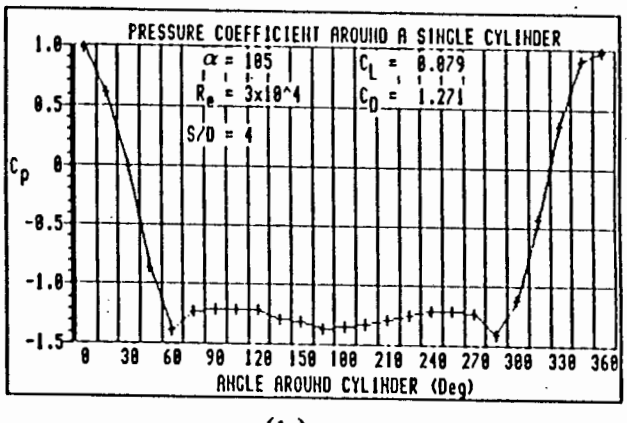


(h)

Fig. D1.6 Pressure coefficient around cylinder 1 in the group of three for various inclination angles. S/D = 4.

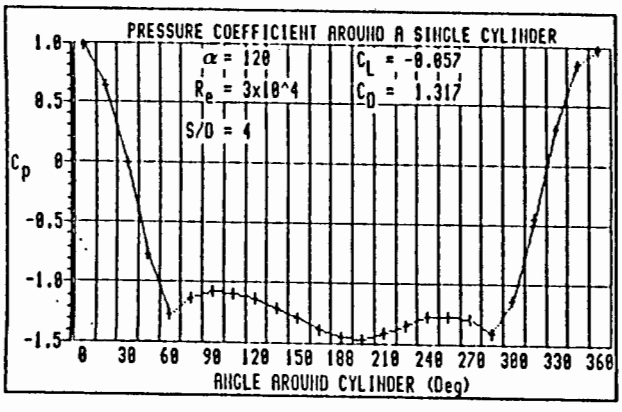


(i)

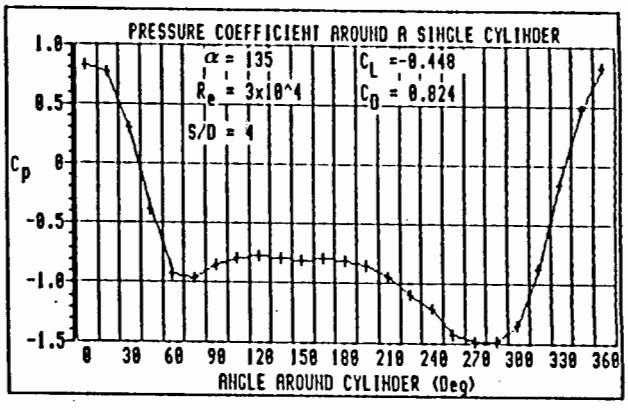


(j)

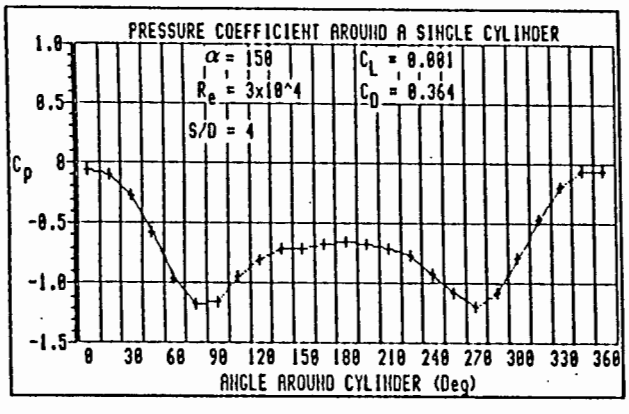


(k)

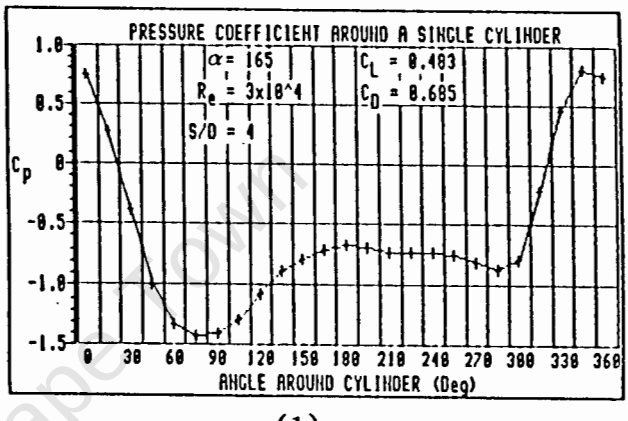


(l)

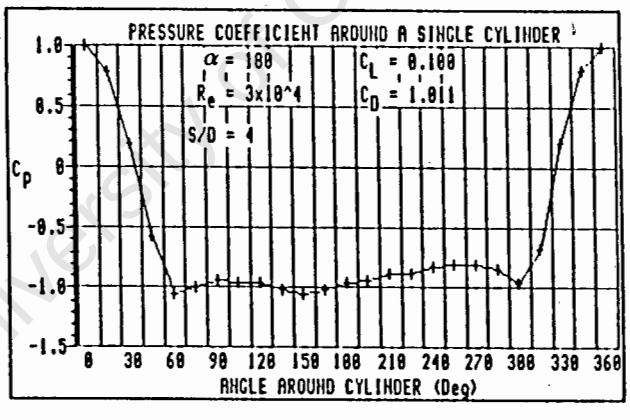


(m)



Fig. D1.6 Pressure coefficient around cylinder 1 in the group of three . for various inclination angles. S/D = 4.

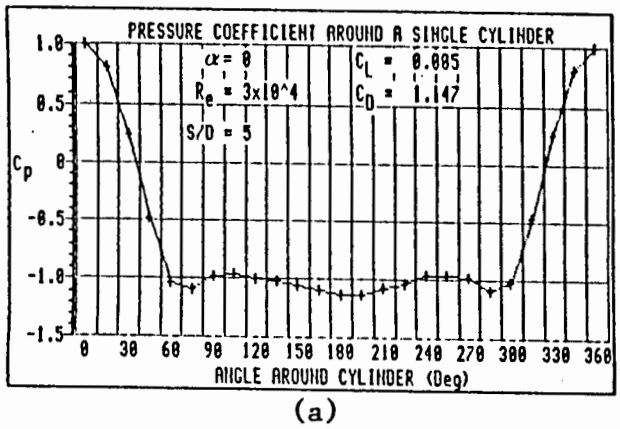


(a)

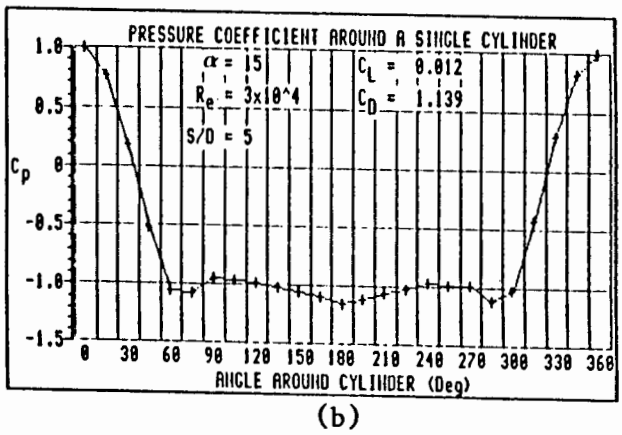


(b)

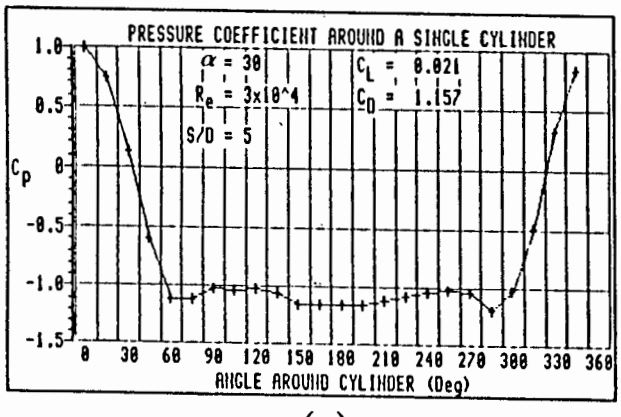


(c)

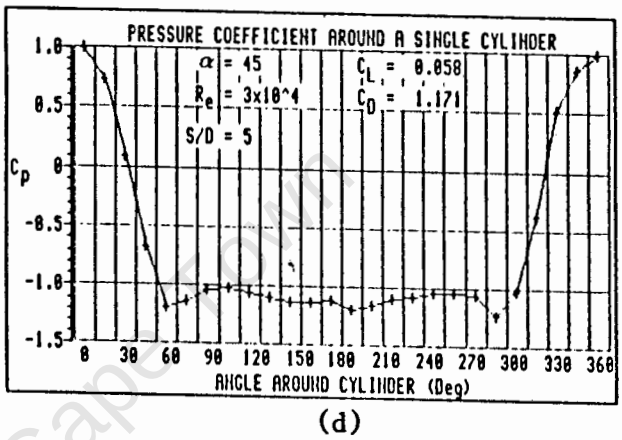


(d)

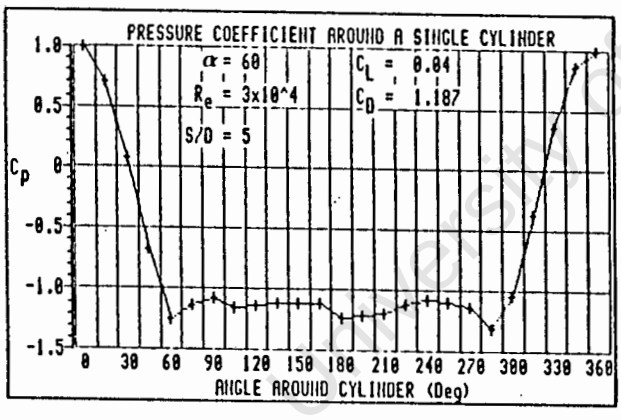


(e)

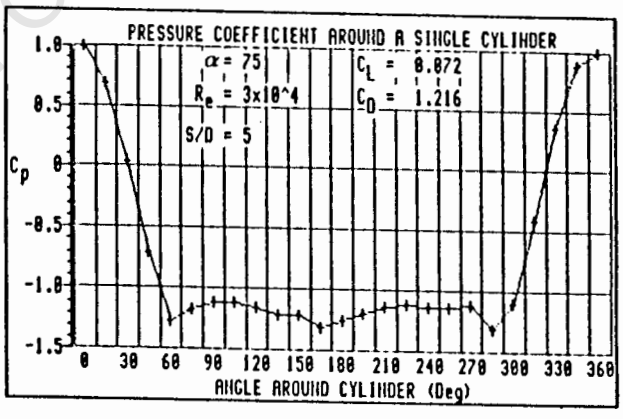


(f)

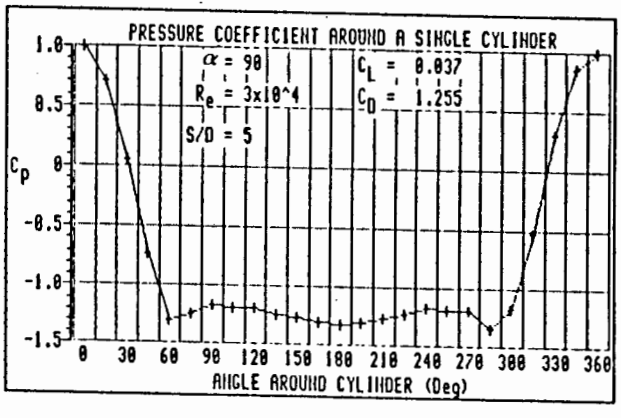


(g)

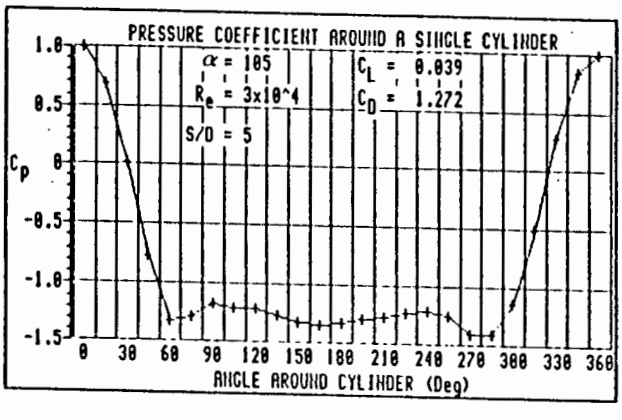


(h)

Fig. D1.7 Pressure coefficient around cylinder 1 in the group of three for various inclination angles. S/D = 5.

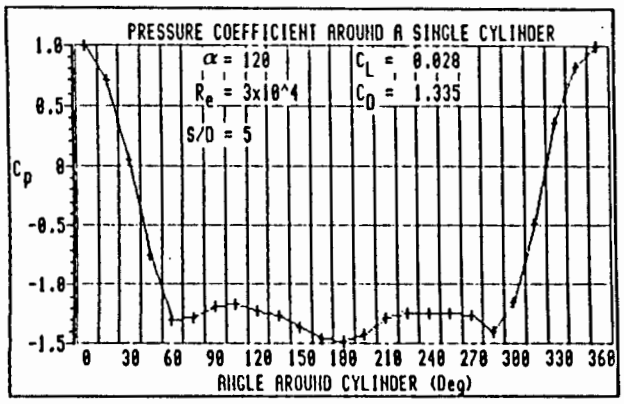


(i)

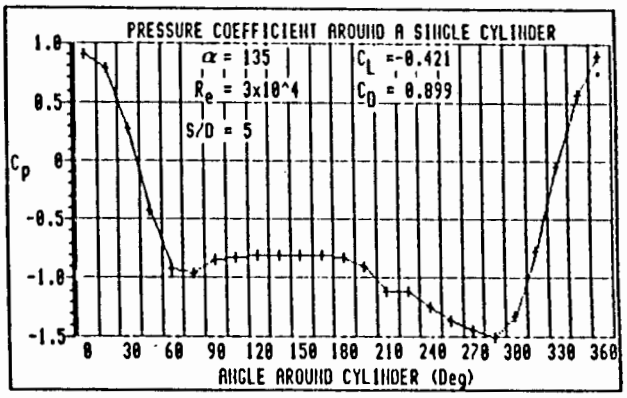


(j)

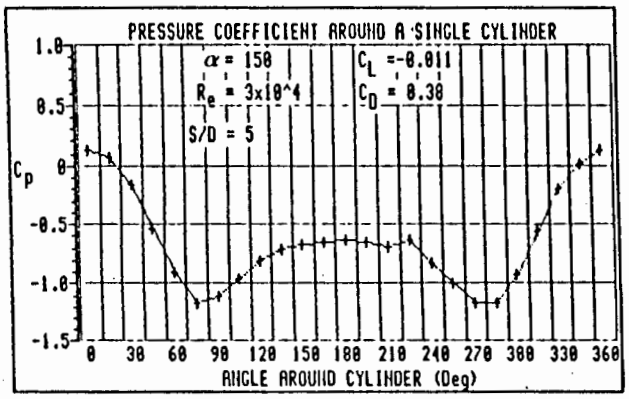


(k)

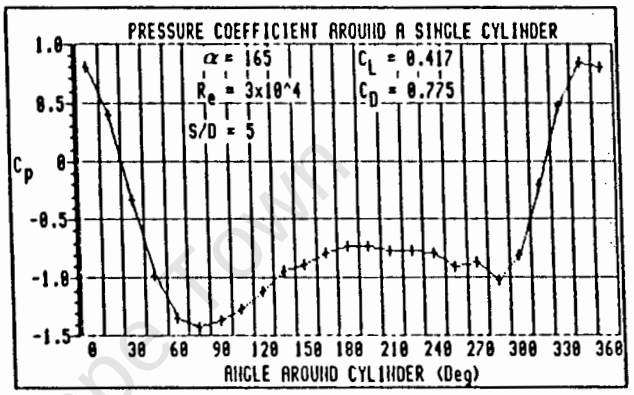


(l)

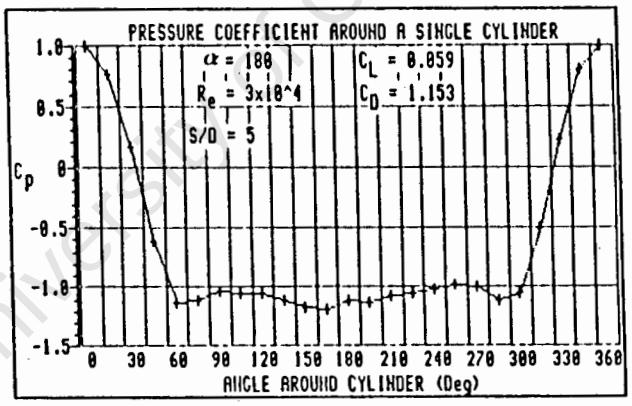


(m)



Fig. D1.7 Pressure coefficient around cylinder 1 in the group of three for various inclination angles. S/D = 5.

D2 PRESSURE COEFFICIENT VERSUS ANGLE $\theta$ AROUND CYLINDER 1 IN THE GROUP OF FOUR CYLINDERS AT VARIOUS INCLINATION ANGLES $\alpha$

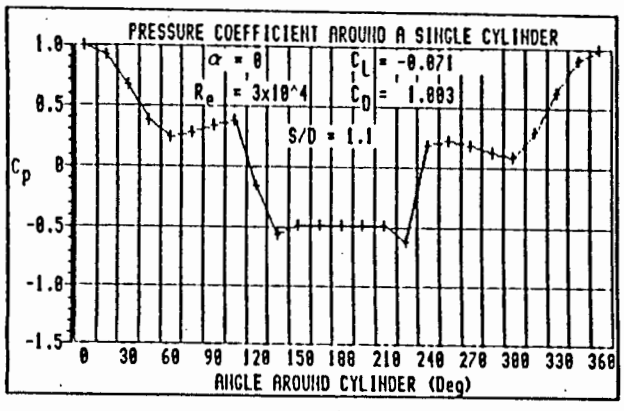


(a)

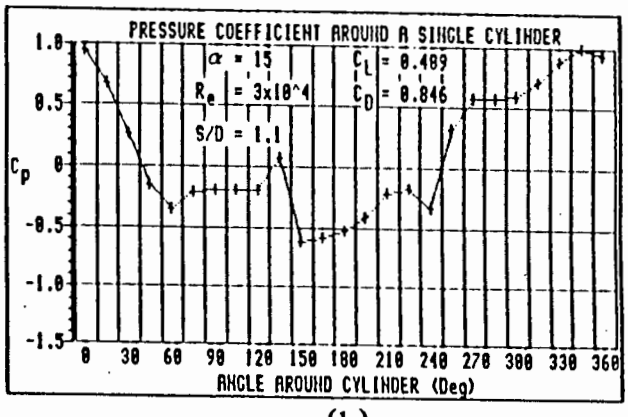


(b)

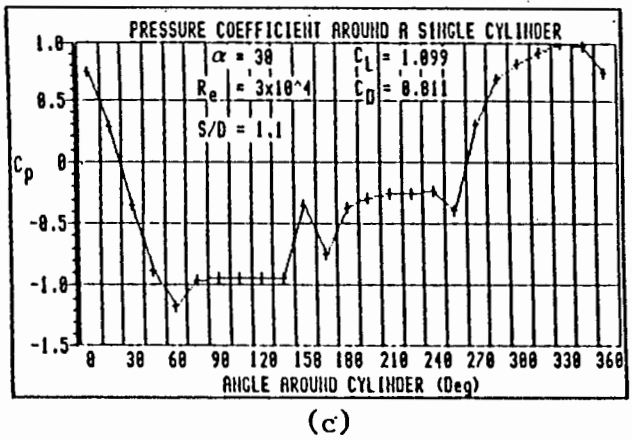


(c)

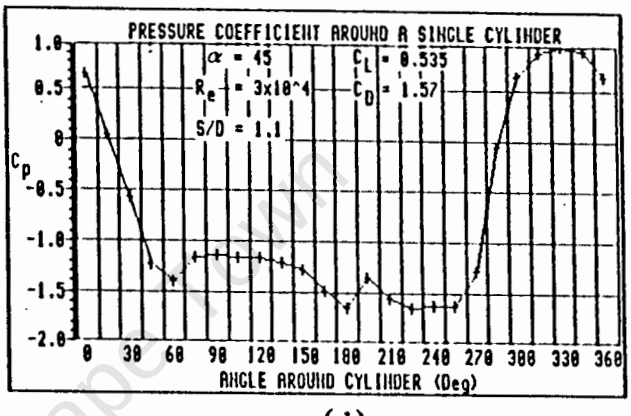


(d)

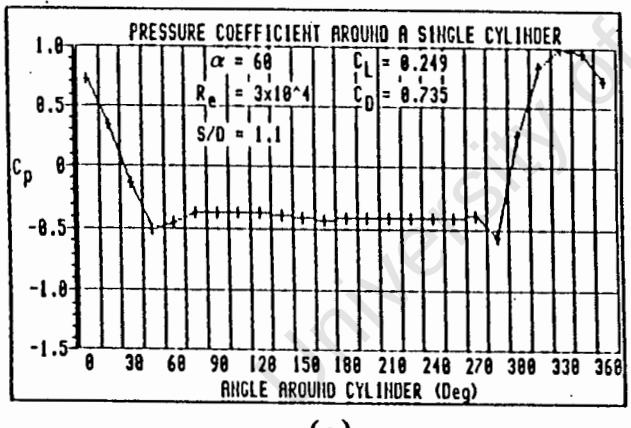


(e)

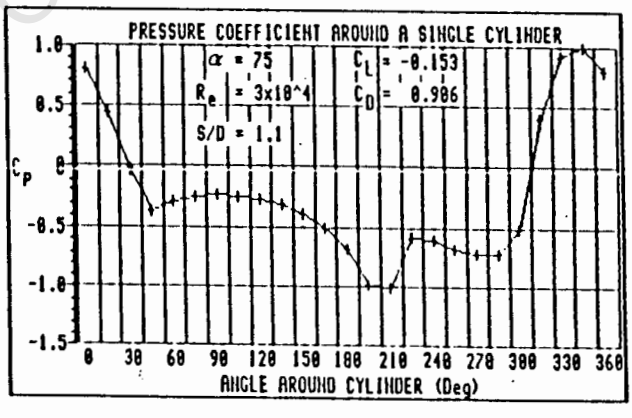


(f)

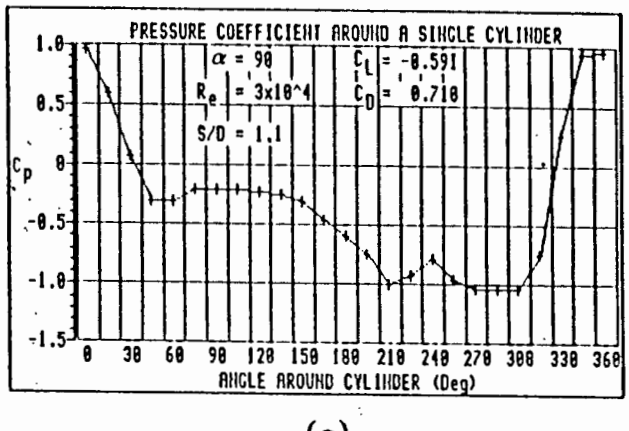


(g)

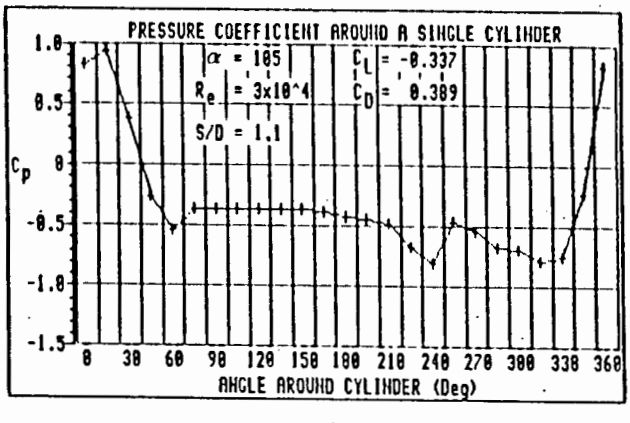


(h)

Fig. D2.1 Pressure coefficient around cylinder 1 in the group of four for various inclination angles. S/D = 1.1.

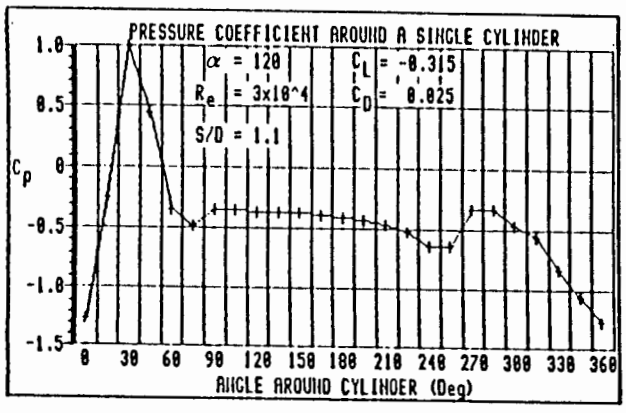


(i)

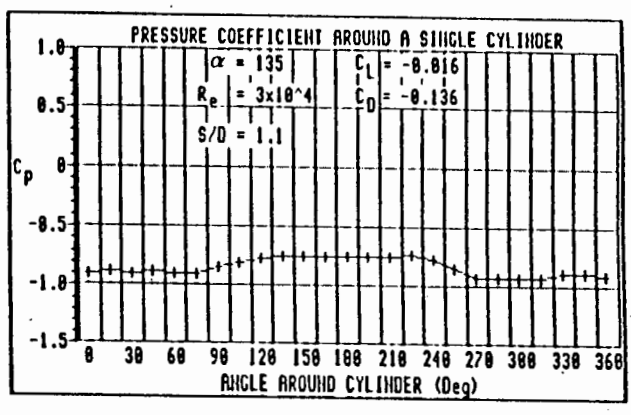


(j)

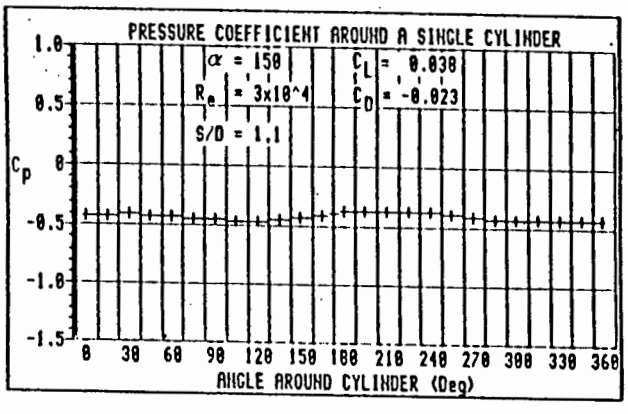


(k)

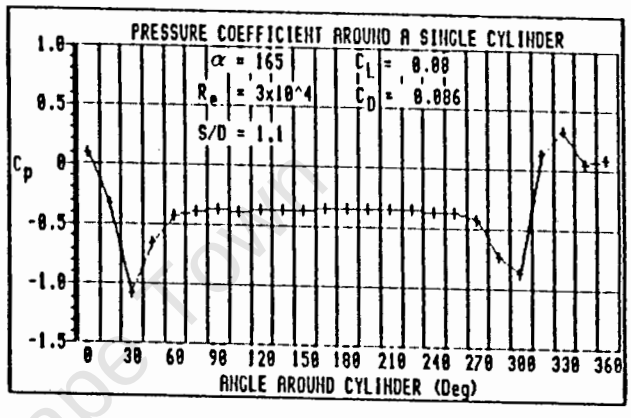


(l)

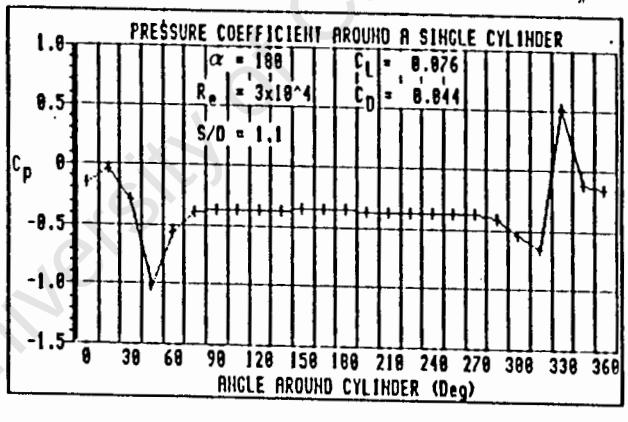


(m)



Fig. D2.1 Pressure coefficient around cylinder 1 in the group of four for various inclination angles. S/D = 1.1.

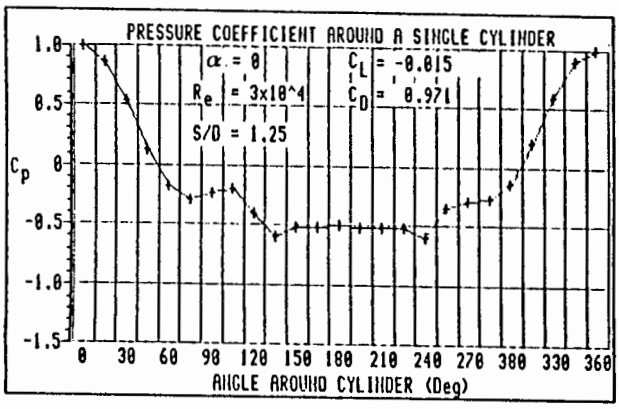


(a)

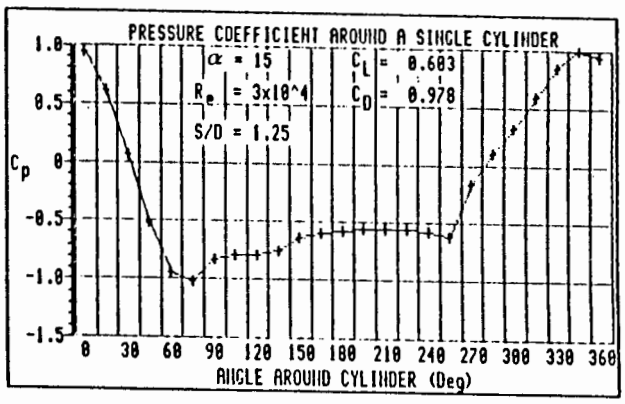


(b)

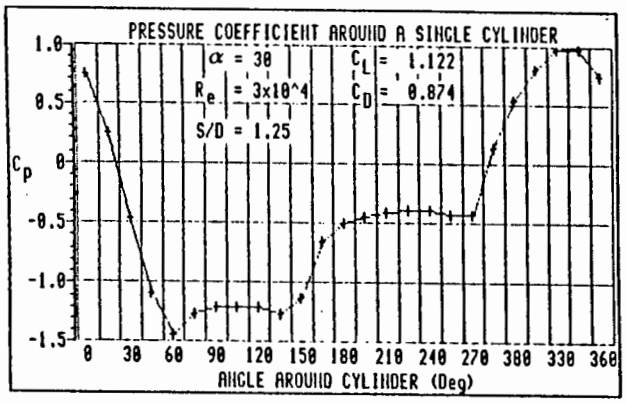


(c)

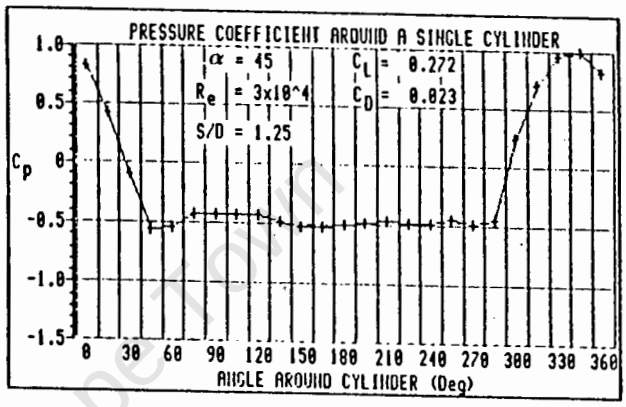


(d)

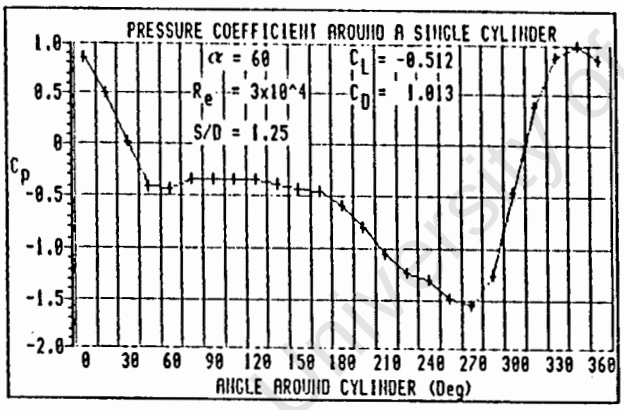


(e)

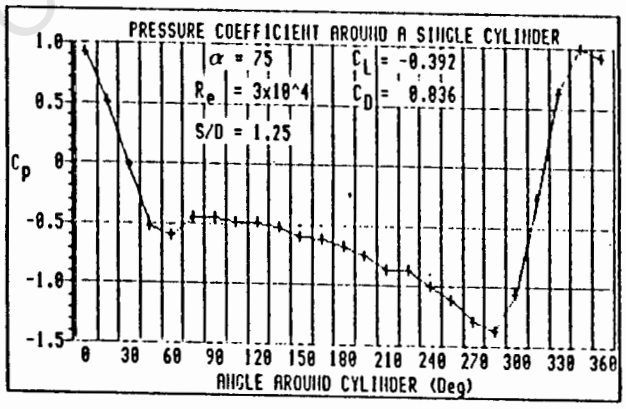


(f)

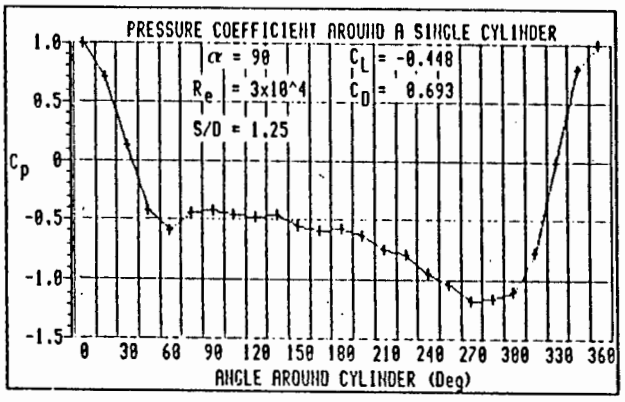


(g)

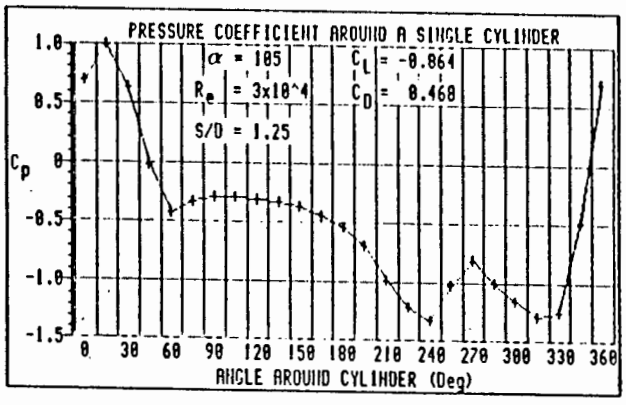


(h)

Fig. D2.2 Pressure coefficient around cylinder 1 in the group of four for various inclination angles. S/D = 1.25.

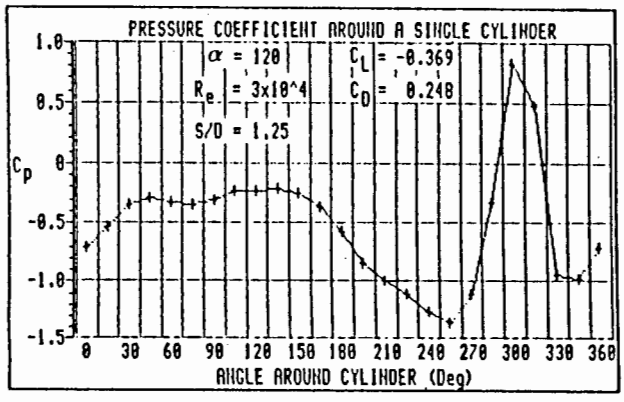


(i)

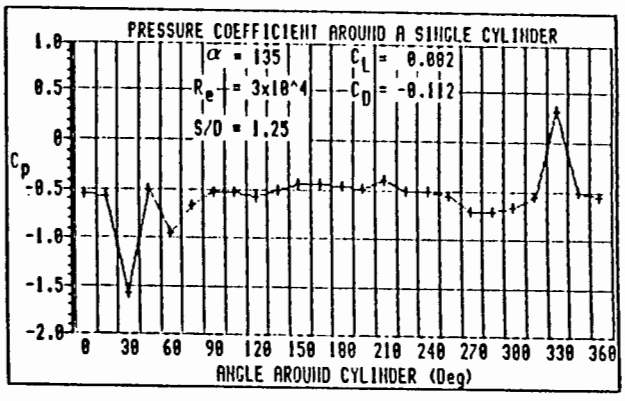


(j)

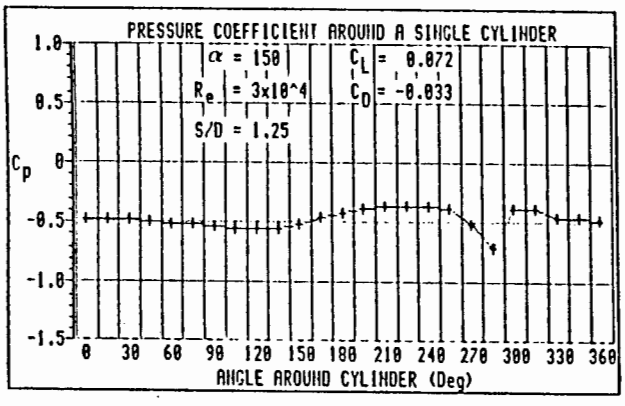


(k)

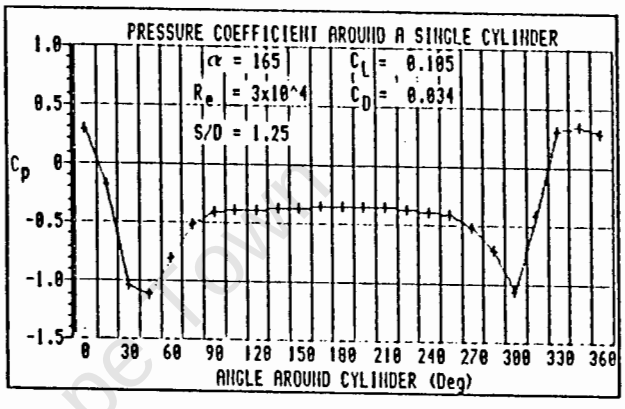


(l)

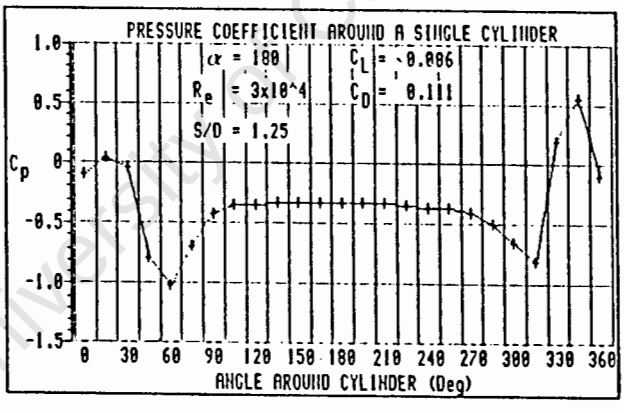


(m)

Fig. D2.2 Pressure coefficient around cylinder 1 in the group of four for various inclination angles. S/D 1.25.

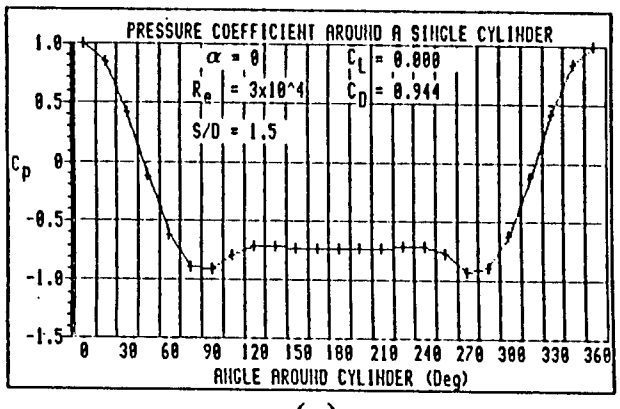


(a)

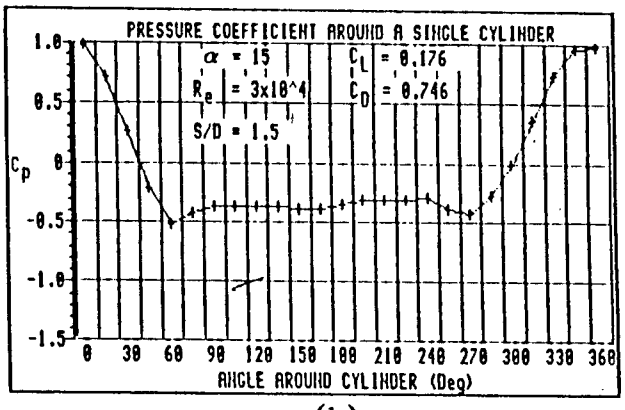


(b)

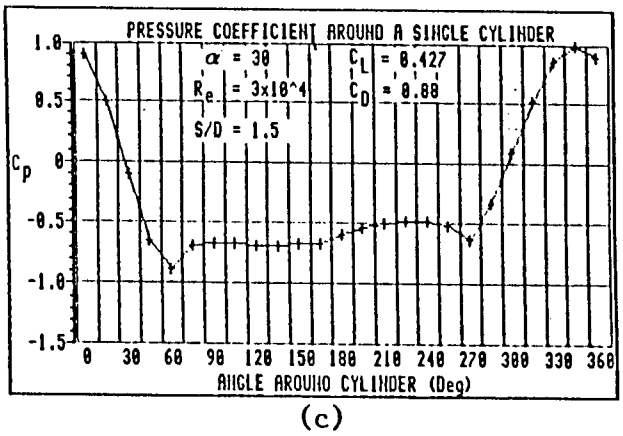


(c)

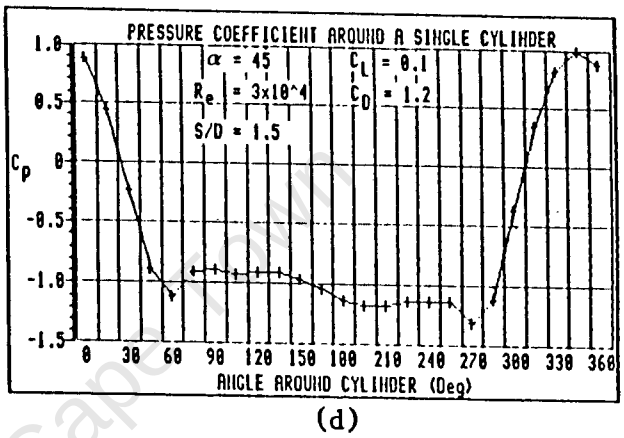


(d)

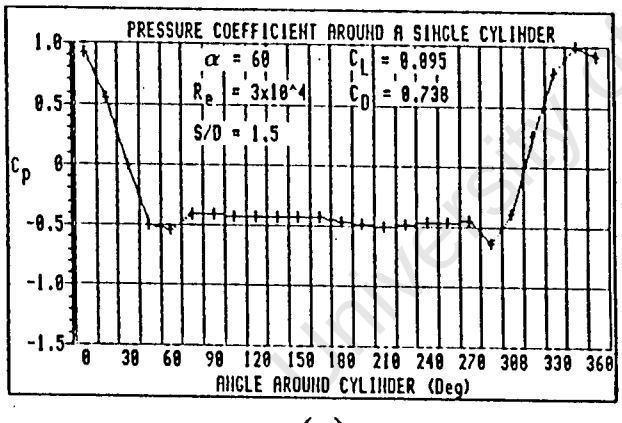


(e)

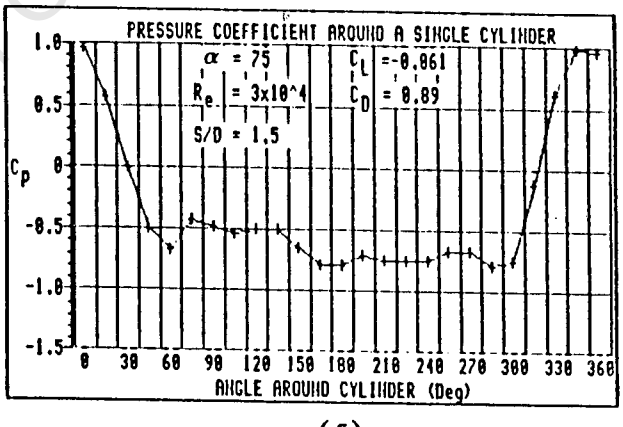


(f)

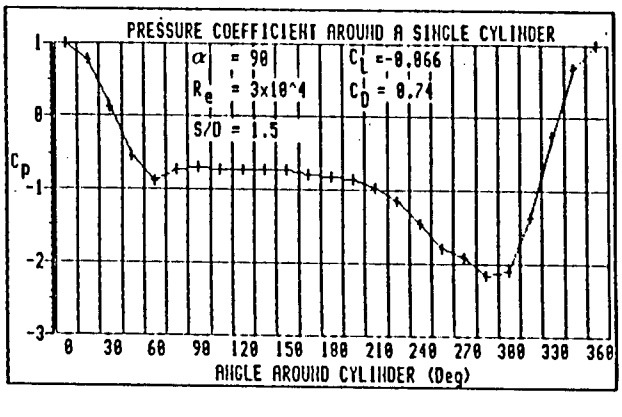


(g)

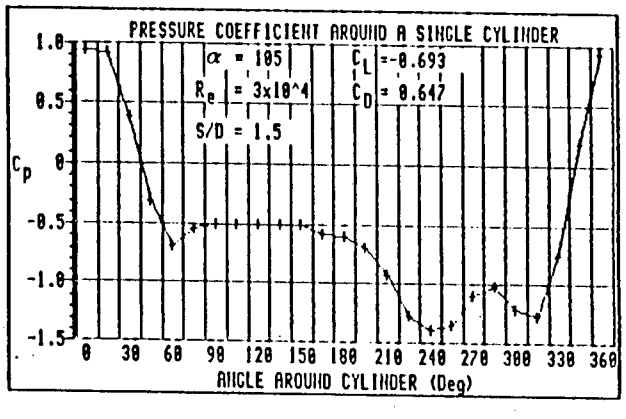


(h)

Fig. D2.3 Pressure coefficient around cylinder 1 in the group of four for various inclination angles. S/D = 1.5.

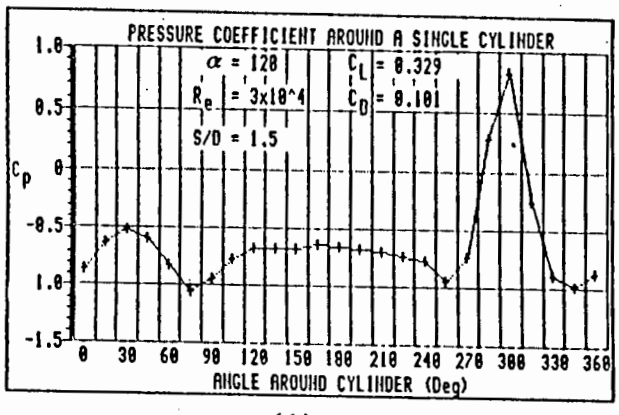


(i)

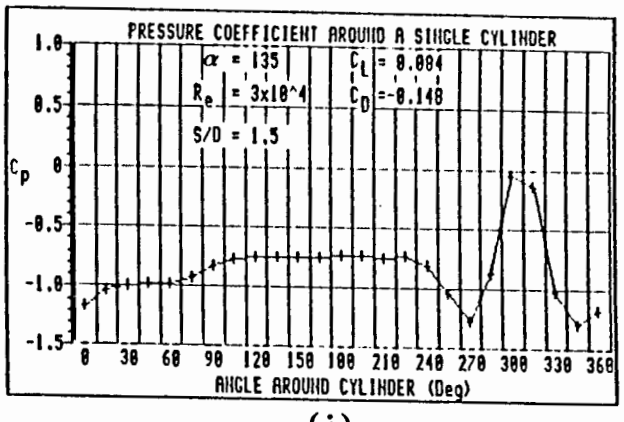


(j)

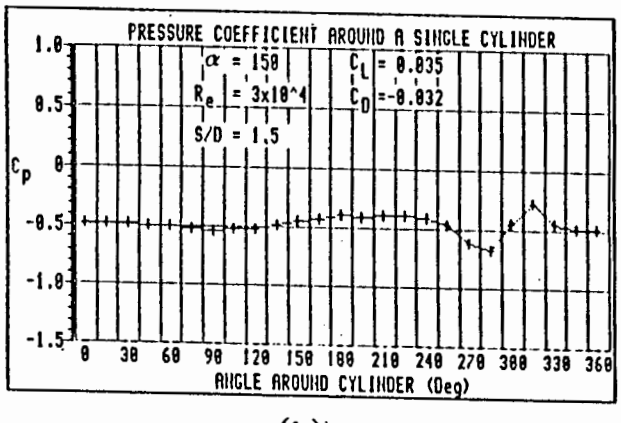


(k)

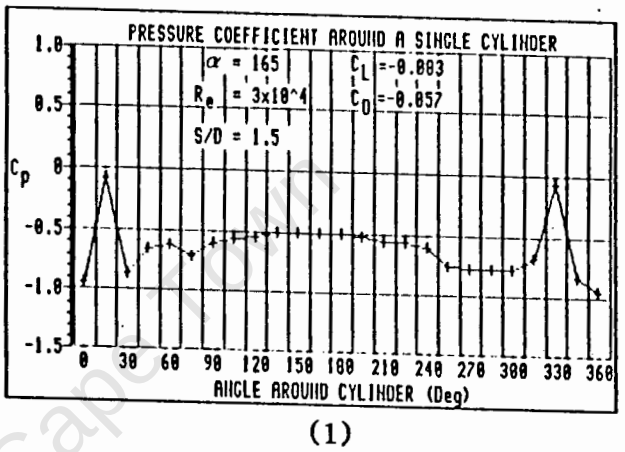


(1)

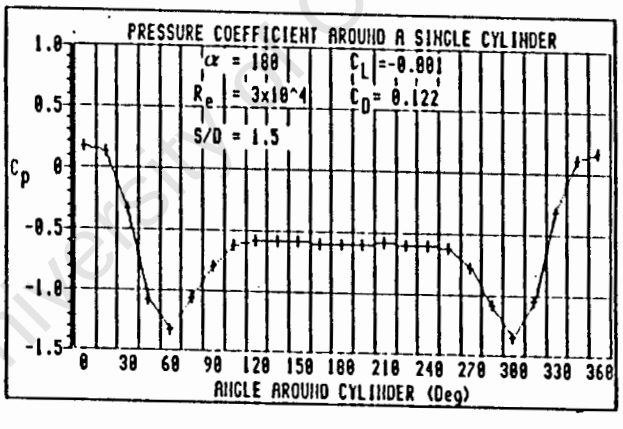


(m)



Fig. D2.3 Pressure coefficient around cylinder 1 in the group of four for various inclination angles. S/D = 1.5.

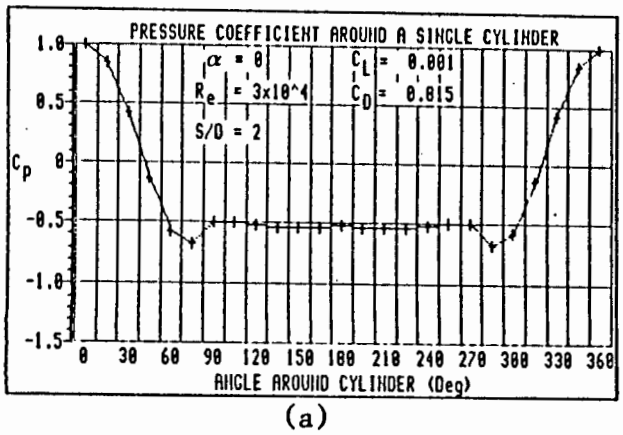


(a)

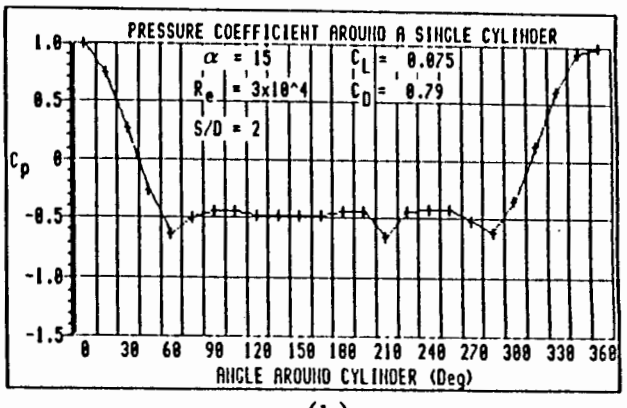


(b)

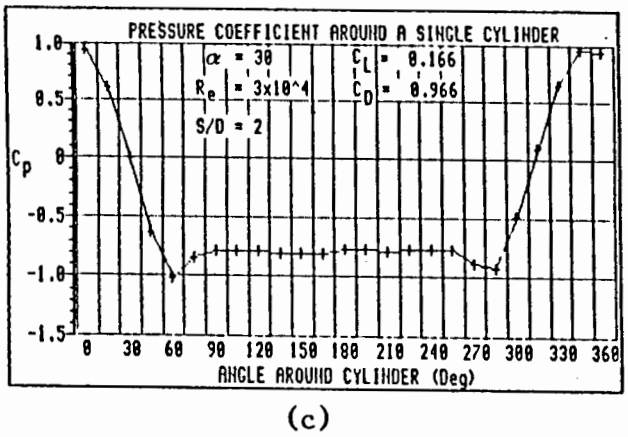


(c)

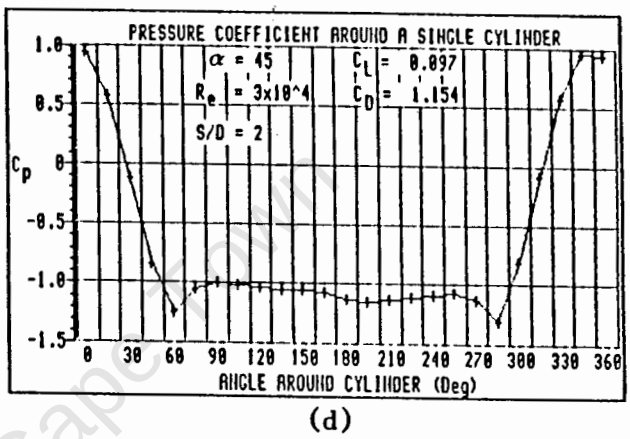


(d)

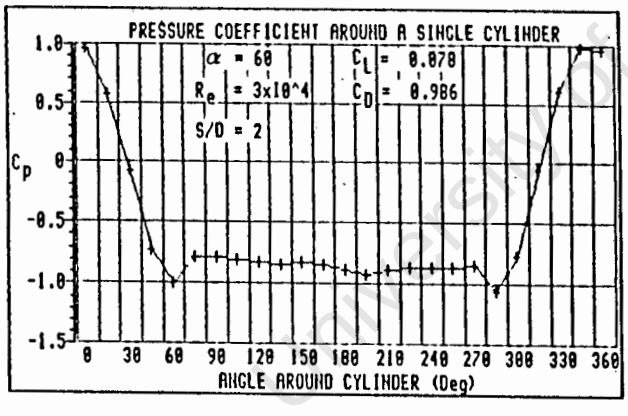


(e)

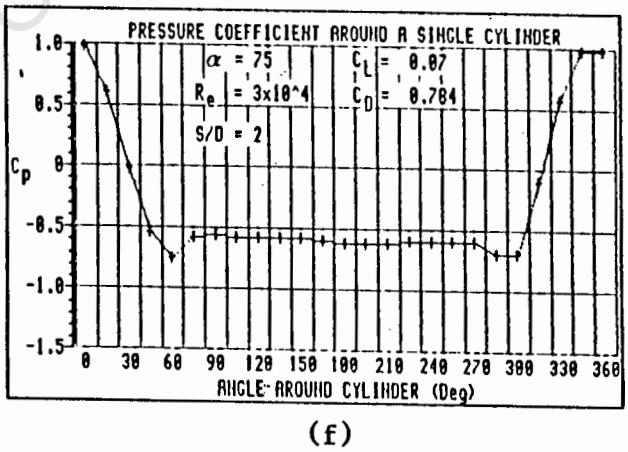


(f)

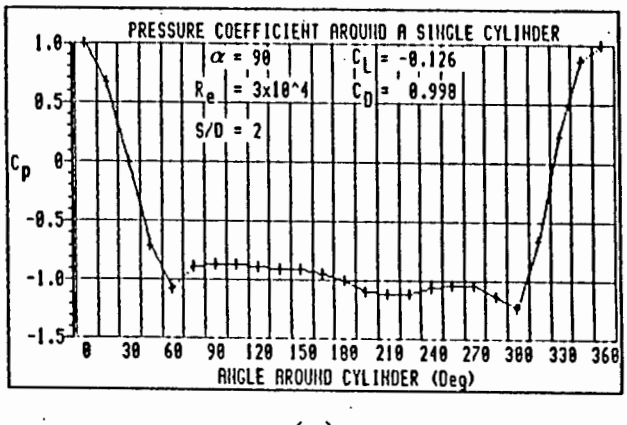


(g)

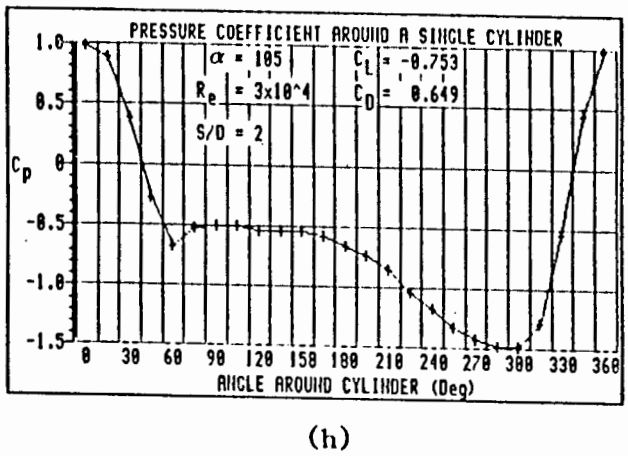


(h)

Fig. D2.4 Pressure coefficient around cylinder 1 in the group of four for various inclination angles. S/D = 2.

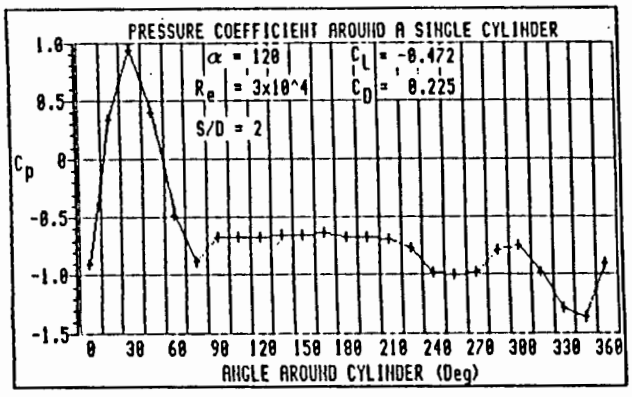


(i)

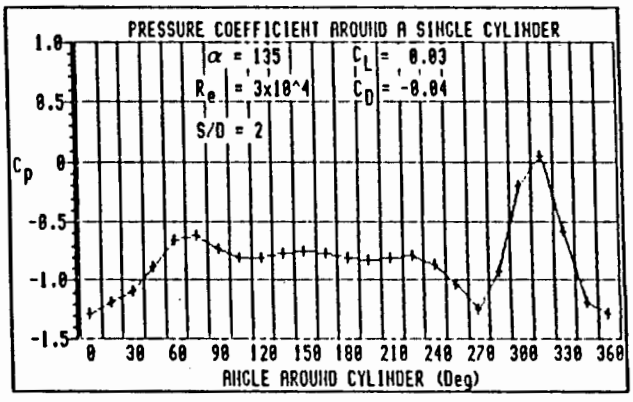


(j)

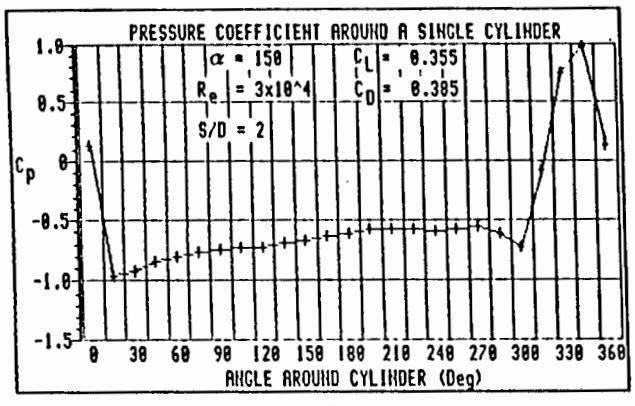


(k)

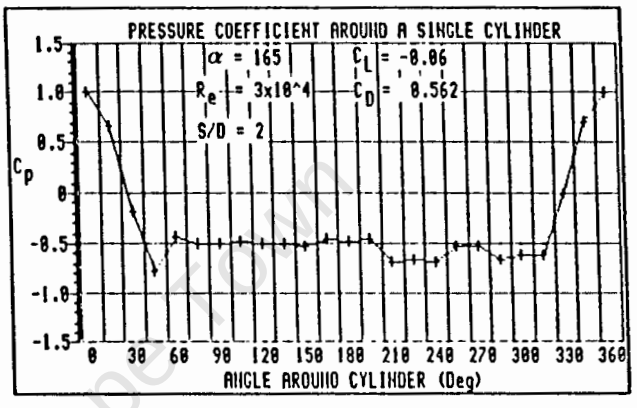


(l)

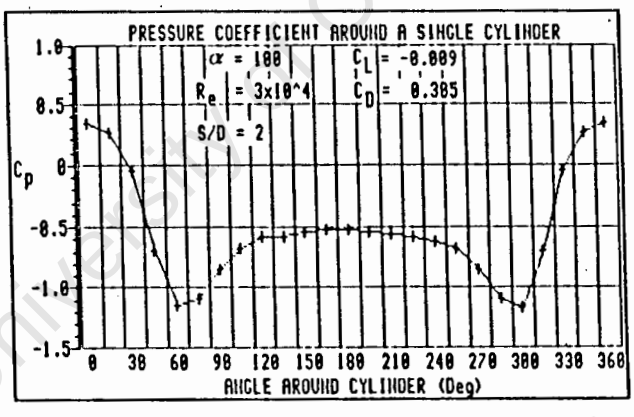


(m)



Fig. D2.4 Pressure coefficient around cylinder 1 in the group of four for various inclination angles. S/D = 2.

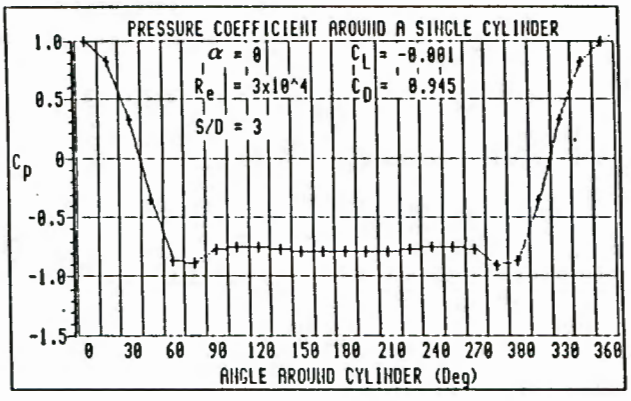


(a)

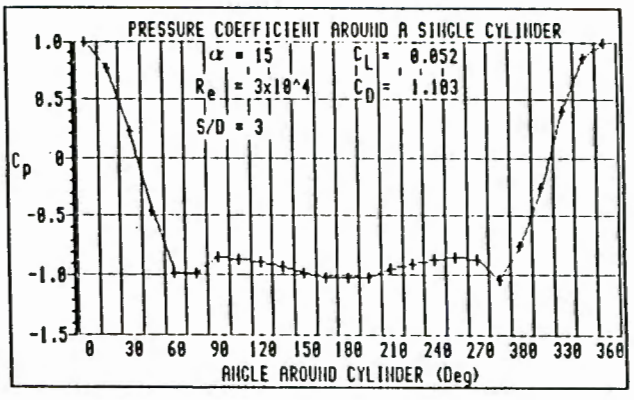


(b)

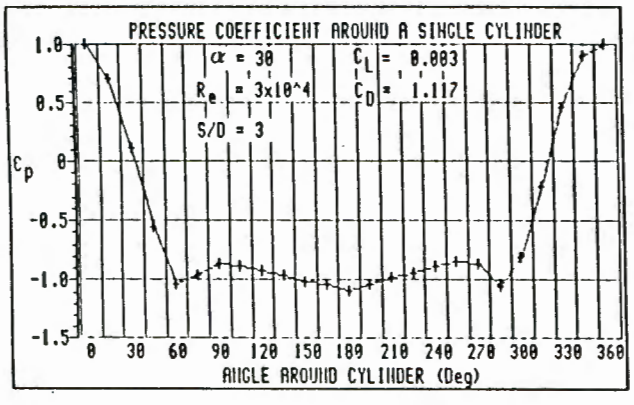


(c)

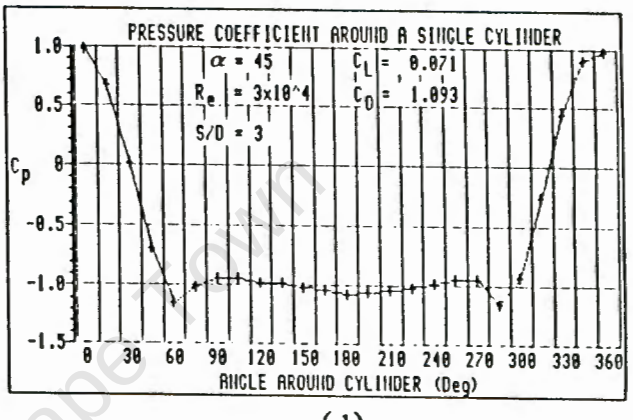


(d)

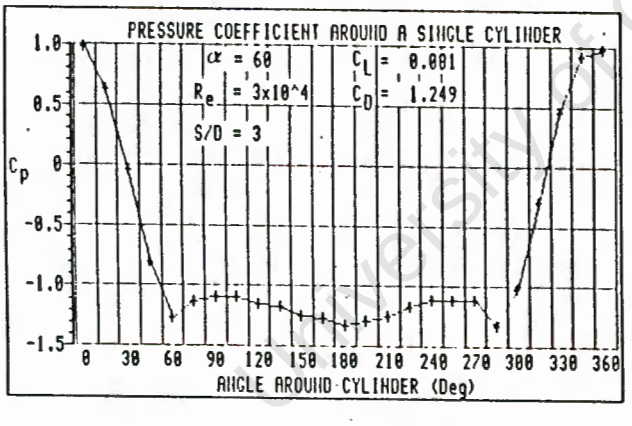


(e)

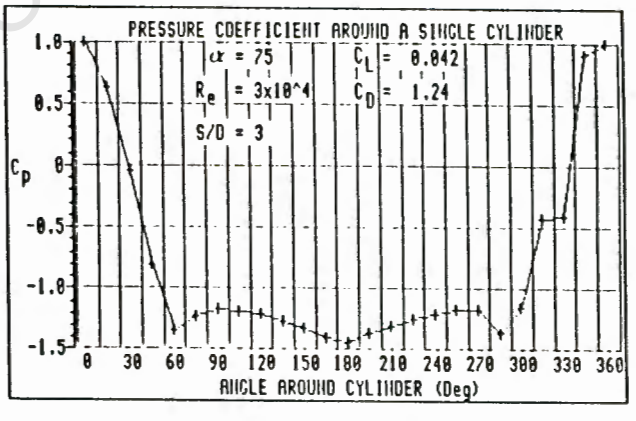


(f)

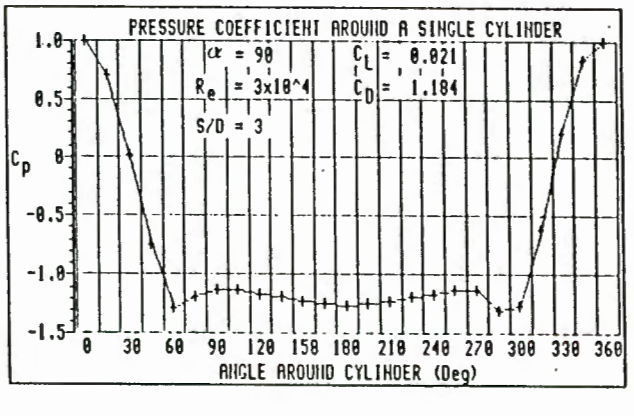


(g)

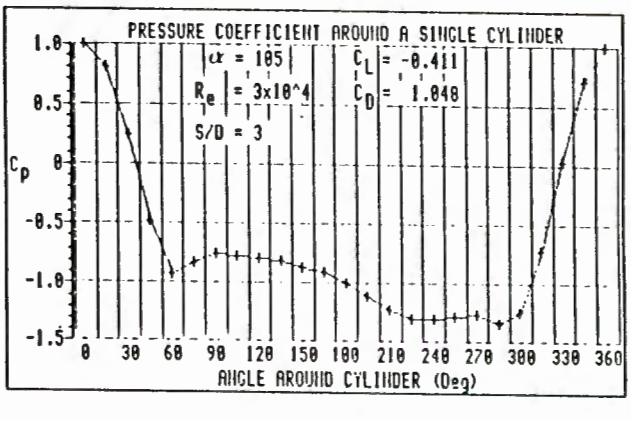


(h)

Fig. D2.5 Pressure coefficient around cylinder 1 in the group of four for various inclination angles. S/D = 3.

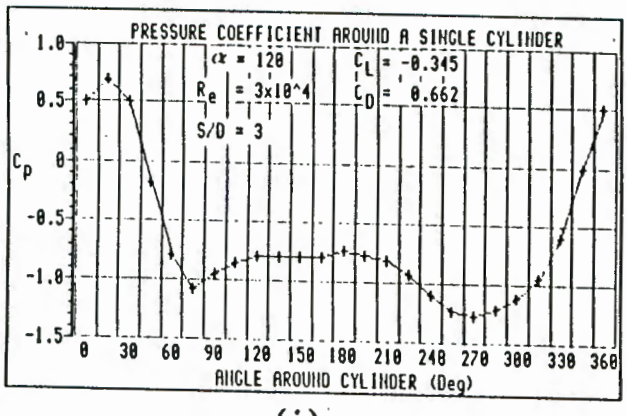


(i)

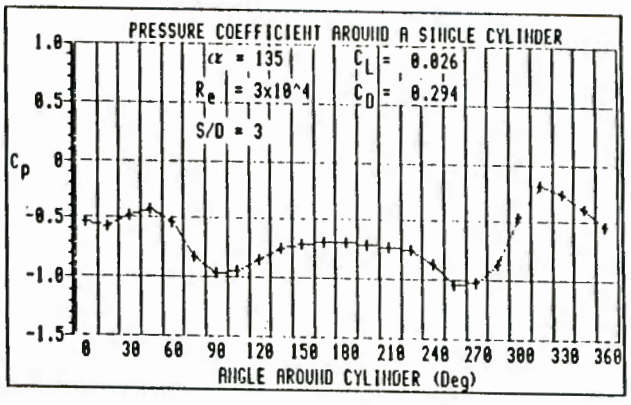


(j)

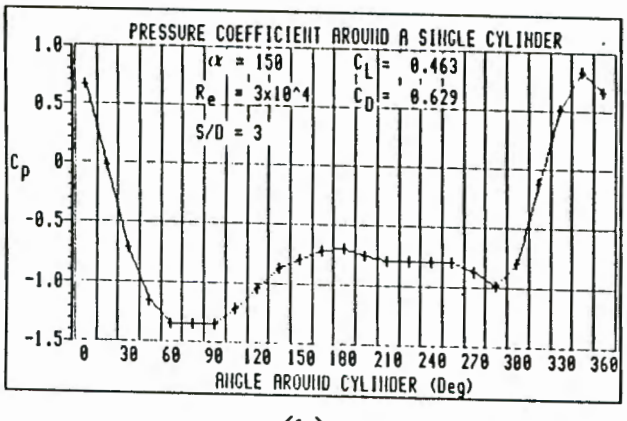


(k)

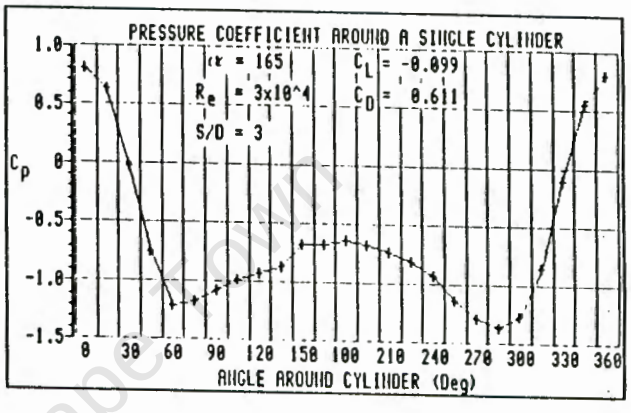


(l)

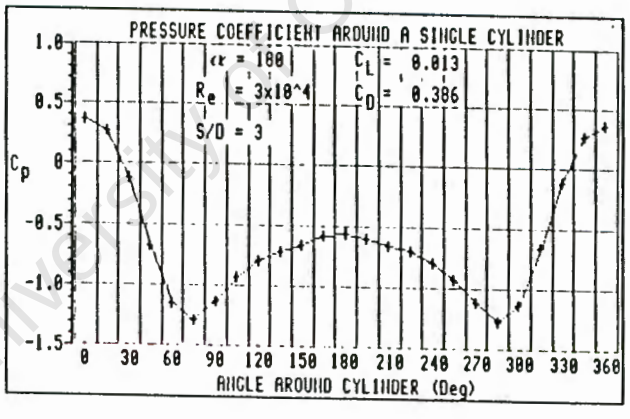


(m)



Fig. D2.5 Pressure coefficient around cylinder 1 in the group of four for various inclination angles. S/D = 3.

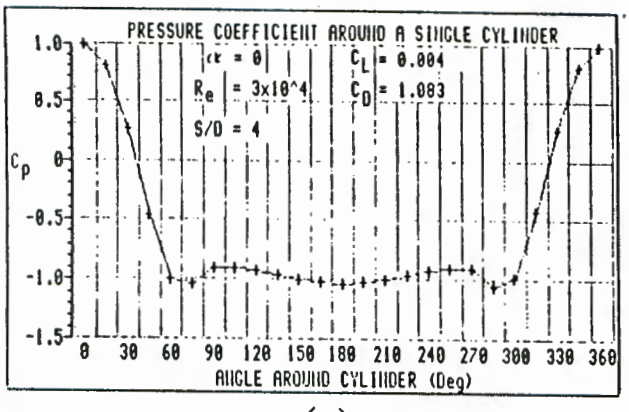


(a)

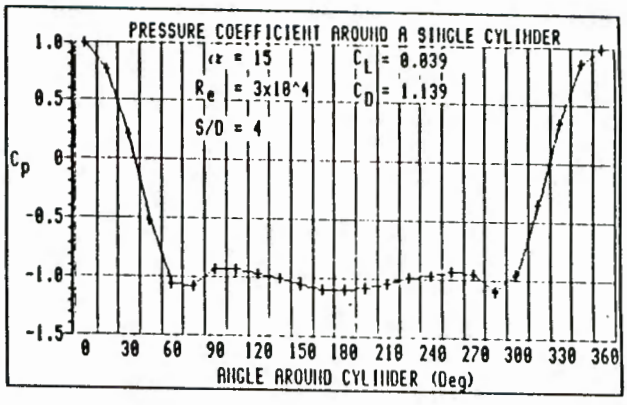


(b)

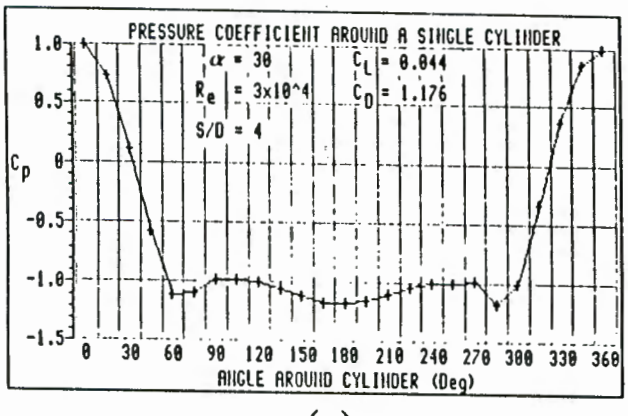


(c)

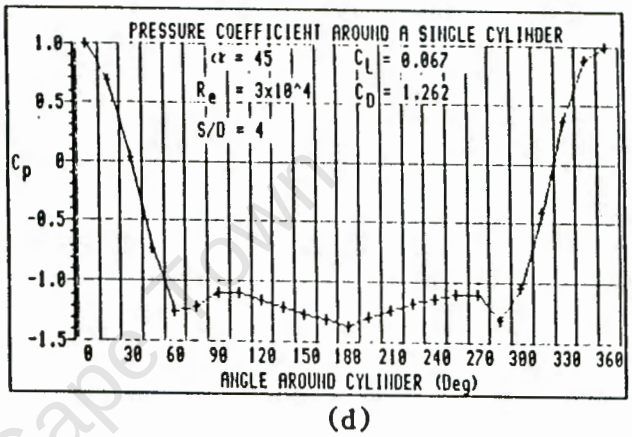


(d)

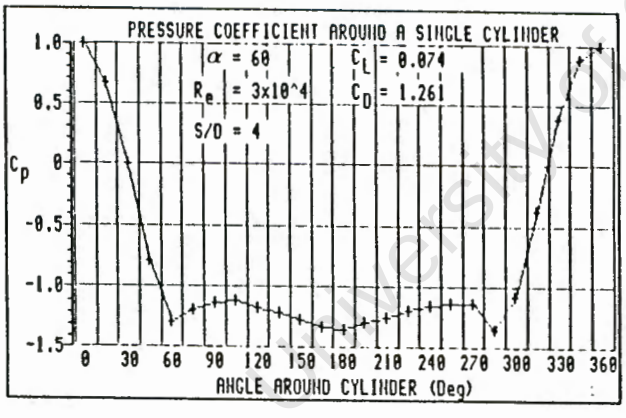


(e)

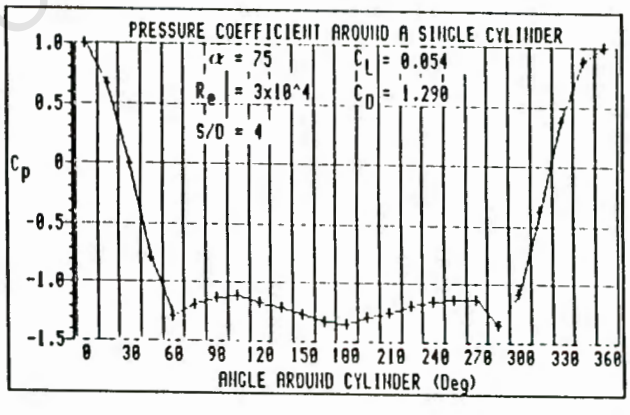


(f)

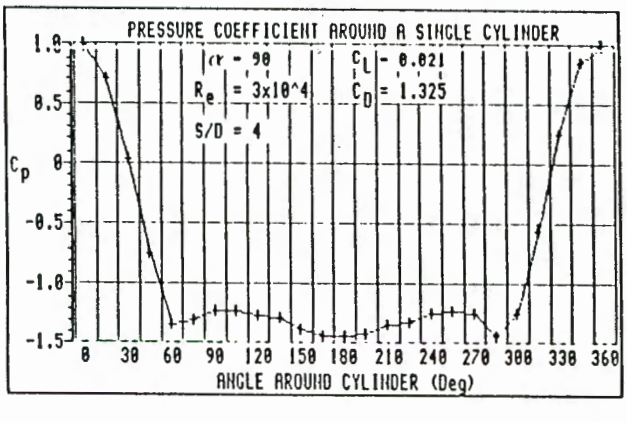


(g)

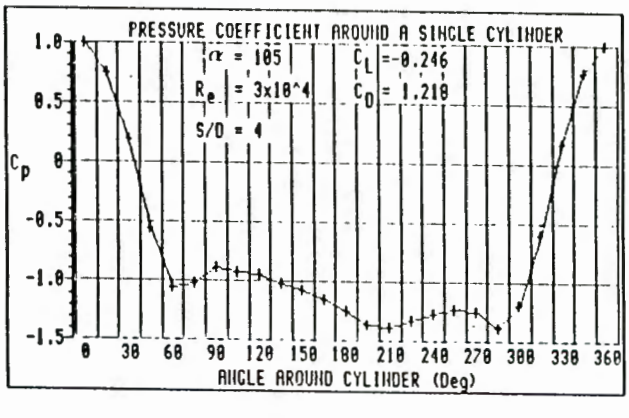


(h)

Fig. D2.6 Pressure coefficient around cylinder 1 in the group of four for various inclination angles. S/D = 4.

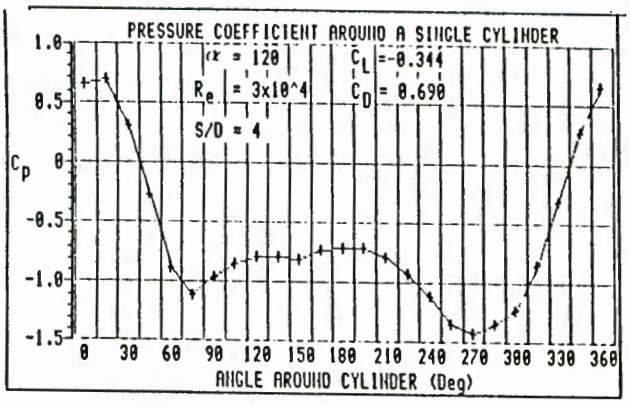


(i)

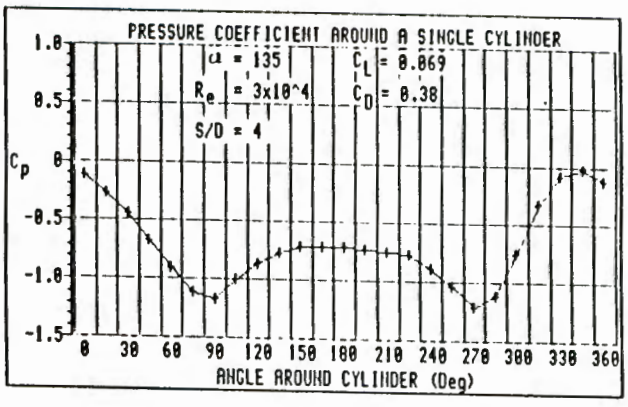


(j)

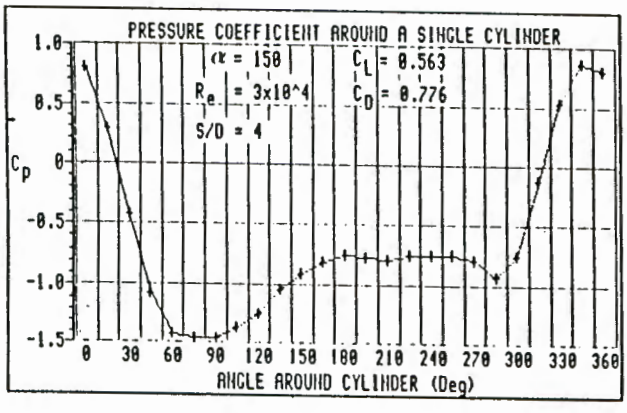


(k)

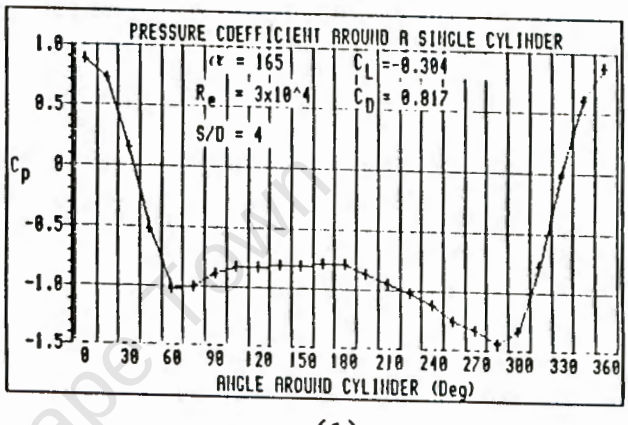


(l)

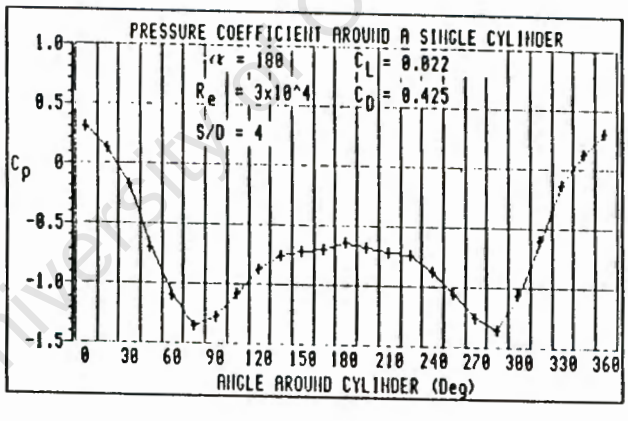


(m)

Fig. D2.6 Pressure coefficient around cylinder 1 in the group of four for various inclination angles. S/D = 4.

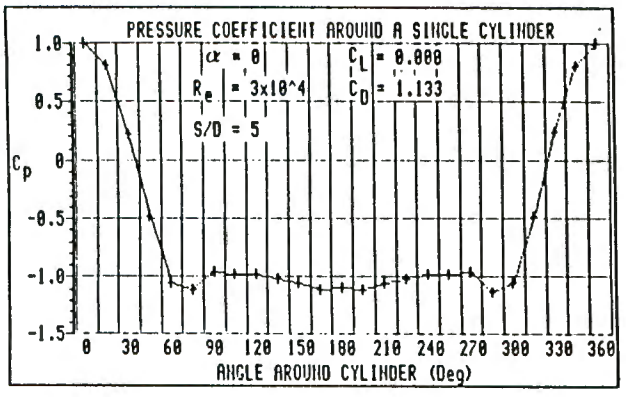


(a)

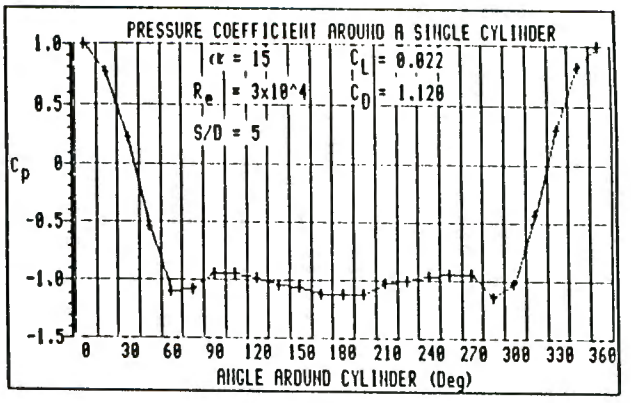


(b)

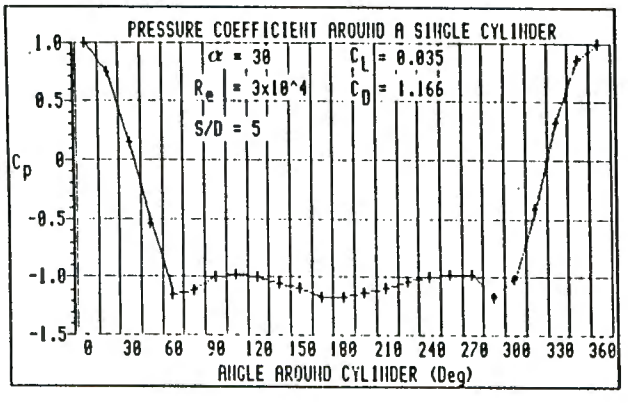


(c)

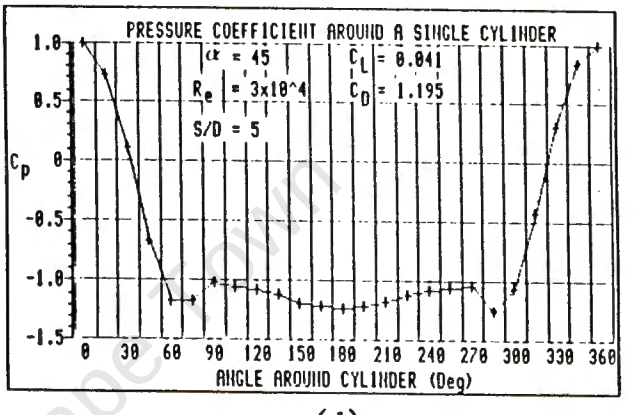


(d)

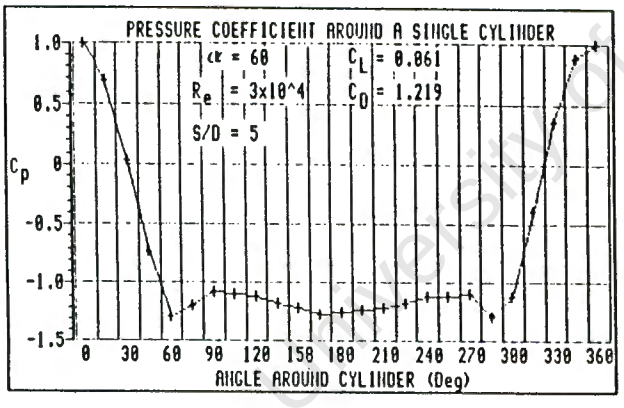


(e)

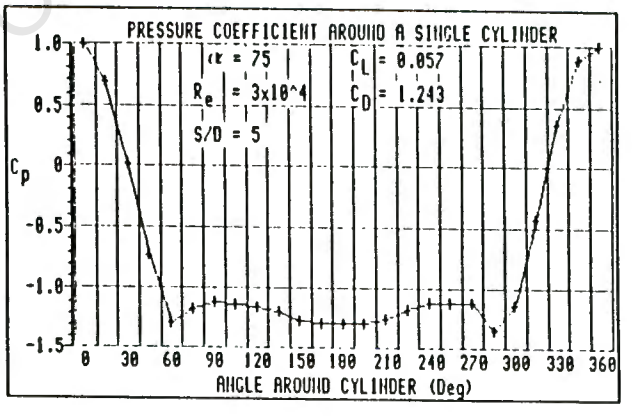


(f)

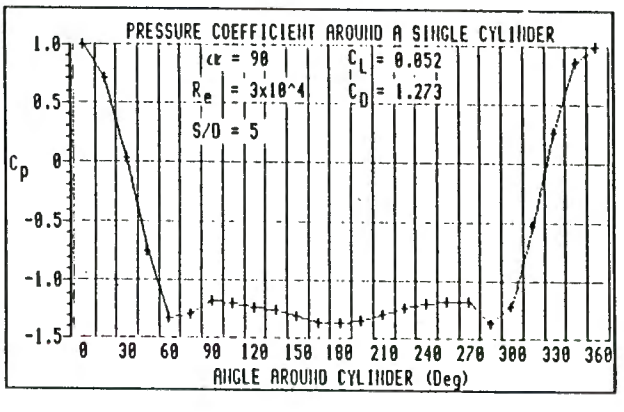


(g)

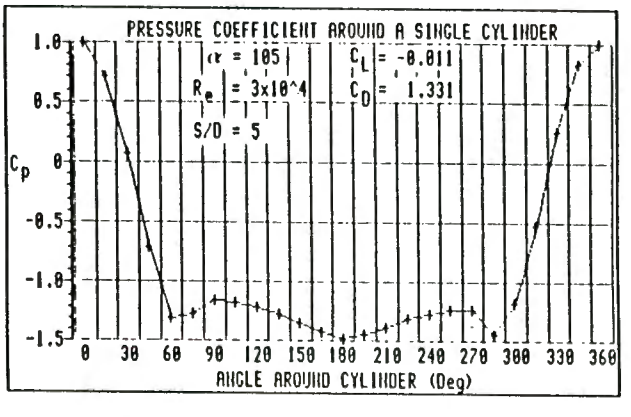


(h)

Fig. D2.7 Pressure coefficient around cylinder 1 in the group of four for various inclination angles. S/D = 5.

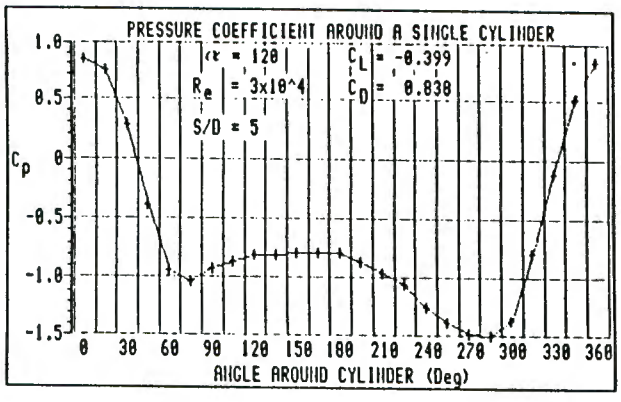


(i)

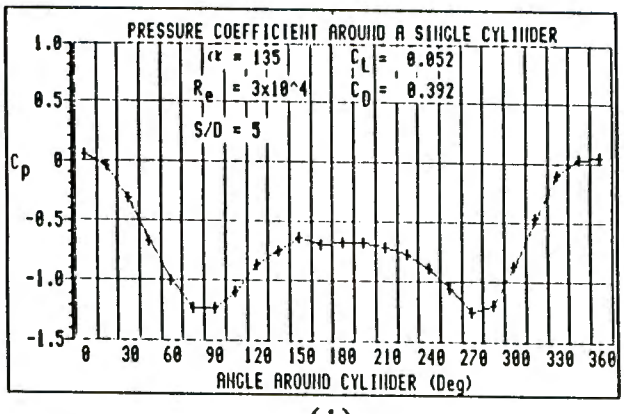


(j)

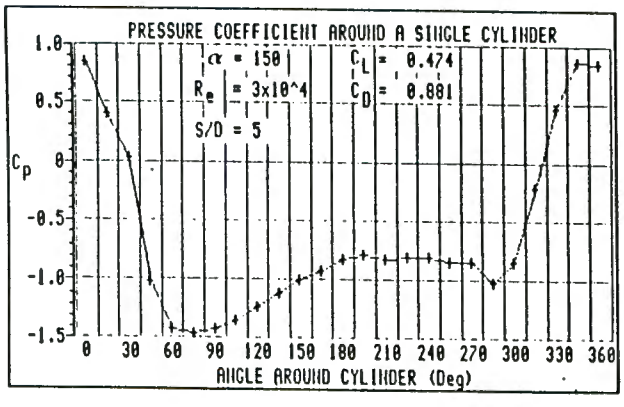


(k)

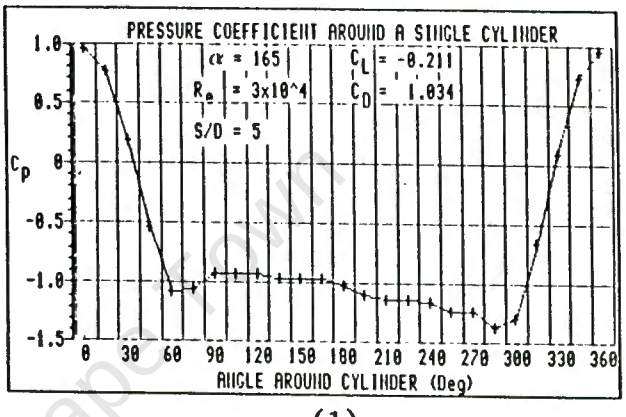


(l)

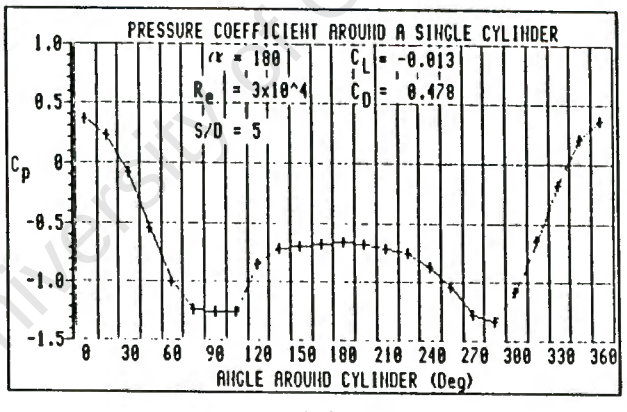


(m)

Fig. D2.7 Pressure coefficient around cylinder 1 in the group of four for various inclination angles. S/D = 5.

# ADDENDUM 1

## HYDROGEN BUBBLE FLOW VISUALISATION

A visual perception of the mean flow between the cylinders forming the group of three enables the lift and drag coefficients as determined by pressure measurements around the cylinders to be explained qualitatively. Using the hydrogen bubble technique, on an adjustable slope perspex water table 1 m long by 240 mm wide, streamlines of the flow over the cylinders were generated and photographically recorded. An 0.4 mm diameter insulated copper wire formed the basis of the cathode and was spanned across the inlet section of the water table. At 10 mm intervals along the wire, 0.25 mm wide circumferential strips of insulation were removed with a modelling knife and it was these sections of uninsulated wire which generated the hydrogen bubble streams. Water was continuously recirculated to an upstream header tank, whilst the water depth and flow velocity were controlled by a downstream weir plate, and the angular tilt of the table respectively. The three 25 mm diameter brass cylinders comprising the group, were located at the required spacings on the surface of the water table. The centre, about which the angle of inclination was varied, being on the longitudinal centre line.

The surface water speed was adjusted by timing a surface marker to approximately 1.2 m/s to give an approximate Reynolds number of $3 \times 10^4$. The bubble positions indicating the streamlines were photographically recorded from a position

vertically above the cylinders against a black background on the underside of the perspex table. The inclination angle of the cylinder group was varied in the range $0° < \alpha < 60°$ in 7.5° intervals anticlockwise for spacing ratios $1.25 < S/D < 5$.

Results

Whilst cylinder 1 was incremented from 0° to 60°, the other two cylinders were at the same time in positions ±120° from cylinder 1. Thus when cylinder 1 was at say 15° we may examine the flow about the other two cylinders, these being at positions equivalent to inclination angles of 105° and 135°. A full table of equivalent angles is given below.

| Inclination angle $\alpha$ for cylinders | | |
|---|---|---|
| 1 | 2 | 3 |
| 0° | 120° | 120° |
| 7.5° | 127.5° | 112.5° |
| 15° | 135° | 105° |
| 22.5° | 142.5° | 97.5° |
| 30° | 150° | 90° |
| 37.5° | 157.5° | 82.5° |
| 45° | 165° | 75° |
| 52.° | 172.5° | 67.5° |
| 60° | 180° | 60° |

Only selected photographic prints are used to identify particularly interesting phenomena and these are shown in Figs. A1.1 to A1.4.

S/D = 3

In Figs. 8.3 and 8.4 the drag and lift coefficient curves are of the same form for spacing ratios of 3, 4 and 5, and therefore the discussion for S/D = 3 also applies to the latter two spacings. Figs. A1.1(a-c) show the streamlines forming the outer edge of the wake of cylinder 1 being constrained to move into the gap between cylinders 2 and 3. This causes acceleration of the flow on the upper surface of cylinder 2 and a corresponding decrease in pressure which manifests itself in the sudden decreased drag and lift coefficient for inclination angles between 105° and 135°. When cylinder 2 is between 142.5° and 165° (Figs. A1.1(d-g)) a streamline from cylinder 1, which lies close to the upper edge of the wake, strikes the surface of cylinder 2, whilst in (f), (g) and (h), the same streamline moves across the wake to flow around the lower side of cylinder 2 and thus cause the sudden reversal in lift coefficient which rises to a peak at 165°.

Fig. A1.1(i) shows cylinder 2 at the 180° position. The streamlines between cylinders 1 and 3 are seen to converge, and the flow to impinge on cylinder 2 with an increased flow velocity, the flow around cylinder 2 being symmetrical. This accounts for the increased drag coefficient and zero lift coefficient exhibited in Figs. 8.3 and 8.4 respectively.

S/D = 2.5

The maximum and minimum $C_D$ occur at 97.5° and 157.5° respectively whilst $C_L$ is zero (Figs. 8d and 9d). In Fig. A1.2(d) when cylinder 3 is at 97.5° and in Fig. A1.2(f) when

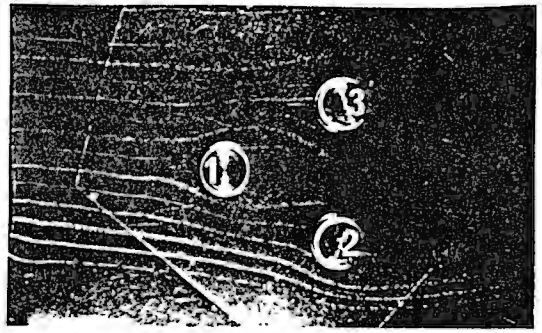


(a) $\alpha=0^0$

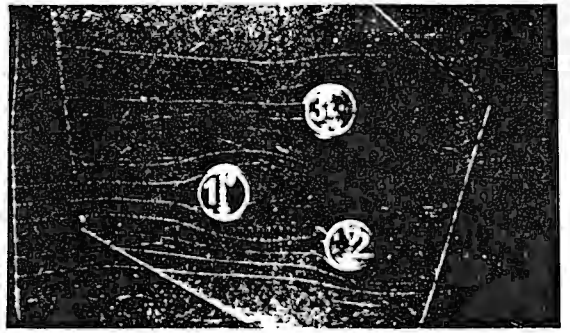


(b) $\alpha=7.5^0$

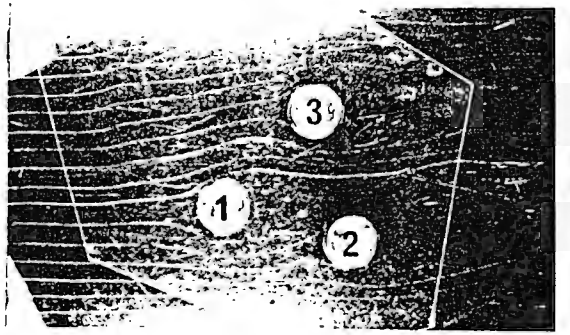


(c) $\alpha=15^0$

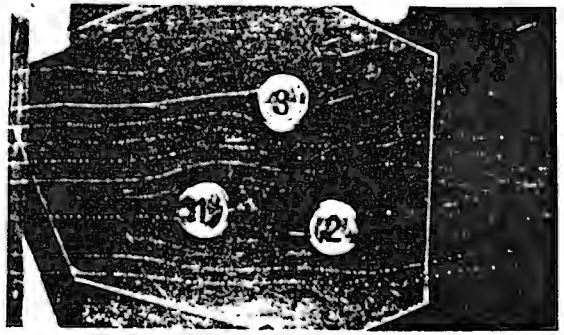


(d) $\alpha=22.5^0$

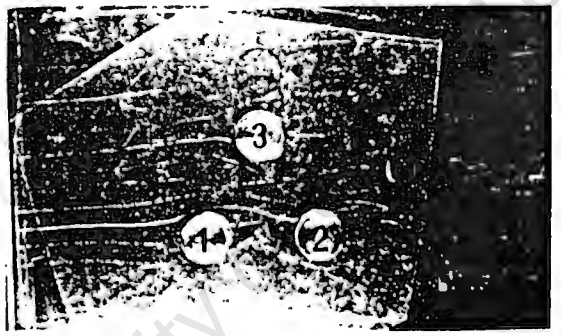


(e) $\alpha=30^0$

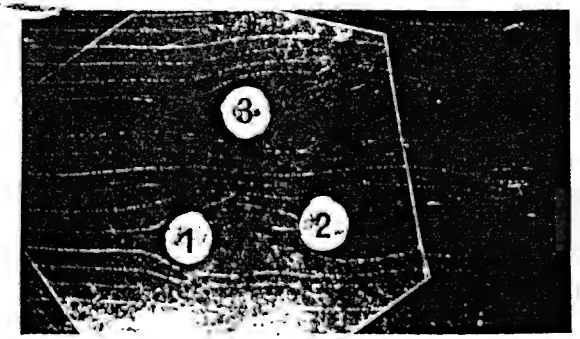


(f) $\alpha=37.5^0$

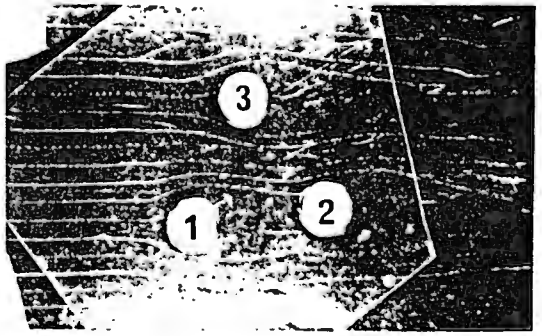


(g) $\alpha=45^0$

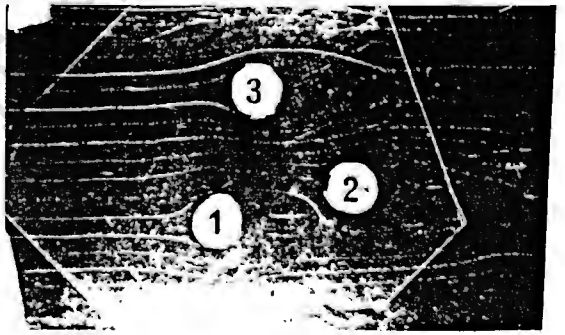


(h) $\alpha=52.5^0$

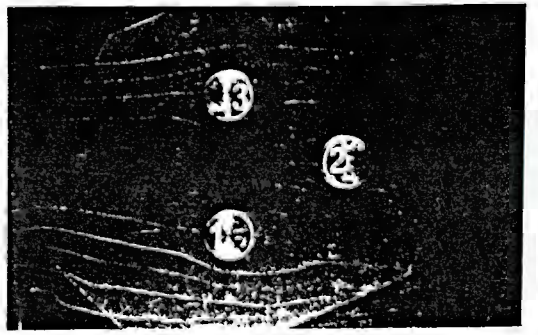


(i) $\alpha=60^0$

Fig. A1.1 Flow visualisation around three cylinders. S/D=3

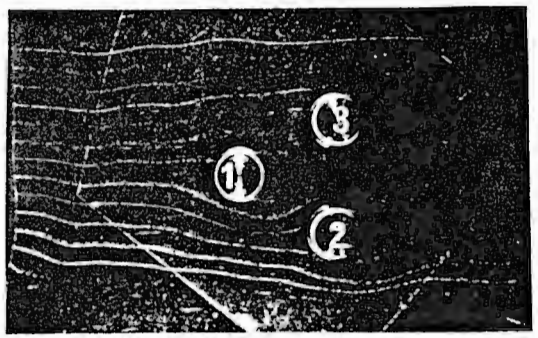


(a) $\alpha=0^0$

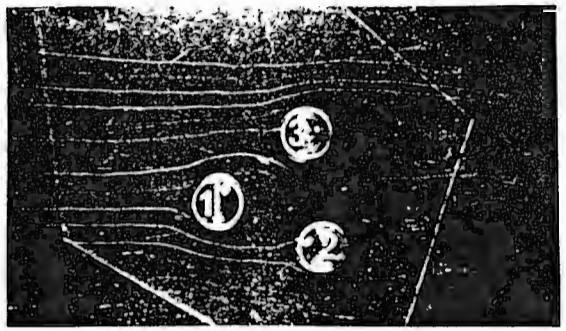


(b) $\alpha=7.5^0$

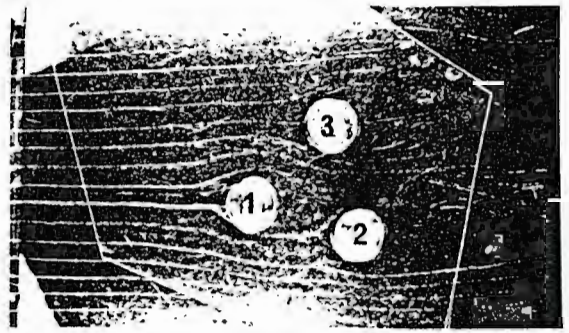


(c) $\alpha=15^0$

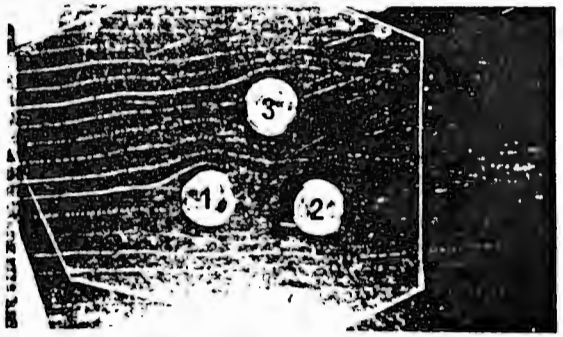


(d) $\alpha=22.5^0$

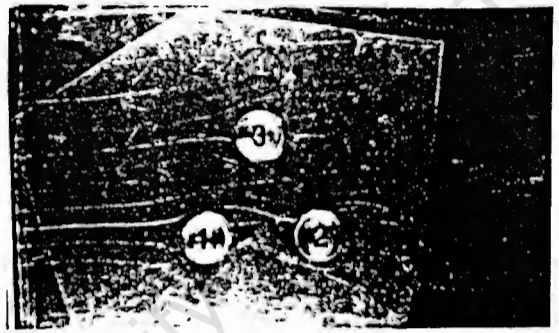


(e) $\alpha=30^0$

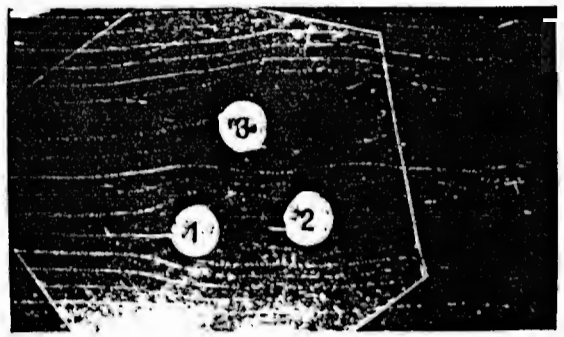


(f) $\alpha=37.5^0$

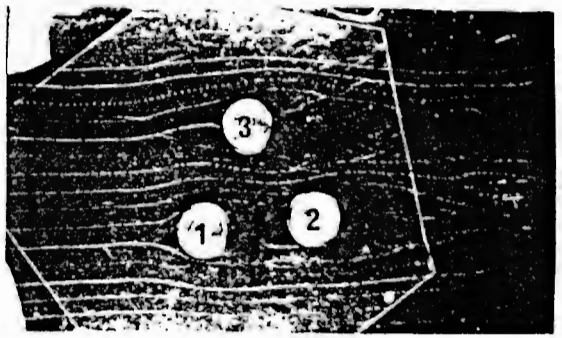


(g) $\alpha=45^0$

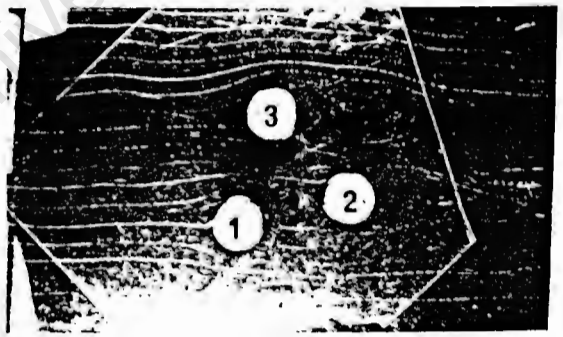


(h) $\alpha=52.5^0$


(i) $\alpha=60^0$

Fig. A1.2 Flow visualation around three cylinders. S/D=2.5

cylinder 2 is at 157.5°, zero lift is due to cylinder 3 being almost in a free stream flow whilst cylinder 2 is immersed in the wake of the upstream cylinder 1. The maximum $C_D$ of 1.4 occurs because of an increase in flow velocity of the fluid impinging on cylinder 3. This increased velocity is caused by the deviated flow around the cylinder 1, and is clearly shown in Fig. A1.2(d). The minimum $C_D$ is almost zero due to cylinder 2 once again being immersed in a quiescent stream, and it remains at zero for S/D of 2 and 1.5.

S/D = 2

Fig. A1.3(i) clearly shows two streamlines passing between cylinders 1 and 3 and then diverging to move symmetrically around cylinder 2 to give the zero lift coefficient at $\alpha$ = 180° in Fig. 9c. As $\alpha$ is decreased from 180°, the velocity in the gap between cylinders 1 and 2 tends to increase whilst that between cylinders 2 and 3 tends to decrease thereby giving rise to a lift coefficient greater than zero on cylinder 2 for the range $142.5° < \alpha < 172.5°$. In this range, the maximum lift occurs at $\alpha$ = 150° where Fig. A1.3e shows a clear streamline moving through the gap between cylinders 1 and 2. Clearly the proximity of cylinder 3 is preventing cylinder 2 being immersed in a uniform wake as is the case for larger spacing ratios; that is the wake is being distorted.

In the range $112.5° < \alpha < 142.5°$ (Figs. A1.3(a-c)) the low pressure wake behind cylinder 1 tends to draw fluid into that region thus increasing the velocity between the three cylinders. This decreases the pressure, and together with the already low pressure wake of cylinder 1 gives the negative

(a) $\alpha=0^0$

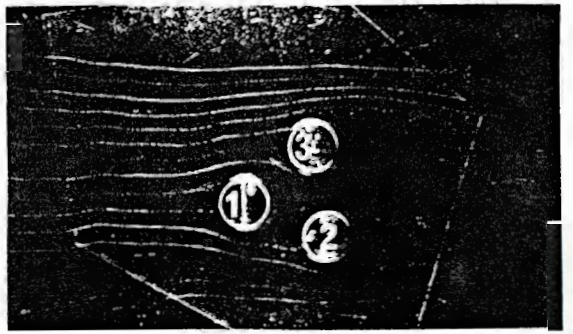

(b) $\alpha=7.5^0$

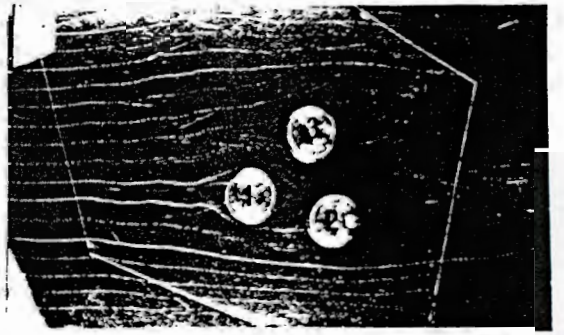

(c) $\alpha=15^0$

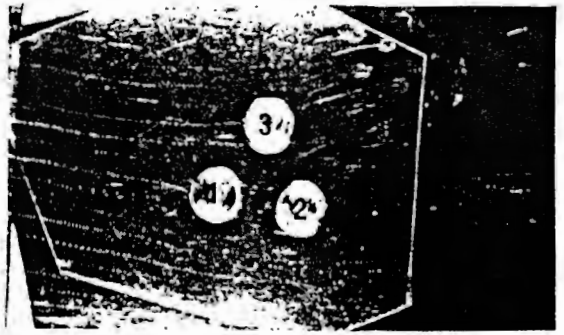

(d) $\alpha=22.5^0$

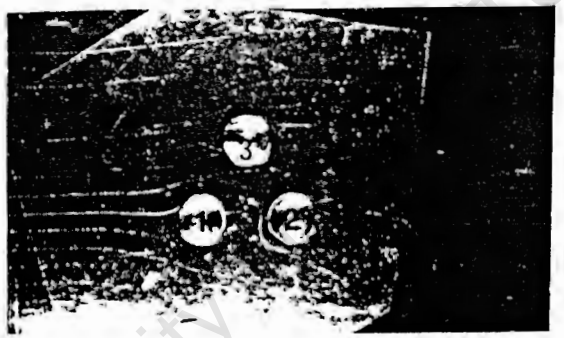

(e) $\alpha=30^0$

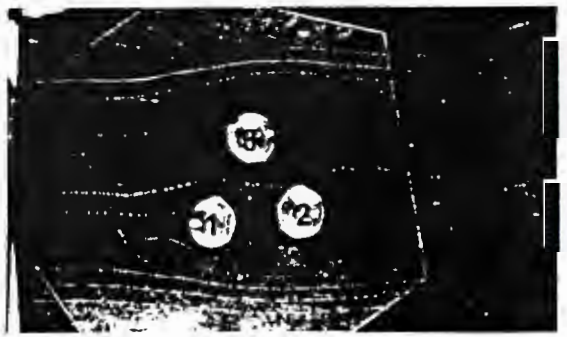

(f) $\alpha=37.5^0$

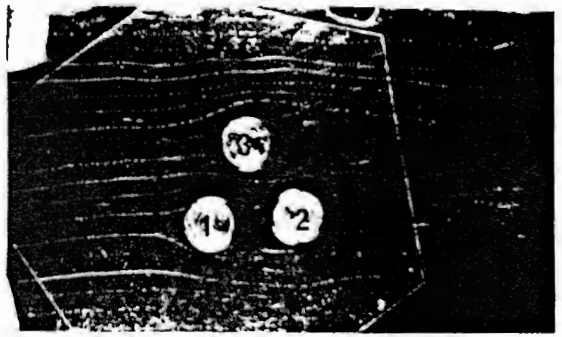

(g) $\alpha=45^0$

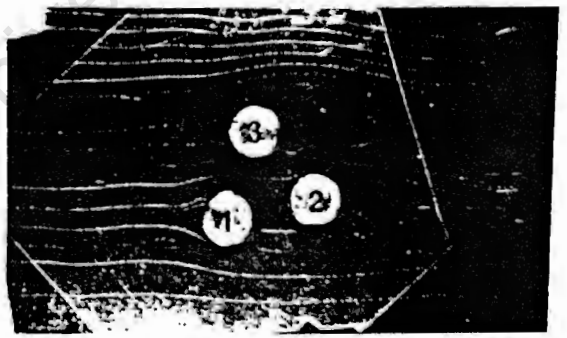

(h) $\alpha=52.5^0$

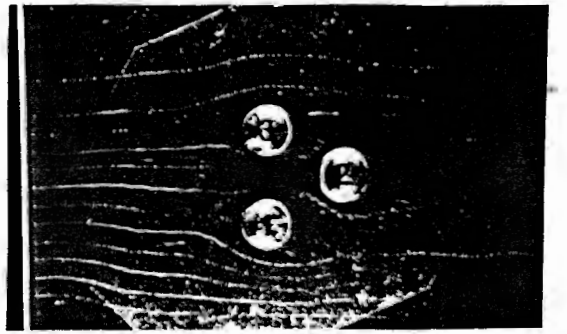

(i) $\alpha=60^0$

Fig. A1.3 Flow visualisation around three cylinders. S/D=2

lift coefficient in Fig. 9c.

Turning to the drag, the spacing of the cylinders is now so close that the streamline flow over cylinder 1 in the range $0° < \alpha < 97.5°$ is no longer similar to free stream flow over a single cylinder and the drag is adjusted accordingly.

S/D = 1.5

From Figs. 8b and 9b, the lift and drag coefficients remain approximately constant and positive in the range $30° < \alpha < 75°$. A clear increased separation of the streamlines around the upper side of cylinder 1 as seen in Figs. A1.4(e-g), and the lower side of cylinder 3, causes an increase of pressure in this region and the consequent increase in $C_D$ and $C_L$.

The peaks at $\alpha$ = 120° and 150° are explained by reasoning similar to that for previous S/D ratios.

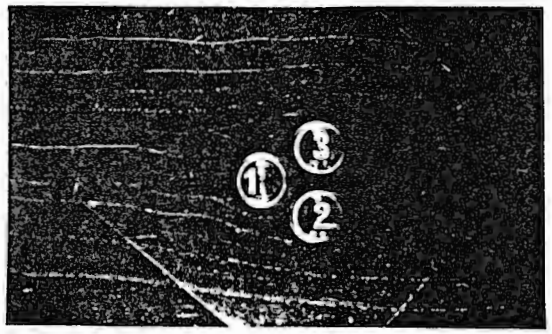


(a) $\alpha=0^0$

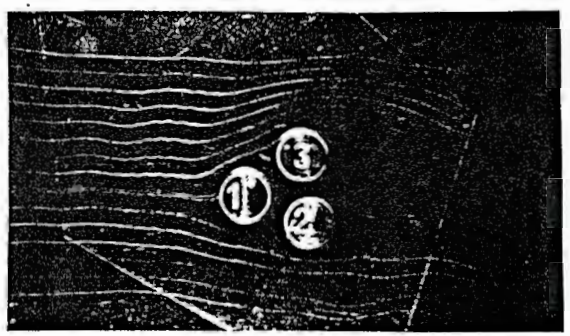


(b) $\alpha=7.5^0$

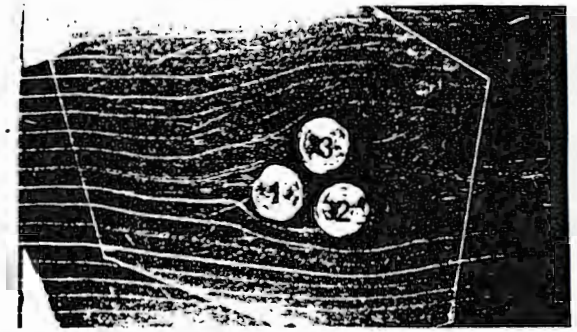


(c) $\alpha=15^0$

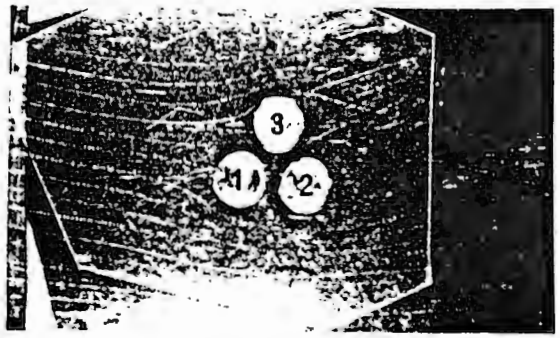


(d) $\alpha=22.5^0$


(e) $\alpha=30^0$

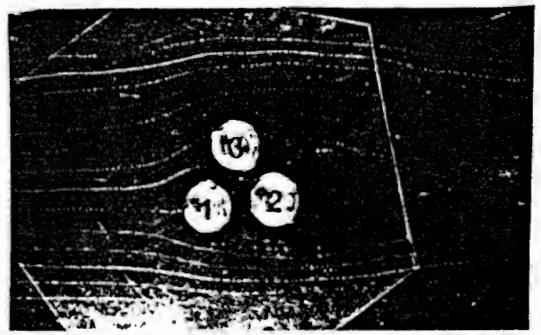


(f) $\alpha=37.5^0$

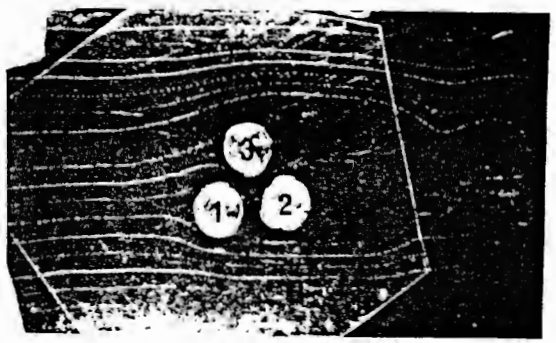


(g) $\alpha=45^0$

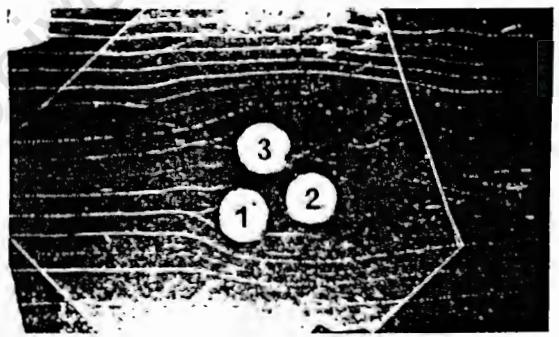


(h) $\alpha=52.5^0$

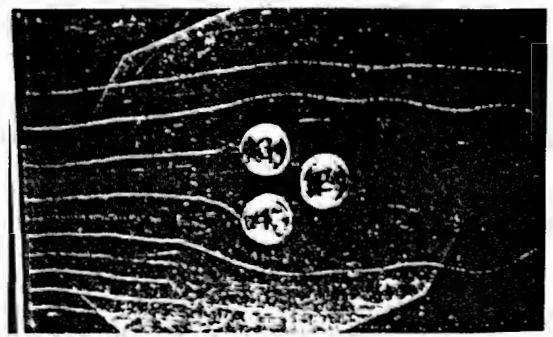


(i) $\alpha=60^0$

Fig. A1.4 Flow visualisation around three cylinders. S/D=1.5

# ADDENDUM 2

## VORTEX SHEDDING FROM THE CYLINDER GROUPS

The frequency of vortex shedding from a single cylinder is linked to the diameter of the cylinder and the free stream velocity through the Strouhal number [29].

$$St = fD/U \qquad (A1)$$

An empirical relationship for St in the range $250<Re<2\times10^5$ is given by

$$St = 0.198(1 - 19.7/Re) \qquad (A2)$$

The frequency of vortex shedding from the cylinders was measured with a DISA type 55D01 anemometer unit using a 5 micron platinum hot wire probe. The output voltage of the probe was continuously recorded against a time base on a digital storage oscilloscope for subsequent analysis. All measurements were made at a nominal free stream velocity of 10 m/s, that is at an equivalent Reynolds number of $3\times10^4$ based on flow over a single cylinder.

The wake behind a single cylinder was first probed to determine where best to position the hot wire to obtain a satisfactory frequency response signal. Frequency measurements were made in various planes downstream from the trailing edge of the cylinder and at various positions across the wake. The frequencies at these points are shown in Fig. A2.1. At distances greater than D/8 downstream and D/2 transversely from the centre line of the cylinder, the vortex shedding frequency was constant at 39.06 Hz. This compares favourably with 39.5 Hz as obtained from equations (A1) and

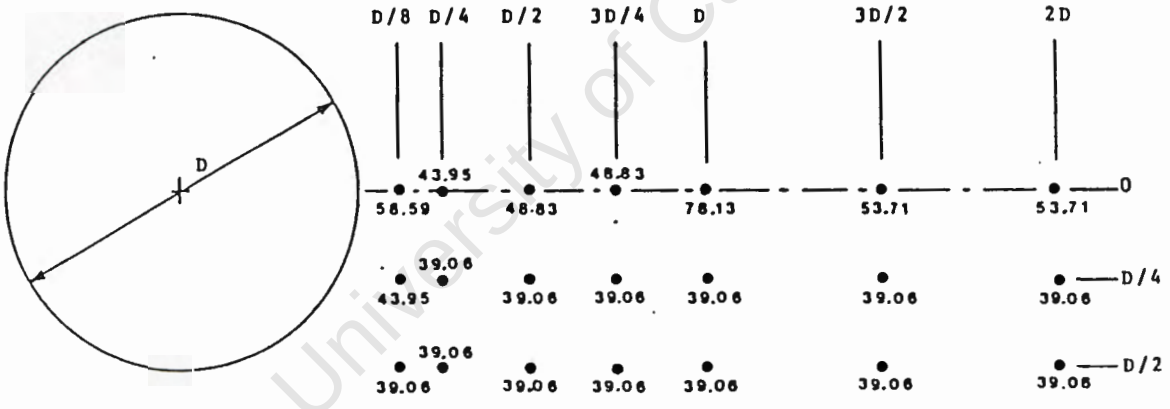


Fig. A2.1 Frequency of vortex shedding from a single cylinder

(A2).

Vortex shedding frequencies were then recorded for the arrays of three and four equispaced cylinders at the two positions A and B shown in Figs. A2.2 and A2.3, that is at D/4 downstream and at D/2 from the centre line of a cylinder. It was however necessary to adjust these positions at some of the lower spacing ratios. This was repeated for cylinder spacings in the range $1.5< S/D <5$ as the group was rotated through the range $0° <\alpha <180°$ in increments of 7.5°.

Results and discussion

The variations in Strouhal number for cylinder 1 as each group of cylinders is rotated are shown in Figs. A2.4 and A2.5. For both groups, at S/D=5, the Strouhal numbers recorded at A and B at all inclination angles are similar in magnitude and lie between 0.19 and 0.21. Thus at this spacing ratio, the vortex shedding frequencies are the same as for an isolated cylinder. At S/D = 4, the Strouhal number is the same at A and B for all increments of $\alpha$ but is no longer constant at about 0.2. The adjacent cylinders 2, 3 and 4 are now influencing the flow over cylinder 1. At S/D = 3 the interference has become well established in that large differences in Strouhal number at A and B occur and these can change suddenly with only small changes in inclination angle. It is also apparent that when cylinder 1 is in the leading position at $\alpha$=0°, the Strouhal number is higher than for the isolated single cylinder despite the fact that the adjacent cylinders are to the rear of cylinder 1. Since at $\alpha$=0° the wake from the other cylinders can not impinge on cylinder 1, the change in Strouhal number

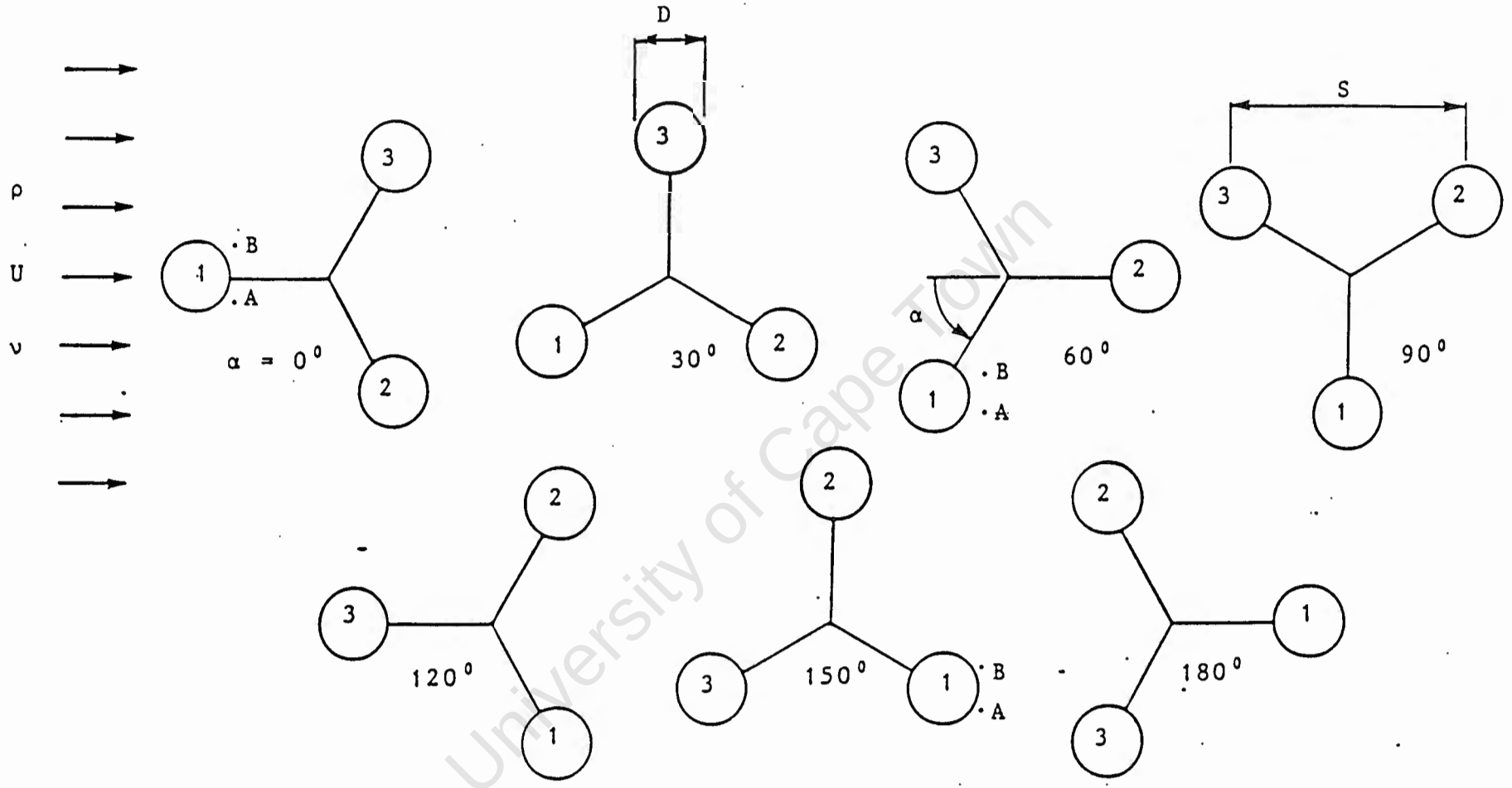


Fig. A2.2 Three cylinder configuration

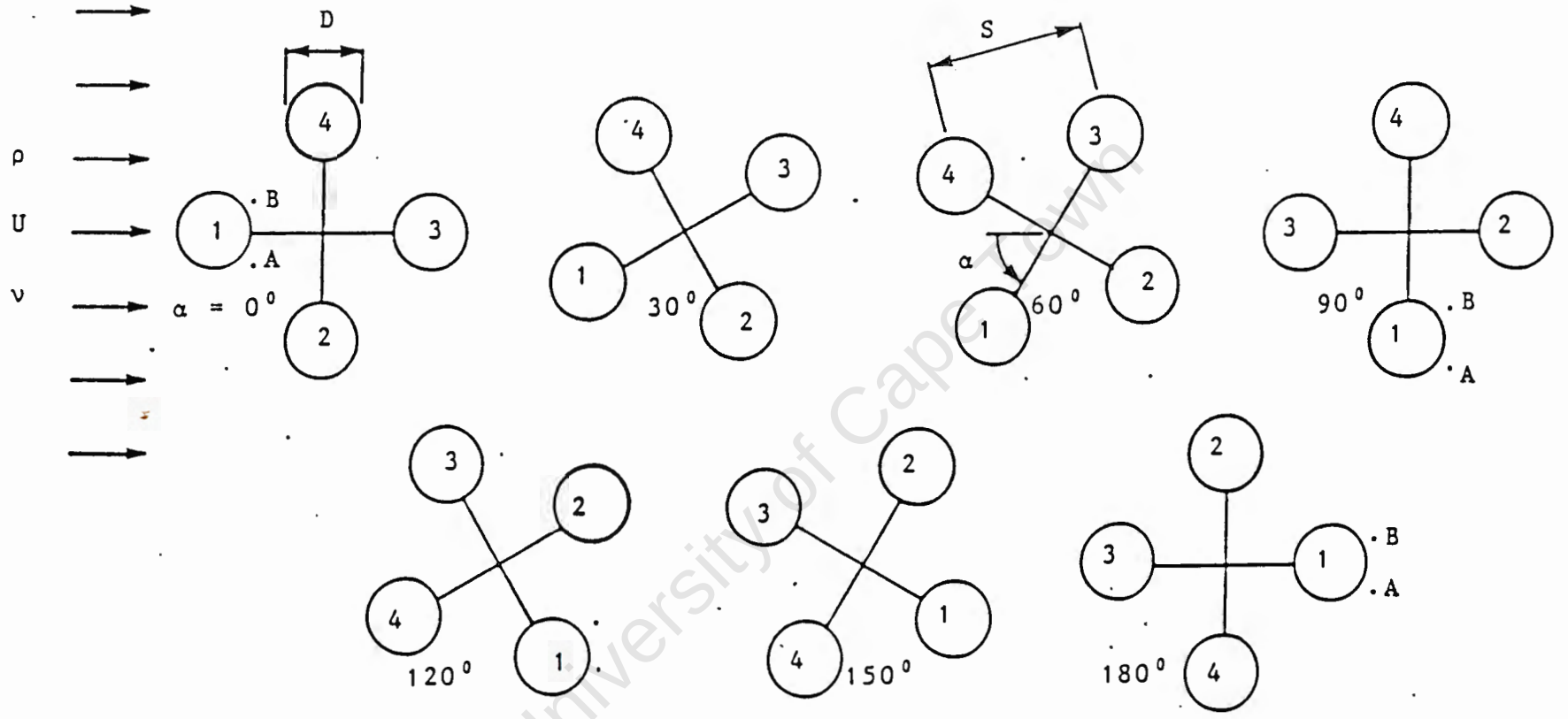


Fig. A2.3 Four cylinder configuration

is due solely to proximity interference. As the group of cylinders is rotated, the vortex shedding frequency of cylinder 1 will be affected by proximity interference, wake interference or a combination of both depending upon the relative positions of the cylinders.

At some orientations at the lower spacing ratios, vortex shedding at position B is totally suppressed whilst still being in evidence at position A, and it is alarming to observe how rapidly vortex shedding is re-established for only a small change in $\alpha$. This could have serious design implications for structures arranged in a similar array especially when situated in a variable direction free stream flow such as tidal currents or atmospheric winds.

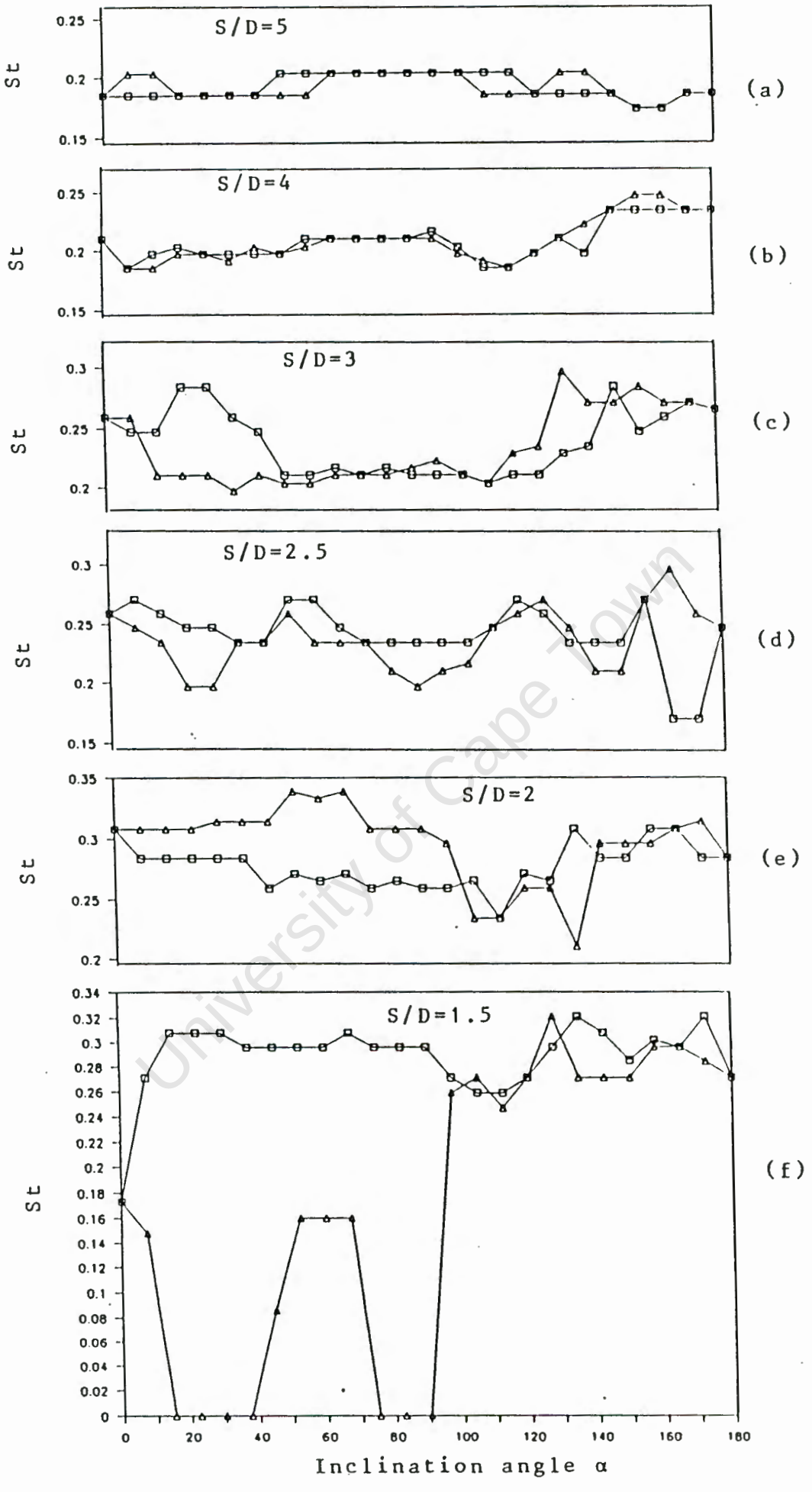


Fig. A2.4 Strouhal number behind cylinder 1 in the group of three equispaced cylinders at variuos orientations to the free stream. (□A,△B) Re=3x10$^4$

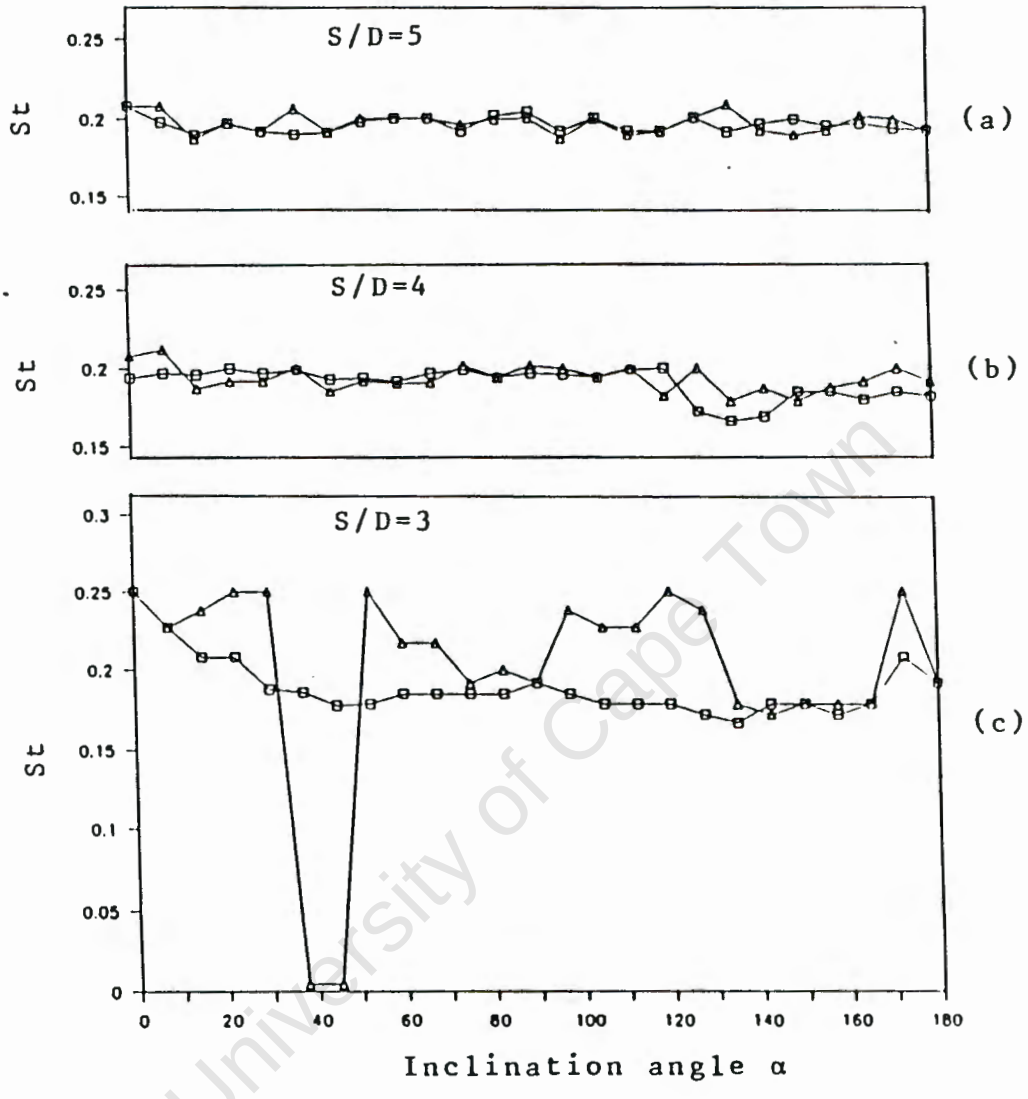




Fig. A2.5 Strouhal number behind cylinder 1 in the group of four equispaced cylinders at various orientations to the free stream. (□A,△B) $Re=3x10^4$

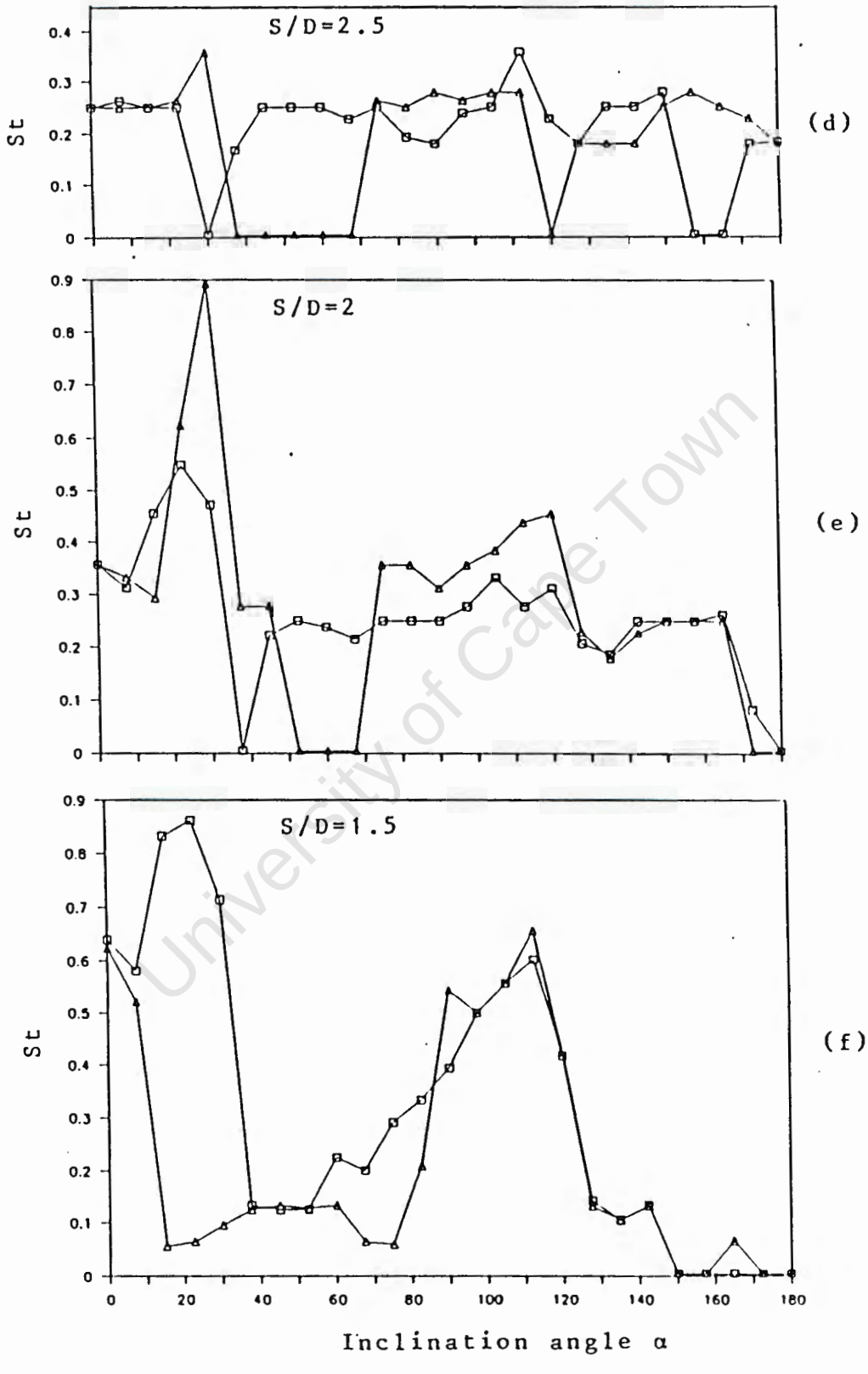


Fig. A2.5 continued

# ADDENDUM 3

## STRAIN AND FREQUENCY RESPONSE OF CYLINDERS

In order that the magnitude of the strain and the frequency of oscillation of the cylinders comprising the group could be determined, it was necessary to reduce the diameter of the cylinders so as to be able to record a high enough value of micro strain. It was also deemed desirable to maintain the same Reynolds number of $3 \times 10^4$ as in the previous tests, and so cylinders of 15.88 mm diameter were chosen whilst the wind tunnel velocity was increased to 32 m/s.

Fig. A3.1 shows the experimental rig designed for these experiments. The three cylinders comprising the group were 580 mm long and were spanned between two 17 mm thick end plates of 236 mm diameter. The ends of the cylinders were a force fit into holes drilled through the end plates at appropriate spacings to give an encastre mounting for the cylinders. This gave an effective cylinder span of 548 mm. At a distance of 23 mm from the end of one of the cylinders, four strain gauges were mounted, at intervals of 90 degrees, around the circumference. Each pair of opposite gauges formed a half bridge which when connected to the strain gauge balance indicated twice the strain due to bending acting at one of the gauges. Each end plate was fitted with a centre pin which in turn were mounted vertically in upper and lower bearings secured to a tubular steel frame. This frame was so designed to be everywhere out of the wind jet when clamped to the mouth of the tunnel. The length of the lower pin was extended to

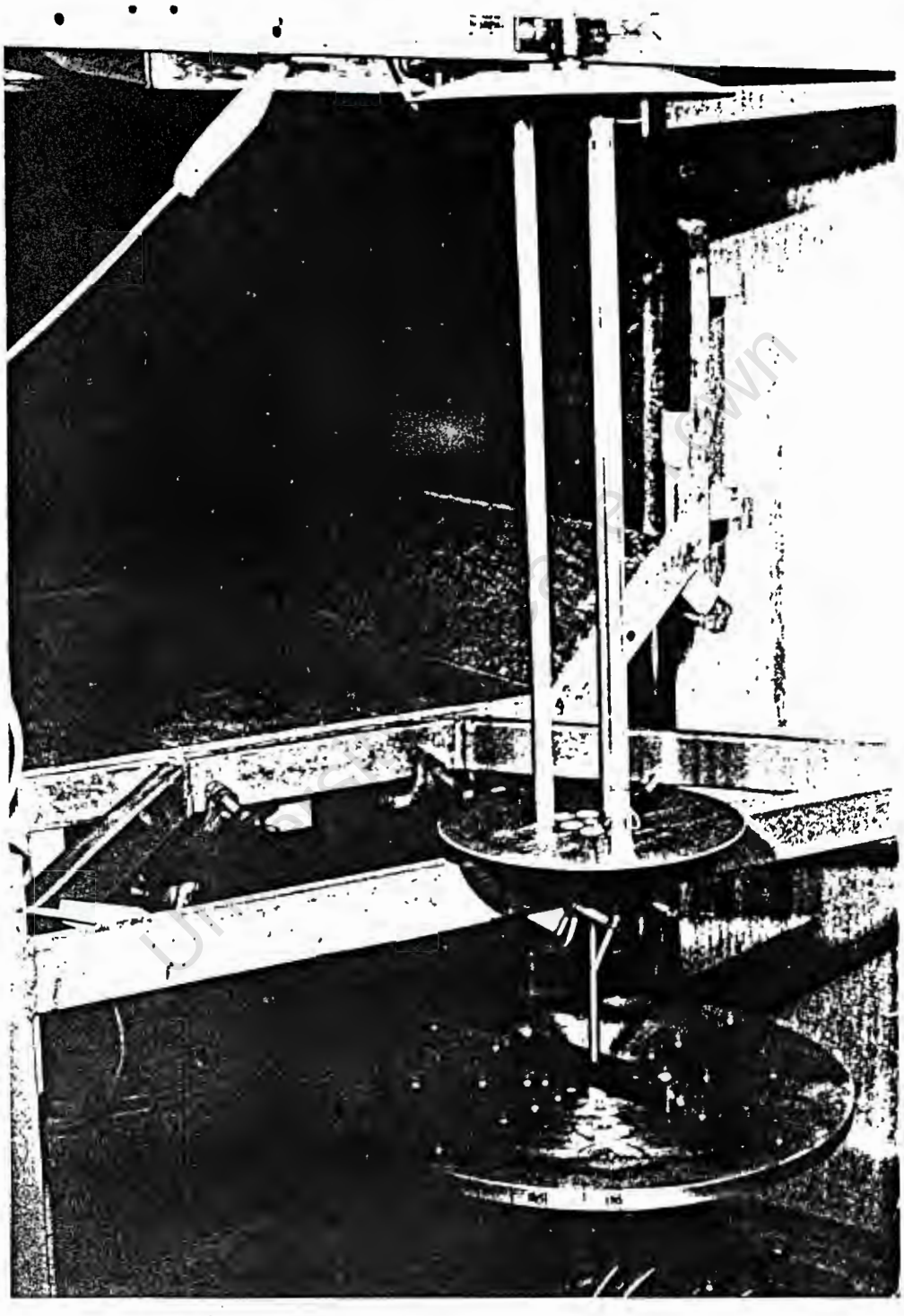

Fig. A3.1 Apparatus for cylinder vibration experiments

reach into a steel block bolted to an indexing head turntable situated below the jet test section such that the assembly of tubes could be rotated to any desired angle of inclination to the free stream.

Strain, due to bending in the free stream and transverse directions was ensured by rotating the strain gauged cylinder an equal amount in the opposite direction to that of the tube assembly. At a nominal wind speed of 31 m/s, recordings of strain variation with time were made for a single cylinder alone, and for a single cylinder in the group of three, at 15 degree increments of $\alpha$ for $0° < \alpha < 180°$. The latter measurements were repeated at various cylinder spacing ratios. The recordings of the strain signals were made onto digital audio recording tape for subsequent analysis using a spectrum analyser. The signals were analysed to obtain the dominant frequencies of tube vibration and the variation in magnitude of the unsteady r.m.s. strains acting on the tubes.

## Results and discussion

### Vibration of a single cylinder

For each cylinder spacing, the background noise signals of the instrumentation and the natural frequencies of vibration of the system were recorded, the latter by lightly tapping the various components comprising the rig. At all cylinder spacings and for the single cylinder the natural frequencies of the apparatus were found to be the same to within 5 Hz. The stiffness of the different systems was therefore statically similar. Natural frequency response curves for a

single cylinder and for S/D = 2 are shown in Fig. A3.2. The natural frequencies of oscillation are 150, 212.5, 237, 612 and 712.5 Hz.

At a nominal free stream velocity of 31 m/s the frequency of von Karmen vortex shedding is calculated, from equations A1 and A2, to be 386 Hz. For flow over the single cylinder, vibration occured at all the natural frequencies, but in the region of 145 Hz particularly large amplitudes were evident as shown in Fig. A3.3. In Fig. A3.3b a frequency of vibration at 397 Hz is noted which is probably due to the reaction to the shed von Karmen vortices. The maximum r.m.s. strain magnitude recorded is 3.32 micro strain.

Streamwise vibration

For all inclination angles at all spacing ratios, the principal vibration frequency lay in the region of 190-220 Hz at an r.m.s. strain magnitude of 2-6 micro strain. Fig. A3.4 illustrates responses at S/D = 5 and 1.5. However, at S/D = 2.5 the strain magnitude at the principal frequency varied widely from one inclination angle to the next, signifying a highly variable flow regime with inclination at this spacing ratio. At S/D = 2, the random peaks disappeared, but at inclinations of 165° and 180°, at the principal frequency of 200 Hz, the r.m.s. amplitude of vibration increased to between 12 and 20 micro strain as shown in Fig. A3.5. At S/D = 1.5, and inclination angles of 165° and 180°, a similar increase in streamwise amplitude of vibration occurs.

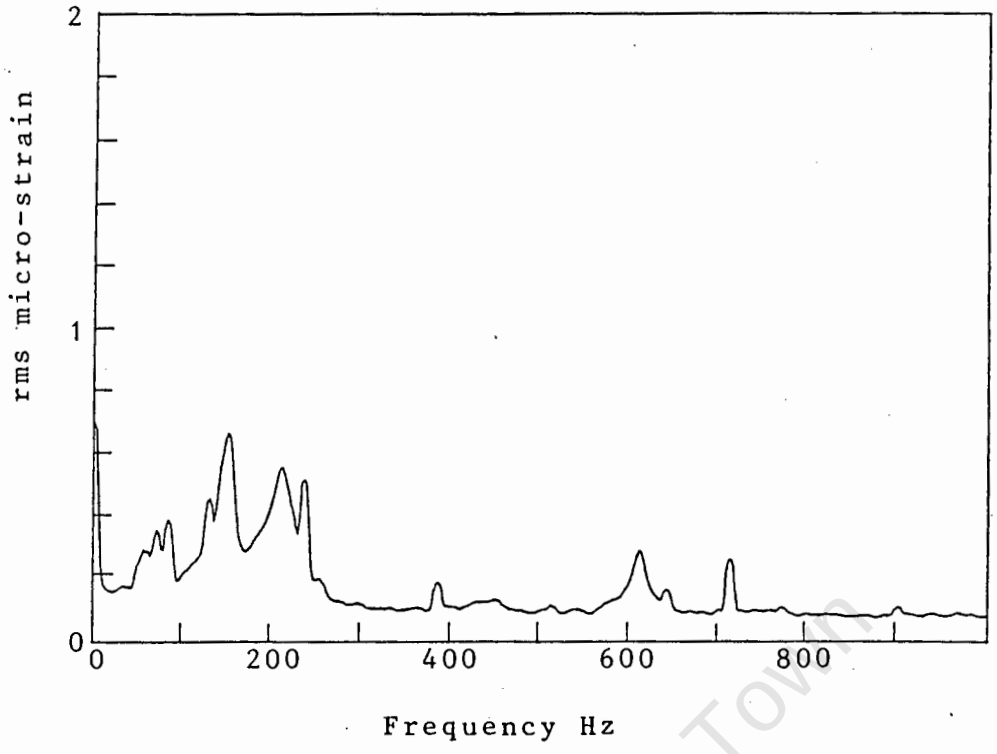


(a) Single cylinder

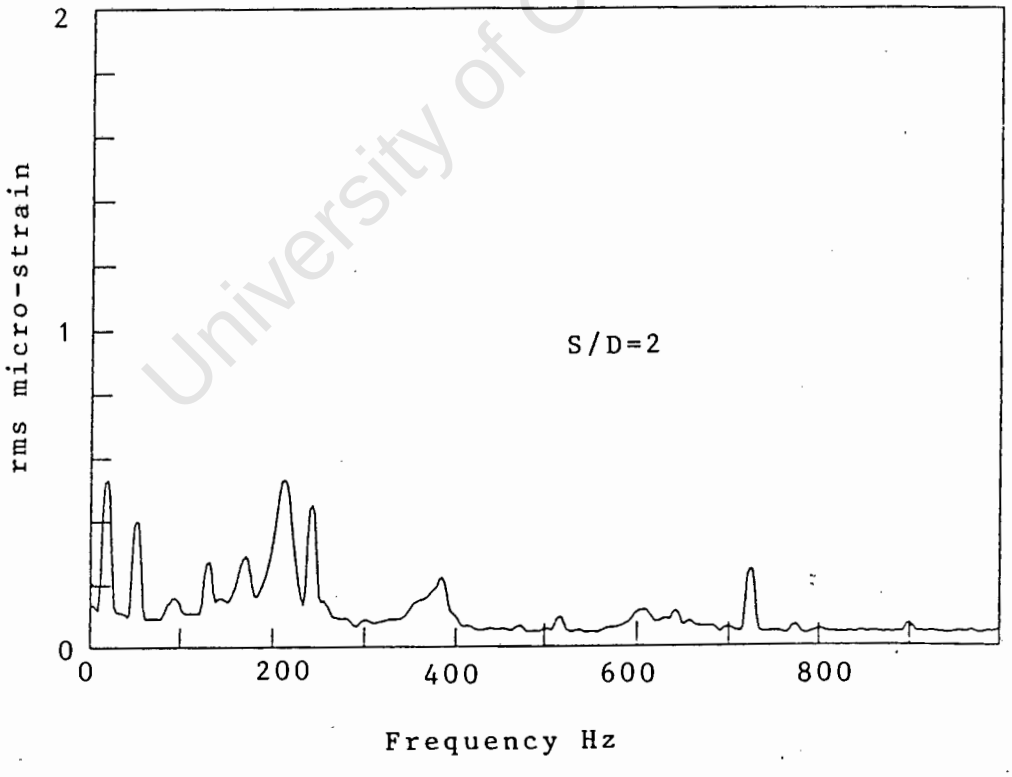


(b) S/D=2

Fig. A3.2 Natural frequencies of strain gauged cylinders

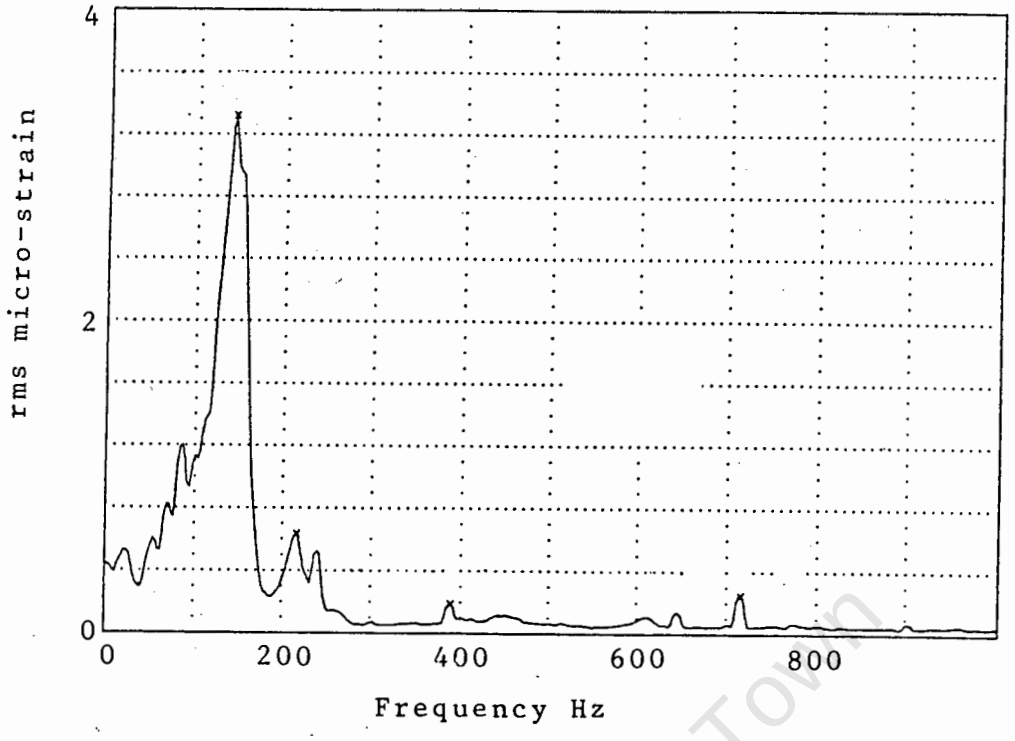


(a) Streamwise vibration

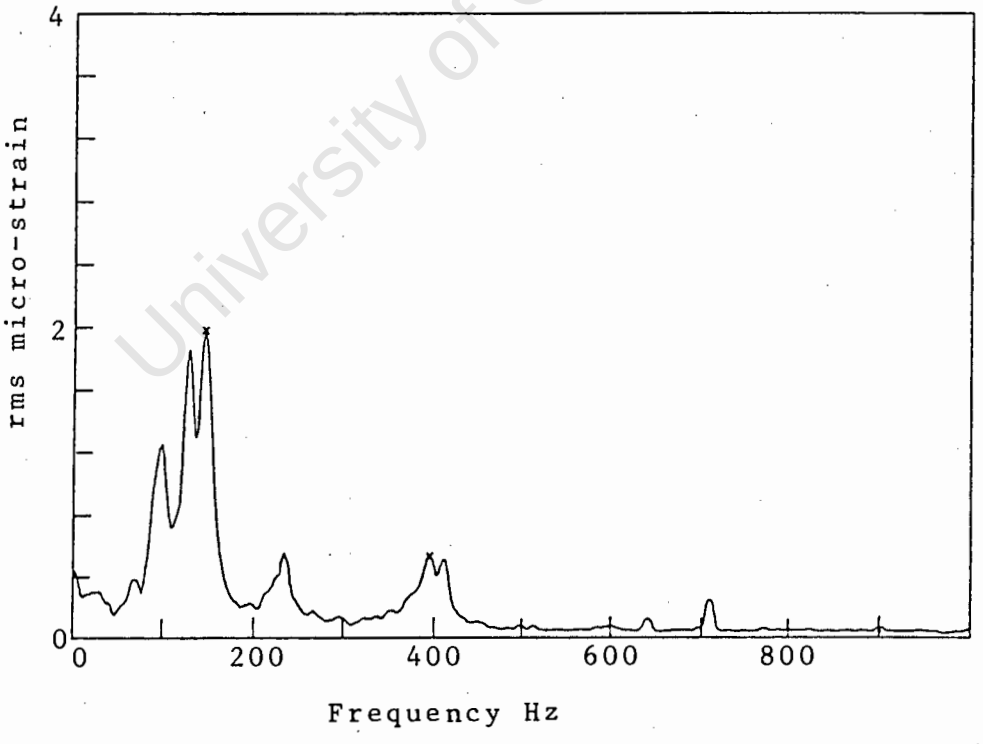


(b) Transverse vibration

Fig. 3.3 Frequency response for flow over a single cylinder

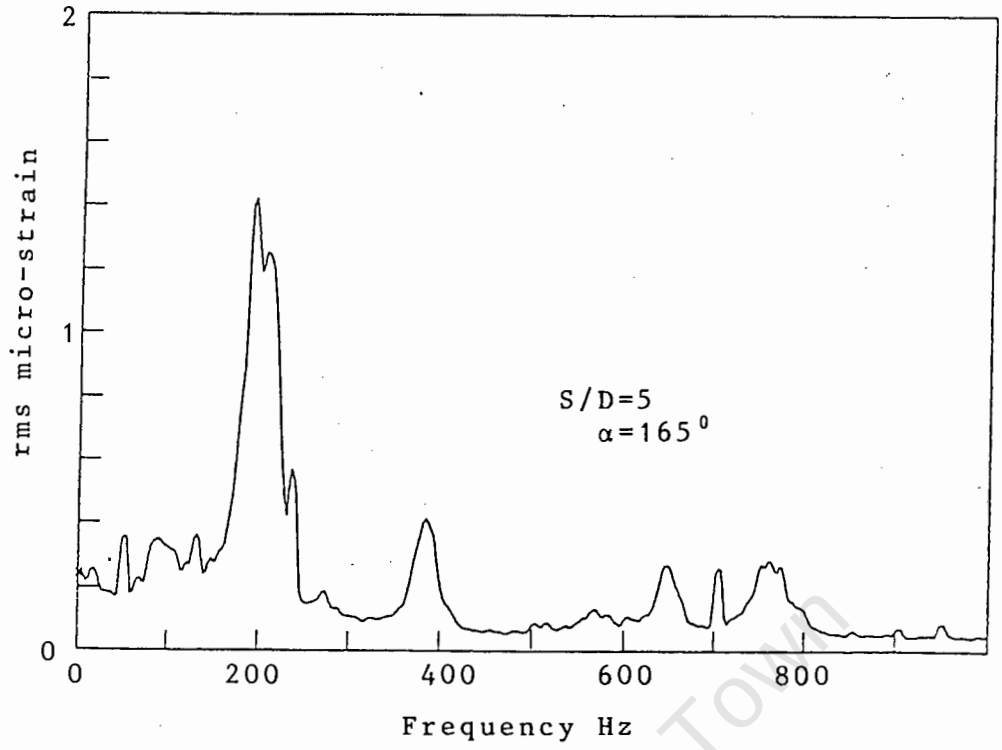


(a) S/D=5; $\alpha=165^0$

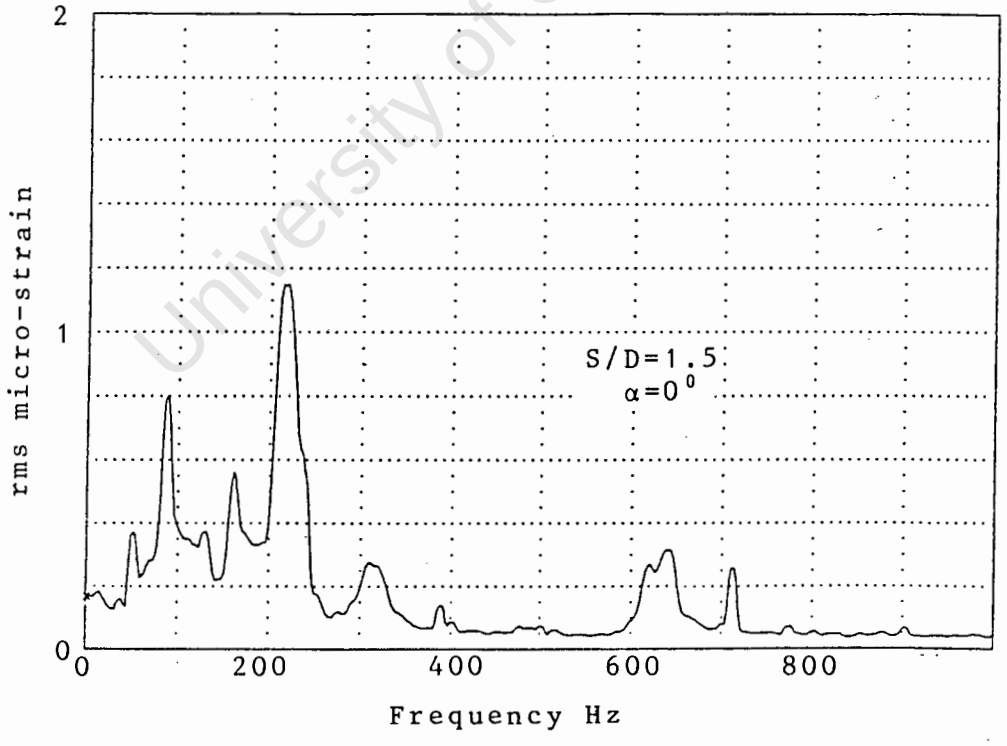


(b) S/D=1.5; $\alpha=0^0$

Fig. A3.4 Streamwise frequency response of a single cylinder in a group of three

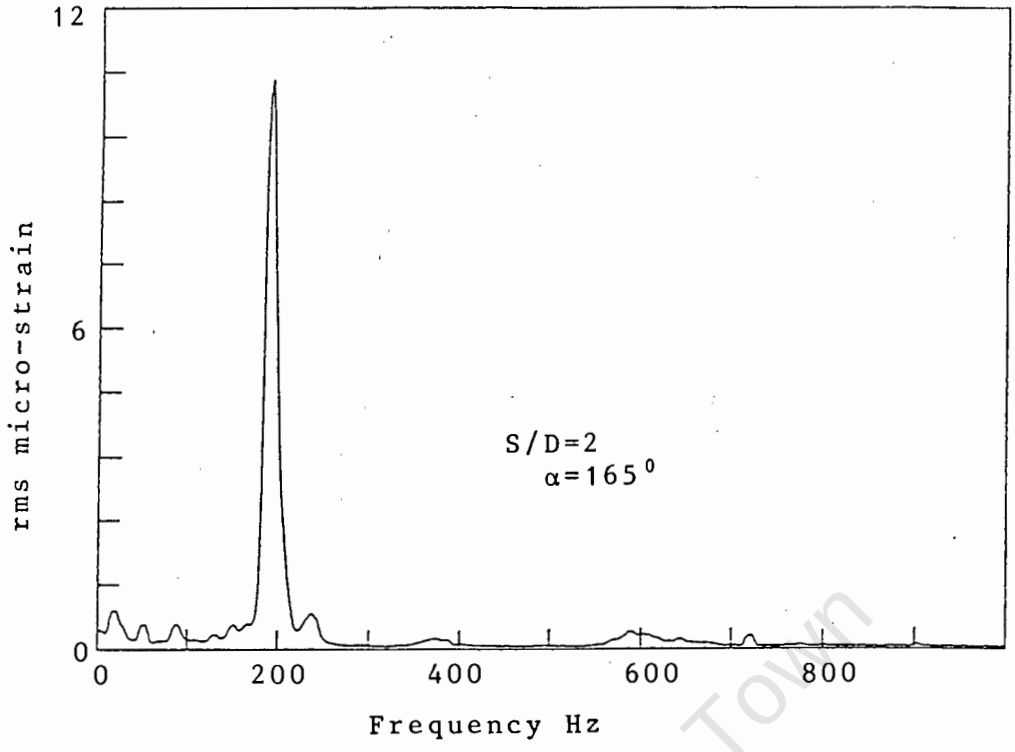


(a) S/D=2; $\alpha=165^0$

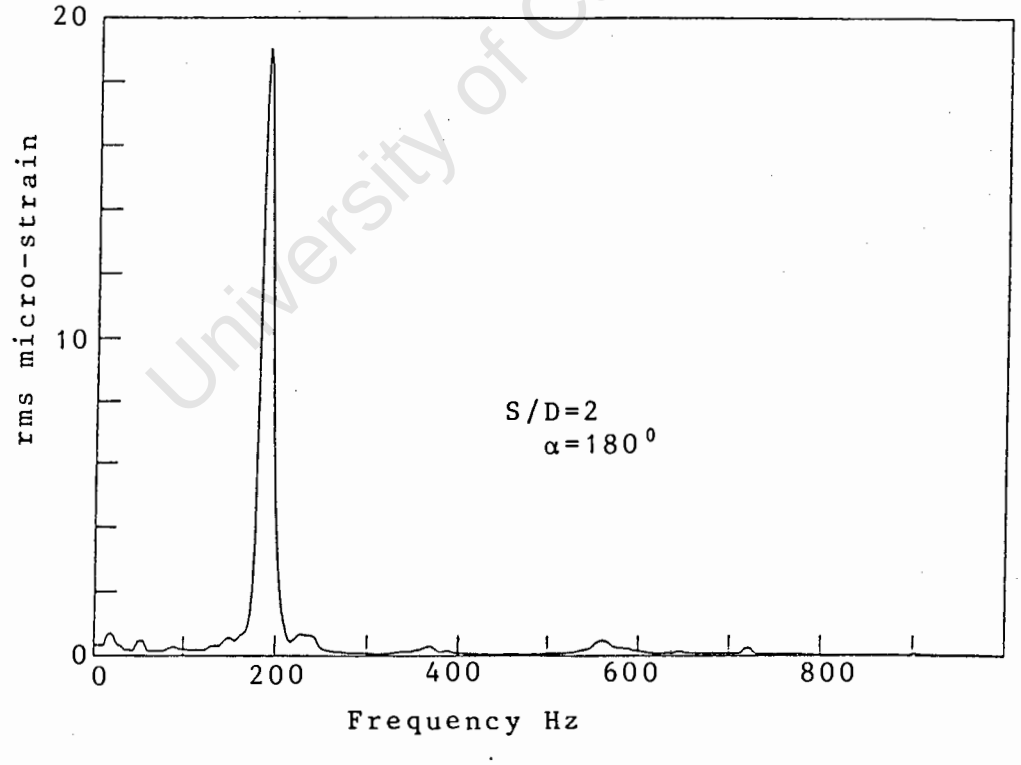


(b) S/D=2; $\alpha=180^0$

Fig. A3.5 Streamwise frequency response of a single cylinder in a group of three

Transverse vibration

For 5< S/D <3 the frequency response curve is characterised by a saddle formation with peak r.m.s. amplitudes at 200 Hz and 380 Hz, the latter being the reaction to the shed von Karmen vortices. These peaks are very distinct and examples are illustrated in Fig. A3.6. At S/D = 2.5, whilst the magnitude of the 200 Hz vibration remains constant, the 380 Hz vibration almost disappears. It reappears in the range 75° < S/D <105° when cylinder 1 is in a position which most closely resembles a single cylinder flow regime. For $\alpha$ >105° the vibration frequencies become random, indicating a wide variation in flow with inclination angle.

For almost all inclination angles at S/D = 2, only the natural frequency of 200 Hz is present, reaching relatively high amplitudes at $\alpha$ = 165° and 180° as shown in Fig. A3.7. Thus for S/D <2.5 it may be inferred that von Karmen vortex shedding is suppressed

At S/D = 1.5, over the range 0° < $\alpha$ <30°, the principal vibration frequency is at 210 Hz. In the range 45° < $\alpha$ <75° the r.m.s. amplitude doubles at a frequency of 170 Hz whilst from 90° < $\alpha$ <150° the principal frequency returns to 210 Hz only to revert to 170 Hz for $\alpha$ = 165° and 180° at amplitudes similar to those for S/D = 2.

From the discussion above, large amplitude vibration takes place at inclination angles of 165° and 180° when the spacing ratio is less than 2.5.

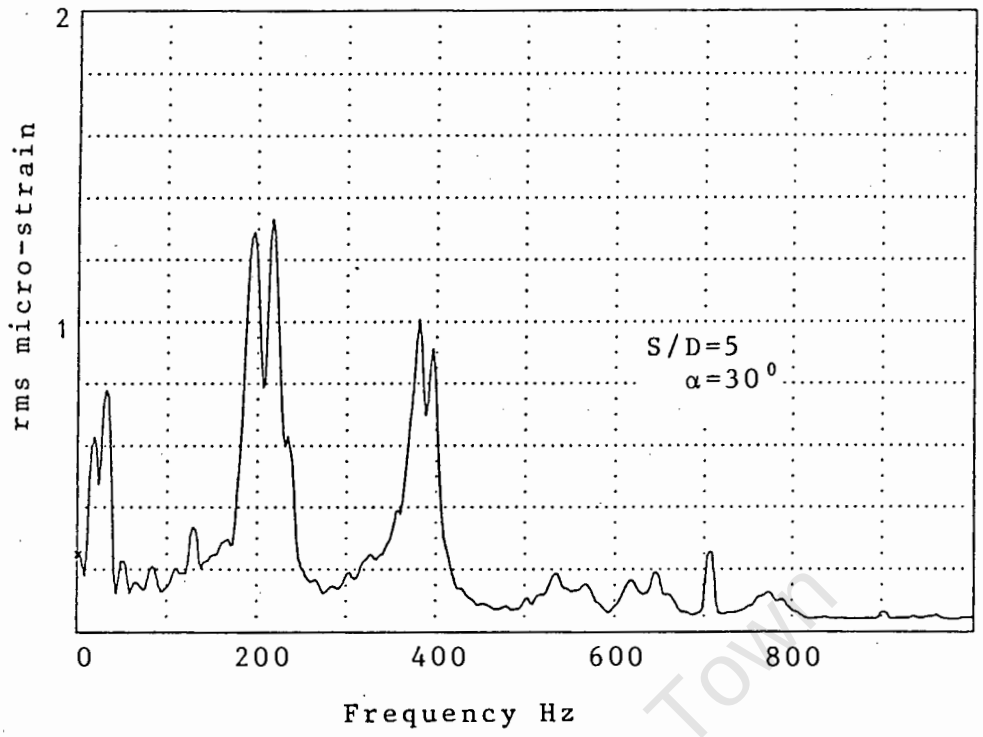


(a) S/D=5; $\alpha=30^0$

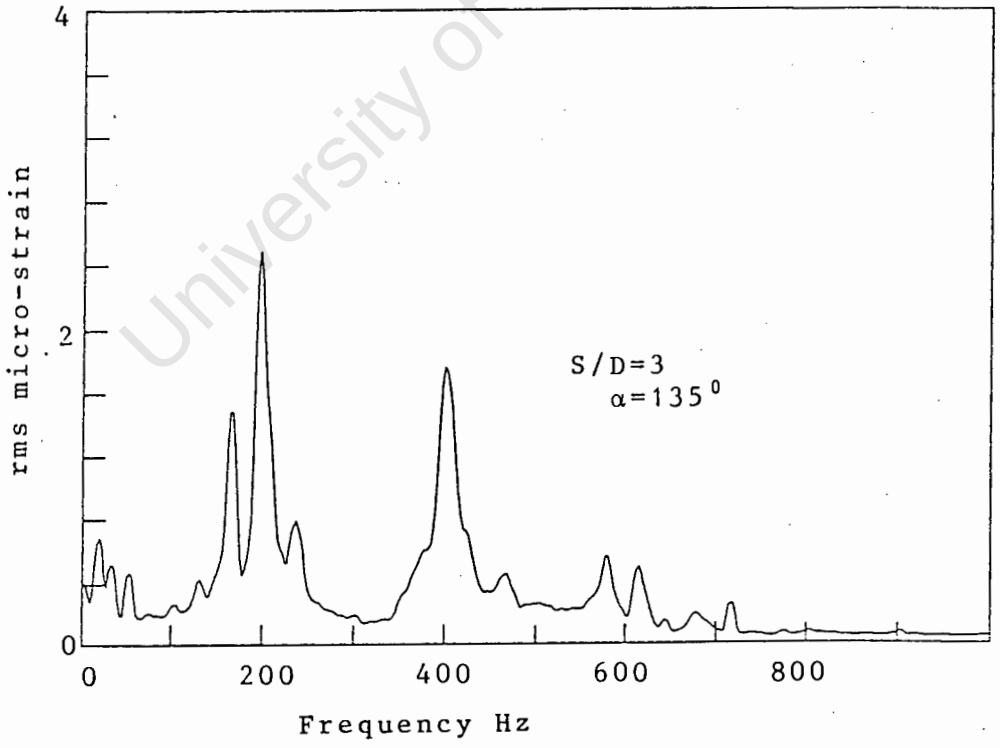


(b) S/D=3; $\alpha=135^0$

Fig. A3.6 Transverse frequency response of a single cylinder in a group of three

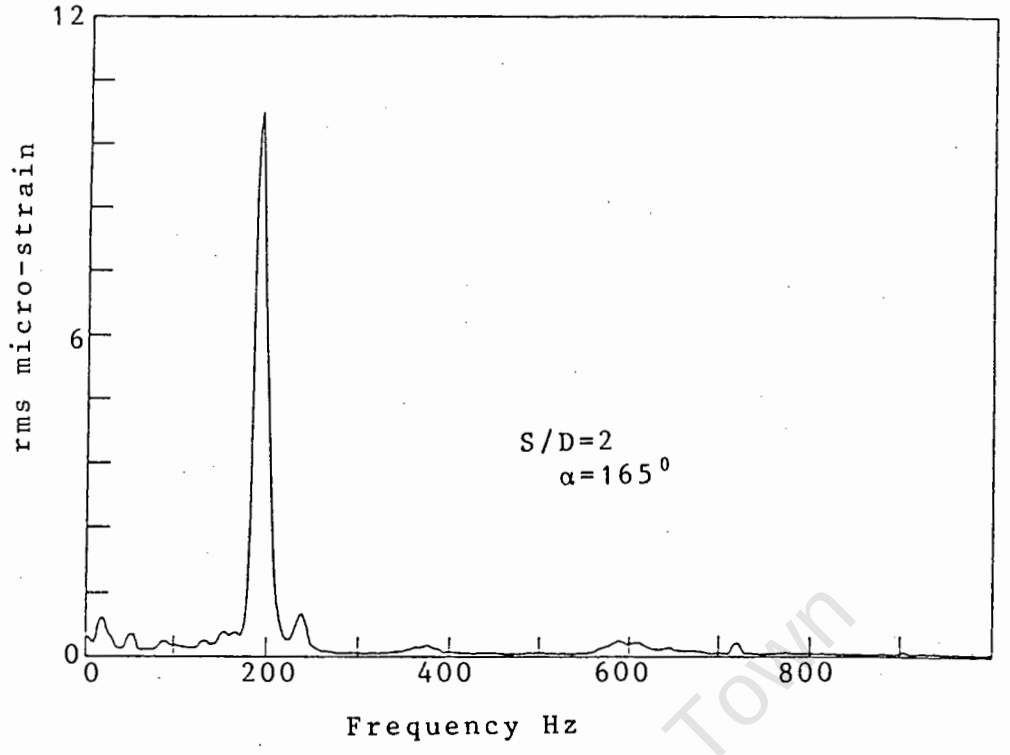


(a) S/D=2; $\alpha=165^0$

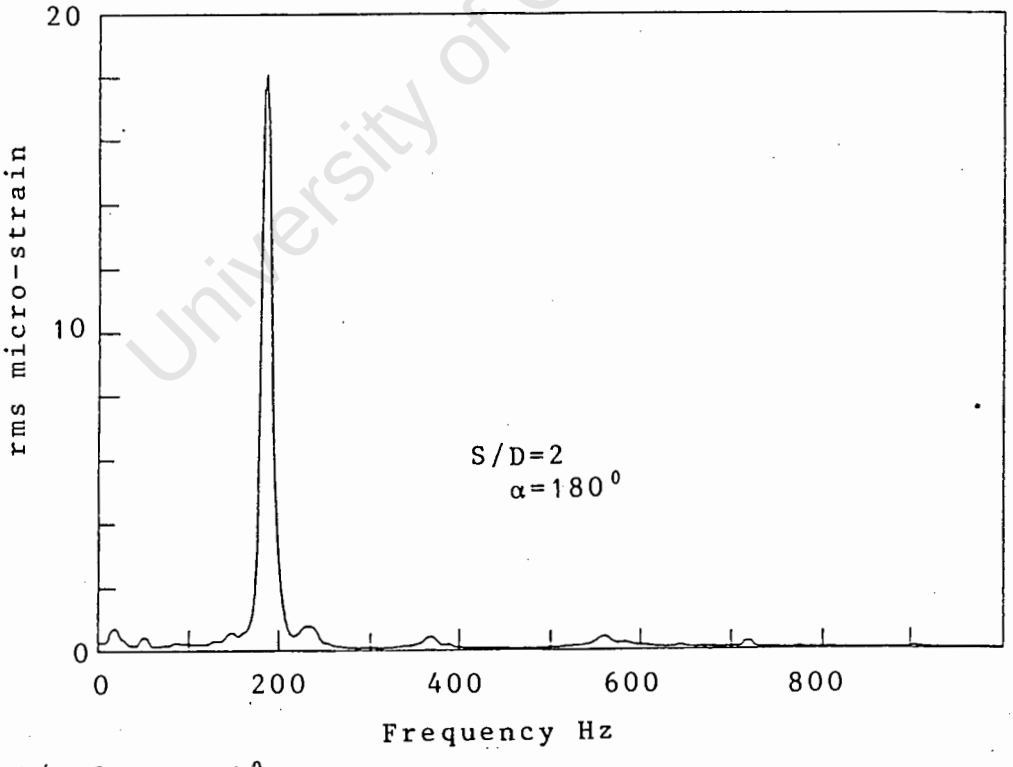


(b) S/D=2; $\alpha=180^0$

Fig. A3.7 Transverse frequency response of a single cylinder in a group of three

*Journal of Wind Engineering and Industrial Aerodynamics*, 31 (1988) 9–28
Elsevier Science Publishers B.V., Amsterdam — Printed in The Netherlands



# FLOW INTERFERENCE BETWEEN FOUR EQUISPACED CYLINDERS WHEN SUBJECTED TO A CROSS FLOW

A.T. SAYERS

*Department of Mechanical Engineering, University of Cape Town, Rondebosch 7700 (South Africa)*

(Received March 26, 1987)

## Summary

This paper presents the results of experiments carried out in an open jet wind tunnel on a group of four equispaced cylinders to determine the lift and drag coefficients for a single cylinder in a group and for the group as a whole. The spacing ratio of their centres was in the range $1.1 < S/D < 5$ while the angle of inclination or stagger angle of the group varied over the range $0° < \alpha < 180°$. In all cases the flow Reynolds number was in the subcritical zone at $Re = 3 \times 10^4$ based on the diameter of a single cylinder. The results are compared with those obtained for flow interference between a group of three cylinders and it is suggested that these results be included with similarly determined data to form a basic code of design.

## Notation

$C_D$ drag coefficient
$C_L$ lift coefficient
$C_{DT}$ total drag coefficient
$C_{LT}$ total lift coefficient
$C_p$ pressure coefficient
$C_{pb}$ base pressure coefficient
$D$ cylinder outside diameter (m)
$p$ static pressure (Pa)
$p_o$ free stream static pressure (Pa)
$Re$ Reynold's number
$r$ radius of cylinder (m)
$S$ distance between cylinder centres (m)
$S/D$ spacing ratio
$U$ free stream velocity (m $s^{-1}$)

*Greek symbols*
$\alpha$ angle of inclination (deg)

$\gamma$ angle of resultant total force (deg)
$\rho$ density of free stream (kg $m^{-3}$)
$\theta$ circumferential angle on the cylinder (deg)

## 1. Introduction

Groups of circular or near-circular structures situated in a flow field with their axes perpendicular to the flow direction are commonly found in engineering practice. Examples are cooling towers in the power generation industry, chimney stacks in the chemical industry, offshore oil drilling platforms, heat exchanger tube banks and overhead power transmission cables. The centreline spacing of the cylinders can range from being very wide to down to one tube diameter, whilst the centre connections can form a rectangular, triangular or linear array, depending upon how many cylinders are involved.

In general, when flow takes place over a group of two or more cylinders, the resultant mean time-averaged forces acting on the cylinders will have lift and drag components perpendicular to and in the direction of the freestream, respectively. The magnitude of the component forces will depend on the number of cylinders in the group, the spacing between the cylinders, the Reynolds number of the flow and the orientation of the cylinders to the freestream flow direction. It is extremely important for the designer of such structures to be aware of the variability of these forces especially in situations where the flow direction is changing, and therefore the need for suitable design codes is evident.

The establishment of such design codes poses problems when one turns to the available experimental data. It is found that most of the data has been determined during research carried out to solve a particular industrial problem and this has led to a rather fragmented set of data points. Indeed, it is only fairly recently that any systematic work has been carried out. Zdravkovich [1] presented a comprehensive review of the studies on flow interference between two circular cylinders in various arrangements. Gerhardt and Kramer [2] investigated the interference effects for groups of three or four stacks whilst Price and Paidoussis [3] found that in certain cases, data for two-cylinder arrangements could be used to predict the forces occuring on certain three-cylinder arrangements. In a later paper, Zdravkovich [4] categorised the flow through pipe clusters and described two basic types of flow interference between two parallel pipes. These are (i) proximity interference, P, which occurs when the pipes are close to each other but neither or only one is submerged in the wake of the other, and (ii) wake interference W, which occurs when one pipe is close to or submerged in the wake of the other; these phenomena can act alone or together. He also concluded that the available experimental data diminished rapidly as the number of pipes increased and that the data for flow over two cylinders could not be used with sufficient accuracy to describe the flow over three or more pipes. Sayers [5] determined the lift and drag coeffi-

cients on one of the cylinders in a group of three equispaced cylinders stressing the need to ensure that flow over the cylinders was two dimensional and that wind tunnel blockage effects were eliminated or suitably accounted for when measurements were being taken.

This paper extends the work of Sayers [5] by describing the determination of the pressure, lift and drag coefficients acting on one cylinder in a group of four as the orientation of the group to the freestream is changed. The cylinders were equispaced forming a regular square and the experiments were conducted in an open jet wind tunnel to eliminate blockage effects. From the data obtained for the individual cylinder, the total drag and lift coefficients for the structure as a whole and the direction in which the resultant force acts are determined.

## 2. Experimental apparatus

The experiments were carried out in a return circuit open jet wind tunnel test section of sides 870 mm $\times$ 580 mm and length 1.6 m, the area ratio between settling chamber and test section being 10:1. The maximum velocity in the test section was 36 m $s^{-1}$; the velocity variation across the test section was $\pm 1\%$ whilst along its length it was 2.6%. The turbulence intensity was 0.4%. All tests were carried out at a nominal wind speed of 10 m $s^{-1}$ and a Reynolds number of $3 \times 10^4$, that is, just before transition in the case of a single cylinder.

The general experimental arrangement of the apparatus is shown in Figs. 1 and 2 and is similar to that described by Sayers [5] except that four cylinders are now used. Each cylinder was a 1-m-long hollow steel tube of 44 mm internal diameter and 50 mm external diameter machined to a smooth finish. One of the tubes was cut in half and a 20-mm-wide brass ring with 24 equispaced (15°) 0.7-mm-diameter pressure tapping holes, was inserted between the two halves. This particular cylinder (the measuring cylinder) was machined smooth after insertion of the ring to ensure that there were no burrs or sharp edges on the surface. At one end of each cylinder a locating screw was secured and the cylinders were screwed vertically into position to a turntable platform the edge of which was graduated in 7.5° divisions. The whole assembly was then located in the wind tunnel test section 500 mm downstream of the tunnel throat, to eliminate blockage effects [6], and its height adjusted such that the 24 pressure tappings lay along the axis of the test section jet with the ends of the cylinders protruding through the jet boundary. Flexible tubing was connected to each pressure tapping of the measuring cylinder and then led up through the hollow tube to one side of an inclined alcohol manometer, the other side of the manometer being connected to the static pressure tapping of a pitot-static tube. The pitot-static tube was placed at the tunnel throat for measurement of freestream velocity. Pressure differences were determined to within 0.025 mm of water and freestream velocity to within 0.25 m $s^{-1}$.

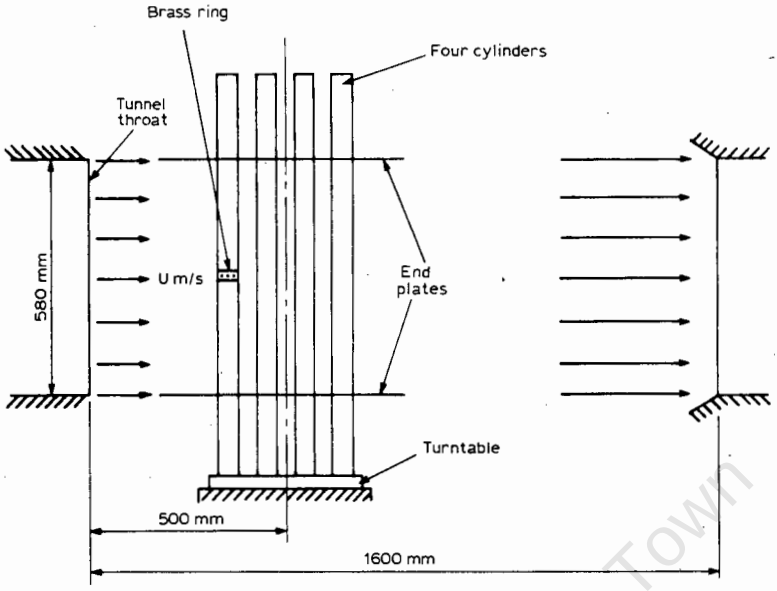


Fig. 1. Experimental arrangement in open jet wind tunnel test section.

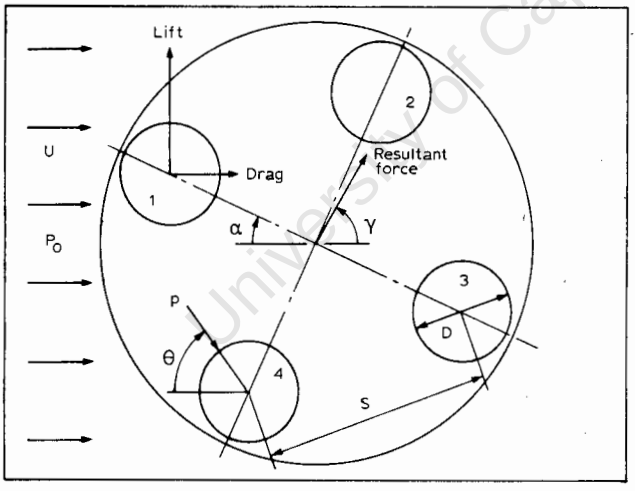


Fig. 2. Cylinder spacing and angles.

To check the uniformity of flow along the span of a cylinder, a fifth cylinder was included with static pressure tappings along its length at $\theta = 180°$. From pressure measurements along the span of this single cylinder it was found necessary to attach end-plates to the cylinders. These took the form of 3-mm-thick boards 760 mm in diameter with 50-mm holes drilled at the positions corresponding to the cylinder spacings.

At all times, great care was taken to ensure that the cylinder separation remained constant across the span and that the axes of the cylinders remained perpendicular to the freestream flow.

## 3. Experimental procedure

The need to attach end plates to a single cylinder in order to achieve two dimensional flow was discussed fully by Sayers [5]. Accordingly, the four cylinders were located on the turntable at a particular spacing ratio with the 760-mm-diameter end plates positioned to give an effective span of 575 mm. With $\alpha$ set at 0°, the measurement cylinder (1) was rotated until one of the mid-span pressure tappings pointed directly upstream when the static pressures at the 24 mid-span tappings were recorded. The turntable was then incremented from 0–180° in steps of 15° in the first instance and then in steps of 7.5° where rapid changes in lift or drag coefficient were evident. The procedure was repeated for the range $1.1 < S/D < 5$ at a nominal freestream velocity of 10 m s$^{-1}$.

## 4. Results and discussion

The experimental results are expressed in terms of dimensionless pressure, lift and drag coefficients. The pressure coefficient is expressed as

$$C_p = (p - p_o)/0.5\rho U^2 \tag{1}$$

The drag coefficient is given by

$$C_D = \int_0^{2\pi} (p - p_o) r\cos\theta \, d\theta / 0.5\rho U^2 D \tag{2}$$

and the lift coefficient by

$$C_L = -\int_0^{2\pi} (p - p_o) r\sin\theta \, d\theta / 0.5\rho U^2 D \tag{3}$$

where the integrals of the pressure distributions of eqns. (2) and (3) were carried out using Simpson's rule.

It was shown by Sayers [5] that the fitting of end-plates to the cylinders gave two dimensional flow between the plates and therefore direct comparison can be made with the results of Sayers [5] for flow over three cylinders. Figs. 3 and 4 show the drag and lift coefficients for cylinder 1 as the group of four cylinders is rotated through 180°. It is assumed that symmetry of flow occurs for the range $180° < \alpha < 360°$ and this was verified by random pressure measurements during the experiments.

The lift and drag coefficients acting on each cylinder of the group for a given

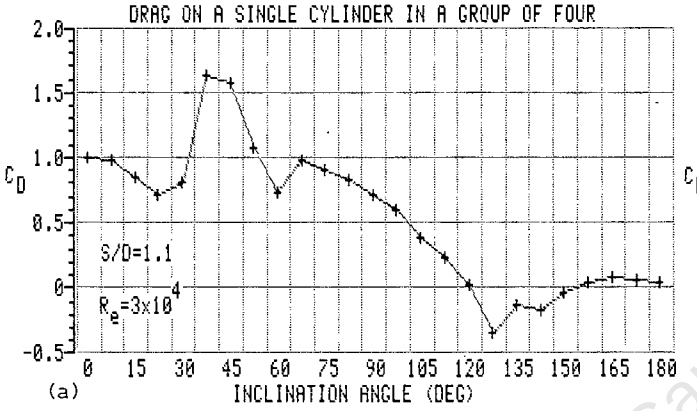


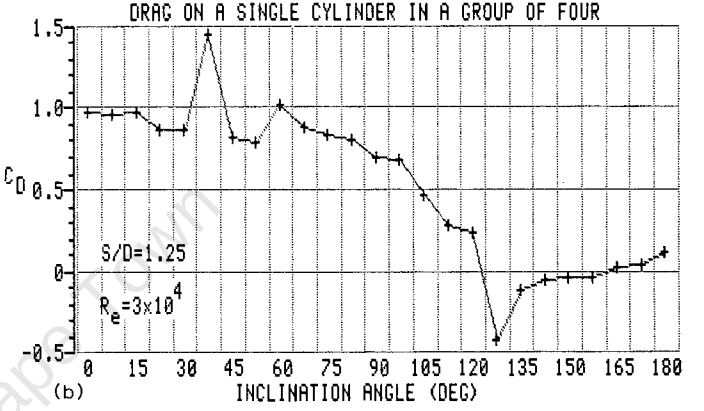


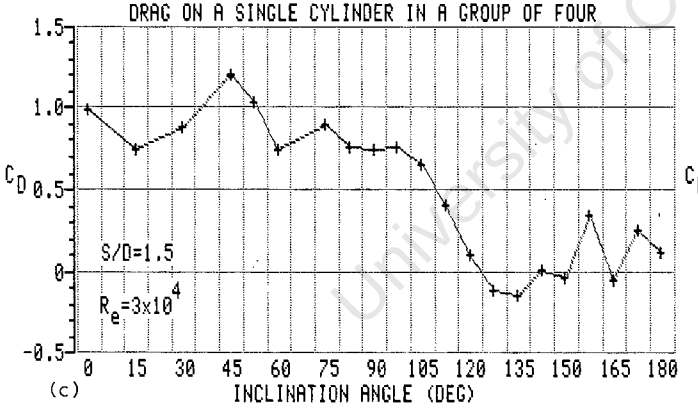


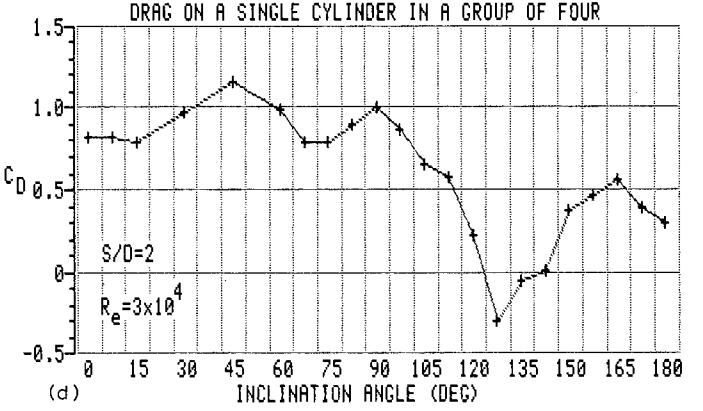

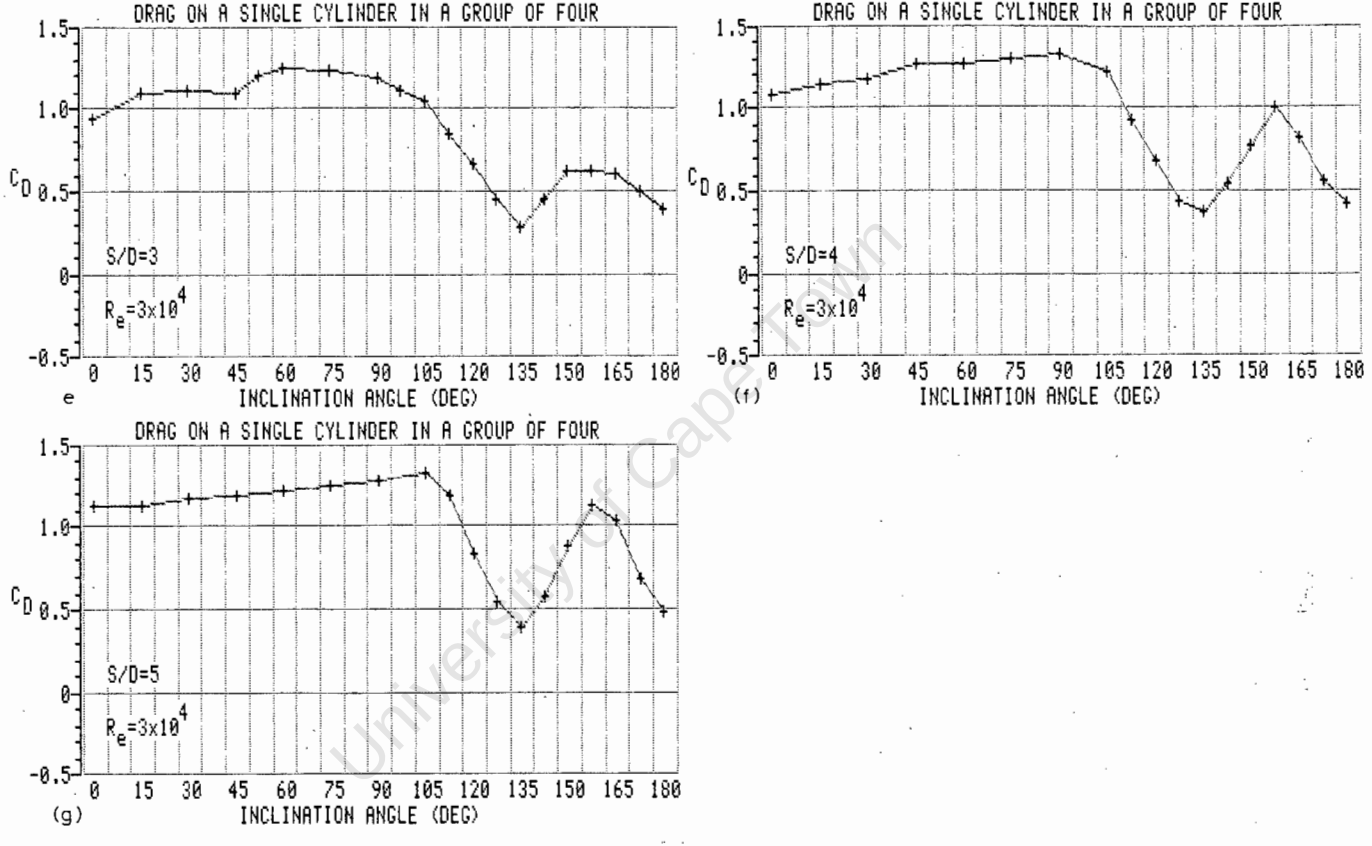


Fig. 3. Drag coefficients on a single cylinder in a group of four.

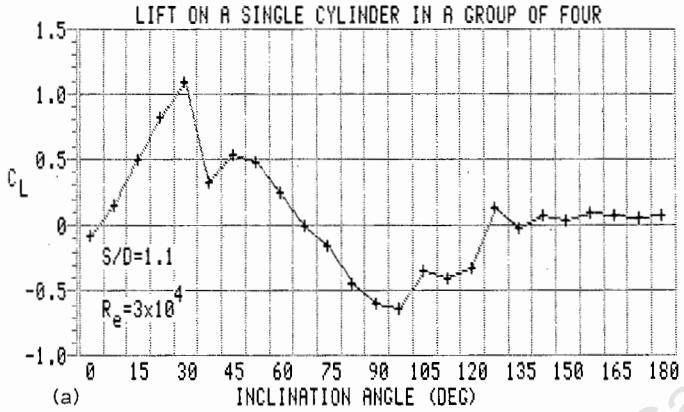


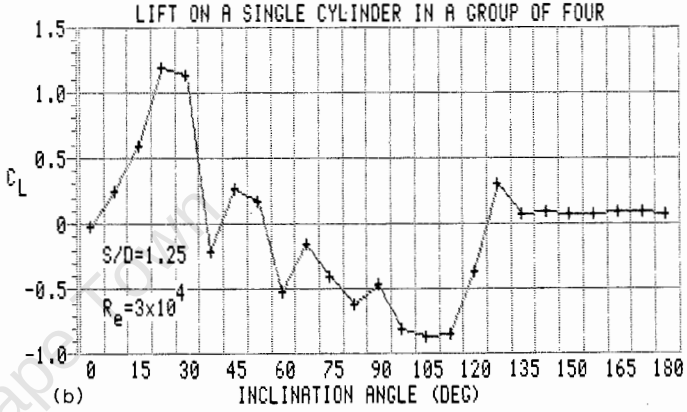


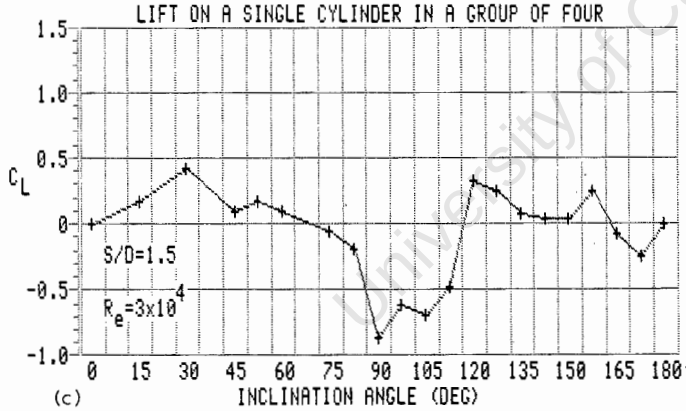


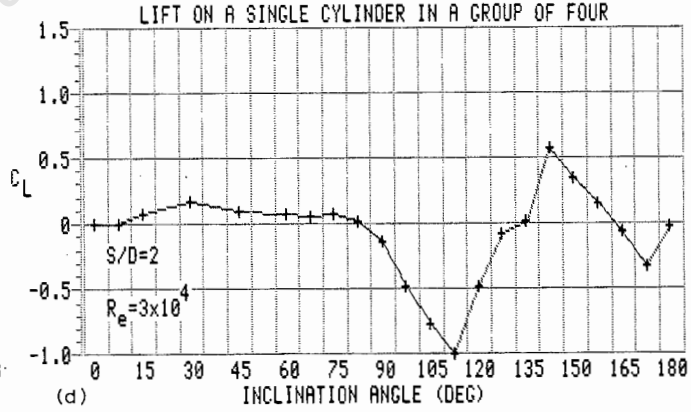

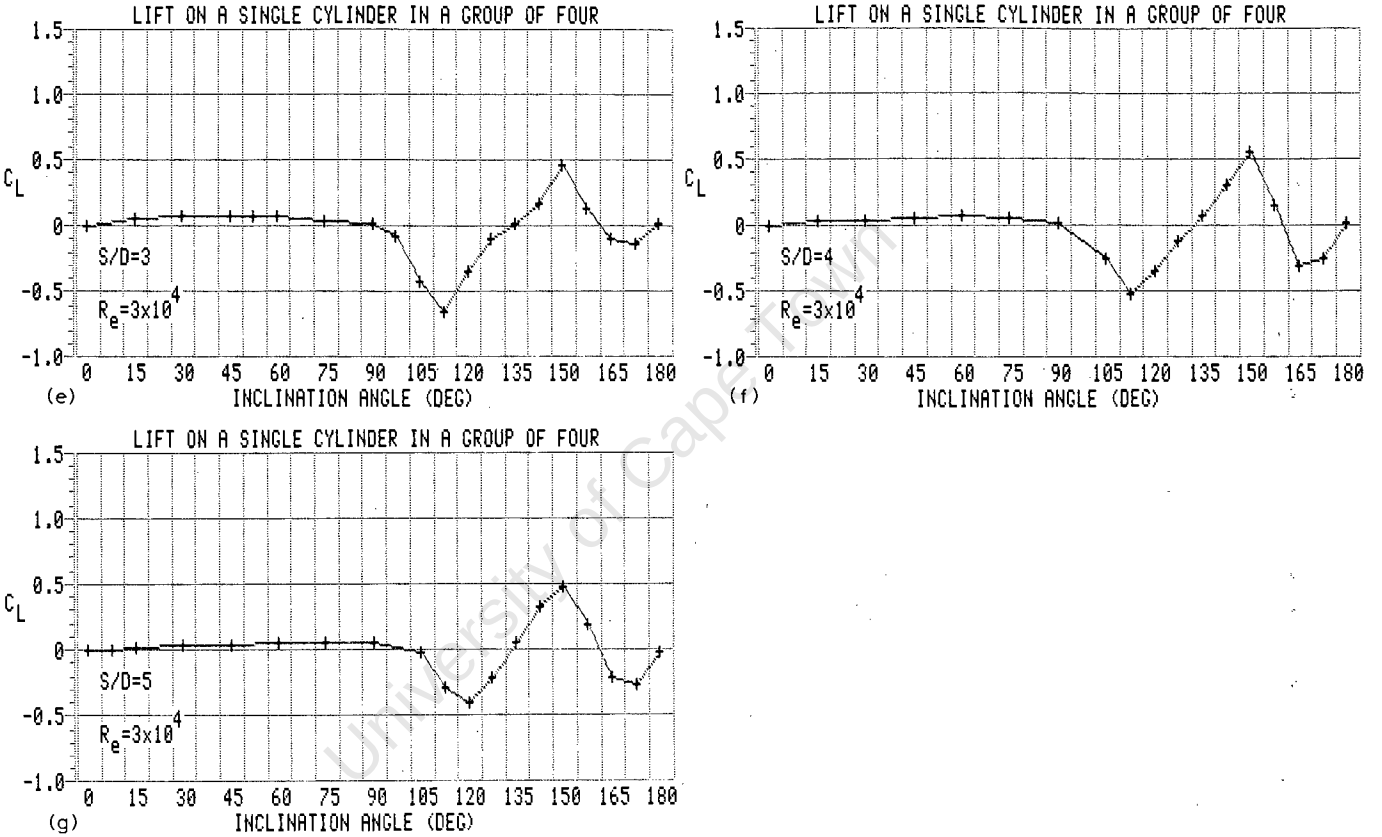


Fig. 4. Lift coefficients on a single cylinder in a group of four.

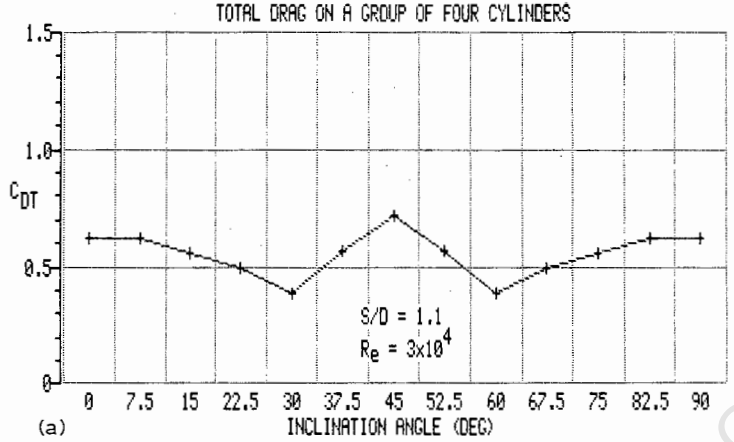


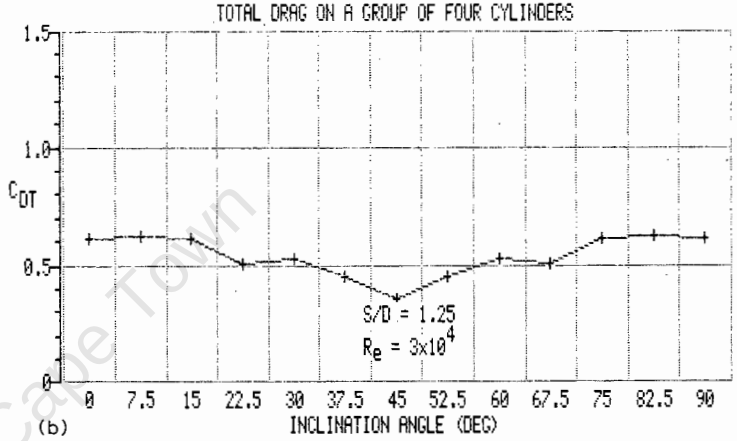


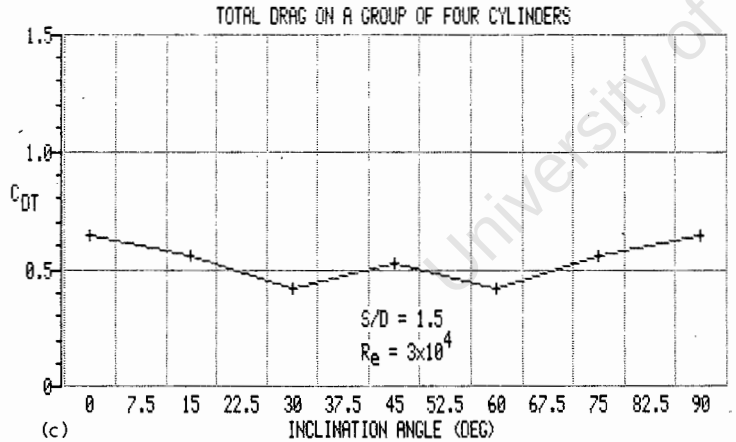


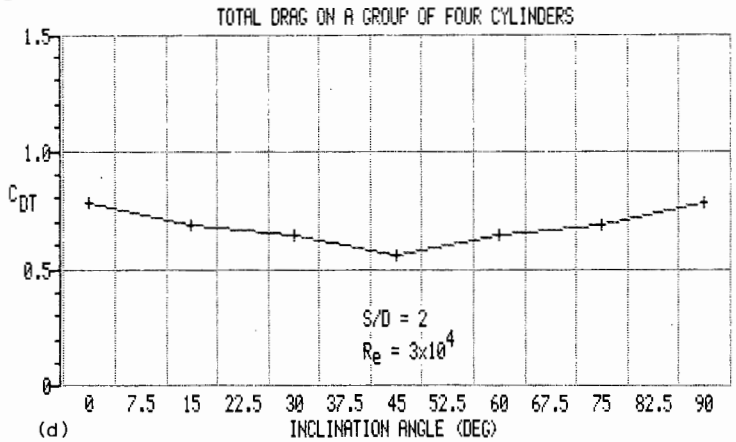

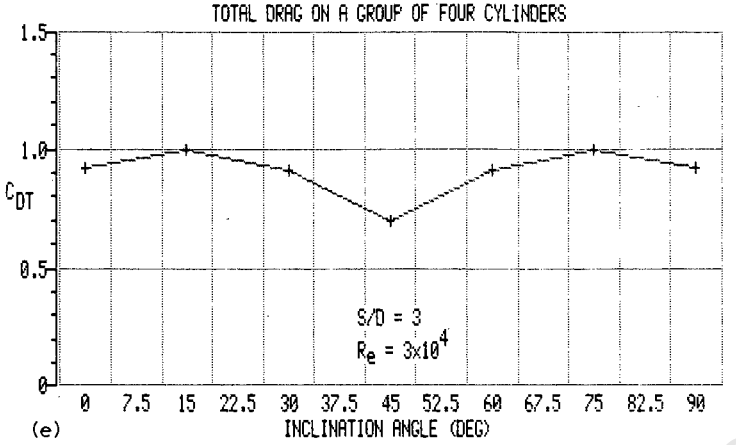


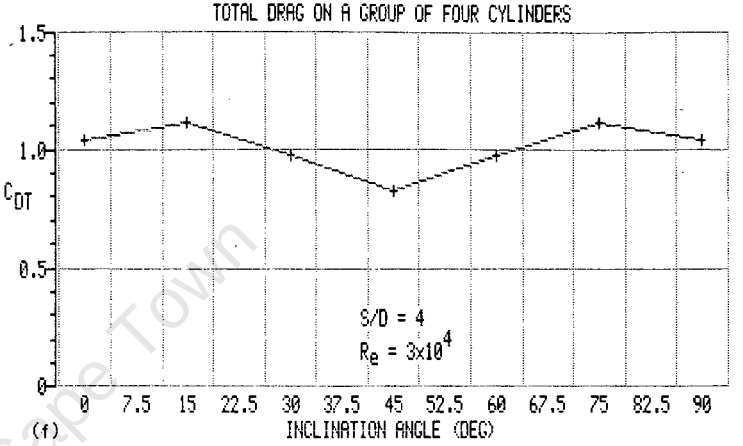


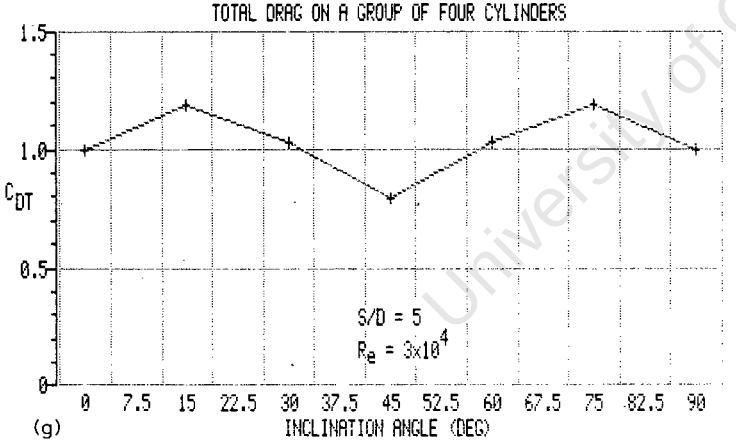


Fig. 5. Total drag coefficients for the group of four cylinders.

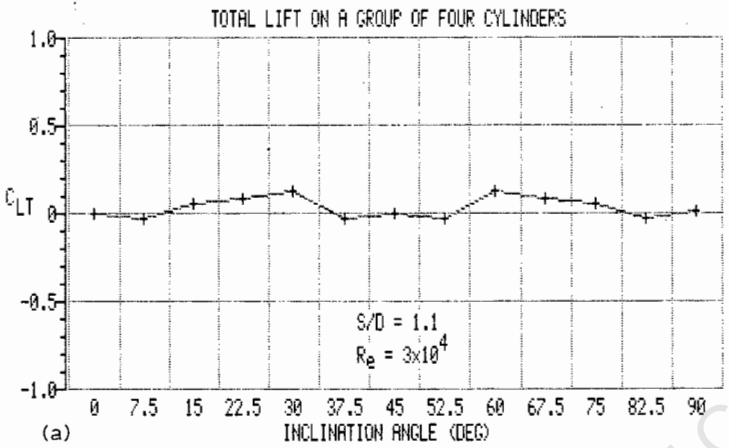

(a)

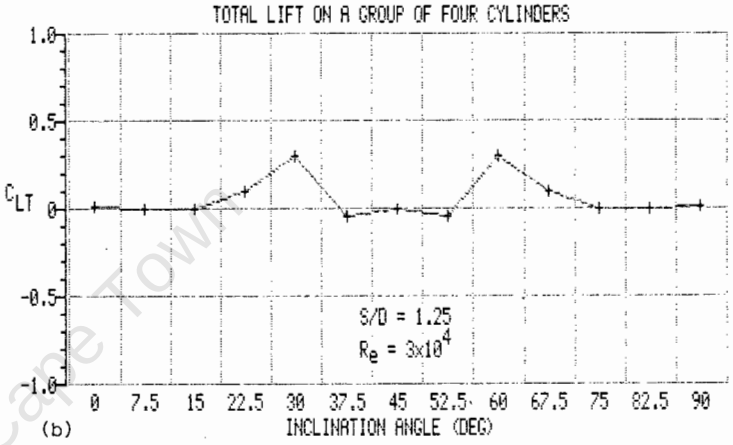

(b)

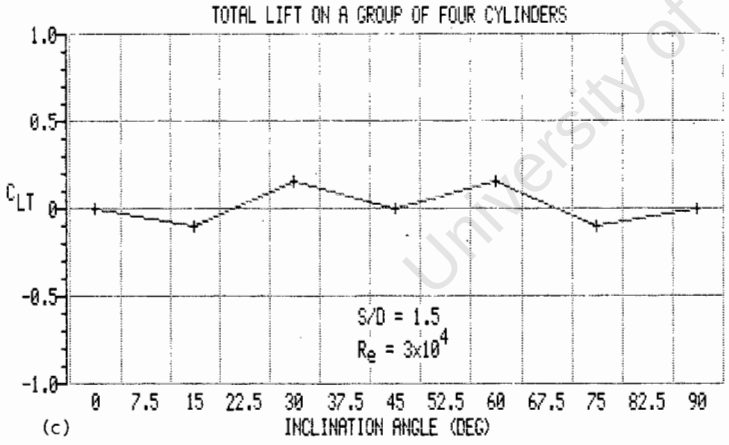

(c)

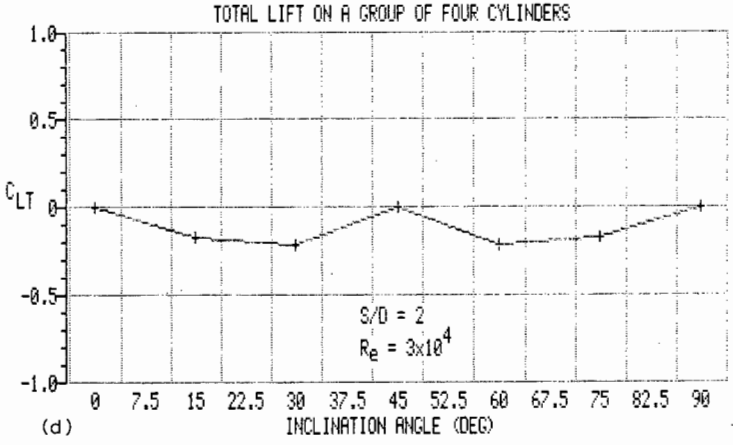

(d)

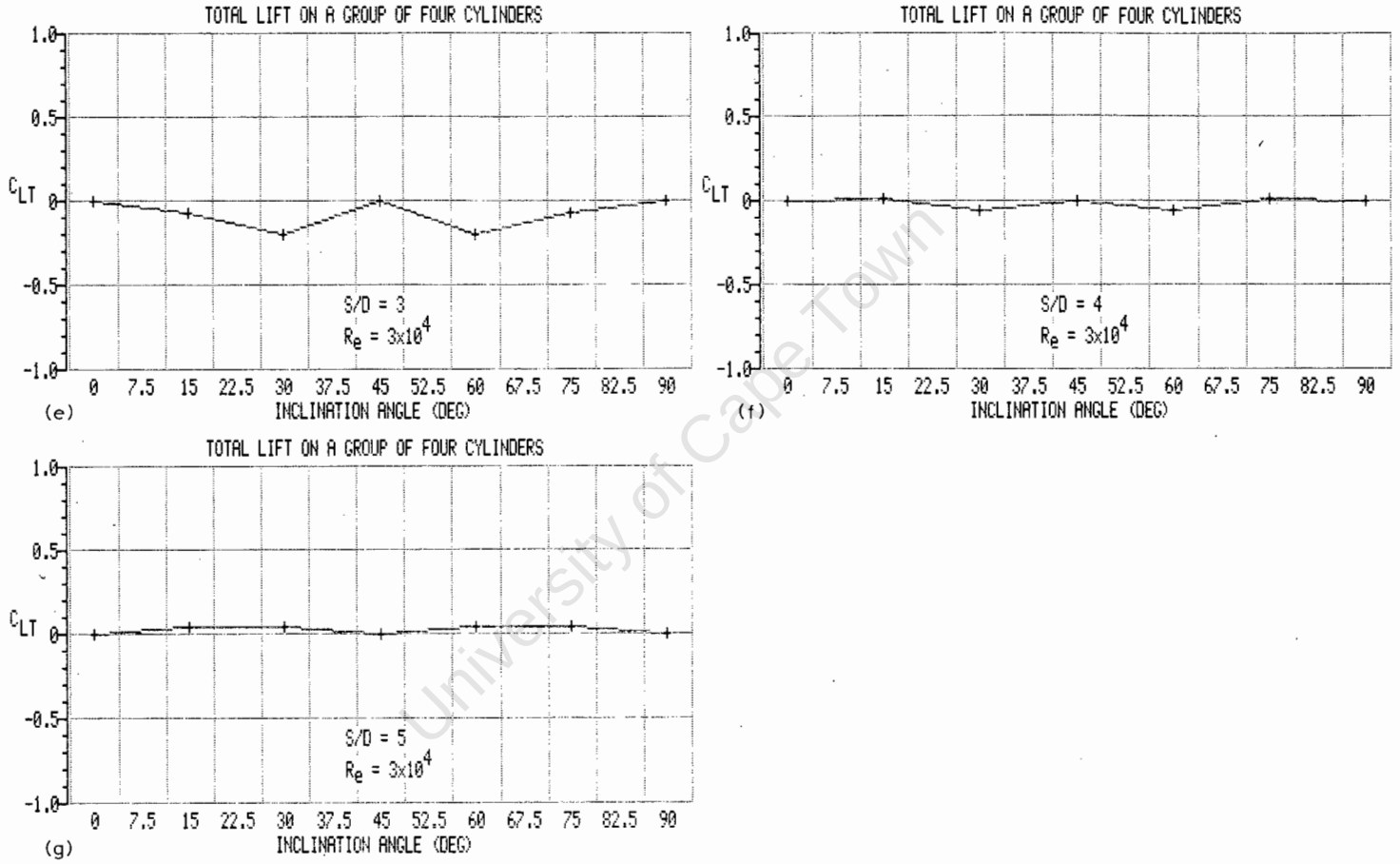


Fig. 6. Total lift coefficients for the group of four cylinders.

TABLE 1

The lift and drag coefficients acting on each of a group of four cylinders with a spacing ratio of 1.1 and an inclination angle of 15°

| Cylinder number | Cylinder angle (deg) | Equivalent angle (deg) | $C_D$ | $C_L$ |
|---|---|---|---|---|
| 1 | 15 | 15 | 0.85 | 0.49 |
| 2 | 105 | 105 | 0.39 | −0.34[a] |
| 3 | 195 | 165 | 0.09 | 0.08 |
| 4 | 285 | 75 | 0.91 | −0.15[a] |

[a]The negative sign indicates a lift force directed towards the axis of the wind tunnel test section.

spacing ratio at a specific inclination angle may now be obtained. Considering a spacing ratio of 1.1 (Figs. 3a and 4a) at an inclination angle of 15°, the drag and lift coefficients of each cylinder are given in Table 1. When these coefficients are summed, noting that the total cross sectional area is now $4D$, the total drag and lift coefficients $C_{DT}$ and $C_{LT}$ are obtained from eqns. (4) and (5).

$$C_{DT} = (C_{D1} + C_{D2} + C_{D3} + C_{D4})/2\rho U^2 D \tag{4}$$

$$C_{LT} = (C_{L1} + C_{L2} + C_{L3} + C_{L4})/2\rho U^2 D \tag{5}$$

The total force coefficients are shown in Figs. 5 and 6 where it is seen that the total coefficients repeat themselves every 90°. The direction of resultant force acting on the group of four cylinders as a whole is given by

$$\gamma = \text{atan}(C_{LT}/C_{DT}) \tag{6}$$

and this variation is shown in Fig. 7.

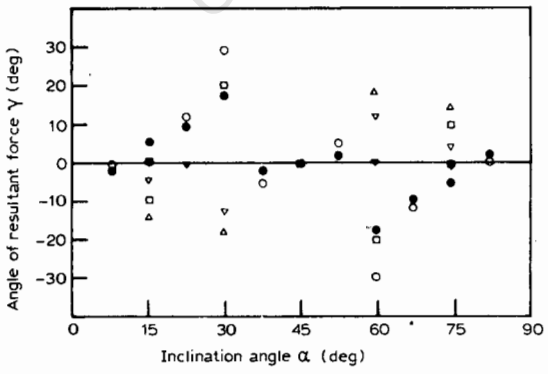


Fig. 7. Variation of direction of the resultant force acting on the group of four cylinders. ($S/D$: ● 1.1; ○ 1.25; □ 1.5; △ 2; ▽ 3; ▼ 4; ■ 5).

*4.1 Drag coefficient*

At $\alpha = 0°$ and spacing ratios of 4 and 5, cylinder 1 behaves as a single isolated cylinder in a two dimensional flow field, the drag coefficient of 1.1 being the same as that determined by Sayers [5] for the isolated cylinder. At a spacing ratio of 2, the drag coefficient drops to 0.82, but for a further decrease in spacing ratio, the drag coefficient recovers to remain steady at $\sim 0.95$. This is due to the presence of the adjacent cylinder affecting the pressure distribution around cylinder 1. Unlike the three cylinder case [5], the negative pressure coefficient (the negative sign indicating a force directed towards the axis of the wind tunnel test section) does not become positive on the downstream part of cylinder 1 but, as shown in Fig. 8, increases from $-1.1$ to only $-0.49$ as the cylinder spacing decreases. Also, the positive pressure coefficient acts over a much wider total angle at the smaller spacings than was the case for three cylinders [5] where it remained virtually unchanged. This spreading of the positive pressure coefficient on the upstream side of cylinder 1 negates the increase in pressure on the downstream side, resulting in only a small change in drag coefficient.

As the group of cylinders is rotated, between 0 and 180°, the shape of the drag coefficient curves for the different spacing ratios are similar in form to those for the three cylinder grouping [5] except that the inclination angles for maximum and minimum $C_D$ of cylinder 1 have changed. At spacings of 1.1 and 1.25, the drag coefficient rises steeply over 7.5° to a maximum value at an inclination angle of 37.5°. For further increases in spacing, the position of maximum $C_D$ occurs at increasing inclination angles when its rate of change and magnitude also become less severe.

$C_D$ drops steeply to a negative value at an inclination angle of 127.5° for $1.1 < S/D < 2$. A similar trend is observed for the range $3 < S/D < 5$ but the

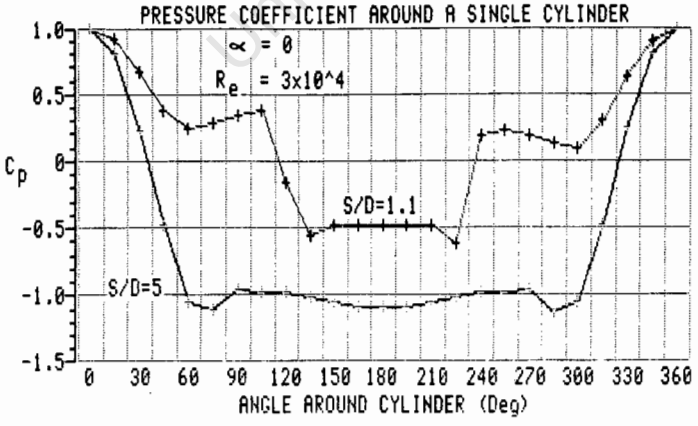


Fig. 8. Pressure distribution around cylinder at $\alpha = 0°$ for $S/D = 1.1$ and 5.

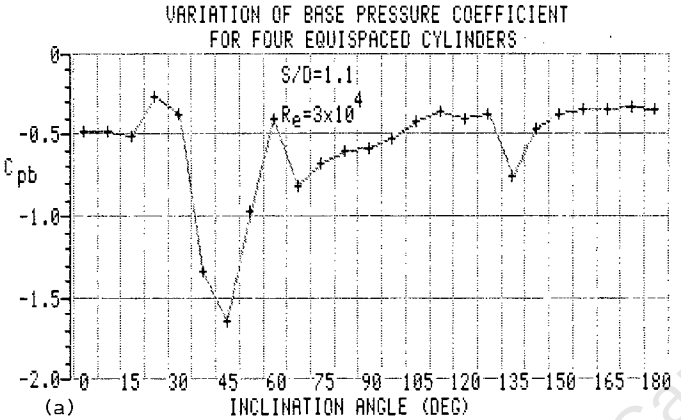


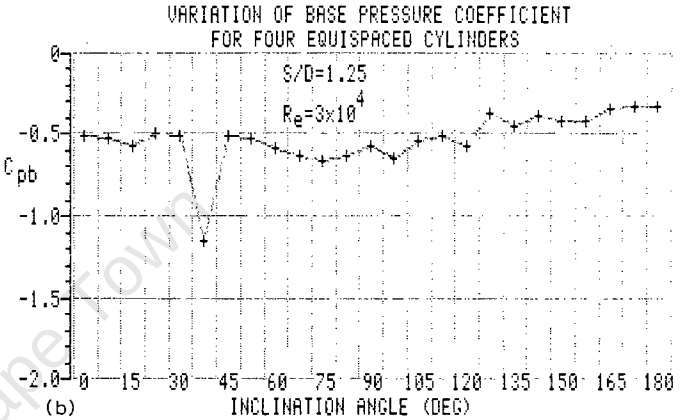


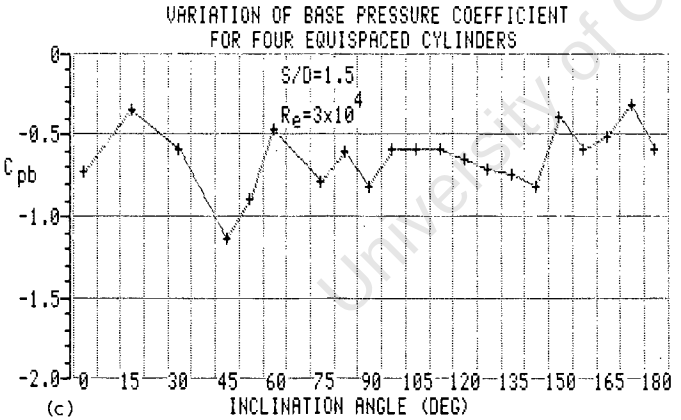


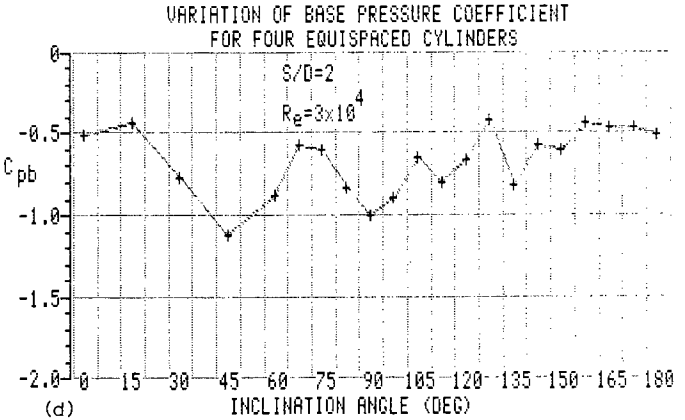

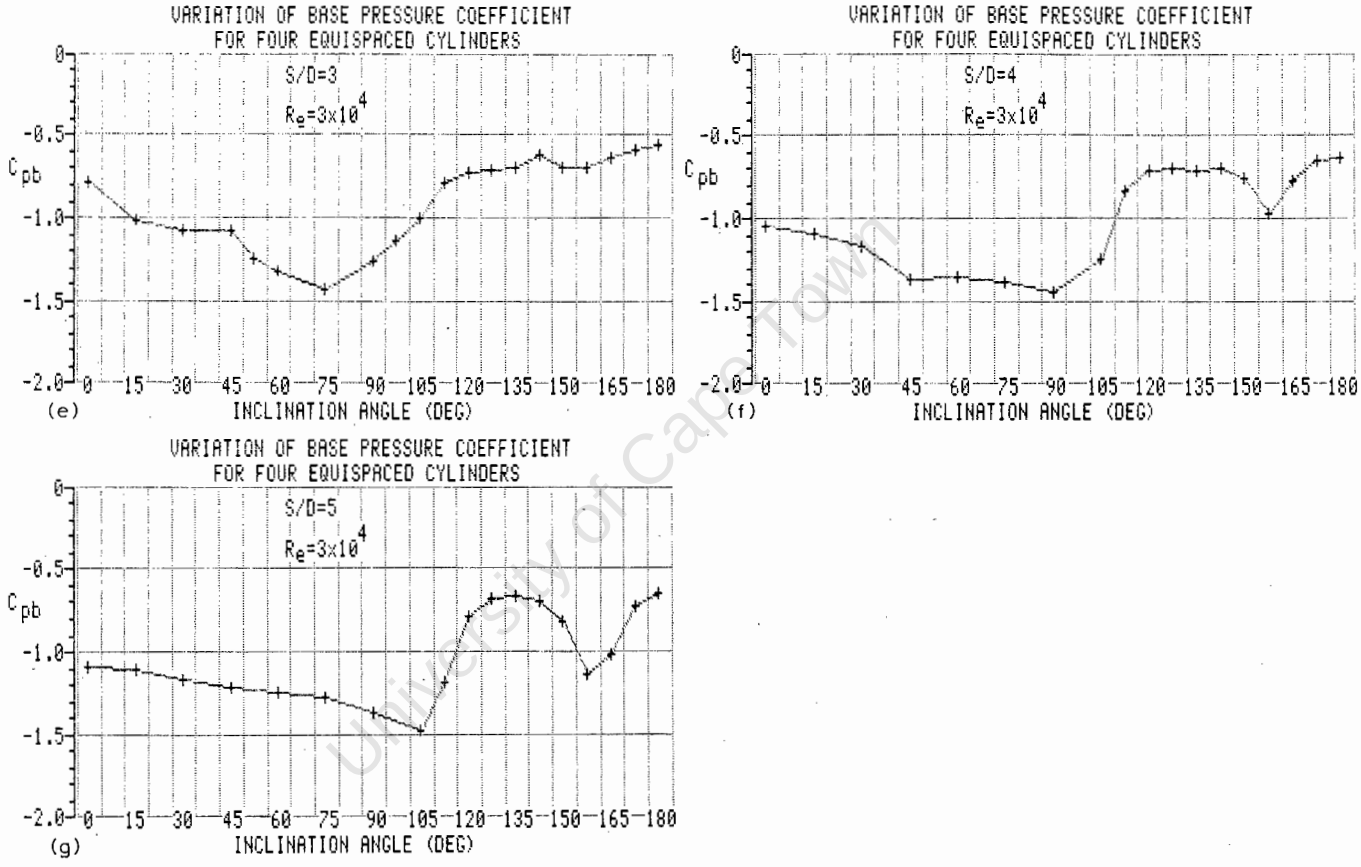




Fig. 9. Variation of base pressure distribution of cylinder 1 with inclination angle.

minimum $C_D$ occurs at $\alpha = 135°$ and remains positive. For the latter spacings, cylinder 1 (at $\alpha = 135°$) is directly behind cylinder 4 (at $\alpha = 45°$) and flow interference is of the W type only since the cylinders are now far enough apart not to affect the flow appreciably. With the lower spacings, both cylinder proximity and wake interference are of importance, the adjacent cylinders deflecting the flow and as a result causing the minimum $C_D$ to occur when the cylinders 1 and 4 are not in line. The changes in $C_D$ are closely mirrored by the variation in the base pressure coefficient shown in Fig. 9, and it may therefore be concluded that the drag coefficient is highly dependent on $C_{pb}$.

For all spacings, $C_D$ recovers from its minimum value and, except for spacings of 1.1 and 1.25, it peaks again at an inclination of 157.5°, this being due to the displacement of the wake from cylinder 4 (at 67.5°) affecting the flow around cylinder 1. This effect diminishes as cylinder 1 moves out of the wake of cylinder 4 for further increases in inclination angle. The drag coefficient also gradually decreases to a value of half that for cylinder 3 (at the 0° position), the flow about cylinder 1 now being strongly affected by the wake shed from cylinder 3. At spacings of 1.1 and 1.25, proximity and wake interference reduce the drag coefficient to about zero.

*4.2 Lift coefficient*

All spacing ratios in Fig. 4 give a zero lift coefficient for cylinder 1 at $\alpha = 0°$, indicating symmetry of flow about that cylinder. Considering first the range $2 < S/D < 5$ of Fig.4d–g, a bias towards a positive outwardly-directed lift coefficient occurs for $0° < \alpha < 90°$. At $\alpha = 90°$, the lift coefficient increases rapidly in the negative direction (i.e. inwards) where it reaches its maximum negative value at $\sim 112.5°$, the magnitude of this value increasing as the cylinder spacing decreases. With cylinder 1 at 112.5°, cylinder 4 is at an inclination angle of 22.5° and therefore lies closer to the axis of symmetry. The edge of the wake of cylinder 4 extends past the lower side of cylinder 1 thereby creating an effective boundary. The flow passing around the lower side of cylinder 1 has a reduced cross sectional area and consequently a higher velocity and lower pressure than that on the upper side. This is clearly shown by the pressure distribution in Fig. 10. A further increase in $\alpha$ causes part of the wake of cylinder 4 to stagnate on cylinder 1 and then to partially flow around it. At $\alpha = 135°$, the cylinders are in line with respect to the freestream, the flow around cylinder 4 being symmetrical as demonstrated by the zero lift coefficients and typical pressure distribution shown in Fig. 10. Increasing $\alpha$ still further now moves cylinder 4 above cylinder 1 and the reverse pressure distribution occurs to give a positive peaking lift coefficient at $\alpha = 150°$. Between 150° and 180°, cylinder 1 becomes increasingly influenced by the wake of cylinder 2 which is moving towards the $\alpha = 0°$ position.

In the range $1.1 < S/D < 1.5$, Fig. 4a–c shows that the lift coefficient increases from zero to peak at 30°, although there is evidence that this phenom-

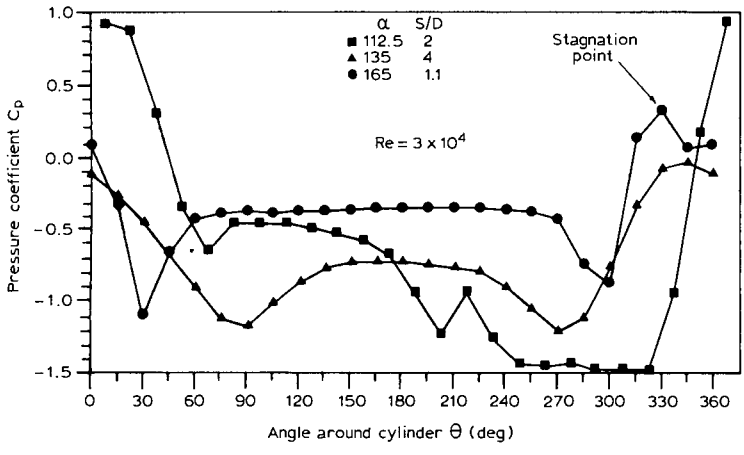


Fig. 10. Pressure distribution around cylinders at various orientations and spacings.

enon is already underway at $S/D=2$ (Fig. 4d). This is due to proximity interference of the lower cylinder 4 before cylinders 1 and 4 are in side by side arrangement, when it might be expected that the greatest proximity interference would occur. However, the close proximity of all cylinders causes intense interaction of the wakes and makes any conclusions based on the two cylinder results of Zdravkovich and Pridden [7], of little value. At spacing ratios of 1.5 and 1.25, rapid fluctuations in $C_L$ indicate a transitory phase before stability is again established at $S/D=1.1$. During this transitory phase, the magnitude of the change from a positive to negative lift coefficient with change in inclination angle becomes greater but less severe whilst the inclination angle at which maximum negative $C_L$ occurs, changes to 90° when cylinder 1 is at its outermost position. This movement from the 112.5° position at the wide spacing ratios indicates strong proximity interference as opposed to wake interference and gives rise to high velocities in the gaps between the cylinders and subsequently high negative pressure coefficients in the range $210° < \theta < 315°$. Increasing $\alpha$ from 90° to 180° sees a return to an almost zero lift coefficient at $\alpha=135°$ when cylinder 1 is in tandem behind cylinder 4. In the range $135° < \alpha < 180°$, the lift coefficient is slightly positive biased and this is due to a prefered stagnation point occuring at $\theta=330°$ as shown in Fig. 10.

*4.3 Total force coefficients*

In comparing Figs. 5 and 6 with the total drag and lift coefficients of Sayers [5] for the three cylinder grouping, it is seen that the variation in $C_{DT}$ with $\alpha$ is of the same order and that at high spacing ratios $C_{DT}$ approaches 1 due to the flow about the cylinders approaching that about a single isolated cylinder. Changes in $C_{LT}$ are less extreme than for the three cylinder case but these changes increase with decreasing spacing ratio whilst the absolute values of

$C_{LT}$ are lower on either side of zero than in the three cylinder case. Fig. 7 shows that the greatest change in $\gamma$ occurs for low values of $S/D$. For spacing ratios of 4 and 5 the change in $\gamma$ is negligible, and therefore in variable direction flow fields structures of this type should be designed with cylinder spacings of at least four diameters to guard against possible fatigue failure.

## 5. Conclusions

The lift and drag coefficients acting on a single cylinder in a group of four situated in a uniform freestream flow have been determined and they show that the forces acting on each cylinder of the group can vary widely. The magnitude of the coefficients is strongly influenced by the orientation of the group to the freestream with minimum drags occurring at inclination angles between 127.5 and 135°. For all spacing ratios, rapid reversals in both lift and drag occur but greatest stability is achieved with higher spacing ratios, when large and rapid changes only take place between inclination angles of 90 and 180°.

These results may be regarded as basic force coefficient data to be included with two and three cylinder data in a design code of practice. It is recommended that further data be obtained for groupings of three by three (9) and four by four (16) equispaced cylinders.



## References

1 M.M. Zdravkovich, Review of flow interference between two circular cylinders in various arrangements, J. Fluids Eng., 99 (1977) 618-633.
2 H.J. Gerhardt and C. Kramer, Interference effects for groups of stacks, J. Wind Eng. Ind. Aerodyn., 8 (1981) 195-202.
3 S.J. Price and M.P. Paidoussis, The aerodynamic forces acting on groups of two and three circular cylinders when subject to a cross flow, J. Wind Eng. Ind. Aerodyn., 17 (1984) 329-347.
4 M.M. Zdravkovich, Forces on pipe clusters, Proc. Conf. on Separated Flow around Marine Structures, Norwegian Institute of Technology, Trondheim, June 1985, pp. 201-226.
5 A.T. Sayers, Flow interference between three equispaced cylinders when subjected to a cross flow, J. Wind Eng. Ind. Aerodyn., 26 (1987) 1-19.
6 A.T. Sayers and D.R. Ball, Blockage corrections for rectangular flat plates mounted in an open jet wind tunnel, Proc. Inst. Mech. Eng., 197C (1983) 259-263.
7 M.M. Zdravkovich and D.L. Pridden, Interference between two circular cylinders; series of unexpected discontinuities, J. Ind. Aerodyn., 2 (1977) 255-270.

*Journal of Wind Engineering and Industrial Aerodynamics*, 26 (1987) 1–19
Elsevier Science Publishers B.V., Amsterdam — Printed in The Netherlands


# FLOW INTERFERENCE BETWEEN THREE EQUISPACED CYLINDERS WHEN SUBJECTED TO A CROSS FLOW

A.T. SAYERS

*Department of Mechanical Engineering, University of Cape Town, Rondebosch 7700 (South Africa)*

(Received May 7, 1986)

## Summary

The drag and lift coefficients occurring on one cylinder in a group of three lying with their axes perpendicular to a uniform stream flow have been measured at a flow Reynolds number of $3\times10^4$ at various inclination angles to the free stream. The cylinders were arranged with their centres equidistant from each other (an equilateral triangle), the spacing ratio of their centres being in the range $1.25 < S/D < 5$.

From the force coefficients for the individual cylinders, total force coefficients for the group as a whole and the direction in which the resultant force acts were determined. It was found that at certain inclination angles the force coefficients were similar to those pertaining to two-cylinder flow, but that in general the effect of the third cylinder was significant. The results presented should aid in the establishment of standard design codes for flow interference around groups of cylinders.



## Notation

| | |
|---|---|
| $C_D$ | drag coefficient |
| $C_L$ | lift coefficient |
| $C_{DT}$ | total drag coefficient |
| $C_{LT}$ | total lift coefficient |
| $C_p$ | pressure coefficient |
| $C_{pb}$ | base pressure coefficient |
| $D$ | cylinder outside diameter (m) |
| $p$ | static pressure (Pa) |
| $p_0$ | free stream static pressure (Pa) |
| $Re$ | Reynold's number |
| $r$ | radius of cylinder (m) |
| $S$ | distance between cylinder centres ($m$) |
| $S/D$ | spacing ratio |
| $U$ | free stream velocity (m $s^{-1}$) |

0167-6105/87/$03.50 

*Greek letters*

$\alpha$ angle of inclination (deg)
$\gamma$ angle of resultant total force (deg)
$\rho$ density of free stream ($kg\ m^{-3}$)
$\theta$ circumferential angle on the cylinder (deg)

## 1. Introduction

Many engineering structures or designs consist of groups of circular or near circular cylinders situated in a flow field with their axes perpendicular to the flow direction. Some examples of such structures are: groups of chimney stacks as found in the chemical industry; groups of cooling towers as those in power plant cooling water systems; oil drilling platform structural members; banks of heat exchanger tubes and bundles of overhead power conduction cables. The distance between the centres of the cylinders can range from very wide spacings to one tube diameter, whilst the centre connections can form a rectangular, triangular or linear array depending on how many cylinders are involved.

For free stream flow of a fluid over a single cylinder situated with its axis perpendicular to the flow, the only mean time-averaged force acting on the cylinder is the drag force in the flow direction. The associated drag coefficients at different Reynolds numbers for this flow regime are well established [1]. When cylinders are grouped together, if the spacing is wide enough, the wake behind the upstream cylinder(s) will have time to re-establish itself into a uniform free stream before flowing over subsequent cylinders. However, for small spacings, the flow patterns of the individual cylinders interact and the cylinders can experience not only a drag force, but also a lift force perpendicular to the free stream direction.

It is extremely important that the designer of such structures is able to predict the forces acting on them and the need for suitable design codes has therefore arisen. However, most of the research carried out in this field has been as a result of the need for a solution to a particular problem and data therefore tends to be rather fragmented. Only relatively recently has any systematic work been carried out. Zdravkovich [2] presented a comprehensive review of the studies on flow interference between two circular cylinders in various arrangements. Gerhardt and Kramer [3] investigated the interference effects for groups of three or four stacks, whilst Price and Païdoussis [4] found that in certain cases, data for two-cylinder arrangements could be used to predict the forces occurring on certain three-cylinder arrangements. In a later paper, Zdravkovich [5] categorised the flow through pipe clusters and described two basic types of flow interference between two parallel pipes. These are proximity interference, $P$, which occurs when the pipes are close to each other but either none or only one is submerged in the wake of the other, and wake interference, $W$, which occurs when one pipe is close to or submerged in the wake

of the other; they can act alone or together. He also concluded that the available experimental data diminished rapidly as the number of pipes increased and that the data for flow over two cylinders could not be used with sufficient accuracy to describe the flow over three or more pipes. Experimental data for various standard configurations of pipe clusters is therefore an urgent necessity.

Most of the existing experimental data has been obtained in tests on cylinders situated in closed test-section wind tunnels. In some cases, account has been taken of blockage effects but in many cases it is not considered. In addition, various methods of measuring the forces have been used along with different support mechanisms for the cylinders [3,4,6–8]. In particular Bardowicks [9] carried out lift and drag measurements on three cylinders arranged as an equilateral triangle at various centre spacings but whose lengths were finite in that the length/diameter ratio was ten with free flow over one of the ends.

In an endeavour to add to the existing basic data, this paper describes a series of tests carried out to determine the pressure, lift and drag coefficients acting on one cylinder in a group of three as the orientation of the group to the free stream is changed. The distance between the centres of adjacent cylinders was equal thus forming the pattern of an equilateral triangle. To minimise blockage effects, all tests were carried out in an open jet wind tunnel test section. From the data obtained for the individual cylinder, the total drag and lift coefficients for the structure as a whole and the direction in which the resultant force acts were determined.

## 2. Experimental apparatus

Figures 1 and 2 illustrate the general experimental arrangement. The tests were conducted in an open jet return circuit wind tunnel driven by a twelve-bladed variable pitch axial flow fan. The open jet test section was $870 \times 580$ mm at the throat with a working length of 1.6 m. Velocity variation across the test section was $\pm 1\%$ and the turbulence intensity was 0.4%. The maximum velocity in the test section was 36 m $s^{-1}$ whilst the area ratio between the settling chamber and test section was 10:1. Pitot-static tube measurements taken in the empty test section along the horizontal axis of the jet showed a velocity variation of 2.6% over the 1.6 m jet length. This was small enough to be considered negligible. All tests were carried out at the nominal wind speed of 10 m $s^{-1}$ and with a Reynolds number of $3 \times 10^4$, that is just before transition in the case of a single cylinder.

Each cylinder of the group was a 1 m long hollow steel tube of 44 mm internal diameter and 50 mm external diameter, machined to a smooth finish. One of the tubes was cut in half and a brass ring 20 mm wide with 24 equispaced (15°) 0.7 mm diameter pressure tapping holes was inserted between the two halves. This particular cylinder (measuring cylinder) was machine finished after

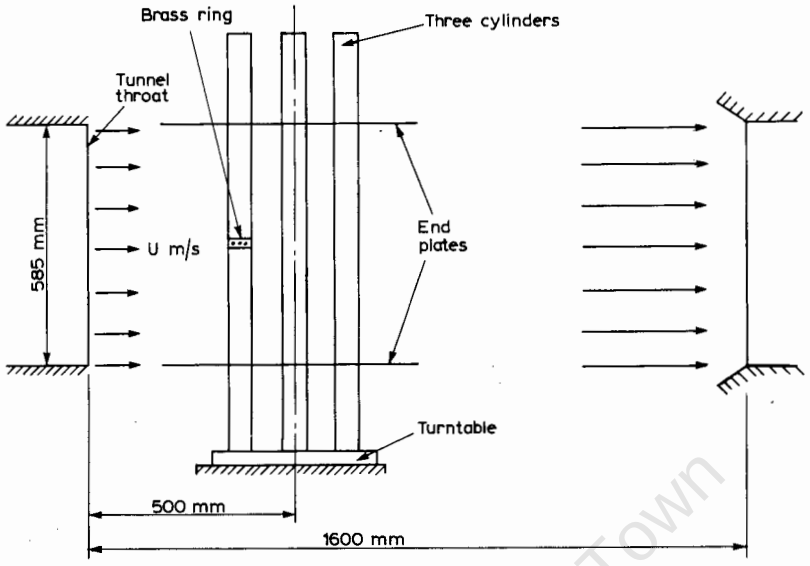


Fig. 1. Experimental arrangement in open jet wind tunnel test section.

insertion of the ring to ensure that there were no burrs or sharp edges on the surface. At one end of each cylinder a locating screw was secured and the cylinders were screwed vertically into position onto a turntable platform, the edge of which was graduated in 7.5° divisions. The whole assembly was then located in the jet at a distance of 500 mm downstream of the tunnel throat and its height adjusted such that the 24 pressure tappings lay along the axis of the test section jet with the ends of the cylinders protruding through the jet boundary.

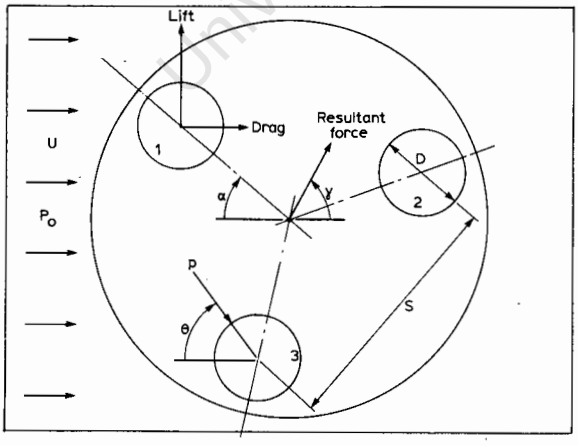


Fig. 2. Cylinder spacing and angles.

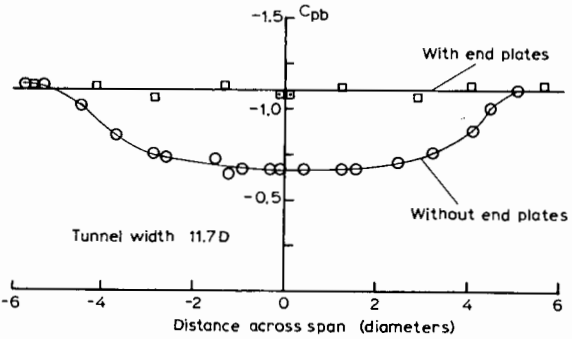


Fig. 3. Spanwise pressure distribution on an isolated cylinder at $Re = 3 \times 10^4$.

Flexible tubing was connected to each pressure tapping of the measuring cylinder and inserted up through the hollow tube to one side of an inclined alcohol manometer, the other side of the manometer being connected to the static pressure tapping of a pitot-static tube. The pitot-static tube was placed at the tunnel throat for measurement of free stream velocity. Pressure differences were determined to within 0.025 mm of water and free stream velocity to within 0.25 m $s^{-1}$.

To check the uniformity of flow along the span of a cylinder, a fourth cylinder was included with static pressure tappings along its length at $\theta = 180°$. From pressure measurements along the span of this single cylinder it was found necessary to attach end plates to the cylinders which were constructed of 3 mm thick boards 620 mm in diameter and with 50 mm holes drilled at the positions corresponding to the cylinder spacings. At all times, great care was taken to ensure that the cylinder separation remained constant across the span and that the axes of the cylinders remained perpendicular to the free stream flow.

### 3. Experimental procedure

The cylinders were purposely made 1 m long so that they would protrude well outside the open jet and thus obviate any end effects which would otherwise occur if the cylinders were of finite length in the free stream. To confirm that uniform flow over the cylinders was being achieved in this way, the single cylinder with the spanwise pressure tappings was first placed in the test section with the static pressure holes facing directly downstream. The base pressure at $\theta = 180°$ was then measured along the span. The resulting pressure distribution is shown in Fig. 3 where it is evident that the flow around the cylinder at the jet boundaries affects the pressure distribution along the span because of the flow being three-dimensional. In order to achieve two-dimensional flow over the cylinder, the 620 mm end plates were attached to the cylinder just

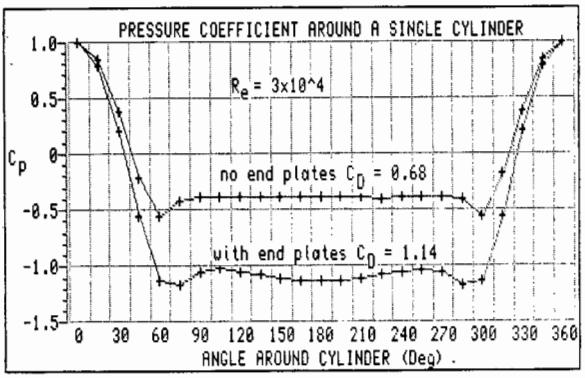


Fig. 4. Pressure coefficient around a single cylinder with and without end plates.

inside the jet boundaries such that the effective span of the cylinder was 575 mm and the new pressure distribution was again measured. The new improved spanwise pressure distribution is also shown in Fig. 3. The static pressures at the 24 tappings at mid-span were recorded both with and without the end plates in position and the pressure coefficients and the associated drag coefficients are illustrated in Fig. 4.

Having satisfied the requirement for two-dimensional flow over the single cylinder, three cylinders were located on the turntable at a particular $S/D$ ratio with 620 mm end plates again attached to give an effective span of 575 mm. The turntable was initially set at $\theta = 0°$ and the measurement cylinder was rotated until one of the mid-span pressure tappings pointed directly upstream. Twenty four static pressure readings were taken around the circumference of the cylinder in increments of 15°. Without further adjustment of the measurement cylinder, the turntable was incremented 0–180° in steps of 7.5°, with sets of pressure readings being taken at each increment. The above procedure was repeated for the range $1.25 < S/D < 5$ at a nominal free stream velocity of 10 m $s^{-1}$.

## 4. Results and discussion

All the experimental results are expressed in terms of dimensionless pressure, drag and lift coefficients. The pressure coefficient is expressed as

$$C_p = (p - p_0)/0.5\rho U^2 \tag{1}$$

The drag coefficient is given by

$$C_D = \int_0^{2\pi} (p - p_0) r\cos\theta \, d\theta / 0.5\rho U^2 D \tag{2}$$

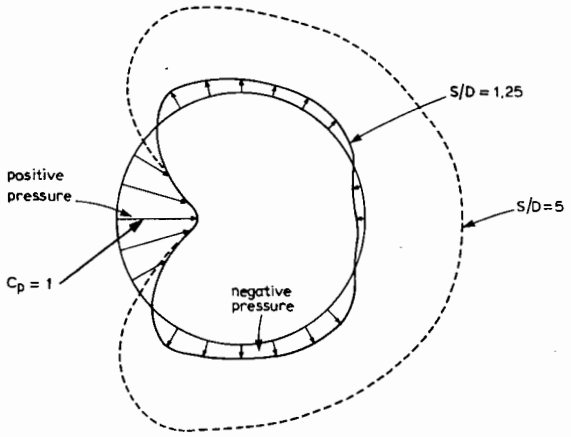


Fig. 5. Polar plots of pressure coefficient around cylinder 1 at $a=0°$, ($C_p$ measured radially from cylinder surface).

and the lift coefficient by

$$C_L = -\int_0^{2\pi} (p-p_0)\, r\sin\theta \, d\theta / 0.5\rho U^2 D \qquad (3)$$

where the integrals of the pressure distributions of eqns. (2) and (3) were carried out using Simpson's rule.

*4.1. Flow over a single cylinder*

The base pressure distribution along the span of the cylinder with no end plates fitted, shows a gradual pressure increase towards the mid-span indicating that atmospheric air is funnelling in from the edge of the jet where the cylinder protrudes through the jet/atmosphere interface. Bearman and Wadcock [6], however, found that for flow over a single cylinder spanning a closed test section, the pressure decreased from the tunnel walls towards mid-span, this being due to the thickening boundary layers built up on the tunnel walls. In both cases, two-dimensional flow was established by fitting end plates to isolate the disturbances.

The pressure distribution around the cylinder at centre-span is shown in Fig. 4 and is in agreement with well established data [1] for two-dimensional flow over an infinitely long cylinder as is the value of drag coefficient. It was considered most important for this flow regime to be established since it may be used as a reference when considering the flow over groups of cylinders.

*4.2. Flow over three cylinders*

Figures 6 and 7 show the drag and lift coefficients of cylinder number 1 as the group of cylinders is rotated through 180° about its axis. It is assumed that

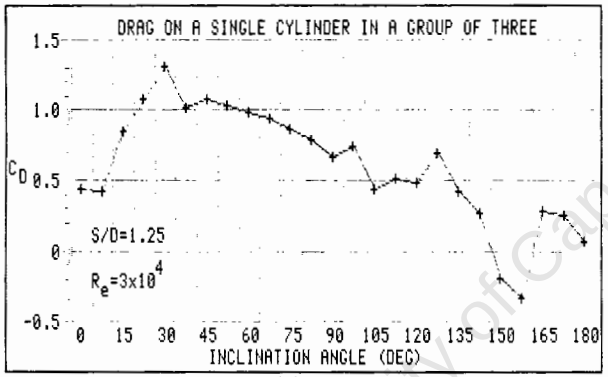


(a)

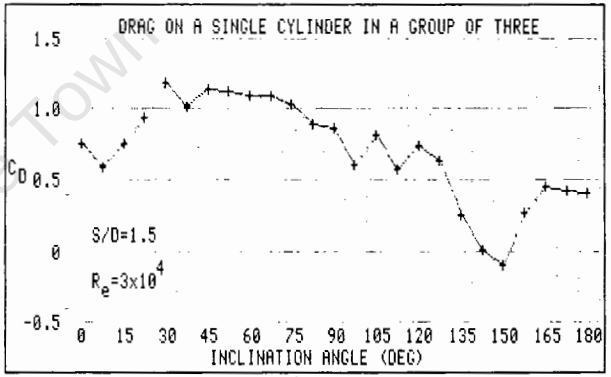


(b)

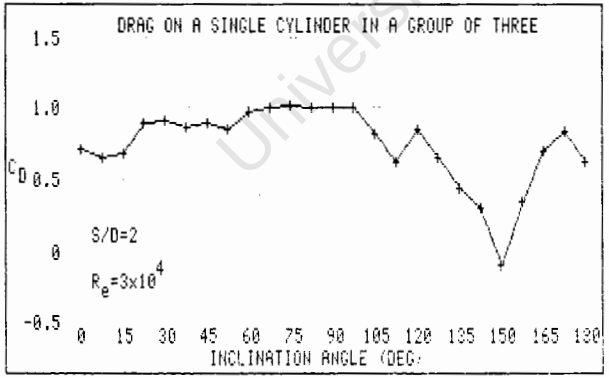


(c)

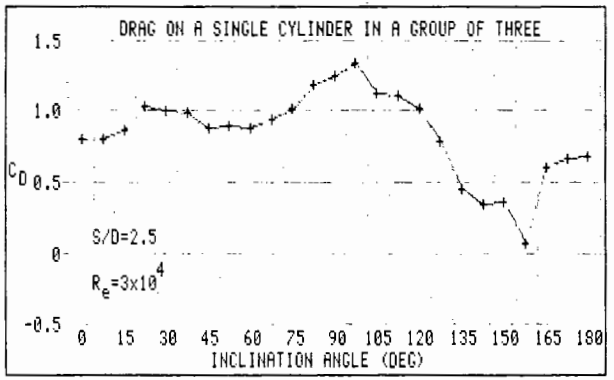


(d)

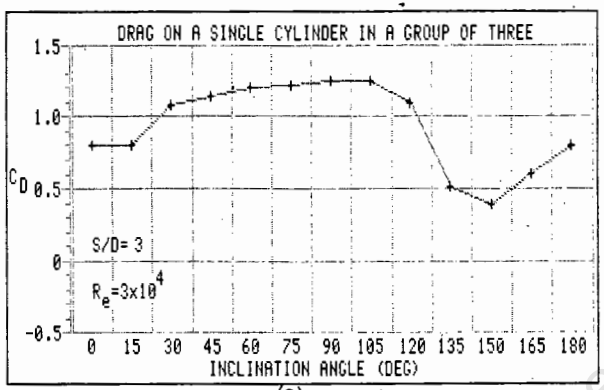


(e)

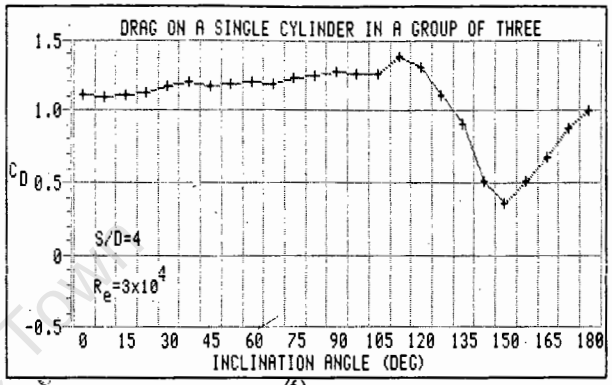


(f)

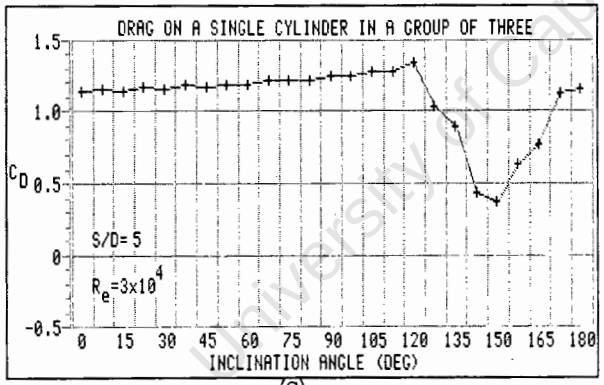


(g)



Fig. 6. Drag coefficients on a single cylinder in a group of three.

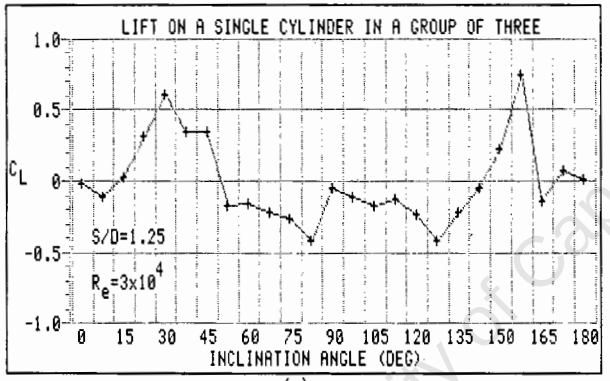


(a)

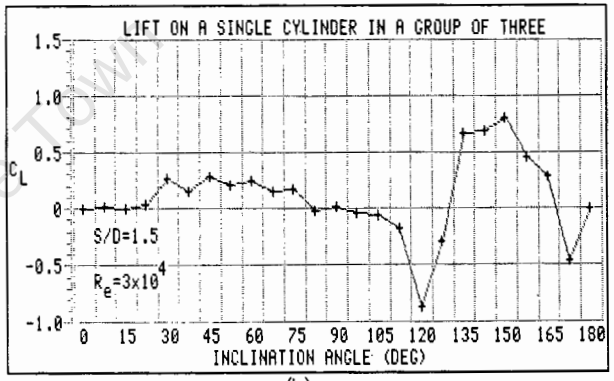


(b)

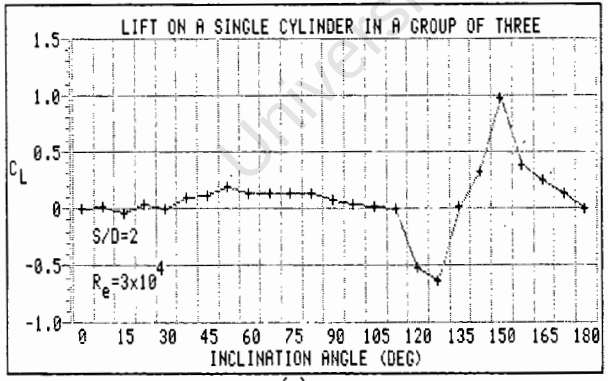


(c)

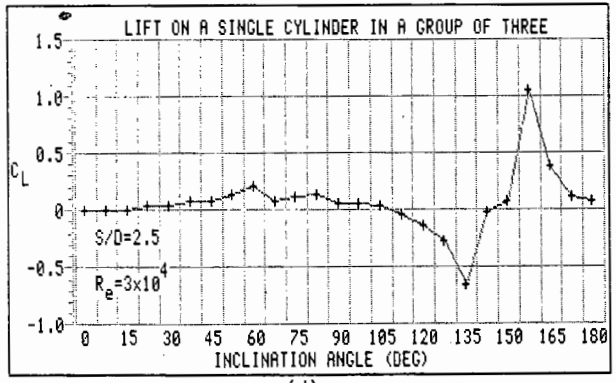


(d)

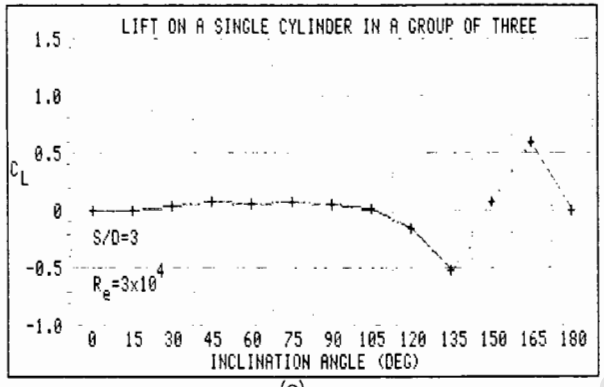


(e)

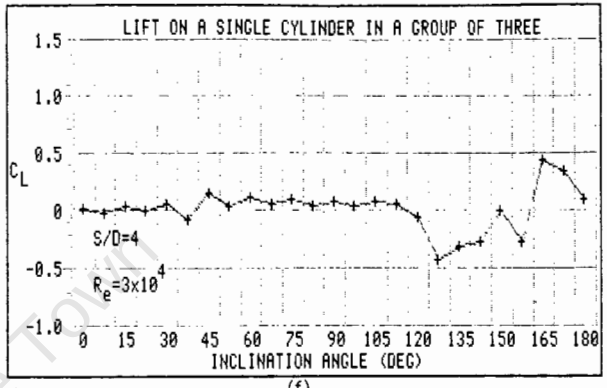


(f)

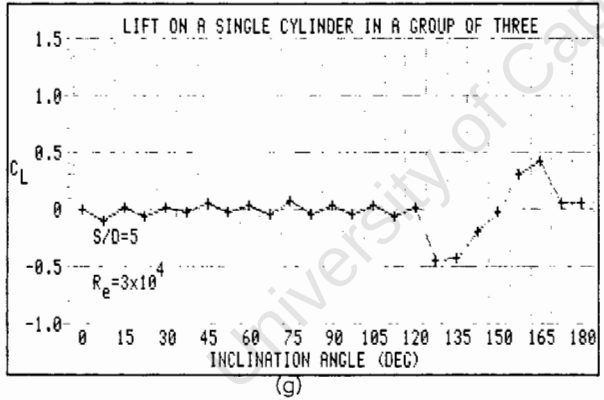


(g)



Fig. 7. Lift coefficients on a single cylinder in a group of three.

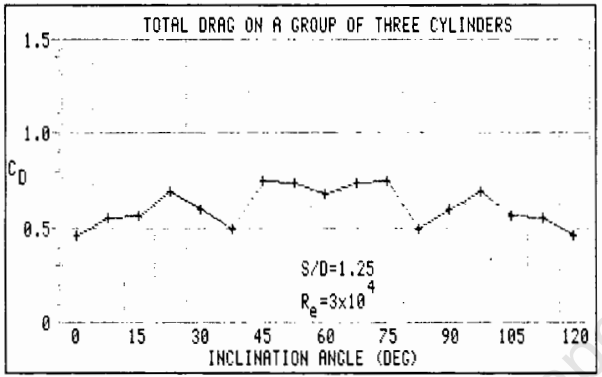


(a)

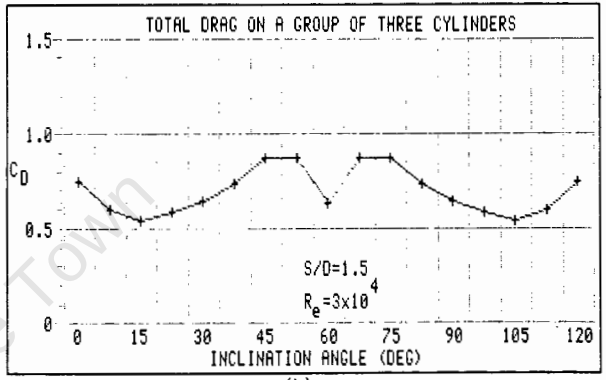


(b)

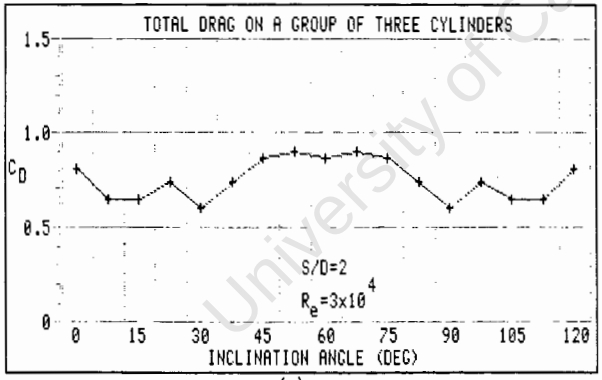


(c)

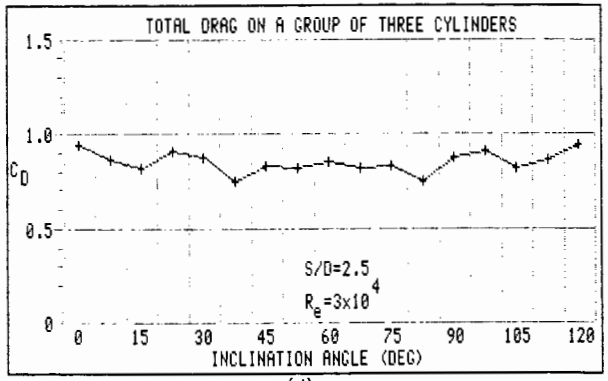


(d)

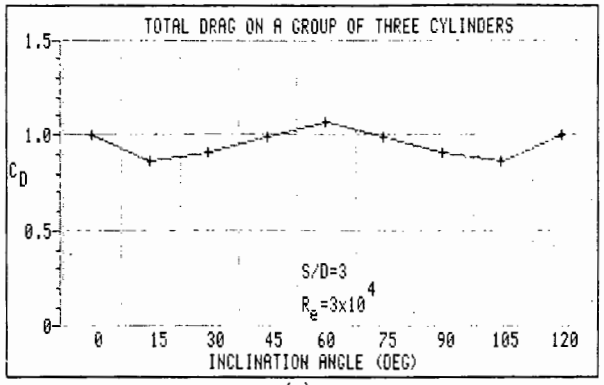

(e)

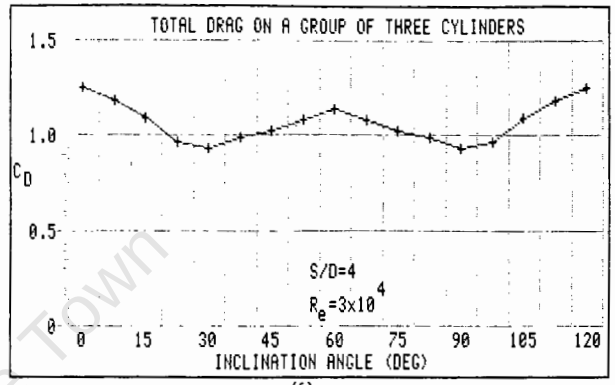

(f)

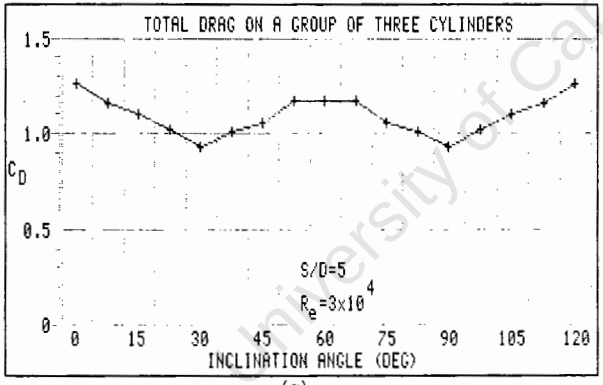

(g)



Fig. 8. Total drag coefficients for the group of three cylinders.

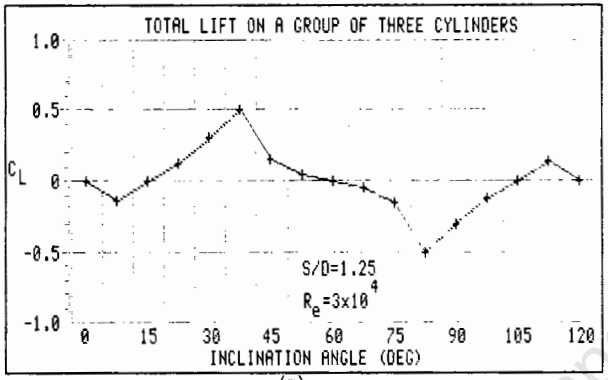

(a)

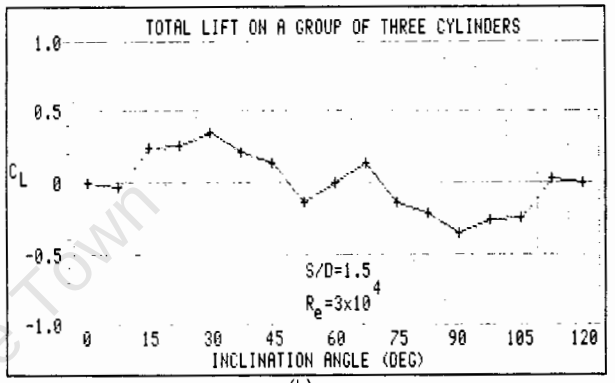

(b)

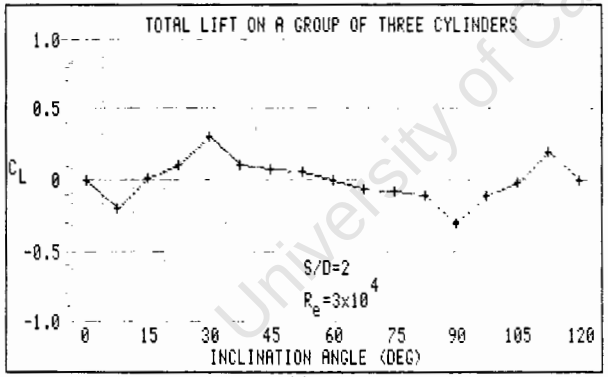

(c)

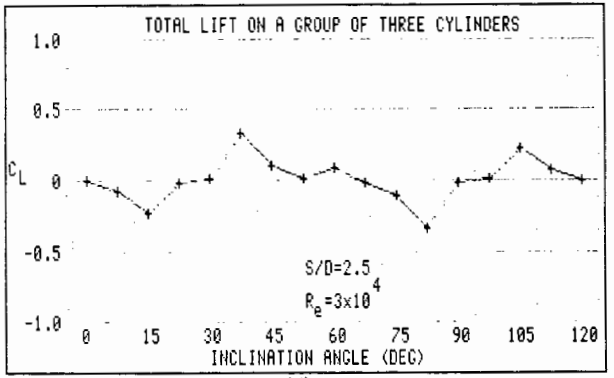

(d)

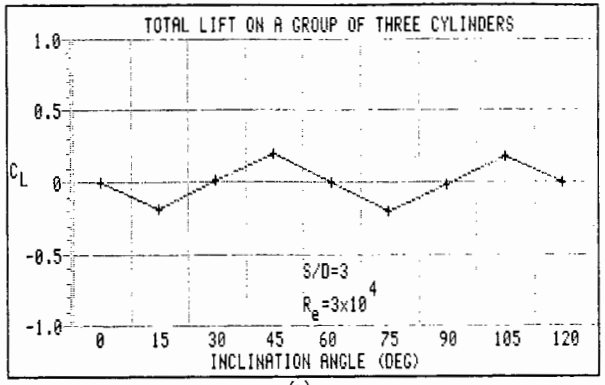

(e)

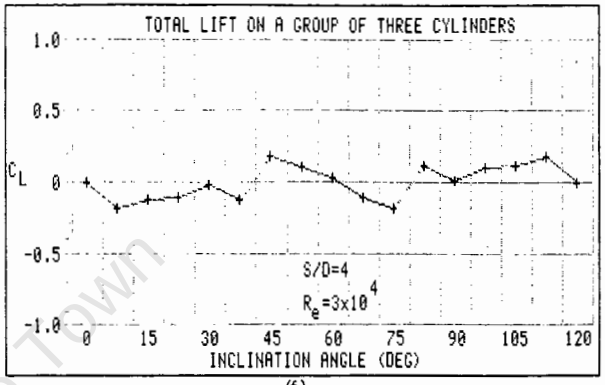

(f)

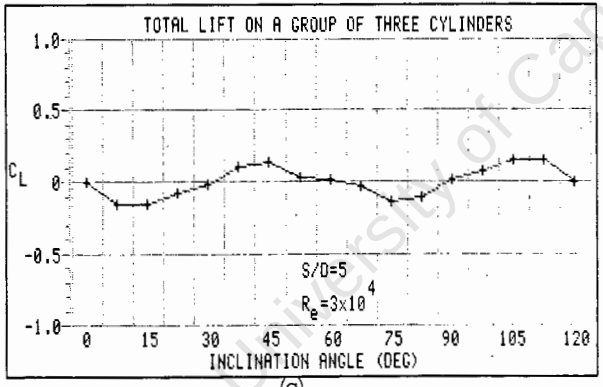

(g)



Fig. 9. Total lift coefficients for the group of three cylinders.

symmetry of flow occurs for the range $180° < \alpha < 360°$ and this was verified by random pressure measurements.

For a given spacing ratio, the lift and drag coefficients acting on each cylinder of the group at any inclination may be obtained. For example, in Figs. 6(a) and 7(a) for an inclination to the free stream of 90°, the drag and lift coefficients of each cylinder are

| Cylinder No. | 1 | 2 | 3 |
|---|---|---|---|
| Cylinder angle (°) | 90 | 210 | 330 |
| Equivalent angle (°) | 90 | 150 | 30 |
| $C_D$ | 0.67 | −0.18 | 1.3 |
| $C_L$ | −0.04 | −0.23 | −0.61 |

By summing these three values of lift and drag coefficients, taking into account their signs and noting that the projected cross sectional area of the cylinders is now $3D$, the total lift and drag coefficients $C_{LT}$ and $C_{DT}$ are obtained from eqns. (4) and (5)

$$C_{LT} = (C_{L1} + C_{L2} + C_{L3})/1.5\rho U^2 D \tag{4}$$

$$C_{DT} = (C_{D1} + C_{D2} + C_{D3})/1.5\rho U^2 D \tag{5}$$

These results are shown in Figs. 8 and 9 where it is noted that the total coefficients repeat themselves every 120°. From the total lift and drag coefficients, the direction of the resultant force acting on the group is determined from

$$\gamma = \text{atan}(C_{LT}/C_{DT}) \tag{6}$$

and this variation is shown in Fig. 10.

For $S/D$ ratios of 4 and 5 at $\alpha = 0°$, cylinder 1 behaves as if it were isolated, the drag coefficients of 1.1 being the same as for the single cylinder in Fig. 4. As $S/D$ decreases, the downstream cylinders 2 and 3 begin to affect the flow over cylinder 1, its drag coefficient dropping to 0.44 at a relative spacing of 1.25. The reason for the decrease is clearly shown in Fig. 5 where the negative pressure coefficient on the downstream part of the cylinder becomes positive, while the front positive pressure coefficient of between $30° > \theta > 270°$ remains virtually unchanged. When the cylinders are rotated, for $S/D$ ratios of 4 and 5, cylinder 1 exhibits a steadily increasing drag coefficient rising to 1.4 at about 120°, although there is some evidence of fluctuating pressures for an $S/D$ of 4. For similar two-cylinder staggered arrangements, Price and Paidoussis [4] and Zdravkovich [5] showed that there was no interference between the two cylinders. It is therefore concluded that the lower cylinder 2 is affecting the flow around cylinder 1, and is of $P$ type interference. For $S/D$ between 3 and 1.25, Fig. 6 shows the maximum $C_D$ on cylinder 1 occurring at decreasing angles of inclination, this being due to increasing combined type $P$ and $W$ interfer-

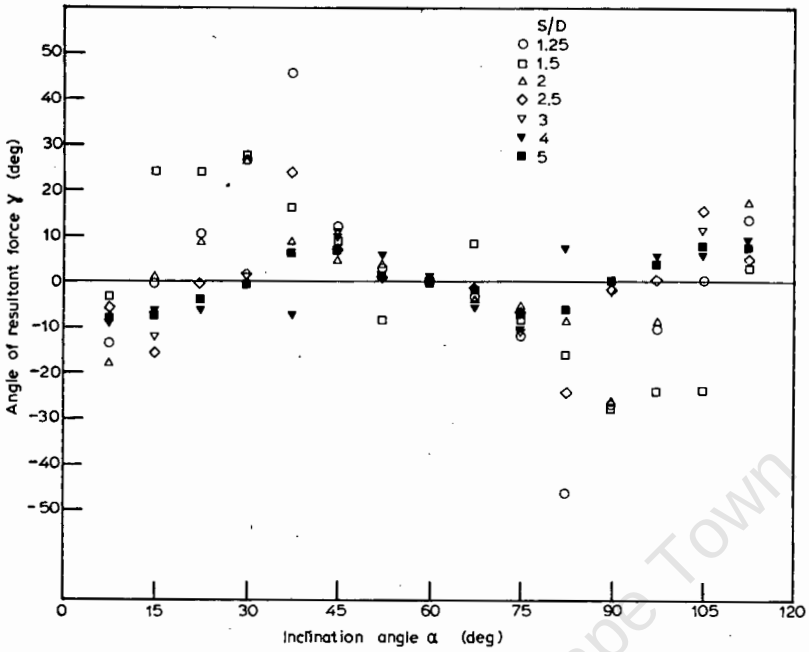


Fig. 10. Variation of direction of resultant force on the group of three cylinders.

ence. From the maximum $C_D$ attained, all spacings show a steep drop to a minimum $C_D$ at an inclination of about 150°. Cylinder 1 is now directly in line with cylinder 3 as if in a two-cylinder tandem arrangement whilst the $C_D$ of 0.4 in Fig. 6(g) is comparable with 0.27 by Price and Paidoussis [4]. The difference can be attributed to the fact that cylinder 2 (now at the 270° position) is affecting the flow pattern around cylinders 1 and 3 and this is indeed confirmed by noting that for the 90° inclination angle, $C_D$ is higher than for the isolated cylinder value. At $\alpha = 180°$, the drag coefficient returns to the isolated cylinder value for the large spacing but is increasingly affected by $P$ and $W$ interference as the spacing decreases. The general trend of the drag curves in Fig. 6 are similar to those obtained by Bardowicks [9]. However, nowhere did he obtain negative drag coefficients at small spacings as obtained in these tests and this is partly attributed to disturbances caused by flow over the ends of his finite length cylinders.

The lift coefficients at the different spacing ratios are shown in Fig. 7 where negative coefficients represent inwardly directed vertical forces. The $S/D = 5$ spacing ratio curve shows almost zero lift in the range $0° < \alpha < 120°$ indicating symmetry of flow about the horizontal axis of the cylinder. At 127.5°, cylinder 1 experiences a sudden inward lift force due to wake interference from cylinder 3 which is now at the 7.5° position. In effect, the edge of the wake generated

by cylinder 3 acts as a boundary and prevents the streamlines on the underside of cylinder 1 from diverging as much as they would were the wake not present. This causes an increase in velocity on the underside of cylinder 1 and a consequent reduction in pressure. The situation persists to 135° at which point the pressure starts to recover to give a positive lift coefficient at $\alpha = 165°$ when cylinder 3 is lying above cylinder 1, its wake now acting on the opposite side of cylinder 1. Cylinder 2 has no effect on the flow around cylinder 1.

As the spacing decreases a bias towards a positive lift force develops for $\alpha > 30°$ whilst the change to the negative lift force become less severe. There is also a tendency for the magnitude of the negative lift to increase as does the magnitude of the recovery on the positive side. For $2 < S/D < 5$, maximum and minimum lift occur at more or less the same inclination angle and the curves in general exhibit the same characteristics. In contrast, at $S/D = 1.25$, rapid changes in lift force are noted at 7.5, 30 and 82.5° and it would appear that at $S/D = 1.5$ a transient state exists between the two types of flow regimes. In the case when two cylinders are in tandem, Zdravkovich [8] found that for $2.7 < S/D < 4$ the lift coefficient on the downstream cylinder was positive or very close to zero. This is confirmed here by examining the lift at $\alpha = 150°$, since in this position cylinders 3 and 1 are situated in tandem with the lift being measured on the effective downstream cylinder 1. However, Zdravkovich [8] also inferred a negative lift coefficient in tandem arrangement for $S/D < 2.7$, but for the three-cylinder case at similar spacings, Figs. 7(a)–7(c) show that the lift is clearly positive indicating a strong interference from the lower cylinder 2. The upstream cylinder 3 at $S/D = 1.25$ also shows a high positive lift at $\alpha = 30°$ indicating proximity interference from the lower cylinder 2.

Cylinders 1 and 3 are in side by side arrangement at $\alpha = 60°$ and Figs. 7(b)–7(g) show positive lift forces, the order of which are in agreement with the results of Zdravkovich [8] for the two-cylinder case. As the spacing decreases the velocity of the flow in the gap increases, with the interference being of $P$ type. At a spacing ratio of 1.25, Bardowicks [9] reported an inward directed lift at $\alpha = 40°$ but no evidence was found of this in these tests. He also found a positive lift force at $\alpha = 120°$ for $S/D = 5$ but once again it was not detected in this work. Since Bardowicks's tests were performed on finite length cylinders, this may again account for these phenomena.

The total lift and drag data points shown in Figs. 8 and 9 and the angle of the resultant force acting on the group shown in Fig. 10 indicate how rapidly the total force components can change with relatively small changes in flow direction. In general, the total drag is greater as the spacing ratio increases due to each of the individual cylinders behaving more as an isolated cylinder. Conversely, the total lift coefficient tends towards zero but shows wide changes as the cylinders move towards each other. Although the magnitude of the resultant force might be low, rapid changes in its direction could present important fatigue problems in situations where the flow direction is constantly changing.

## 5. Conclusions

It has been shown that for a standard three-cylinder cluster, the angle of orientation to the free stream will strongly influence the force coefficients acting on any one of the cylinders. Large reversals in lift magnitude and direction occur at inclination angles lying between 120 and 165° for all cylinder spacings tested, whilst a minimum drag is found at about 150°. At some spacings the force coefficients were similar to those for flow interference between two cylinders but it is recommended that extrapolation of this sort should be used with caution. The total force coefficients for the three-cylinder structure as a unit also shows large variations in direction and care should be taken in the design of such structures especially when a variable direction free stream flow is present.

## References


1 J.F. Douglas, J.M. Gasiorek and J.A. Swaffield, Fluid Mechanics, Pitman, London, 1979, pp. 318-319.

2 M.M. Zdravkovich, Review of flow interference between two circular cylinders in various arrangements. ASME J. Fluids Eng., 99 (1977) 618-633.

3 H.J. Gerhardt and C. Kramer, Interference effects for groups of stacks, J. Wind Eng. Ind. Aerodyn., 8(1981) 195-202.

4 S.J. Price and M.P. Paidoussis, The aerodynamic forces acting on groups of two and three circular cylinders when subjected to a cross flow, J. Wind Eng. Ind. Aerodyn., 17(1984) 329-347.

5 M.M. Zdravkovich, Forces on pipe clusters, Proc. Conf. on Separated Flow Around Marine Structures, Norwegian Institute of Technology, Trondheim, June 1985, pp. 201-226.

6 P.W. Bearman and A.J. Wadcock, The interaction between a pair of cylinders normal to a stream, J. Fluid Mech., 61 (1973) 499-511.

7 C. Dalton and J.M. Szabo, Drag on a group of cylinders, ASME J. Pressure Vessel Tech., 99(1977) 152-157.

8 M.M. Zdravkovich and D.L. Pridden, Interference between two circular cylinders; series of unexpected discontinuities, J. Ind. Aerodyn., 2(1977) 255-270.

9 H. Bardowicks, A new six-component balance and applications on wind tunnel models of slender structure, 1980, private communication with M.M. Zdravkovich.

Engineering Sciences Division

# Blockage corrections for rectangular flat plates mounted in an open jet wind tunnel

A T Sayers, BSc, MSc, CEng, MIMechE and D R Ball, BSc
Department of Mechanical Engineering, University of Cape Town, South Africa

*The correction that must be applied to the upstream wind velocity, when a rectangular flat plate normal to the flow direction is placed in an open jet wind tunnel, is determined and is found to be at all times equal to or greater than unity. It is also found to be dependent upon the distance of the body from the tunnel outlet, and the projected area of the body. Comparisons with previous work carried out in closed wind tunnels are made to confirm the experimental technique used.*

## NOTATION

| | |
|---|---|
| $A$ | wind tunnel mouth cross-sectional area, $m^2$ |
| $D_1$ | drag on a body in an unlimited flow field, N |
| $D_2$ | drag on a body in a limited (wind tunnel) flow field, N |
| $C_{DC}$ | drag coefficient for bluff body in unlimited flow field |
| $C_D$ | drag coefficient for bluff body in limited (wind tunnel) flow field |
| $S$ | projected area of bluff body (rectangular plate), $m^2$ |
| $S/A$ | area or blockage ratio |
| $V$ | free stream velocity in limited flow field, m/s |
| $V_C$ | corrected free stream velocity in limited (wind tunnel) flow field, m/s |
| $\rho$ | density of fluid, $kg/m^3$ |

## 1 INTRODUCTION

The energy crisis of the last decade has focused attention on the use of wind turbines as energy producing devices. The Department of Mechanical Engineering at the University of Cape Town is currently investigating the coefficients of performance of various designs of rotor blades using a horizontal axis model wind turbine incorporating a dynamometer (1). In order to obtain meaningful results, the power output of the model should be as large as possible and this entails maximizing the turbine swept area in the wind tunnel test section.

When any model is tested in a wind tunnel, solid and wake blockage cause the air velocity in the vicinity of the model in the wind tunnel to be different from the air velocity in the vicinity of the same model placed in an unlimited free air stream, the upstream velocity being the same in both cases. A velocity correction factor must therefore be applied to the value of the wind tunnel upstream velocity used in the calculation of performance, torque and thrust coefficients of a model wind turbine, particularly if the model power output is very low.

For flow past streamlined bodies blockage corrections are fairly well established and have been discussed by Pankhurst and Holder (2) amongst others (3). In such cases it is usual to express the blockage correction as the sum of individual components due to solid blockage, $\varepsilon_s$, and wake blockage, $\varepsilon_w$, such that:

$$V_C = V(1 + \varepsilon_s + \varepsilon_w) \quad (1)$$

For a closed working section continuity of mass demands that velocities in the vicinity of the body are greater than they would be for zero blockage and so $V_C > V$. For an open jet wind tunnel the constant (atmospheric) pressure boundary means that $V_C < V$. In addition the correction is due almost entirely to solid blockage since $\varepsilon_w$ is usually small.

However for wind tunnel tests on wind turbines blockage corrections for streamlined flows are not really relevant, whereas blockage corrections for bluff body flows such as rectangular flat plates or discs placed normal to the stream are of far greater relevance. Blockage corrections for such flows are generally much larger than for streamlined flows (4), and are also far more difficult to treat theoretically since they require a detailed understanding of the wake properties and wake distortion effects. It is also difficult to break down the correction into components in the manner of equation (1), although one would still expect $V_C > V$ for closed working sections and $V_C < V$ for open jet wind tunnels.

Maskell (4) considered theoretically the bluff body blockage problem for closed working sections. For low aspect ratio bodies, such as square plates and discs normal to the flow, his theory gives:

$$\frac{V_C}{V} = \sqrt{\left[1 + 2.5C_D\left(\frac{S}{A}\right)\right]} \quad (2)$$

He verified this expression by comparison with existing data for square plates which only extended up to 4.5 per cent blockage. Subsequently Alexander (5), Fackrell (6) and Awbi (7) have validated Maskell's theory for higher blockage ratios.

The wind tunnel at the University of Cape Town is of the open jet type, for which the authors are not aware of any information in the literature relating to bluff body blockage corrections. It is to this problem to which the work described in this paper is addressed, by making measurements on a series of rectangular flat plates and extrapolating the results down to zero blockage. In addition a few measurements were made with the plates

*The MS was received on 12 July 1982 and was accepted for publication on 12 July 1983.*

mounted in the closed section of the wind tunnel upstream of the open jet. This enabled comparison with the earlier work of Maskell (4) and Alexander (5).

## 2 THEORY

Consider the two cases shown in Figs. 1 and 2 respectively, where a body is placed in an unlimited and limited flow field. From Fig. 1, the correct value of drag coefficient is given by:

$$C_{DC} = D_1/0.5\rho V^2 S \quad (3)$$

where $D_1$ is the measured drag.

In Fig. 2, the uncorrected drag coefficient will be given by:

$$C_D = D_2/0.5\rho V^2 S \quad (4)$$

but whilst the free stream velocity, $V$, may be the same in both cases, $D_1$ and $D_2$ are not equal due to the velocity at the body in each case being unequal. Therefore $C_{DC}$ and $C_D$ are not equal.

To obtain the correct value for the drag coefficient for Fig. 2, the value of the free stream velocity used in equation (4) must be modified by a velocity correction factor, $V_C/V$, so that the correct value of drag coefficient is obtained from:

$$C_{DC} = D_2/0.5\rho[V(V_C/V)]^2 S \quad (5)$$

Combining equations (3) and (5) gives $(V_C/V)^2 = D_2/D_1$ and substituting for $D_1$ and $D_2$ from equations (3) and (4) gives:

$$V_C/V = (C_D/C_{DC})^{1/2} \quad (6)$$

For a bluff body with sharp edge flow separation the effect of Reynolds number is expected to be small and therefore $C_{DC}$ is unaffected by changes in upstream nominal flow velocity. The value of $C_{DC}$ can be determined experimentally by plotting the drag coefficients of progressively smaller bluff bodies against the cross-sectional area of the body and extrapolating the resultant curve to zero cross-sectional area where the value of $C_{DC}$ will be obtained. Hence for a measured $C_D$ and $V$, knowing $C_{DC}$, the corrected velocity $V_C$ may be determined.

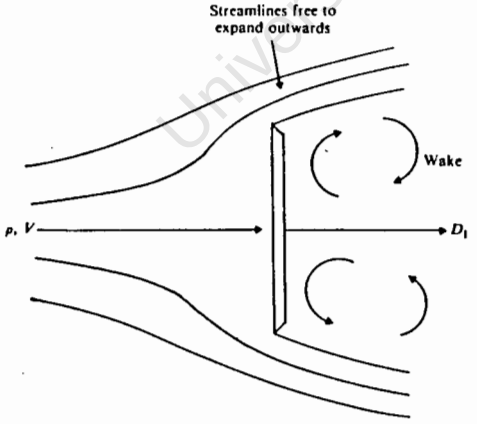


**Fig. 1** Flow over a body with sharp edge flow separation in an unlimited flow field

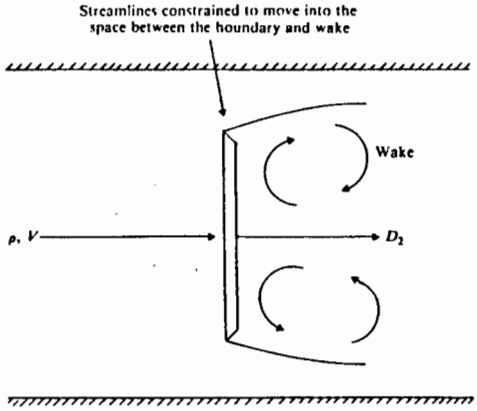


**Fig. 2** Flow over a body with sharp edge flow separation in a limited flow field

## 3 EXPERIMENTAL APPARATUS

### 3.1 Wind tunnel

The wind tunnel used was of the open jet return circuit type, the surrounding pressure in the open jet section being atmospheric. It was driven by a twelve-bladed Woods Varafoil variable pitch axial flow fan which was powered by a two-speed 380 V three-phase motor. The open jet test section was 875 mm × 583 mm × 1600 mm long with a velocity variation across the jet of ±1 per cent and a maximum velocity of 36 m/s. Pitot-static tube measurements taken in the empty test section along the horizontal axis of the jet showed a velocity variation of 2.6 per cent over the 1600 mm jet length. This was small enough to be considered negligible. Tests were carried out at nominal wind speeds of 5, 10 and 15 m/s.

### 3.2 Bluff bodies

The bluff bodies used were flat 5 mm thick rectangular plywood plates of the dimensions given in Table 1, the area ratio ranging from 0.005 to 0.3. The plates were mounted at their centres on a flat rectangular bar sting and the sting was bolted to a horizontal beam drilled with location holes for altering the longitudinal position of the plates in the air jet. A rectangular frame 800 mm × 1100 mm was constructed from flat rectangular bar and wires which were attached to the four corners of the frame allowed suspension of the rectangular plates in the centre of the frame. It was therefore possible to remove a plate from its sting, and with the sting remaining in position, suspend the plate from the wires in the same position as if mounted on the sting but unattached to it, thus the drag on the sting alone could be determined under the conditions prevailing when the plate was attached. The frame size was such that only the support wires and suspended plates were in the air jet.

**Table 1** Dimensions of flat plates
Exact cross-sectional area of tunnel = 0.48 m²

| | | | | | | | | | | | |
|---|---|---|---|---|---|---|---|---|---|---|---|
| Width, | $X$, mm | 60 | 105 | 150 | 195 | 240 | 285 | 330 | 375 | 420 | 465 |
| Height, | $Y$, mm | 40 | 70 | 100 | 130 | 160 | 190 | 220 | 250 | 280 | 310 |

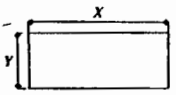


### 3.3 Drag balance

A three-component balance employing strain gauges, enabled a digital read-out of drag force to be measured to within 0.02 N.

### 3.4 Free stream velocity measurement

The velocity head was obtained from a pitot-static tube with pressure tappings connected to an inclined alcohol manometer, the velocity being determined to within 0.25 m/s.

The influence of the plates on the free stream velocity extended at the most a distance of 600 mm upstream from the plates, this distance decreasing for progressively smaller plates. The nominal free stream velocity was set at the proposed plate position in the empty test section by adjusting the velocity head of a pitot-static tube to the required value. The pitot-static tube was then moved 700 mm upstream from the proposed plate position and the velocity head again noted. When the plate was now placed in the air stream the wind speed was adjusted until the previously noted velocity head at the 700 mm upstream position was again obtained on the pitot-static tube.

The difference between the two velocity heads when both were measured in the open jet section proper lay within the 2.6 per cent longitudinal velocity variation noted previously. As the plate position moved upstream towards the start of the open section of the wind tunnel, the velocity head at the 700 mm upstream position was now measured in the contraction section and was substantially below that at the plate location when the plate was not in position. However, by ensuring that the plate again had no effect on the upstream pitot-static tube, measurement was not affected by the plate in the contraction section and the nominal free stream velocity could be maintained for all plate positions.

## 4 EXPERIMENTAL METHOD

For a selected axial distance from the wind tunnel mouth, each plate and sting assembly was in turn mounted in the drag balance, the plate being normal to the air stream as shown in Fig. 3. The tunnel upstream velocity, $V$, was set at 10 m/s for each plate and the drag force on the plate and sting were recorded. The plate was then removed from the sting and suspended by the four tie wires of the suspension frame. The frame was positioned such that, with the sting still mounted in the drag balance, the plate was in almost the same position as when mounted on the sting but completely separate from it. The drag force on the sting alone was recorded. The drag force, $D_2$, on the plate, was calculated from the difference between the two drag readings. This was repeated for five positional settings of the plates relative to the tunnel mouth, one setting being inside the closed section of the tunnel.

At a position 430 mm from the tunnel mouth, the above experiment was repeated for upstream velocities of 5 m/s and 15 m/s to verify the assumption that Reynolds number effects could be neglected.

## 5 RESULTS

Using the values of $V$ and $D_2$ as calculated from the experimental measurements, the uncorrected drag coefficient, $C_D$, was calculated from equation (4) and plotted against the area ratio in Fig. 4 for the different plate positions. The curve labelled −125 mm refers to the plate situated 125 mm upstream from the tunnel mouth in the closed section of the tunnel. Each curve has been extrapolated to zero $S/A$ where the value of $C_D$ (= $C_{DC}$) tends towards 1.1 for plates in the open jet test section. For plates in the closed section, the value of $C_{DC}$ also tends to 1.1. These values of $C_{DC}$ were used in equation (6) for the calculation of the velocity ratio, $V_C/V$.

The velocity ratio is shown plotted against area ratio in Fig. 5 for all plates along with Alexander's results (5). The drag coefficients were also substituted into Maskell's equation (1) and this has been plotted up to an area ratio of 0.3.

The effect of changing tunnel upstream velocity is shown in Fig. 6 where $C_D$ is plotted against $S/A$, some of the points falling on top of each other.

## 6 DISCUSSION

The value of $C_{DC}$ at zero area ratio would be expected to be the same for both a closed and open jet wind tunnel and compares favourably with Alexander's value of 1.15 the difference being 4.5 per cent. As the plate was moved away from the mouth of the tunnel the drag coefficient decreased until at 430 mm from the tunnel mouth, the drag coefficient remained constant with change in area ratio. Only the curves for the 120, 430,

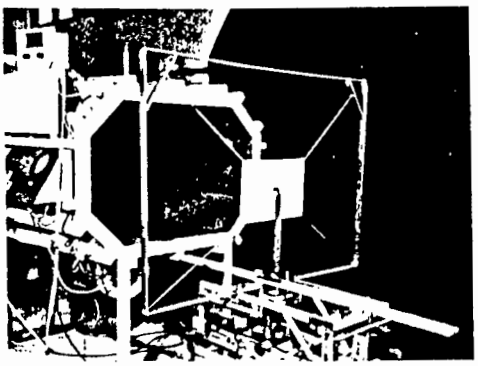

**Fig. 3** Plate suspended in front of, but separate from, the sting

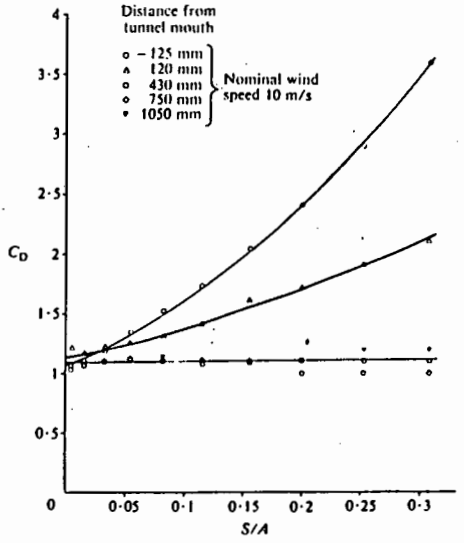


Fig. 4 Drag coefficient versus area ratio for varying distance of plate from tunnel mouth

750 and 1050 mm positions are shown in Fig. 4, since the purpose of plotting Fig. 4 was to determine the value $C_{DC}$ at zero area ratio.

The velocity ratios for flat plates in the open jet section are compared with those for the closed wind tunnel in Fig. 5 where it is seen that the corrected velocity, $V_C$, is always greater than or equal to $V$ which is contrary to the statements made in references (2) and (5) with respect to open jet wind tunnels. As the body was

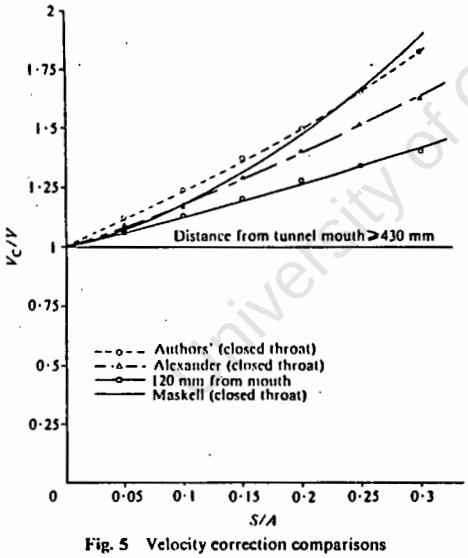


Fig. 5 Velocity correction comparisons

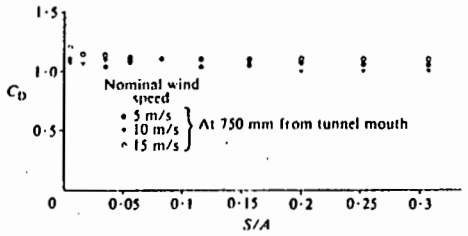


Fig. 6 Effect of Reynolds number on drag coefficient at 750 mm from tunnel mouth

moved away from the tunnel mouth, the velocity ratio decreased to a minimum value of 1 at a distance of 430 mm from the tunnel mouth and remained at that value for further distances indicating that the corrected velocity $V_C$ does not drop below the free stream tunnel velocity.

When the air leaves the closed section of the wind tunnel and becomes the open jet, a distance is required for the jet bounding streamlines to adjust to the new boundary conditions of surrounding atmospheric pressure. If a plate is placed within this adjustment length, the bounding streamlines are unable to expand quickly enough to their naturally fully expanded state. The velocity at the plate between the bounding streamlines and the streamlines forming the edge of the wake at the separation point will therefore have a value between that for the plate in the closed section and that in the fully adjusted open jet. This intermediate velocity decreases as the plate is moved away from the closed section until the velocity at the plate attains its naturally fully expanded streamline value, when $V_C/V$ becomes unity.

The velocity ratios for a position 125 mm upstream of the tunnel mouth are seen to correspond closely with Maskell's equation (1) but are higher than those of Alexander particularly at high area ratios where the difference is in the order of 8.7 per cent at an area ratio of approximately 0.3. If the measured drag coefficients by Alexander for a given area ratio were the same as the authors', a difference in the $C_{DC}$ value of 0.05 would result in a velocity ratio difference of only 2 per cent, and therefore no explanation can be given for this high difference. Although Maskell's curve is based on an equation derived from results obtained using plates of area ratio up to only 0.045, the present results tend to confirm Maskell's equation at higher area ratios.

## 7 CONCLUSIONS

To obtain the corrected wind velocity for a rectangular flat plate placed normal to the flow direction in an open jet wind tunnel test section, the upstream tunnel velocity must be multiplied by a correction factor that will depend upon the distance of the body from the tunnel mouth and which is always positive and greater than or equal to 1. The correction factor decreases with distance from the tunnel mouth until a point is reached where no correction to the upstream velocity needs to be made.

In the calculation of performance coefficients of a model wind turbine, since the coefficient of performance

is inversely proportional to the cube of the wind speed, a 1 per cent error in wind speed results in a 3 per cent error in performance coefficient. The velocity corrections obtained in this investigation will therefore significantly increase the accuracy of calculations made from wind turbine test results.

## REFERENCES


1 **Sayers, A. T.** and **Christoper, A. F.** Performance characteristics of a horizontal axis model wind turbine. *Proc. Instn. Mech. Engrs.*, 1981, **195**, 223–229.

2 **Pankhurst, R. C.** and **Holder, D. W.** *Wind tunnel technique*. Pitman, London, 1952

3 **Pope, A.** and **Harper, J. J.** *Low speed wind tunnel testing*. Wiley, New York, 1966.

4 **Maskell, E. C.** A theory of the blockage effects on bluff bodies and stalled wings in a closed wind tunnel. Aero Res. Council, Reports and Memoranda 3400, 1965, pp 1–22.

5 **Alexander, A. J.** Wind tunnel corrections for Savonius rotors. 2nd International Symposium on Wind Energy Systems, Amsterdam, Oct. 1978.

6 **Fackrell, J. E.** Blockage effects on two-dimensional bluff body flow. *Aero. Quart.*, 1975, **26**, 243–253.

7 **Awbi, H. B.** Wind tunnel wall constraint on two-dimensional rectangular-section prisms. *J. Indust. Aero.*, 1972, **3**, 285–306.

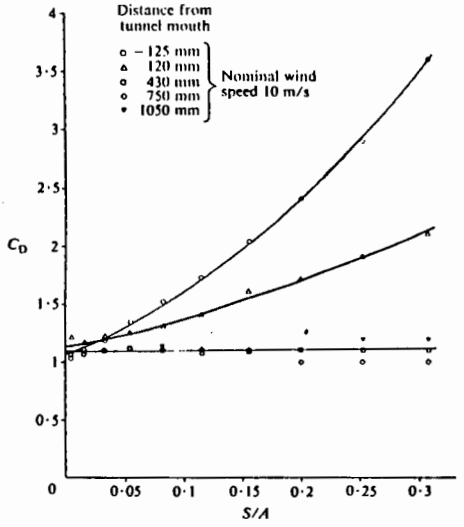


Fig. 4 Drag coefficient versus area ratio for varying distance of plate from tunnel mouth

750 and 1050 mm positions are shown in Fig. 4, since the purpose of plotting Fig. 4 was to determine the value $C_{DC}$ at zero area ratio.

The velocity ratios for flat plates in the open jet section are compared with those for the closed wind tunnel in Fig. 5 where it is seen that the corrected velocity, $V_C$, is always greater than or equal to $V$ which is contrary to the statements made in references (2) and (5) with respect to open jet wind tunnels. As the body was moved away from the tunnel mouth, the velocity ratio decreased to a minimum value of 1 at a distance of 430 mm from the tunnel mouth and remained at that value for further distances indicating that the corrected velocity $V_C$ does not drop below the free stream tunnel velocity.

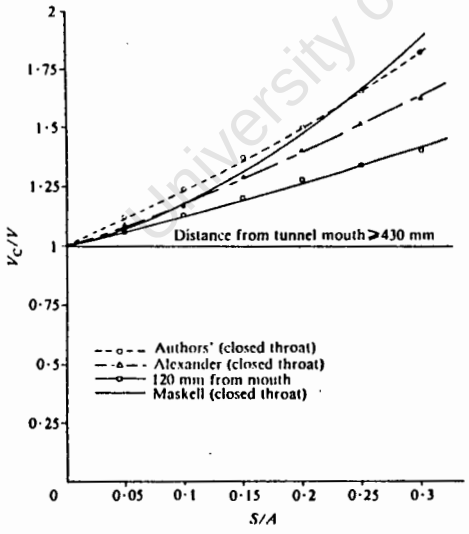


Fig. 5 Velocity correction comparisons

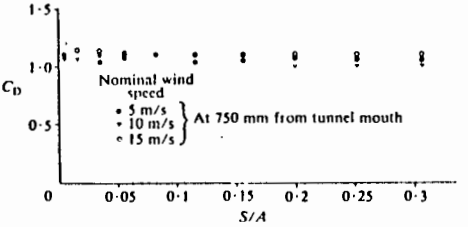


Fig. 6 Effect of Reynolds number on drag coefficient at 750 mm from tunnel mouth

When the air leaves the closed section of the wind tunnel and becomes the open jet, a distance is required for the jet bounding streamlines to adjust to the new boundary conditions of surrounding atmospheric pressure. If a plate is placed within this adjustment length, the bounding streamlines are unable to expand quickly enough to their naturally fully expanded state. The velocity at the plate between the bounding streamlines and the streamlines forming the edge of the wake at the separation point will therefore have a value between that for the plate in the closed section and that in the fully adjusted open jet. This intermediate velocity decreases as the plate is moved away from the closed section until the velocity at the plate attains its naturally fully expanded streamline value, when $V_C/V$ becomes unity.

The velocity ratios for a position 125 mm upstream of the tunnel mouth are seen to correspond closely with Maskell's equation (1) but are higher than those of Alexander particularly at high area ratios where the difference is in the order of 8.7 per cent at an area ratio of approximately 0.3. If the measured drag coefficients by Alexander for a given area ratio were the same as the authors', a difference in the $C_{DC}$ value of 0.05 would result in a velocity ratio difference of only 2 per cent, and therefore no explanation can be given for this high difference. Although Maskell's curve is based on an equation derived from results obtained using plates of area ratio up to only 0.045, the present results tend to confirm Maskell's equation at higher area ratios.

## 7 CONCLUSIONS

To obtain the corrected wind velocity for a rectangular flat plate placed normal to the flow direction in an open jet wind tunnel test section, the upstream tunnel velocity must be multiplied by a correction factor that will depend upon the distance of the body from the tunnel mouth and which is always positive and greater than or equal to 1. The correction factor decreases with distance from the tunnel mouth until a point is reached where no correction to the upstream velocity needs to be made.

In the calculation of performance coefficients of a model wind turbine, since the coefficient of performance